Development and Application of Leaf Wax Geochemistry to Reconstruct Late Cenozoic Climate and Environmental Change in Australia

A thesis submitted in fulfilment of the requirements for the degree of

Doctor of Philosophy

Jake William Andrae BSc (Hons Geology)

School of Physical Sciences - Department of Earth Science

THE UNIVERSITY of ADELAIDE

August 2019

This page is intentionally left blank

Table of contents

Abstract

Leaf wax *n*-alkanes are hydrocarbon compounds that are biosynthesized by higher plants. These compounds can be preserved in the geological record as molecular fossil biomarkers for tens of millions of years. Molecular and isotopic properties of these biomarkers hold great potential as proxy systems for reconstructing various aspects of plant physiology, vegetation structure and climate of the past. Still, uncertainty remains around certain aspects of these proxy systems and their application to past vegetation and climate dynamic reconstructions. The first half of this thesis aimed to provide a more nuanced understanding of aspects of leaf wax *n*-alkane molecular and isotopic proxy systematics. Major outcomes of this research include an increased understanding of the scale at which *n*-alkane molecular distributions in modern plants reflect the climate in which they live, with results suggesting population scale responses of *n*-alkane molecular distributions to climatic conditions. Additionally, carbon isotope systematics of discrete leaf wax *n*-alkane compounds are found to vary significantly as a function of mixed vegetation group inputs to sedimentary records, particularly in relation to aquatic plant contributions. These results provide new insights into the application of leaf wax *n*-alkane proxy systems to reconstructions of past vegetation and climate dynamics. The second half of the thesis aimed to apply leaf wax *n*-alkane molecular and isotopic proxy systems to reconstruct aspects of Australia's palaeo-environment across the late Cenozoic, focusing primarily on the timing and drivers of the expansion of C4 vegetation on the Australian continent. Across many geographic regions, isotope ratios of plant derived carbon in geological archives indicate that plants using the C4 photosynthetic pathway began to proliferate during the late Miocene and Pliocene. While Australia is today the most C4 dominated continent on Earth, little is known of the history of this important aspect of the Australian vegetation. Using carbon isotope ratios measured from leaf wax *n*-alkanes in

sediments from offshore Western Australia, it is demonstrated that C4 vegetation expanded in north-western Australia much more recently than most other geographic regions, within the last 3.5 million years. *n*-Alkane molecular distributions indicate C4 proliferation was the final step in opening of the landscape likely related to increasing aridification. These research outcomes suggest strongly regional drivers for C4 proliferation across the globe. Because of the strong links between the distribution of C4 vegetation and warm season precipitation in Australia today, this aspect of the climate is reconstructed in the context of C4 proliferation since ~3.5 Ma. Through measuring hydrogen isotope ratios of leaf wax *n*-alkanes, an increased amount of summer rainfall in northern Australia since the Pliocene is demonstrated to be a plausible driver for this significant ecological shift on the Australian continent. The research presented in this thesis furthers our understanding of the systematics and application of leaf wax *n*-alkane molecular and isotopic proxy systems. Late Cenozoic palaeo-environmental reconstructions for the Australian continent using these proxy systems further our understanding of the development of important aspects of modern Australian vegetation and climate.

Statement of certification

I certify that this work contains no material which has been accepted for the award of any other degree or diploma in my name in any university or other tertiary institution and, to the best of my knowledge and belief, contains no material previously published or written by another person, except where due reference has been made in the text. In addition, I certify that no part of this work will, in the future, be used in a submission in my name for any other degree or diploma in any university or other tertiary institution without the prior approval of the University of Adelaide and where applicable, any partner institution responsible for the joint award of this degree. I acknowledge that copyright of published works contained within this thesis resides with the copyright holder(s) of those works. I give permission for the digital version of my thesis to be made available on the web, via the University's digital research repository, the Library Search and also through web search engines, unless permission has been granted by the University to restrict access for a period of time. I acknowledge the support I have received for my research through the provision of an Australian Government Research Training Program Scholarship.

Jake William Andrae

27/08/19

Acknowledgments

It really does "…take a village". Without the support and guidance of many people, as well as significant financial support from several sources, the completion of this thesis would not have been possible.

First and foremost, I would like to sincerely thank my three academic supervisors; Francesca McInerney, Jonathan Tyler and Tony Hall. Cesca, you have been an inspiring mentor and friend, and a constant source of support and good humour. You have enthusiastically encouraged me to take every opportunity presented during my PhD and have been pivotal in my professional development by sharing your skills, knowledge and experience as a scientist. Jon, you have been an enthusiastic mentor and have always been willing to make time for me when I needed advice about my project, or anything else for that matter. You greatly inspire the way I think about scientific research and science communication. Tony, you have graciously shared your extensive knowledge of analytical instrumentation and techniques with me, and I appreciate your unceasing energy in this regard. I greatly respect all three of you, and without your significant contributions as mentors, I would not be the confident and well-rounded researcher that I feel I am today.

Thank you to Pratigya Polissar, Billy d'Andrea, Kevin Uno, Jonathan Nichols and all the graduate students in the Lamont-Doherty Earth Observatory organic geochemistry research group for incorporating me so graciously into your lab and lives. The memories of time spent in New York during research visits are something I dearly cherish. I would like to thank Pratigya Polissar and Sam Phelps in particular for your patience and enthusiasm in helping me to generate high quality isotopic data and achieve my research goals. Thank you to Pratigya Polissar, Heather Savage, Nick O'Mara and Chris Carchedi for hosting me

during these visits. In addition, I would like to thank the staff and students of the Mawson Centre for Geoscience and the Sprigg Geobiology Centre at the University of Adelaide. Your support, guidance and friendship has been immeasurable throughout my PhD.

Thank you to the Australian and New Zealand IODP Consortium and the Royal Society of South Australia, whose significant financial support enabled the work presented in this thesis to be undertaken.

I owe a great deal of gratitude to my family. The paths I have taken in life, including undertaking this work, would not have been possible with your unending support. Thank you for being my backbone, holding me up during the hardest times and being there to laugh with me during the best times. Thank you for sharing your wisdom and insight, and for always encouraging me to take advantage of every opportunity that comes my way. I could never have been the person I am today without you.

Finally, I would like to express my sincerest thanks to my partner Erin. You have been by my side through this PhD with a constant supply of love, humour, encouragement and patience. You ensured that I maintained a healthy work-life balance and provided important perspective during the hardest times. I can only hope I am able to provide the same level of support to you in your endeavours.

Chapter 1: Background and literature review

The common theme of this thesis is the calibration and application of leaf wax *n*-alkane proxy systems in palaeo-environmental studies, with an emphasis on reconstructing aspects of Australia's palaeo-environment during the late Cenozoic (~10 Ma to present). The late Cenozoic was a time of significant ecological and climatic change across many regions of the globe, but there has been little work to understand these changes and their impacts in the Australian region. Constraining these changes for the Australian region is of great importance for developing projections about how modern ecosystems may respond to future climate perturbations. In this thesis, four research chapters are presented that have either been published in the scientific literature or prepared in a manuscript style ready for submission to a peer-reviewed journal. In addition, three other chapters are presented; a comprehensive background and literature review (here), a summary of the research outcomes of the thesis along with study limitations and future directions, and appendices that include other research items published and a list of conference papers authored during candidature.

In Section 1 of this background and literature review, I outline leaf wax *n*-alkane molecular and isotopic proxy systems used for reconstructing past changes in plant physiology, vegetation structure on the landscape and climate, and highlight uncertainties associated with these proxy systems. In Section 2, Australia's environment and climate during the late Cenozoic are discussed. I highlight key knowledge gaps pertaining to Australia's environment and climate during this this period, and the potential for leaf wax *n*-alkane proxy systems to address these. In Section 3, the specific aims of the research are outlined, with a summary of each research chapter in context with these aims.

1 Leaf wax *n*-alkane proxy systems

1.1 Background

Leaf waxes, comprising a mixture of organic compounds, are biosynthesized by higher plants and deposited primarily as a component of the leaf cuticle (Jetter et al., 2006; Kunst & Samuels, 2003). Leaf waxes play critical physiological and ecological roles, with a key function of reducing water loss through the cuticle (Jetter & Riederer, 2016; Riederer & Schreiber, 2001). Other roles include the reduction of solute leaching from inside cells, protection against UV-radiation damage and minimization of dust, pollen and air pollutant deposition (Koch & Ensikat, 2008; Kunst & Samuels, 2003). Leaf waxes are in general comprised of long chain aliphatic *n*-alkyl derivatives (e.g., *n*-alkanes, *n*-alkanols, *n*-alkanoic acids), along with triterpenoids and minor secondary metabolites, in varying proportions (Eglinton & Hamilton, 1967; Eglinton et al., 1962; Jetter et al., 2006; Kunst & Samuels, 2003; Schuster et al., 2016). Mid-long chain *n*-alkanes (C21–C37) are a ubiquitous component of leaf waxes in higher plants (Bush & McInerney, 2013) with odd chain lengths typically dominating as a function of fatty acid elongation during biosynthesis (Kunst & Samuels, 2003).

Because of their molecular simplicity (i.e. lack of double bonds and functional groups), leaf wax *n*-alkanes are robust and relatively stable compounds that can potentially be preserved for tens of millions of years in sedimentary archives (Eglinton & Logan, 1991), where they subsequently become molecular fossils. Leaf wax *n*-alkanes can be transported to and preserved in deep marine and lacustrine sediments as well as soils (Diefendorf & Freimuth, 2017; Schreuder et al., 2018), with transport occurring through several avenues. Leaf wax *n*-alkanes can be delivered in association with whole or partial leaf material, that can be either allochthonous or autochthonous to the sedimentary deposit, generally through riverine or leaf-litter fall processes. Leaf wax *n*-alkanes can be also

delivered as a stand-alone aerosol or adsorbed to dust or smoke particles through aeolian processes, subsequent to ablation of waxes from leaf surfaces predominantly by wind or biomass burning (Diefendorf & Freimuth, 2017; Gagosian & Peltzer, 1986; Rosell-Mele & McClymont, 2007; Schefuss et al., 2003; Schreuder et al., 2018). In addition, leaf wax *n*-alkanes can be delivered as a component of sediment that has been eroded and re-deposited (Diefendorf & Freimuth, 2017; Gagosian & Peltzer, 1986). In all these cases, *n*-alkane inputs are spatially and temporally integrated.

Various molecular and isotopic properties of leaf wax *n*-alkanes reflect aspects of plant physiology and growth environment. As such, several *n*-alkane palaeo-environmental proxy systems exist that can be applied to *n*-alkane molecular fossils, as a means to reconstruct past ecological and climate change. Still, there are several significant knowledge gaps surrounding aspects of these proxy systems, with implications for confidently interpreting ancient environmental conditions from geological archives. Here, I outline commonly used leaf wax *n*-alkane proxy systems and how they are applied, along with uncertainties associated with these.

1.2 *n*-Alkane molecular distributions as a proxy for vegetation composition

One approach to reconstructing environments of the past is to identify abundances of different plant functional types (PFTs) which inhabited the landscape, which in turn may be used to indicate environmental conditions in a region. Leaf wax *n*-alkane distributions of plants are observed to differ in relation to PFT, which refers to groupings of plants through their physical, phylogenetic and phenological characteristics; for example, grasses, trees and shrubs. In terrestrial plants, *n*-alkanes commonly display abundance maxima at C27, C29 or C31 (Kunst & Samuels, 2003), while in non-emergent aquatic macrophytes, abundance maxima generally occur at C23 or C25 (Chikaraishi & Naraoka, 2003; Ficken

et al., 2000; Liu & Liu, 2016). Modern studies of vegetation have shown that PFTs can also be distinguished within the realm of terrestrial plants through *n*-alkane molecular distributions. In terrestrial plants, certain *n*-alkane compounds are also produced to a greater extent than others as a function of PFT. This distinction is most evident between grasses and woody vegetation such as trees and shrubs. In Australia, grasses produce a higher proportion of the C33 *n*-alkane than trees or shrubs (Howard et al., 2018). This pattern is mirrored in North America and Africa, where grasses have higher abundances of longer chain *n*-alkanes (C33 and C35) than trees that show higher abundances of the shorter chain *n*-alkanes C27 and C29 (Bush & McInerney, 2013; Garcin et al., 2014; Rommerskirchen et al., 2006; Vogts et al., 2009).

Leaf wax *n*-alkanes present in sediments represent the integrated inputs from vegetation in a catchment. The abundance of certain *n*-alkane compounds relative to others in that mixture will therefore, in part, be a function of the relative abundance of different PFTs in the catchment, with changes in vegetation composition through time reflected (Diefendorf & Freimuth, 2017). The ratio of C33 to C29 *n*-alkanes in a sedimentary mixture can be used to estimate relative abundances of grassy versus woody vegetation in a catchment through time (Carr et al., 2014). Similarly, the different *n*-alkane molecular distributions that exist between terrigenous plants and non-emergent aquatic macrophytes can also be exploited using a ratio of their respective dominant compounds (C29; C31, and C23; C25, respectively) and can be used to estimate the relative abundance of terrigenous and submerged/floating aquatic vegetation in a catchment through time (Ficken et al., 2000).

1.3 *n*-Alkane molecular distributions as a climate proxy

A key function of leaf wax *n*-alkanes is to reduce water loss through the cuticle (Jetter & Riederer, 2016; Riederer & Schreiber, 2001). The prevailing mechanism for how leaf waxes reduce water loss through the cuticle is explained by the so-called barrier membrane model, where impermeable crystallites formed by *n*-alkanes (among other aliphatic compounds) force water through a more amorphous matrix created by alicyclic compounds. The lengthened transport pathway that this creates increases cuticular resistance to the passage of water (Jetter & Riederer, 2016; Reynhardt & Riederer, 1994; Riederer & Schneider, 1990; Riederer & Schreiber, 1995). As such, greater concentrations of longer and more narrowly distributed *n*-alkanes should theoretically be produced by plants living in climatic conditions where the prevention of non-stomatal water loss is important to limit desiccation (Dodd & Afzal-Rafii, 2000; Dodd & Poveda, 2003; Dodd et al., 1998; Koch & Ensikat, 2008; Riederer & Schneider, 1990; Riederer & Schreiber, 1995; Shepherd & Griffiths, 2006). Correlations between *n*-alkane molecular distributions and aridity have been observed in a number of spatial transect studies that quantify *n*-alkanes from modern vegetation, top soil and sediment core tops (Bush & McInerney, 2015; Carr et al., 2014; Hoffman et al., 2013; Leider et al., 2013; Tipple & Pagani, 2013; Vogts et al., 2009). Association between major climate change events in the past and shifts in fossil *n*-alkane molecular distributions is also observed within sediments which track the Paleocene-Eocene Thermal Maximum (PETM) (Baczynski et al., 2016; Smith et al., 2007).

While there is strong evidence to suggest that leaf wax *n*-alkanes play a significant role in managing water loss under arid conditions, the interpretation of leaf wax *n*-alkane molecular distributions in this context from sedimentary records is not straightforward. As outlined previously, *n*-alkane distributions in sedimentary records are likely to be largely influenced by mixing of different PFT inputs. The potential for plant community change

119 independent of climate is an important factor to consider when interpreting the distribution
120 of sedimentary *n*-alkanes in a climatic context (Diefendorf et al., 2011; Diefendorf &
121 Freimuth, 2017; Freeman & Pancost, 2014; Garcin et al., 2014; Howard et al., 2018;
122 Jansen & Wiesenberg, 2017; Vogts et al., 2009). Another factor to consider is that most
123 sedimentary records likely represent a complex mixture of regionally and locally sourced
124 leaf wax *n*-alkanes, and as such could reflect inputs of leaf wax from vegetation growing in
125 vastly different climate regimes (Diefendorf et al., 2011; Diefendorf & Freimuth, 2017;
126 Freeman & Pancost, 2014; Garcin et al., 2014; Howard et al., 2018; Jansen & Wiesenberg,
127 2017; Rouillard et al., 2016; Schefuss et al., 2003). In addition, complexity in the
128 production of leaf wax *n*-alkanes and their subsequent transport to sedimentary archives
129 means that it is likely to be difficult to isolate robust climate signals from sedimentary leaf
130 wax *n*-alkane distributions (Diefendorf et al., 2011; Howard et al., 2018; Jansen &
131 Wiesenberg, 2017; Rouillard et al., 2016).

132 There is potential for these complexities to be minimised where leaf wax *n*-alkane
133 distributions can be isolated from fossil leaves of a single species preserved in a
134 sedimentary record. These types of records exist, with examples including Holocene
135 *Melaleuca quinquenervia* sub-fossil leaves from the perched lake Swallow Lagoon on
136 North Stradbroke Island, Queensland (Barr et al., 2019; Tibby et al., 2016) and Paleogene
137 *Metasequoia* fossil leaves from the Canadian Arctic (Yang & Leng, 2009). There is
138 however minimal modern calibration data for relationships between leaf wax *n*-alkane
139 distributions and climate from single plant species. In many cases, calibration studies do
140 not consider species turnover along climate transects. In addition, there is uncertainty
141 surrounding the scale at which *n*-alkane distributions respond to climate variability, with
142 two opposing schools of thought. *n*-Alkane distributions could reflect plastic responses to
143 short-term climate variability, or they could reflect potentially genetically fixed features of

plants related to the ambient climate conditions they evolved in or adapted to (Bender et al., 2017; Diefendorf et al., 2015). There is evidence to suggest that genetics plays a large role in *n*-alkane biosynthesis (Diefendorf et al., 2015; Dodd & Afzal-Rafii, 2000; Dodd et al., 1998; Rajčević et al., 2014; Schreiber & Riederer, 1996; Shepherd & Griffiths, 2006). Confidently interpreting palaeo-climatic changes from changes in *n*-alkane characteristics from single species geological records therefore requires a much better understanding of the scale at which modern *n*-alkane distributions reflect climate.

1.4 *n*-Alkane carbon isotope ratios as a proxy for photosynthetic pathway

In addition to *n*-alkane molecular distributions, *n*-alkane compound-specific carbon isotope analysis can be used to investigate vegetation dynamics through time, including changes in the proportion of plants using different photosynthetic pathways on the landscape. Higher plants use two main physiological pathways for photosynthesis; C3 and C4 (Ehleringer & Monson, 1993). A third photosynthetic pathway; Crassulacean Acid Metabolism (CAM), is also prevalent throughout many biomes (Silvera et al., 2010), but the importance of this pathway in the fossil record is minimal. This is due to generally low biomass and predominant occurrence in very arid regions where organic matter preservation is limited (Raven & Spicer, 1996). C4 plants account for only ~3% of plant species (Kellogg, 2013; Sage et al., 2012), however C4 vegetation is a significant component of modern ecosystems globally, comprising ~23% of global gross primary productivity (Kellogg, 2013; Sage et al., 2012; Still et al., 2003). Most species using the C4 photosynthetic pathway are clustered within the PFTs of grasses and sedges, particularly the family Poaceae (Gowik & Westhoff, 2011). C4 photosynthesis is also common within the families Chenopodiaceae, Amaranthaceae, Euphorbiaceae and Asteraceae (Muhaidat et al., 2007).

C3 photosynthesis involves the fixation of atmospheric CO_2 through catalysis by the enzyme ribulose-1,5-biphosphate carboxylase/oxygenase, more commonly known as Rubisco. The fixation of CO_2 to ribulose-1,5-biphosphate (RuBP) in the presence of Rubisco within the mesophyll cell produces an unstable enzyme bound intermediate, 2-carboxy-3-ketoarabinitol-1,5-bisphosphate which is hydrolyzed to form a pair of the 3-carbon molecule phosphoglycerate (PGA). A series of intermediate products are formed from the reduction of PGA by the products of photosynthetic light reactions during the photosynthetic carbon reduction (PCR) cycle, to ultimately produce the 3-carbon sugar glyceraldehydes-3-phosphate (G3P), the molecule after which C3 photosynthesis is named. Subsequently, one of every six of these molecules is converted to a simple sugar while the rest are used for the regeneration of RuBP for continuation of the carbon fixing process (Ehleringer & Monson, 1993).

C4 photosynthesis is more complex and first involves the fixation of aqueous HCO_3^- derived from atmospheric CO_2 to phosphoenolpyruvate (PEP) in a plant's mesophyll cells by the cytosolic enzyme phosphoenolpyruvate carboxylase (PEP-C). The product of this fixation is the 4-carbon dicarboxylic acid oxaloacetate (the molecule that gives C4 photosynthesis its name) which is reduced to either malate or aspartate depending on the photosynthetic pathway enzymatic subtype. These dicarboxylic acids are then transported to the bundle sheath cells of the plant, and subsequently decarboxylated, and the CO_2 produced during the decarboxylation fixed to RuBP in the presence of Rubisco, as occurs in mesophyll cells during C3 photosynthesis. The products of this process are then converted to sucrose and starch through the photosynthetic carbon reduction (PCR) cycle. The spatial separation of processes in the mesophyll and bundle sheath cells, and the resultant ringed cell arrangement is known as Kranz anatomy (Ehleringer & Monson, 1993; Kanai & Edwards, 1999; Tipple & Pagani, 2007).

C4 plants are better adapted than C3 plants to low atmospheric CO_2, high seasonal aridity; where any rainfall is generally confined to the warm season, as well as conditions of high light intensity. An elevated CO_2 concentration from decarboxylation of C4 acids at the site of fixation by Rubisco in the bundle sheath results in better function of C4 plants under low atmospheric CO_2 conditions (Long, 1999). The initial fixation of CO_2 by the enzyme PEP-C in C4 plants takes place at a much faster rate than Rubisco in C3 plants. This allows for higher rates of photosynthesis during times of lower stomatal conductance in C4 plants and means a high water use efficiency for the plant due to decreased transpiration through the stomatal boundary (Long, 1999; Osborne & Sack, 2012). In high light intensity environments, C3 plant photosynthesis is limited by both the quantity of Rubisco available for CO_2 fixation and the rate at which the plant can regenerate RuBP in the mesophyll cell, resulting in photorespiration; the loss of CO_2 back to the atmosphere through the stomatal boundary. This problem is avoided in C4 plants due to CO_2 being concentrated at the site of Rubisco in the bundle sheath cell (Long, 1999). Photorespiration relative to photosynthesis in C3 plants is temperature dependent, with more deleterious effects at higher temperatures (Long, 1999). Because C4 plants do not experience photorespiration, C4 has a competitive advantage where growing season temperatures are warm (i.e. where warm season precipitation is high) (Ehleringer et al., 1997).

The physiological and biochemical differences between C3 and C4 photosynthesis result in differences in carbon isotope discrimination during photosynthesis (O'Leary, 1981). Two stable isotopes of carbon exist; carbon-12 (^{12}C) and carbon-13 (^{13}C). ^{12}C has a natural abundance of 98.9% while ^{13}C is rare naturally, with an abundance of only ~1%. The relative abundance of these isotopes in natural materials varies and can be quantified by measuring the carbon isotope ratio. This is expressed using the delta notation, a ratio of

the two isotopes relative to a standard (the Vienna Pee Dee Belemnite; VPDB). It is calculated as follows, with units of per thousand, or per mil (‰) (O'Leary, 1981):

$$\delta^{13}C = \left[\frac{13C/12C\ (sample)}{13C/12C\ (standard)} - 1\right] \times 1000$$

Though both ^{12}C and ^{13}C as a component of atmospheric CO_2 are utilized by plants during photosynthesis, discrimination of ^{13}C occurs. The carbon concentrating mechanism of C4 photosynthesis results in less isotopic fractionation than C3 photosynthesis (Farquhar et al., 1989; O'Leary, 1981). The mechanisms for fractionation of atmospheric CO_2 $\delta^{13}C$ during C3 and C4 photosynthesis can be represented quantitatively with the following models, respectively (Farquhar, 1983; Farquhar et al., 1989; O'Leary, 1981):

$$\delta^{13}C_{C3} = \delta^{13}C_{CO2atm} - a - (b - a)\frac{Pi}{Pa}$$

Term *a* represents the fractionation of carbon isotopes that occurs as atmospheric CO_2 diffuses into the leaf through the stomata (4.4‰). The fractionation during carboxylation by Rubisco is represented by *b* (27‰). The partial pressure of CO_2 inside the leaf and of the atmosphere is expressed by p_i and p_a respectively.

$$\delta^{13}C_{C4} = \delta^{13}C_{CO2atm} - a - (b4 + b\varphi - a)\frac{Pi}{Pa}$$

Terms *a, b,* p_i and p_a represent the same fractionation as in the equation for C3 photosynthesis, *b4* represents fractionation that occurs during carboxylation associated with PEP-C (−5.7‰), while the proportion of PEP-C fixed carbon that leaks subsequent to transfer to and prior to de-carboxylation in the bundle sheath cells is represented by φ.

233 Consequently, $\delta^{13}C$ of plant tissue is indicative of the photosynthetic pathway that a plant
234 utilizes. For C3 plants, $\delta^{13}C$ values of bulk plant tissue range from -20 to -35‰ (σ = -
235 26.5‰). C4 plant bulk tissue exhibits a range in $\delta^{13}C$ of -10 to -14‰, (σ = -12.5‰)
236 (Cerling & Harris, 1999; O'Leary, 1981; Tipple & Pagani, 2007).

237 Information about the proportional use of the C3 and C4 photosynthesis by
238 vegetation through time in the catchment of a sedimentary archive can be ascertained by
239 measuring the $\delta^{13}C$ signature of a variety of substrates that preserve the carbon isotope
240 signatures of vegetation. These include herbivore fossil bioapatite (tooth enamel),
241 vegetation macro- and micro-fossils, palaeosol carbonates and molecular fossil *n*-alkanes
242 (Cerling, 1984; Cerling & Harris, 1999; Cerling et al., 1991; Morgan et al., 1994; Urban et
243 al., 2016; Wang et al., 1994). The deposition and taxonomy of these substrates differs
244 significantly, and as such vary in their presence or ubiquity in different geological archives
245 (Tipple & Pagani, 2007). Of the available substrates for analyzing $\delta^{13}C$ as a C3/C4 proxy,
246 measurement of carbon isotope ratios from molecular fossil *n*-alkanes has a demonstrated
247 global utility compared to other substrates. Leaf wax *n*-alkanes are highly recalcitrant and
248 are often preserved in temporally continuous geological successions that extend across
249 millions of years (Eglinton & Logan, 1991). Their transport properties also make them
250 ideal for assessing broad spatial and temporal trends in vegetation changes. Isotopic
251 fractionation during biosynthesis of *n*-alkanes occurs, resulting in systematically even
252 more ^{13}C depleted $\delta^{13}C$ that is measured from these compounds than bulk plant material. In
253 African plants, mean $\delta^{13}C$ of *n*-alkanes biosynthesized by C3 plants is -33.8‰, while mean
254 $\delta^{13}C$ of *n*-alkanes biosynthesized by C4 plants is -20.1‰ (Garcin et al., 2014).

1.5 *n*-Alkane carbon isotope ratios as a proxy for carbon sources

One of the dominant controls on *n*-alkane compound specific $\delta^{13}C$ differences in plants, aside from photosynthetic pathway, is postulated to be terrestrial/emergent versus non-emergent aquatic plant physiology (Naafs et al., 2019). Theoretically, *n*-alkane compounds produced by non-emergent aquatic macrophytes should be more enriched in ^{13}C than those produced by C3 terrestrial plants, as a function of CO_2 limitation, increased CO_2 diffusional resistance through water, and uptake of ^{13}C enriched HCO_3^- from geological sources (Keeley, 1990; Keeley & Sandquist, 1992). As such, *n*-alkane compound specific $\delta^{13}C$ in sedimentary records deposited in certain settings (e.g. bogs and lakes) could reflect mixing of non-emergent aquatic macrophytes and C3 terrestrial vegetation to sedimentary records. Still, there has been limited work to quantify the impact of vegetation source mixing impacts on $\delta^{13}C$ values of discrete leaf wax *n*-alkanes in sedimentary records. There is great potential for this to provide insights into lake hydrology (i.e. variability in habitat favouring emergent versus submerged plants) (Naafs et al., 2019). Constraining this would have important implications for interpretation of past vegetation dynamics from leaf wax *n*-alkane carbon isotopes in lacustrine sedimentary systems.

1.6 *n*-Alkane hydrogen isotope ratios as a hydrological proxy

Hydrogen isotope ratios of *n*-alkanes are another source of palaeo-environmental information. There are two naturally occurring stable isotopes of hydrogen; protium (^1H; designated as H) and deuterium (^2H; designated as D), with abundances on Earth of 99.98% and ~0.02% respectively. The relative abundance of hydrogen isotopes in natural materials is calculated as follows, with units of per thousand, or per mil (‰) (White, 1989):

$$\delta D = \left[\frac{D/H\ (sample)}{D/H\ (standard)} - 1\right] \times 1000$$

δD values of precipitation can be related to various environmental and geographical factors that influence Rayleigh-type processes during evaporation and condensation of water (Craig, 1961; Marshall et al., 2007; Sachse et al., 2012). The strongest environmental and geographical influences on precipitation δD values are known as the continental, temperature and amount effects (Dansgaard, 1964; Rozanski et al., 1993; Sachse et al., 2012). The continental effect impacts precipitation δD values due to D being preferentially lost from moist air masses as they progressively move away from the coast, resulting in more negative δD values further inland. Values of precipitation δD are impacted by the temperature effect by two mechanisms; an increase in equilibrium isotopic fractionation between vapor and condensate at higher temperatures, and the correlation between condensation and temperature influencing rainout. The temperature effect has a significant influence on precipitation δD values at higher latitudes, where temperature variability is high (Dansgaard, 1964; Sachse et al., 2012). The amount effect describes the phenomenon of higher rainout resulting in more precipitation with more negative δD values (Dansgaard, 1964). This is a function of condensation enriched in D being preferentially lost from an air mass until condensation depleted in D cannot be discriminated against any longer and will subsequently rainout. This effect is most pronounced in tropical regions, where temperature variability is relatively low (Rozanski et al., 1993).

Soil moisture is generally considered the primary environmental water source used by terrestrial higher plants (Dawson, 1998; Sachse et al., 2012), with soil moisture ultimately originating from precipitation. Still, there are fractionation effects between precipitation and soil moisture to consider, stemming from evaporation at soil-air

boundaries (Riley et al., 2002; Sachse et al., 2012). These fractionation effects are often considered to be negligible because water will generally be taken up by root systems at depths not affected by evaporation (Sachse et al., 2012). As a result, δD values of precipitation and δD values of soil moisture can be considered equivalent. Plants uptake this soil moisture, and it is used during biosynthesis of organic compounds, including *n*-alkanes (Chikaraishi & Naraoka, 2003; Sternberg, 1988). Isotopic fractionation related to eco-physiological factors takes place between initial uptake of soil moisture by a plant and the biosynthesis of organic compounds from intracellular water, with a resultant net apparent fractionation between values of precipitation δD and plant leaf wax *n*-alkane δD (Feakins & Sessions, 2010; Sachse et al., 2012; Sauer et al., 2001; Smith & Freeman, 2006) (Fig. 2). This apparent fractionation is observed to vary between different plant functional types (Sachse et al., 2012). Grasses in particular have biosynthetic processes that are less sensitive to transpirational D-enrichment (McInerney et al., 2011). Photosynthetic pathway also plays a significant role, with higher δD values by more than 20‰ in C4 grasses relative to C3 grasses (Smith & Freeman, 2006). Precipitation δD can therefore be related to leaf wax *n*-alkane δD when variability in apparent fractionation for different PFTs and photosynthetic pathway is accounted for.

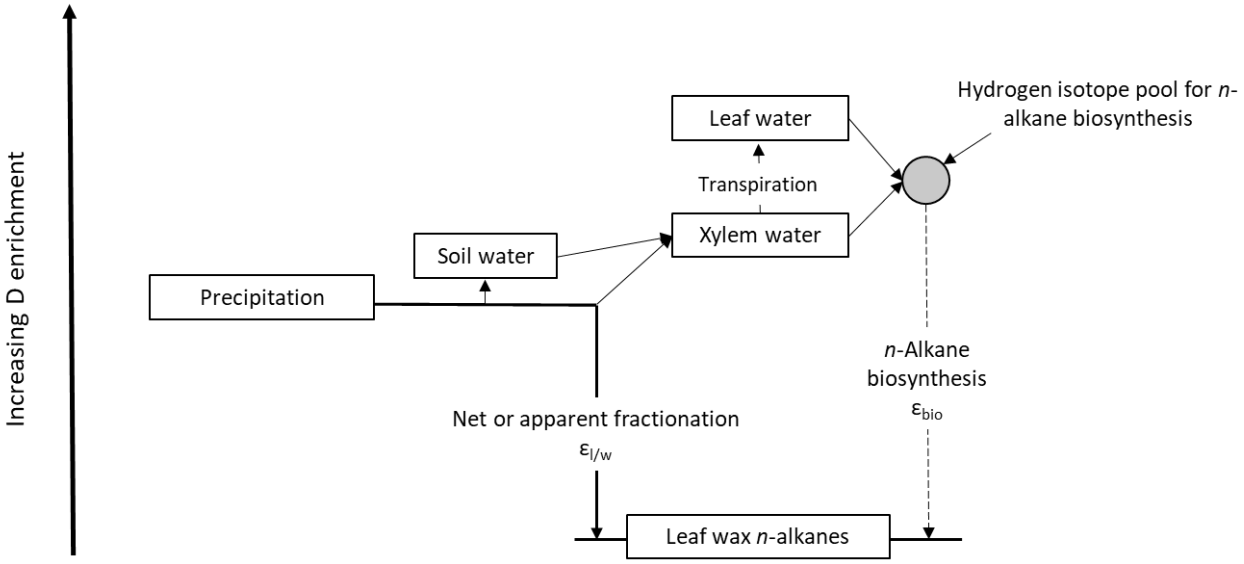

Figure 2. Simple schematic illustrating the pathway of precipitation hydrogen isotopes through water uptake by plants to incorporation into leaf wax *n*-alkane molecular structure during biosynthesis, and how leaf wax *n*-alkane δD ultimately can be related to precipitation δD through apparent fractionation (after Sachse et al., 2012).

Measurement of δD values from leaf wax *n*-alkanes preserved in sedimentary archives can be used to quantify aspects of precipitation though time. In regions close to the equator, the δD signature of precipitation is predominantly controlled by the amount of precipitation (Sachse et al., 2012). δD values of leaf wax *n*-alkanes biosynthesized by plants in these regions will reflect this signature, and as a result, changes in molecular fossil *n*-alkane δD values in sedimentary time-series records from tropical regions will reflect any changes in precipitation amount through time (Bi et al., 2005; Chikaraishi & Naraoka, 2003; Sachse et al., 2004; Sauer et al., 2001; Smith & Freeman, 2006; Yang & Leng, 2009). In more temperate regions, precipitation δD values are more strongly controlled by air temperature (Sachse et al., 2012). As such, leaf wax *n*-alkane δD values of plants in temperate regions will reflect this to a greater extent. Changes in sedimentary

329 *n*-alkane δD values in time-series records from more temperate regions are more likely to
330 reflect variability in precipitation δD values as a function of temperature.

331 **2 Late Cenozoic global and Australian palaeo-environments**

332 **2.1 Late Cenozoic expansion of C4 vegetation**

333 Palaeo-ecological studies from widely separated geographic regions show that
334 between 3 and 10 Ma (Fig. 3), there was a significant expansion of C4 vegetation
335 worldwide (Polissar et al., 2019). Pollen and phytolith assemblage data from the same
336 period suggest ecosystems underwent systematic vegetation shifts. In many regions, C3
337 dominated closed canopy forest ecosystems were replaced by C3 open habitat grasslands,
338 before proliferation of C4 dominated open savanna ecosystems (Edwards et al., 2010;
339 Keeley & Rundel, 2005). In the region of the Indian sub-continent, ecosystem shifts
340 beginning at ~ 7.4 Ma are observed in Siwalik Group sedimentary records. Palaeosol
341 carbonate $\delta^{13}C$ values cross a C3 dominated/C4 dominated threshold by ~5 Ma, with C4
342 floodplain biomass inferred to have displaced earlier C3 dominated biomass (Barry et al.,
343 2002; Quade et al., 1989). Enamel apatite $\delta^{13}C$ of Miocene fauna from this formation
344 records C4 vegetation as a dietary component at 9.4 Ma (Morgan et al., 1994), while
345 analysis of a sequence of ratite egg shells suggests that faunal diets comprised
346 predominantly C4 vegetation by 4 Ma (Stern et al., 1994). Analysis of molecular fossil
347 $\delta^{13}C$ preserved in both terrestrial and marine sedimentary archives from the region suggest
348 the onset of a shift toward C4 dominance between 6-8 Ma (Freeman & Colarusso, 2001).
349 Horse tooth enamel bioapatite $\delta^{13}C$ preserved in records of central North America as well
350 as South America suggest C4 vegetation as a dietary component increased across the
351 Miocene/Pliocene boundary (~4-6 Ma) (Cerling et al., 1997; Cerling et al., 1993; Jacobs et
352 al., 1999; Stromberg, 2011; Willis & McElwain, 2002). Palaeosol carbonate $\delta^{13}C$ values
353 suggest increasing dominance of C4 vegetation beginning at ~7.3 Ma in north-west

Argentina (Latorre et al., 1997; Stromberg, 2011). In Africa, C4 vegetation became a primary dietary resource by ~6 Ma as evidenced by fossil tooth enamel increasingly enriched in ^{13}C (Cerling et al., 1997; Morgan et al., 1994). $\delta^{13}C$ values measured from leaf wax *n*-alkanoic acids in marine sediments off the Horn of Africa record an onset of C4 expansion at 3.8 Ma, with the greatest variability occurring after 3.4 Ma (Feakins et al., 2005; Stromberg, 2011). ^{13}C enriched leaf wax *n*-alkanes in Arabian Sea sediments would suggest a marked increase in C4 biomass between 5.5 and 10 Ma (Huang et al., 2007; Uno et al., 2016). In Eurasia, herbivore tooth enamel records suggest replacement of a dominantly C3 vegetation food source at the Miocene/Pliocene boundary (~4-6 Ma) (Jacobs et al., 1999; Willis & McElwain, 2002).

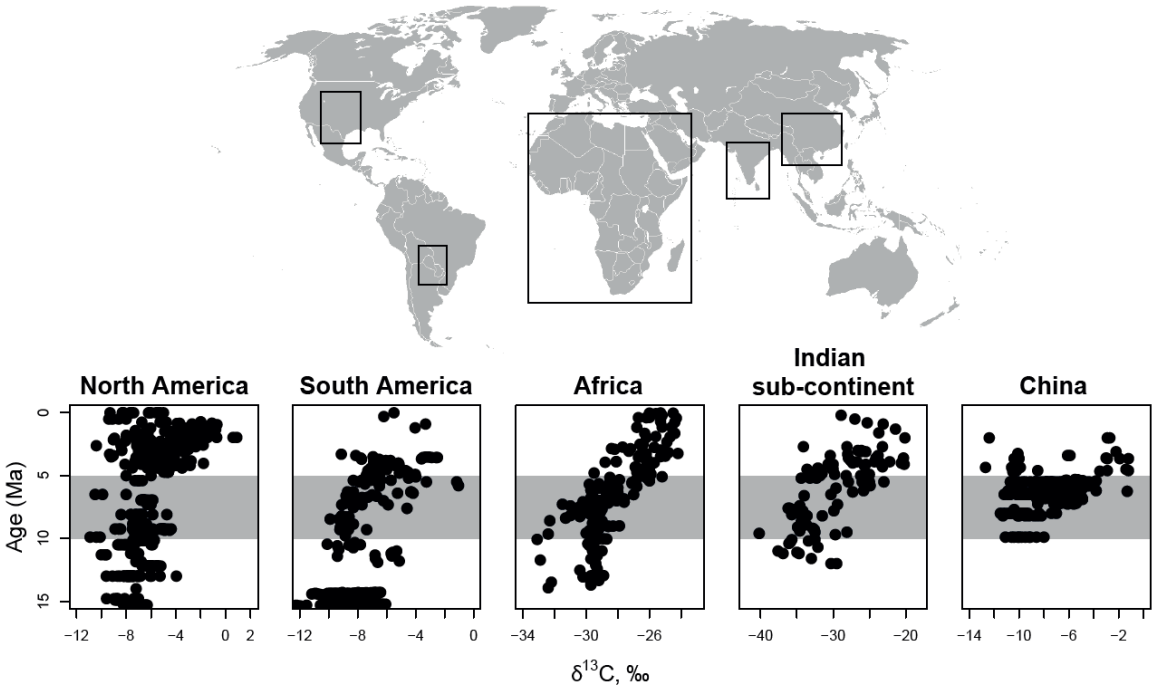

Figure 3. Compiled $\delta^{13}C$ records derived from plant derived substrates illustrating a secular shift between ~5-10 Ma towards higher $\delta^{13}C$ values indicating increased C4 dominance in various regions. Different x-axis scales reflect differences in isotope fractionation in various plant derived substrates. North American and South American records (Fox et al., 2018) are derived from soil carbonates, African and Indian sub-continent records (Dupont et al., 2013; Freeman & Colarusso,

2001; Hoetzel et al., 2013; Uno et al., 2016) are derived from leaf wax *n*-alkanes, and the Chinese record (Passey et al., 2009) is derived from a combination of herbivore tooth enamel and soil carbonates.

Australia is one place where we have little constraint on the expansion of C4 vegetation. Australia has the highest proportional cover of C4 vegetation on Earth today (Murphy & Bowman, 2007; Still et al., 2003), with C4 taxa particularly dominant in arid and tropical to subtropical grasslands and savannas in northern Australia (Hattersley, 1983; Murphy & Bowman, 2007). There is evidence for significant vegetation change in central and northern Australia across the middle to late Miocene and into the Pliocene. Pollen assemblage records show dry woodland and chenopod shrub lands beginning to expand in central Australia from the late Miocene onwards, where more temperate to wet forest environments had previously dominated (Macphail, 1997; Martin, 2006). Rainforest decline is postulated to have begun during the Eocene in this region (Martin, 2006). During the Pliocene, the development of large-scale grasslands is recorded as increases in charcoal, grass and Asteraceae pollen and grass phytoliths in Australian terrestrial and marine sedimentary archives (Locker & Martini, 1986; Martin, 1990; Martin & McMinn, 1993; Martin & McMinn, 1994; McMinn & Martin, 1992). Hypsodont wombats and high crowned kangaroos began to proliferate and diversify during this time, indicating that habitats suited to large scale grazing were beginning to appear (Couzens & Prideaux, 2018).

In Australia, there is a lack of temporally continuous sedimentary records that cover this interval of time and preserve the required plant derived substrates to investigate C4 expansion. Most terrestrial geological successions of Miocene/Pliocene age that do preserve plant derived substrates in Australia are in the temperate eastern and south-eastern

regions of the continent, while sedimentary archives from the central and northern regions are mostly restricted to the Miocene. Other terrestrial sites consist of lake, swamp and fluvial sediments which are limited in their temporal continuity (Kershaw et al., 1994). In addition, age control of these sedimentary archives is often poor. This has hampered our ability to understand C4 vegetation expansion in a truly global context. Miocene/Pliocene marine sediment packages from off the coast of Australia do however preserve molecular fossil *n*-alkanes. These successions are much more temporally continuous and long, with strong bio-stratigraphic and palaeo-magnetic age control (Haq et al., 1990; Tang, 1992). A significant portion of the research undertaken in this thesis pertains to the measurement of $\delta^{13}C$ from molecular fossil leaf wax *n*-alkanes in Australian marine records, and the development of a late Cenozoic photosynthetic pathway reconstruction for the Australian region.

2.2 Environmental drivers for C4 expansion

Several drivers have been proposed for the expansion of C4 vegetation during the late Cenozoic across different geographic regions (Keeley & Rundel, 2003; Osborne, 2008). C4 photosynthesis may have evolved as a response to decreasing atmospheric CO_2 concentration (pCO_2) beginning as far back as the Cretaceous (Cerling et al., 1997; Cerling et al., 1993; Christin et al., 2008; Ehleringer et al., 1997; Vicentini et al., 2008). Evolution of the C4 photosynthetic pathway as a result of decreasing pCO_2 has been postulated (Christin et al., 2008; Vicentini et al., 2008). Quantum yield studies have indicated that C4 plants are favored over C3 plants in high growing season temperature environments where atmospheric CO_2 levels are lower than 500 parts per million by volume (Cerling et al., 1997). Still, other records based on independent proxies have suggested that atmospheric CO_2 levels during the time interval of inferred C4 vegetation expansion were largely static (Osborne, 2008; Pagani et al., 1999; Pearson & Palmer, 2000; Royer et al., 2001). Recent

work, however, has refuted that notion, with analysis of fossil coccolithophores using isotope vital effects as a proxy for CO_2 concentrations indicating decreasing atmospheric CO_2 levels from ~7 to 5 Ma (Bolton et al., 2016; Bolton & Stoll, 2013). Even so, the asynchronous timing of C4 expansions globally indicates that decreased pCO_2 cannot be the only driving factor for C4 proliferation. While changes in pCO_2 have the potential to transform global vegetation states, the main control on vegetation state transformation is found to be dominated by regional differences in the timing and rates of change of temperature, rainfall amount, rainfall seasonality, and fire severity (Higgins & Scheiter, 2012).

It is postulated that hydrological change in combination with other factors played a significant role in C4 ecosystem expansion globally. Various studies suggest changes in hydrological conditions across the period of C4 ecosystem expansion in different regions (Dupont et al., 2013; Huang et al., 2007; Pagani et al., 1999; Quade et al., 1995). Changing environmental conditions in eastern Asia as a consequence of the evolution of the East Asian monsoon phases beginning in the early Neogene would have resulted in environmental stresses for C3 plants and a competitive advantage for C4 vegetation (Jia et al., 2003). Increases in seasonality of aridity and precipitation over long time scales would have been advantageous to plants using C4 photosynthesis, due to their high water use efficiency (Pagani et al., 1999). Changing fire occurrence and intensity during the late Miocene and into the Pliocene (Bond, 2015; Karp et al., 2018; Keeley & Rundel, 2005) may have resulted from the development of more intense monsoon conditions with an increased emergence of wet and dry seasons. A strong wet season would have promoted growth of fuel, while long, hot dry seasons allowed that fuel to burn unabated. It is postulated that changes in fire regimes could have exacerbated the influence of hydrological change, as a function of the interplay between climate, vegetation and fire

feedbacks (Bond, 2015; Karp et al., 2018; Keeley & Rundel, 2005). In this context, the leaf wax *n*-alkane hydrogen isotope proxy system holds great potential for quantifying hydrological variability to better understand the extent to which C4 vegetation expansion was controlled by hydrological change. Quantifying this would have significant implications for our understanding of differences in ecosystem sensitivity to climate and environmental change across different regions.

3 Thesis outline and research aims

The research chapters of the thesis are broadly structured as two groups. Research in the first group (chapters 2 and 3) was undertaken to fill knowledge gaps in leaf wax *n*-alkane molecular and isotopic proxy systems. A major goal of this work was to provide new insights into how palaeo-environmental change is interpreted from the geological record using *n*-alkane molecular distributions and isotope geochemistry. The research aims to be addressed constitute the following:

1. For a single species, do leaf wax *n*-alkane molecular distributions respond plastically to climate variability, or are they fixed for distinct climate regimes?
2. How do carbon isotope ratios of different *n*-alkanes in lacustrine sediments reflect mixing of *n*-alkanes derived from terrestrial and aquatic vegetation?

In chapter two, I present a modern study that elucidates the scale at which *n*-alkane distributions respond to climate variability. Relationships between leaf wax *n*-alkane molecular distributions and water availability/temperature are quantified for individuals of *Melaleuca quinquenervia* across spatially variable climate conditions in Queensland, Australia. In addition, molecular distributions are measured for leaves of the same species collected periodically across an 11-year period in one location. The outcomes of this work

458 have significant implications for interpretations of climate variability from leaf wax *n*-
459 alkane distributions in sedimentary records, particularly for cases where *n*-alkanes can be
460 isolated from single species.

461 Chapter three quantifies the impact that mixing of *n*-alkanes derived from terrestrial
462 and aquatic vegetation has on the carbon isotope ratio of different *n*-alkane chain-lengths
463 in a Pleistocene lacustrine sedimentary record from south-eastern Australia. Variable
464 inputs of terrestrial vegetation and non-emergent aquatic macrophyte derived *n*-alkanes to
465 a time-series lacustrine sedimentary record are estimated using an *n*-alkane molecular
466 distribution metric. Relationships between these inputs and carbon isotope ratios of
467 discrete leaf wax *n*-alkanes are quantified. Significant implications are found to exist for
468 use of *n*-alkanes in palaeo-environmental reconstructions, with certain chain-lengths found
469 to be more suited than others to reconstructing aspects of terrestrial vegetation from
470 lacustrine sedimentary archives, particularly the proportion of photosynthetic pathway on
471 the landscape.

472 The second group of research chapters (Chapters 4 and 5) aim to apply relatively
473 well-constrained aspects of leaf wax *n*-alkane molecular and isotopic proxy systems to
474 reconstruct aspects of Australia's vegetation and climate during the late Cenozoic, with a
475 focus on the timing and drivers of the expansion of C4 vegetation in the region. Here, the
476 research aims to be addressed are:

477 1. What was the timing of C4 vegetation expansion on the Australian continent?
478 2. Was regional hydrology an important control on the expansion of C4 vegetation on
479 the Australian continent?

In chapter four, a record of leaf wax *n*-alkane carbon isotope ratios and molecular distributions is presented, along with fossil pollen assemblages, from a 10-million-year marine sedimentary record from off north-west Australia. These measurements are used to quantify changes in the proportion of C4 vegetation on the landscape through time, as well as estimate changes in vegetation structure (i.e. closed forests, open grasslands). This record elucidates the timing of C4 expansion on the Australian continent for the first time and proposes that hydrological change was a strong control on this ecological shift.

Chapter five presents a record of leaf wax *n*-alkane hydrogen isotope ratios derived from the same sediment core as in chapter four. In addition, an interpretive framework for this record is developed, based on a synthesis of modern precipitation δD data from northern Australia. Regional hydrology, with a focus on seasonality of precipitation, is reconstructed through the late Cenozoic. The record provides evidence for hydrological change being an important factor in the expansion of C4 vegetation in northern Australia during this time.

References

Baczynski, A. A., McInerney, F. A., Wing, S. L., Kraus, M. J., Morse, P. E., Bloch, J. I., et al. (2016). Distortion of carbon isotope excursion in bulk soil organic matter during the Paleocene-Eocene thermal maximum. *Geological Society of America Bulletin, 128*(9-10), 1352-1366.

Barr, C., Tibby, J., Leng, M. J., Tyler, J. J., Henderson, A. G. C., Overpeck, J. T., et al. (2019). Holocene El Niño-Southern Oscillation variability reflected in subtropical Australian precipitation. *Scientific Reports, 9*.

Barry, J. C., Morgan, M. E., Flynn, L. J., Pilbeam, D., Behrensmeyer, A. K., Raza, S. M., et al. (2002). Faunal and environmental change in the Late Miocene Siwaliks of northern Pakistan. *Paleobiology, 28*(2), 1-71.

Bender, A. L. D., Chitwood, D. H., & Bradley, A. S. (2017). Heritability of the structures and ^{13}C fractionation in tomato leaf wax alkanes: a genetic model system to inform paleoenvironmental reconstructions. *Frontiers in Earth Science, 5*(47), 1-13.

Bi, X., Sheng, G., Liu, X., Li, C., & Fu, J. (2005). Molecular and carbon and hydrogen isotopic composition of *n*-alkanes in plant leaf waxes. *Organic Geochemistry, 36*(10), 1405-1417.

Bolton, C. T., Hernandez-Sanchez, M. T., Fuertes, M.-A., Gonzalez-Lemos, S., Abrevaya, L., Mendez-Vicente, A., et al. (2016). Decrease in coccolithophore calcification and CO_2 since the middle Miocene. *Nature Communications, 7*.

Bolton, C. T., & Stoll, H. M. (2013). Late Miocene threshold response of marine algae to carbon dioxide limitation. *Nature, 500*, 558-562.

Bond, W. J. (2015). Fires in the Cenozoic: a late flowering of flammable ecosystems. *Frontiers in Plant Science, 5*, 1-11.

Bush, R. T., & McInerney, F. A. (2013). Leaf wax *n*-alkane distributions in and across modern plants: implications for paleoecology and chemotaxonomy. *Geochimica et Cosmochimica Acta, 117*, 161-179.

Bush, R. T., & McInerney, F. A. (2015). Influence of temperature and C4 abundance on *n*-alkane chain length distributions across the central USA. *Organic Geochemistry, 79*, 65-73.

Carr, A. S., Boom, A., Grimes, H. L., Chase, B. M., Meadows, M. E., & Harris, A. (2014). Leaf wax *n*-alkane distributions in arid zone South African flora: environmental controls, chemotaxonomy and palaeoecological implications. *Organic Geochemistry, 67*, 72-84.

528 Cerling, T. E. (1984). The stable isotopic composition of modern soil carbonate and its
529 relationship to climate. *Earth and Planetary Science Letters, 71*(2), 229-240.
530 Cerling, T. E., & Harris, J. M. (1999). Carbon isotope fractionation between diet and
531 bioapatite in ungulate mammals and implications for ecological and
532 paleoecological studies. *Oecologia, 120*(3), 347-363.
533 Cerling, T. E., Harris, J. M., MacFadden, B. J., Leakey, M. G., Quade, J., Eisenmann, V.,
534 & Ehleringer, J. R. (1997). Global vegetation change through the Miocene/Pliocene
535 boundary. *Nature, 389*, 153-158.
536 Cerling, T. E., Quade, J., Ambrose, S. H., & Sikes, N. E. (1991). Fossil soils, grasses, and
537 carbon isotopes from Fort Ternan, Kenya: grassland or woodland? *Journal of*
538 *Human Evolution, 21*(4), 295-306.
539 Cerling, T. E., Wang, Y., & Quade, J. (1993). Expansion of C4 ecosystems as an indicator
540 of global ecological change in the late Miocene. *Letters to Nature, 361*, 344-345.
541 Chikaraishi, Y., & Naraoka, H. (2003). Compound-specific δD–δ^{13}C analyses of *n*-alkanes
542 extracted from terrestrial and aquatic plants. *Phytochemistry, 63*(3), 361-371.
543 Christin, P.-A., Besnard, G., Samaritani, E., Duvall, M. R., Hodkinson, T. R., Savolainen,
544 V., & Salamin, N. (2008). Oligocene CO_2 decline promoted C4 photosynthesis in
545 grasses. *Current Biology, 18*(1), 37-43.
546 Couzens, A. M. C., & Prideaux, G. J. (2018). Rapid Pliocene adaptive radiation of modern
547 kangaroos. *Science, 362*, 72-75.
548 Craig, H. (1961). Isotopic Variations in Meteoric Waters. *Science, 133*, 1702-1703.
549 Dansgaard, W. (1964). Stable isotopes in precipitation. *Tellus, 1*6, 436-468.
550 Dawson, T. E. (1998). Fog in the California redwood forest: ecosystem inputs and use by
551 plants. *Oecologia, 117*(4), 476-485.

552 Diefendorf, A. F., Freeman, K. H., Wing, S. L., & Graham, H. V. (2011). Production of *n*-
553 alkyl lipids in living plants and implications for the geologic past. *Geochimica et*
554 *Cosmochimica Acta, 75*(23), 7472-7485.
555 Diefendorf, A. F., & Freimuth, E. J. (2017). Extracting the most from terrestrial plant-
556 derived *n*-alkyl lipids and their carbon isotopes from the sedimentary record: A
557 review. *Organic Geochemistry, 103*, 1-21.
558 Diefendorf, A. F., Leslie, A. B., & Wing, S. L. (2015). Leaf wax composition and carbon
559 isotopes vary among major conifer groups. *Geochimica et Cosmochimica Acta,*
560 *170*, 145-156.
561 Dodd, R. S., & Afzal-Rafii, Z. (2000). Habitat-related adaptive properties of plant cuticular
562 lipids. *Evolution, 54*(4), 1438-1444.
563 Dodd, R. S., & Poveda, M. M. (2003). Environmental gradients and population divergence
564 contribute to variation in cuticular wax composition in *Juniperus communis*.
565 *Biochemical Systematics and Ecology, 31*(11), 1257-1270.
566 Dodd, R. S., Rafii, Z. A., & Power, A. B. (1998). Ecotypic adaptation in *Austrocedrus*
567 *chilensis* in cuticular hydrocarbon composition. *The New Phytologist, 138*(4), 699-
568 708.
569 Dupont, L. M., Rommerskirchen, F., Mollenhauer, G., & Schefuß, E. (2013). Miocene to
570 Pliocene changes in South African hydrology and vegetation in relation to the
571 expansion of C4 plants. *Earth and Planetary Science Letters, 375*, 408-417.
572 Edwards, E. J., Osborne, C. P., Stromberg, C. A. E., & Smith, S. A. (2010). The origins of
573 C4 grasslands: integrating evolutionary and ecosystem science. *Science, 328*, 587-
574 591.
575 Eglinton, G., & Hamilton, R. J. (1967). Leaf epicuticular waxes. *Science, 156*, 1322-1335.
576 Eglinton, G., Hamilton, R. J., & Raphael, R. A. (1962). Hydrocarbon constituents of the
577 wax coatings of plant leaves: a taxonomic survey. *Nature, 193*, 739-742.

578 Eglinton, G., & Logan, G. A. (1991). Molecular preservation. *Philosophical Transactions -*
579 *Royal Society of London B, 333*, 315-328.
580 Ehleringer, J. R., Cerling, T. E., & Helliker, B. R. (1997). C4 photosynthesis, atmospheric
581 CO_2, and climate. *Oecologia, 112*(3), 285-299.
582 Ehleringer, J. R., & Monson, R. K. (1993). Evolutionary and ecological aspects of
583 photosynthetic pathway variation. *Annual Review of Ecology and Systematics, 24*,
584 411-439.
585 Farquhar, G. D. (1983). On the nature of carbon isotope discrimination in C4 species.
586 *Australian Journal of Plant Physiology, 10*(2), 205-226.
587 Farquhar, G. D., Ehleringer, J. R., & Hubick, K. T. (1989). Carbon isotope discrimination
588 and photosynthesis. *Annual Review of Plant Physiology and Plant Molecular*
589 *Biology, 40*, 503-537.
590 Feakins, S. J., deMenocal, P. B., & Eglinton, T. I. (2005). Biomarker records of late
591 Neogene changes in northeast African vegetation. *Geology, 33*(12), 977-980.
592 Feakins, S. J., & Sessions, A. L. (2010). Controls on the D/H tatios of plant leaf waxes in
593 an arid ecosystem. *Geochimica et Cosmochimica Acta, 74*(7), 2128-2141.
594 Ficken, K. J., Li, B., Swain, D. L., & Eglinton, G. (2000). An *n*-alkane proxy for the
595 sedimentary input of submerged/floating freshwater aquatic macrophytes. *Organic*
596 *Geochemistry, 31*(7), 745-749.
597 Fox, D. L., Pau, S., Taylor, L., Strömberg, C. A. E., Osborne, C. P., Bradshaw, C., et al.
598 (2018). Climatic Controls on C4 Grassland Distributions During the Neogene: a
599 Model-Data Comparison. *Frontiers in Ecology and Evolution, 6*, 1-19.
600 Freeman, K. H., & Colarusso, L. A. (2001). Molecular and isotopic records of C4
601 grassland expansion in the late Miocene. *Geochimica et Cosmochimica Acta, 65*(9),
602 1439–1454.

603 Freeman, K. H., & Pancost, R. D. (2014). Biomarkers for terrestrial plants and climate. In
604 H. D. Holland & K. K. Turekian (Eds.), *Treatise on Geochemistry* (2nd ed., pp.
605 395-416). Oxford: Elsevier.
606 Gagosian, R. B., & Peltzer, E. T. (1986). The importance of atmospheric input of terrestrial
607 organic material to deep sea sediments. *Organic Geochemistry, 10*(4–6), 661-669.
608 Garcin, Y., Schefuß, E., Schwab, V. F., Garreta, V., Gleixner, G., Vincens, A., et al.
609 (2014). Reconstructing C3 and C4 vegetation cover using *n*-alkane carbon isotope
610 ratios in recent lake sediments from Cameroon, Western Central Africa.
611 *Geochimica et Cosmochimica Acta, 142*, 482-500.
612 Gowik, U., & Westhoff, P. (2011). The path from C3 to C4 photosynthesis. *Plant*
613 *Physiology, 155*, 56-63.
614 Haq, B. U., von Rad, U., O'Connell, S., Bent, A., Blome, C. D., Borella, P. E., et al.
615 (1990). Site 763. *Proceedings of the ODP Initial Reports, 122*.
616 Hattersley, P. W. (1983). The distribution of C3 and C4 grasses in Australia in relation to
617 climate. *Oecologia, 57*(1-2), 113-128.
618 Higgins, S. I., & Scheiter, S. (2012). Atmospheric CO_2 forces abrubt vegetation shifts
619 locally, but not globally. *Nature, 488*, 209-213.
620 Hoetzel, S., Dupont, L., Schefuß, E., Rommerskirchen, F., & Wefer, G. (2013). The role of
621 fire in Miocene to Pliocene C4 grassland and ecosystem evolution. *Nature*
622 *Geoscience, 6*, 1027-1030.
623 Hoffman, B., Kahmen, A., Cernusak, L. A., Arndt, S. K., & Sachse, D. (2013). Abundance
624 and distribution of leaf wax *n*-alkanes in leaves of *Acacia* and *Eucalyptus* trees
625 along a strong humidity gradient in northern Australia. *Organic Geochemistry, 62*,
626 62-67.

627 Howard, S., McInerney, F. A., Caddy-Retalic, S., Hall, P. A., & Andrae, J. W. (2018).
628 Modelling leaf wax *n*-alkane inputs to soils along a latitudinal transect across
629 Australia. *Organic Geochemistry, 121*, 126-137.
630 Huang, Y., Clemens, S. C., Liu, W., Wang, Y., & Prell, W. L. (2007). Large-scale
631 hydrological change drove the late Miocene C4 plant expansion in the Himalayan
632 foreland and Arabian Peninsula. *Geology, 35*(6), 531–534.
633 Jacobs, B. F., Kingston, J. D., & Jacobs, L. L. (1999). The origin of grass-dominated
634 ecosystems. *Annals of the Missouri Botanical Garden, 86*(2), 590-643.
635 Jansen, B., & Wiesenberg, G. L. B. (2017). Opportunities and limitations related to the
636 application of plant-derived lipid molecular proxies in soil science. *SOIL, 3*(4),
637 211-234.
638 Jetter, R., Kunst, L., & Samuels, A. L. (2006). Composition of plant cuticular waxes. In M.
639 Riederer & C. Muller (Eds.), *Biology of the plant cuticle* (Vol. Annual Plant
640 Reviews 23, pp. 145-181). Oxford: Blackwell Publishing.
641 Jetter, R., & Riederer, M. (2016). Localization of the transpiration barrier in the epi- and
642 intracuticular waxes of eight plant species: water transport resistances are
643 associated with fatty acyl rather than alicyclic components. *Plant Physiology,*
644 *170*(2), 921-934.
645 Jia, G., Peng, P. a., Zhao, Q., & Jian, Z. (2003). Changes in terrestrial ecosystem since 30
646 Ma in East Asia: stable isotope evidence from black carbon in the South China Sea.
647 *Geology, 31*(12), 1093-1096.
648 Kanai, R., & Edwards, G. E. (1999). The biochemistry of C4 photosynthesis In R. F. Sage
649 & R. K. Monson (Eds.), *C4 Plant Biology* (pp. 49-87). London: Academic Press.
650 Karp, A. T., Behrensmeyer, A. K., & Freeman, K. H. (2018). Grassland fire ecology has
651 roots in the late Miocene. *Proceedings of the National Academy of Sciences,*
652 *115*(48), 12130.

653 Keeley, J. E. (1990). Photosynthetic pathways in freshwater aquatic plants. *Trends in*
654 *Ecology & Evolution, 5*(10), 330-333.
655 Keeley, J. E., & Rundel, P. W. (2003). Evolution of CAM and C4 carbon-concentrating
656 mechanisms. *International Journal of Plant Science, 164*(S3), 555-577.
657 Keeley, J. E., & Rundel, P. W. (2005). Fire and the Miocene expansion of C4 grasslands.
658 *Ecology Letters, 8*(7), 683–690.
659 Keeley, J. E., & Sandquist, D. R. (1992). Carbon: freshwater plants. *Plant, Cell &*
660 *Environment, 15*(9), 1021-1035.
661 Kellogg, E. A. (2013). C4 photosynthesis. *Current Biology, 23*(14), R594-R599.
662 Kershaw, A. P., Martin, H. A., & McEwen-Mason, J. R. C. (1994). The Neogene: a period
663 of transition. In R. S. Hill (Ed.), *History of the Australian vegetation: Cretaceous to*
664 *recent*. New York: Cambridge University Press.
665 Koch, K., & Ensikat, H.-J. (2008). The hydrophobic coatings of plant surfaces: epicuticular
666 wax crystals and their morphologies, crystallinity and molecular self-assembly.
667 *Micron, 39*(7), 759-772.
668 Kunst, L., & Samuels, A. L. (2003). Biosynthesis and secretion of plant cuticular wax.
669 *Progress in Lipid Research, 42*(1), 51-80.
670 Latorre, C., Quade, J., & McIntosh, W. C. (1997). The expansion of C4 grasses and global
671 change in the late Miocene: stable isotope evidence from the Americas. *Earth and*
672 *Planetary Science Letters, 146*(1-2), 83-96.
673 Leider, A., Hinrichs, K.-U., Schefuß, E., & Versteegh, G. J. M. (2013). Distribution and
674 stable isotopes of plant wax derived *n*-alkanes in lacustrine, fluvial and marine
675 surface sediments along an eastern Italian transect and their potential to reconstruct
676 the hydrological cycle. *Geochimica et Cosmochimica Acta, 117*, 16-32.

677 Liu, H., & Liu, W. (2016). *n*-Alkane distributions and concentrations in algae, submerged
678 plants and terrestrial plants from the Qinghai-Tibetan Plateau. *Organic*
679 *Geochemistry, 99*, 10-22.
680 Locker, S., & Martini, E. (1986). Phytoliths from the southwest Pacific, Site 591. *Initial*
681 *reports of the Deep Sea Drilling Project, 90*, 1079-1084.
682 Long, S. P. (1999). Environmental Responses. In R. F. Sage & R. K. Monson (Eds.), *C4*
683 *Plant Biology*. London: Academic Press.
684 Macphail, M. K. (1997). Late Neogene climates in Australia: fossil pollen- and spore-
685 based estimates in retrospect and prospect. *Australian Journal of Botany, 45*(3),
686 425-464.
687 Marshall, J. D., Brooks, J. R., & Lajtha, K. (2007). Sources of varation in the stable
688 isotopic composition of plants. In R. Michener & K. Lajtha (Eds.), *Stable isotopes*
689 *in ecology and environmental science* (pp. 22-60). Massachussets, USA; Oxford
690 UK; Carlton, Australia: Blackwell Publishing.
691 Martin, H. A. (1990). The palynology of the Namba Formation in the Wooltana-1 bore,
692 Callabonna Basin (Lake Frome), South Australia, and its relevance to Miocene
693 grasslands in central Australia. *Alcheringa, 14*(3), 247-255.
694 Martin, H. A. (2006). Cenozoic climatic change and the development of the arid vegetation
695 in Australia. *Journal of Arid Environments, 66*(3), 533-563.
696 Martin, H. A., & McMinn, A. (1993). Palynology of Sites 815 and 823; the Neogene
697 vegetation history of coastal northeastern Australia. *Proceedings of the Ocean*
698 *Drilling Program, Scientific Results, 133*, 115.
699 Martin, H. A., & McMinn, A. (1994). Late Cainozoic vegetation history of north-western
700 Australia, from the palynology of a deep sea core (ODP site 765). *Australian*
701 *Journal of Botany, 42*(1), 95-102.

McInerney, F. A., Helliker, B. R., & Freeman, K. H. (2011). Hydrogen isotope ratios of leaf wax *n*-alkanes in grasses are insensitive to transpiration. *Geochimica et Cosmochimica Acta, 75*(2), 541-554.

McMinn, A., & Martin, H. A. (1992). Late Cenozoic pollen history from Site 765, eastern Indian Ocean. *Proceedings of the Ocean Drilling Program, 123*, 421-427.

Morgan, M. E., Kingston, J. D., & Marino, B. D. (1994). Carbon isotopic evidence for the emergence of C4 plants in the Neogene from Pakistan and Kenya. *Letters to Nature, 367*, 162-165.

Muhaidat, R., Sage, R. F., & Dengler, N. G. (2007). Diversity of Kranz anatomy and biochemistry in C4 eudicots. *American Journal of Botany, 94*(3), 362-381.

Murphy, B. P., & Bowman, D. M. J. S. (2007). Seasonal water availability predicts the relative abundance of C3 and C4 grasses in Australia. *Global Ecology and Biogeography, 16*(2), 160-169.

Naafs, B. D. A., Inglis, G. N., Blewett, J., McClymont, E. L., Lauretano, V., Xie, S., et al. (2019). The potential of biomarker proxies to trace climate, vegetation, and biogeochemical processes in peat: a review. *Global and Planetary Change, 179*, 57-79.

O'Leary, M. H. (1981). Carbon isotope fractionation in plants. *Phytochemistry, 20*(4), 553-567.

Osborne, C. P. (2008). Atmosphere, ecology and evolution: what drove the Miocene expansion of C4 grasslands? *Journal of Ecology, 96*(1), 35-45.

Osborne, C. P., & Sack, L. (2012). Evolution of C4 plants: a new hypothesis for an interaction of CO_2 and water relations mediated by plant hydraulics. *Philisophical Transactions of The Royal Society, 367*, 583-600.

Pagani, M., Freeman, K. H., & Arthur, M. A. (1999). Late Miocene atmospheric CO_2 concentrations and the expansion of C4 grasses. *Science, 285*, 876-879.

728 Passey, B. H., Ayliffe, L. K., Kaakinen, A., Zhang, Z., Eronen, J. T., Zhu, Y., et al. (2009).
729 Strengthened East Asian summer monsoons during a period of high-latitude
730 warmth? Isotopic evidence from Mio-Pliocene fossil mammals and soil carbonates
731 from northern China. *Earth and Planetary Science Letters*, *277*(3-4), 443-452.
732 Pearson, P. N., & Palmer, M. R. (2000). Atmospheric carbon dioxide concentrations over
733 the past 60 million years. *Nature, 406*, 695-6999.
734 Polissar, P. J., Rose, C., Uno, K. T., Phelps, S. R., & deMenocal, P. (2019). Synchronous
735 rise of African C4 ecosystems 10 million years ago in the absence of aridification.
736 *Nature Geoscience, 12*, 657-660.
737 Quade, J., Cater, J. M. L., Ojha, T. P., Adam, J., & Harrison, T. M. (1995). Late Miocene
738 environmental change in Nepal and the northern Indian subcontinent: stable
739 isotopic evidence from paleosols. *Geological Society of America Bulletin, 107*(12),
740 1381-1397.
741 Quade, J., Cerling, T. E., & Bowman, J. R. (1989). Development of Asian monsoon
742 revealed by marked ecological shift during the latest Miocene in northern Pakistan.
743 *Nature, 342*, 163-166.
744 Rajčević, N., Janaćković, P., Dodoš, T., Tešević, V., & Marin, P. D. (2014). Biogeographic
745 variation of foliar *n*-alkanes of *Juniperus communis var. saxatilis pallas* from the
746 Balkans. *Chemistry & Biodiversity, 11*(12), 1923-1938.
747 Raven, J. A., & Spicer, R. A. (1996). The evolution of Crassulacean Acid Metabolism. In
748 K. Winter & J. A. C. Smith (Eds.), *Crassulacean Acid Metabolism: Biochemistry,*
749 *Ecophysiology and Evolution* (pp. 360-385). Berlin: Springer Berlin Heidelberg.
750 Reynhardt, E. C., & Riederer, M. (1994). Structures and molecular dynamics of plant
751 waxes. *European Biophysics Journal, 23*(1), 59-70.
752 Riederer, M., & Schneider, G. (1990). The effect of the environment on the permeability
753 and composition of Citrus leaf cuticles. *Planta, 180*(2), 154-165.

754 Riederer, M., & Schreiber, L. (1995). Waxes - The transport barriers of plant cuticles. In R.
755 J. Hamilton (Ed.), *Waxes: chemistry, molecular biology, and functions* (pp. 130-
756 156). Dundee: Oily Press.
757 Riederer, M., & Schreiber, L. (2001). Protecting against water loss: analysis of the barrier
758 properties of plant cuticles. *Journal of Experimental Botany, 52*(363), 2023-2032.
759 Riley, W. J., Still, C. J., Torn, M. S., & Berry, J. A. (2002). A mechanistic model of $H_2{}^{18}O$
760 and $C^{18}OO$ fluxes between ecosystems and the atmosphere: model description and
761 sensitivity analyses. *Global Biogeochemical cycles, 16*(4), 42-41-42-14.
762 Rommerskirchen, F., Plader, A., Eglinton, G., Chikaraishi, Y., & Rullkötter, J. (2006).
763 Chemotaxonomic significance of distribution and stable carbon isotopic
764 composition of long-chain alkanes and alkan-1-ols in C4 grass waxes. *Organic*
765 *Geochemistry, 37*(10), 1303-1332.
766 Rosell-Mele, A., & McClymont, E. L. (2007). Biomarkers as paleoceanographic proxies.
767 In C. Hillaire-Marcel & A. De Vernal (Eds.), *Proxies in Late Cenozoic*
768 *Paleoceanography* (Vol. 1, pp. 441-490): Elsevier.
769 Rouillard, A., Greenwood, P. F., Grice, K., Skrzypek, G., Dogramaci, S., Turney, C., &
770 Grierson, P. F. (2016). Interpreting vegetation change in tropical arid ecosystems
771 from sediment molecular fossils and their stable isotope compositions: a baseline
772 study from the Pilbara region of northwest Australia. *Palaeogeography,*
773 *Palaeoclimatology, Palaeoecology, 459*, 495-507.
774 Royer, D. L., Wing, S. L., Beerling, D. J., Jolley, D. W., Koch, P. L., Hickey, L. J., &
775 Berner, R. A. (2001). Paleobotanical evidence for near present-day levels of
776 atmospheric CO_2 during part of the Tertiary. *Science, 292*, 2310-2313.
777 Rozanski, K., Araguas-Araguas, L., & Gonfiantini, R. (1993). Isotopic patterns in modern
778 global precipitation. In P. K. Swart, K. C. Lohmann, J. McKenzie, & S. Savin

779 (Eds.), *Climate Change in Continental Isotopic Records Geophysical Monograph*
780 (Vol. 78, pp. 1-36): American Geophysical Union.
781 Sachse, D., Billault, I., Bowen, G. J., Chikaraishi, Y., Dawson, T. E., Feakins, S. J., et al.
782 (2012). Molecular paleohydrology: interpreting the hydrogen-isotopic composition
783 of lipid biomarkers from photosynthesizing organisms. *Annual Review of Earth and*
784 *Planetary Sciences, 40*, 221-249.
785 Sachse, D., Radke, J., & Gleixner, G. (2004). Hydrogen isotope ratios of recent lacustrine
786 sedimentary *n*-alkanes record modern climate variability. *Geochimica et*
787 *Cosmochimica Acta, 68*(23), 4877-4889.
788 Sage, R. F., Sage, T. L., & Kocacinar, F. (2012). Photorespiration and the Evolution of C4
789 Photosynthesis. *Annual Review of Plant Biology, 63*(1), 19-47.
790 Sauer, P. E., Eglinton, T. I., Hayes, J. M., Schimmelmann, A., & Sessions, A. L. (2001).
791 Compound-specific D/H ratios of lipid biomarkers from sediments as a proxy for
792 environmental conditions. *Geochimica et Cosmochimica Acta, 65*(2), 213-222.
793 Schefuss, E., Ratmeyer, V., Stuut, J.-B. W., Jansen, J. H. F., & Damste, J. S. S. (2003).
794 Carbon isotope analyses of *n*-alkanes in dust from the lower atmosphere over the
795 central eastern Atlantic. *Geochimica et Cosmochimica Acta, 67*(10), 1757-1767.
796 Schreiber, L., & Riederer, M. (1996). Ecophysiology of cuticular transpiration:
797 comparative investigation of cuticular water permeability of plant species from
798 different habitats. *Oecologia, 107*(4), 426-432.
799 Schreuder, L. T., Stuut, J.-B. W., Korte, L. F., Sinninghe Damsté, J. S., & Schouten, S.
800 (2018). Aeolian transport and deposition of plant wax *n*-alkanes across the tropical
801 North Atlantic Ocean. *Organic Geochemistry, 115*, 113-123.
802 Schuster, A.-C., Burghardt, M., Alfarhan, A., Bueno , A., Hedrich, R., Leide, J., et al.
803 (2016). Effectiveness of cuticular transpiration barriers in a desert plant at
804 controlling water loss at high temperatures. *AoB Plants, 8*(1), 1-14.

805 Shepherd, T., & Griffiths, D. W. (2006). The effects of stress on plant cuticular waxes.
806 *New Phytologist*, *171*(3), 469-499.
807 Silvera, K., Neubig, K. M., Whitten, W. M., Williams, N. H., Winter, K., & Cushman, J.
808 C. (2010). Evolution along the crassulacean acid metabolism continuum.
809 *Functional Plant Biology*, *37*(11), 995-1010.
810 Smith, F. A., & Freeman, K. H. (2006). Influence of physiology and climate on δD of leaf
811 wax *n*-alkanes from C3 and C4 grasses. *Geochimica et Cosmochimica Acta*, *70*(5),
812 1172-1187.
813 Smith, F. A., Wing, S. L., & Freeman, K. H. (2007). Magnitude of the carbon isotope
814 excursion at the Paleocene–Eocene thermal maximum: the role of plant community
815 change. *Earth and Planetary Science Letters*, *262*(1), 50-65.
816 Stern, L. A., Johnson, G. D., & Chamberlain, C. P. (1994). Carbon isotope signature of
817 environmental change found in fossil ratite eggshells from a South Asian Neogene
818 sequence. *Geology*, *22*(5), 419-422.
819 Sternberg, L. d. S. L. (1988). D/H ratios of environmental water recorded by D/H ratios of
820 plant lipids. *Nature*, *333*, 59-61.
821 Still, C. J., Berry, J. A., Collatz, G. J., & DeFries, R. S. (2003). Global distribution of C3
822 and C4 vegetation: carbon cycle implications. *Global Biogeochemical cycles*,
823 *17*(1), 1-14.
824 Stromberg, C. A. E. (2011). Evolution of grasses and grassland ecosystems. *Annual Review*
825 *of Earth and Planetary Sciences*, *39*, 517–544.
826 Tang, C. (1992). Paleomagnetism of Cenozoic sediments in holes 762B and 763A, central
827 Exmouth Plateau, Northwest Australia. *Proceedings of the ODP*, *122*, 717-733.
828 Tibby, J., Barr, C., McInerney, F. A., Henderson, A. C. G., Leng, M. J., Greenway, M., et
829 al. (2016). Carbon isotope discrimination in leaves of the broad-leaved paperbark

tree, *Melaleuca quinquenervia*, as a tool for quantifying past tropical and sub-tropical rainfall. *Global Change Biology, 22*(10), 3474–3486

Tipple, B. J., & Pagani, M. (2007). The early origins of terrestrial C4 photosynthesis. *Annual Review of Earth and Planetary Sciences, 35*, 435–461.

Tipple, B. J., & Pagani, M. (2013). Environmental control on eastern broadleaf forest species' leaf wax distributions and D/H ratios. *Geochimica et Cosmochimica Acta, 111*, 64-77.

Uno, K. T., Polissar, P. J., Jackson, K. E., & deMenocal, P. B. (2016). Neogene biomarker record of vegetation change in eastern Africa. *Proceedings of the National Academy of Sciences, 113*(23), 6355-6363.

Urban, M. A., Nelson, D. M., Jimenez-Moreno, G., & Hu, F. S. (2016). Carbon isotope analyses reveal relatively high abundnace of C4 grasses during early-middle Miocene in southwestern Europe. *Palaeogeography, Palaeoclimatology, Palaeoecology, 443*, 10-17.

Vicentini, A., Barber, J. C., Alisciono, S. S., Giussani, L. M., & Kellogg, E. A. (2008). The age of the grasses and clusters of origins of C4 photosynthesis. *Global Change Biology, 14*(12), 2963-2977.

Vogts, A., Moossen, H., Rommerskirchen, F., & Rullkötter, J. (2009). Distribution patterns and stable carbon isotopic composition of alkanes and alkan-1-ols from plant waxes of African rain forest and savanna C3 species. *Organic Geochemistry, 40*(10), 1037-1054.

Wang, Y., Cerling, T. E., & MacFadden, B. J. (1994). Fossil horses and carbon isotopes: new evidence for Cenozoic dietary, habitat, and ecosystem changes in North America. *Palaeogeography, Palaeoclimatology, Palaeoecology, 107*(3-4), 269-279.

White, J. W. C. (1989). *Stable Hydrogen Isotope Ratios in Plants: A Review of Current Theory and Some Potential Applications.* Paper presented at the Stable Isotopes in Ecological Research, New York, NY.

Willis, K. J., & McElwain, J. C. (2002). *The evolution of plants*. New York: Oxford University Press.

Yang, H., & Leng, Q. (2009). Molecular hydrogen isotope analysis of living and fossil plants - *Metasequoia* as an example. *Progress in Natural Science, 19*(8), 901-912.

Statement of Authorship

Title of Paper	Variation in leaf wax *n*-alkane characteristics with climate in the broad-leaved paperbark (*Melaleuca quinquenervia*)
Publication Status	☑ Published ☐ Accepted for Publication ☐ Submitted for Publication ☐ Unpublished and Unsubmitted work written in manuscript style
Publication Details	Published in Organic Geochemistry: Andrae, J.W., McInerney, F.A., Tibby, J., Henderson, Andrew C.G., Hall, P.A., Marshall, J.C., McGregor, G.B., Barr, C. and Greenway, M. (2019) Variation in leaf wax *n*-alkane characteristics with climate in the broad-leaved paperbark (*Melaleuca quinquenervia*), *Organic Geochemistry*, 130, 33-42

Principal Author

Name of Principal Author (Candidate)	Jake W. Andrae
Contribution to the Paper	Led research design and undertook sample acquisition, sample preparation and geochemical analysis for the spatial aspect of the study. Processed data and undertook statistical analysis and interpretation for both the spatial and temporal aspects of the study. Led the development and drafting of the manuscript, produced all figures, and acted as the corresponding author.
Overall percentage (%)	70%
Certification:	This paper reports on original research I conducted during the period of my Higher Degree by Research candidature and is not subject to any obligations or contractual agreements with a third party that would constrain its inclusion in this thesis. I am the primary author of this paper.

Signature Date 29/05/19

Co-Author Contributions

By signing the Statement of Authorship, each author certifies that:

i. the candidate's stated contribution to the publication is accurate (as detailed above);
ii. permission is granted for the candidate in include the publication in the thesis; and
iii. the sum of all co-author contributions is equal to 100% less the candidate's stated contribution.

Name of Co-Author	Dr Francesca A. McInerney
Contribution to the Paper	Contributed extensively to research design, sample acquisition and statistical analysis and data interpretation. Edited and provided feedback on drafts of the paper and approved final manuscript.

Signature Date 04/07/19

Name of Co-Author	Dr John Tibby
Contribution to the Paper	Contributed extensively to research design, sample acquisition and statistical analysis and data interpretation. Edited and provided feedback on drafts of the paper and approved final manuscript.

Signature Date 25/06/19

Name of Co-Author	Dr Andrew C.G. Henderson
Contribution to the Paper	Contributed to research design and undertook sample preparation and geochemical analysis for the temporal aspect of the study. Provided feedback on drafts of the paper and approved final manuscript.

Signature Date 25/06/19

Name of Co-Author	Dr P. Anthony Hall
Contribution to the Paper	Contributed extensively to geochemical analysis of samples and wrote the geochemical analysis methods section. Provided feedback on drafts of the paper and approved final manuscript

Signature Date 25/06/19

Name of Co-Author	Dr Jonathan C. Marshall
Contribution to the Paper	Was involved in sample acquisition for the spatial aspect of the study. Contributed extensively to the discussion section, particularly regarding population genetics. Provided feedback on drafts of the paper and approved final manuscript.

Signature Date 26/06/19

Name of Co-Author	Dr Glenn B. McGregor
Contribution to the Paper	Was involved in sample acquisition for the spatial aspect of the study. Contributed extensively to data interpretation and provided feedback on drafts of the paper and approved final manuscript.

Signature Date 26/06/19

Name of Co-Author Dr Cameron Barr

Contribution to the Paper	Was involved in sample acquisition for the spatial aspect of the study. Contributed extensively to data interpretation and provided feedback on drafts of the paper and approved final manuscript.

Signature Date 26/06/19

Name of Co-Author	Dr Margaret Greenway
Contribution to the Paper	Undertook sample acquisition for the temporal aspect of the study. Provided feedback on drafts of the paper and approved final manuscript.

Signature Date 10/07/19

Chapter 2: Variation in leaf wax *n*-alkane characteristics with climate in the broad-leaved paperbark (*Melaleuca quinquenervia*)*

*Originally published as Andrae, J.W., McInerney, F.A., Tibby, J., Henderson, Andrew C.G., Hall, P.A., Marshall, J.C., McGregor, G.B., Barr, C. and Greenway, M. (2019) Variation in leaf wax *n*-alkane characteristics with climate in the broad-leaved paperbark (*Melaleuca quinquenervia*), *Organic Geochemistry*, 130, 33-42

Keywords

Leaf wax *n*-alkanes; Chain length distribution; Precipitation; Temperature; *Melaleuca quinquenervia*

Abstract

In higher plants, leaf waxes provide a barrier to non-stomatal water loss, and their composition varies both between and within species. Characteristics of *n*-alkanes, a suite of ubiquitous compounds in these waxes, are thought to be influenced by the availability of water and the temperature in a plant's growing environment. Longer *n*-alkane distributions with less variability in chain length are hypothesised to confer greater resistance to non-stomatal water loss and thus are expected in higher abundance in desiccating environments. Relationships between the distribution of *n*-alkanes and both precipitation and temperature have previously been observed. Despite this, it is unclear whether *n*-alkane chain length distributions vary plastically in response to climate, or whether they are fixed within populations in different climate settings. To better understand this, we examine the relationship between *n*-alkane characteristics of *Melaleuca quinquenervia* and both spatial and temporal climate variation. Across eastern Australia, we find that *n*-alkane homolog concentrations and distributions in leaves of *M. quinquenervia* do not vary with

climate where samples are proximate, even when climate shows significant variability. However, the concentration and distribution of *n*-alkane homologs do differ considerably between geographically separated populations in very different climate regimes. These results suggest *n*-alkane characteristics are not a plastic response to climate variability, and instead are likely fixed and could be driven by genetic differences between populations. This has important implications for the use of *n*-alkane characteristics as palaeo-environmental proxies.

1 Introduction

The leaf waxes of higher plants contain a mixture of long chain aliphatic *n*-alkyl derivatives (e.g., *n*-alkanes, *n*-alkanols, *n*-alkanoic acids), triterpenoids (Schuster et al., 2016) and minor secondary metabolites (Eglinton et al., 1962; Eglinton and Hamilton, 1967; Kunst and Samuels, 2003; Jetter et al., 2006; Schuster et al., 2016). Long chain *n*-alkanes (C25–C35) are a ubiquitous component of leaf waxes, with their distribution in leaf wax typically displaying odd over even predominance of homologs with maxima at C27, C29 or C31 (Kunst and Samuels, 2003). A key function of leaf waxes is to reduce water loss through the cuticle (Riederer and Schreiber, 2001; Jetter and Riederer, 2016), with other roles including the reduction of solute leaching from inside cells and protection against UV-radiation damage (Koch and Ensikat, 2008). The prevailing mechanism for how leaf waxes reduce water loss through the cuticle is explained by the barrier membrane model (Riederer and Schneider, 1990; Reynhardt and Riederer, 1994; Riederer and Schreiber, 1995; Jetter and Riederer, 2016). In this model, leaf waxes form micro-crystalline (crystallite) and unstructured (amorphous) zones, with alignment of hydrocarbon (i.e. *n*-alkane) backbones in crystallites creating impermeable zones in the leaf cuticle (Riederer and Schreiber, 1995; Koch and Ensikat, 2008).

It is hypothesised that the impermeability of the crystallites forces water to travel around them through a more amorphous matrix created by alicyclic compounds. This creates a lengthened transport pathway that increases the resistance of the cuticle to water passing through it (Riederer and Schneider, 1990; Reynhardt and Riederer, 1994; Riederer and Schreiber, 1995; Jetter and Riederer, 2016). A prediction of this model is that greater resistance to water loss is associated with greater concentrations of long-chain *n*-alkanes, as well as longer and more narrowly distributed *n*-alkane homologs i.e. low variability in constituent chain lengths. This would be advantageous to plants living in arid conditions (Riederer and Schneider, 1990; Riederer and Schreiber, 1995; Dodd et al., 1998; Dodd and Afzal-Rafii, 2000; Dodd and Poveda, 2003; Shepherd and Griffiths, 2006; Koch and Ensikat, 2008).

Modern calibration studies of *n*-alkanes in the context of climate from plants, soils and sediment have shown correlations between *n*-alkane characteristics and aridity (e.g., Vogts et al., 2009; Hoffman et al., 2013; Leider et al., 2013; Tipple and Pagani, 2013; Carr et al., 2014; Bush and McInerney, 2015). Moreover, major climate events in the past are associated with large shifts in *n*-alkane chain length distributions (e.g., Smith et al., 2007; Baczynski et al., 2016). Together, observations of modern and ancient systems demonstrate potential for *n*-alkanes preserved in the geological record to hold palaeoclimate information (Smith et al., 2007; Bush and McInerney, 2013; Hoffman et al., 2013; Leider et al., 2013; Carr et al., 2014; Bush and McInerney, 2015; Baczynski et al., 2016; Diefendorf and Freimuth, 2017). Even so, the interpretation of bulk plant wax *n*-alkane signatures in the geological record using modern climate calibrations is not straightforward.

Many modern climate calibration studies of *n*-alkanes in plants and surface sediments rely on 'space-for-time' substitution where variations in space are used to infer variations in time. This approach can limit the ability to perceive the responsiveness of the proxy to environmental change in modern systems (Pickett, 1989; Diefendorf and Freimuth, 2017). This is compounded in many cases by a lack of control on plant community turnover (e.g., Vogts et al., 2009; Hoffman et al., 2013; Carr et al., 2014; Bush and McInerney, 2015), with intrinsic differences in *n*-alkane production by different taxa having the potential to bias calibrations of *n*-alkane response to climate (Vogts et al., 2009; Diefendorf et al., 2011, 2015; Freeman and Pancost, 2014; Garcin et al., 2014; Diefendorf and Freimuth, 2017; Jansen and Wiesenberg, 2017; Howard et al., 2018). Complexities in plant wax *n*-alkane inputs to sediments are also inherent, with most sedimentary records likely representing a complex mixture of regionally and locally sourced leaf wax *n*-alkanes (Schefuss et al., 2003; Diefendorf et al., 2011; Freeman and Pancost, 2014; Garcin et al., 2014; Rouillard et al., 2016; Diefendorf and Freimuth, 2017; Jansen and Wiesenberg, 2017; Howard et al., 2018). This complexity and the biases imposed suggests a need for careful interpretation of bulk sedimentary leaf wax *n*-alkane records (Diefendorf et al., 2011; Rouillard et al., 2016; Diefendorf and Freimuth, 2017; Jansen and Wiesenberg, 2017; Howard et al., 2018).

These complexities can be minimised through the application of single-species calibrations to single-species leaf wax *n*-alkane records. Such single-species records are rare, but Holocene subfossil leaves of the species *Melaleuca quinquenervia* (Cav. S.T. Blake) are well preserved in lake sediments from south-east Queensland, Australia (Tibby et al., 2016; Barr et al., 2019). These types of records present an opportunity to better use plant wax *n*-alkanes to understand Holocene climate in a region that is particularly sensitive to changes in the El Niño–Southern Oscillation. There is uncertainty, however, in

whether relationships between leaf wax *n*-alkane characteristics and climate in a single species reflect plastic responses to short-term climate variability or whether they reflect potentially genetically fixed features of plants in different ambient climate conditions (Diefendorf et al., 2015; Bender et al., 2017). There is evidence to suggest that genetics plays a large role in *n*-alkane biosynthesis, and that there is potential for ecotypes of species, in terms of their *n*-alkane characteristics, to emerge where populations are geographically and climatically distinct (Schreiber and Riederer, 1996; Dodd et al., 1998; Dodd and Afzal-Rafii, 2000; Shepherd and Griffiths, 2006; Rajčević et al., 2014; Diefendorf et al., 2015). Confidently interpreting palaeoclimate from changes in *n*-alkane characteristics of sub-fossil leaves requires a better understanding of modern *n*-alkane characteristics in relation to climate.

In this study, we explore variation in *n*-alkane characteristics with climate of *M. quinquenervia* through time in one place as well as on large and small spatial climatic transects. We aim to provide unique insights into the responsiveness of *n*-alkane characteristics to climate within a single species, thereby removing the effects of *n*-alkane production differences between plant groups, functional types and species. If *n*-alkane characteristics reflect a plastic response to short-term climate variability, then we expect to see significant correlation between climate and *n*-alkane characteristics of *M. quinquenervia* at all scales, both temporally and spatially. If, however, *n*-alkane characteristics reflect genetically fixed features of ecotypes living in different ambient climates, we expect to observe distinct *n*-alkane characteristics in geographically and climatically distinct populations of *M. quinquenervia*. We measure leaf wax *n*-alkane characteristics of *M. quinquenervia* across variable precipitation and temperature conditions in three different sampling sets of living plants: (1) a time-series of 11 years at a single site, (2) a south-east Queensland (SEQ) transect across ~150 km and (3) a cross-

115 Queensland (QLD) sample set comparing SEQ with Cape York, that are separated by

116 ~1500 km (Fig. 1).

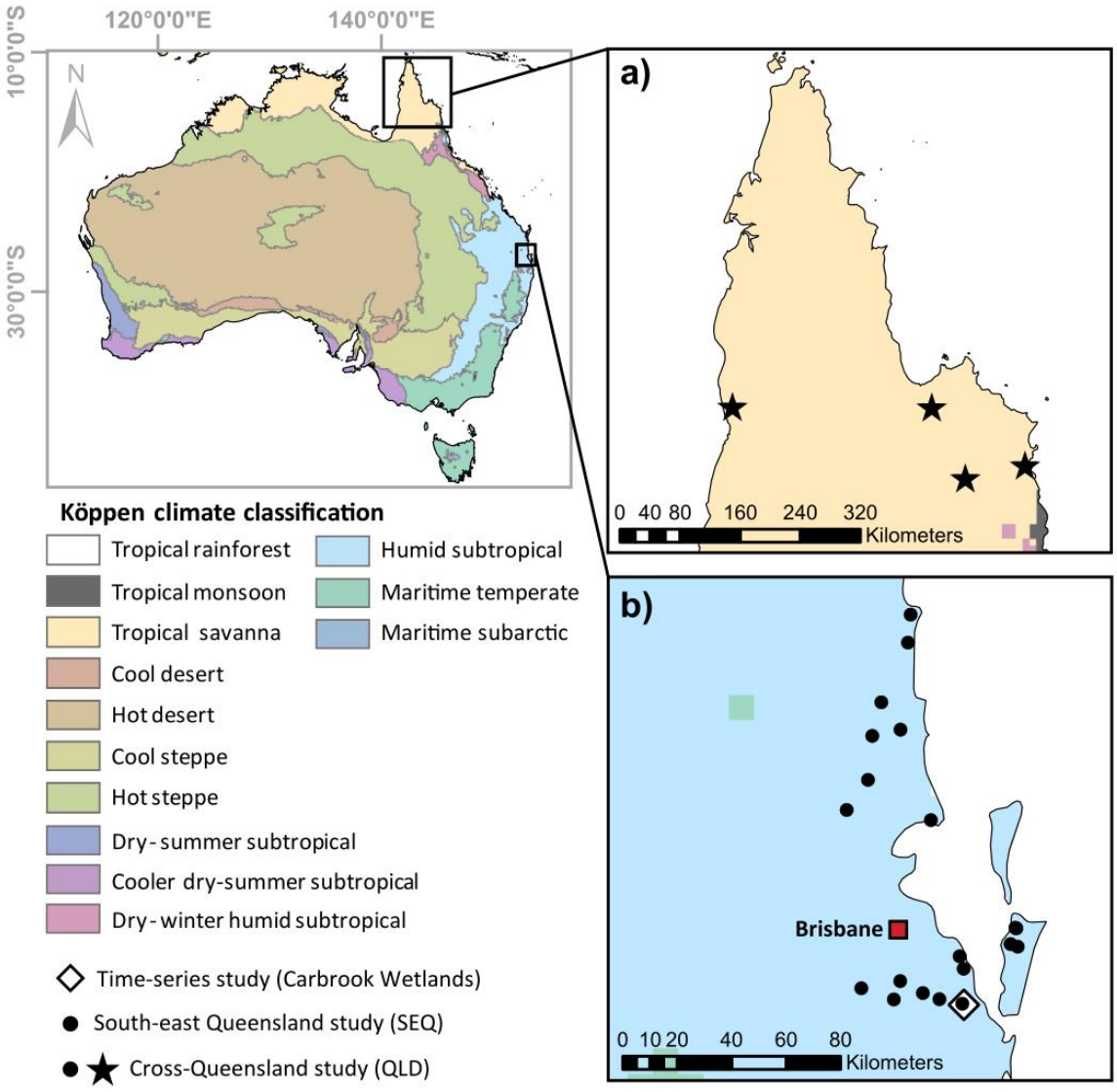

Figure 1. A modified Köppen climate classification map of Australia (Peel et al., 2007) with extents of the (a) Cape York and (b) south-east Queensland sampling regions indicated. Time-series, SEQ and QLD components of the study are marked.

2 Material and methods

2.1 Study species

Melaleuca quinquenervia, the broad-leaved paperbark or five veined paperbark, is an evergreen tree of the family Myrtaceae that typically ranges in height in mature trees from 8 to 12 m, though smaller or larger trees are not uncommon (4–25 m) (Boland et al., 2006). This species inhabits coastal areas and is associated with wetlands, with its native geographic range extending from southern New South Wales to Cape York within Australia and continuing into southern Papua New Guinea and New Caledonia. The species is naturalised in other regions, notably the southern United States of America (Ireland et al., 2002). In Australia, new leaf growth in this species begins in mid-winter and continues through to early summer (Serbesoff-King, 2003). The growing season for this species is therefore considered as the Austral winter and spring (June to November, inclusive).

2.2 Study sites and sampling

2.2.1 Time-series study

Long term sampling (11 years) for our time-series study was undertaken via a litter trap approach at Carbrook Wetlands (27.690 ºS, 153.276 ºE), a part of the Native Dog Creek catchment and the Logan River floodplain (Fig. 1). Approximately 164 ha of the wetland is comprised of *M. quinquenervia* forest (Greenway, 1994; Tibby et al., 2016). The sample collection area for our time-series study had a tree density of 2175 trees per ha, with a mean tree height of 18.6 m (±4 m, 1 standard deviation). The mean tree diameter at the site was 17.8 cm (±9 cm, 1 standard deviation). The tree density and the presence of leaves from species not overhanging the litter traps suggests leaves were integrated from many individuals in the sampling area. Litterfall was collected in a raised 0.25 m^2 (0.5 m × 0.5 m) tray in one area of Carbrook Wetlands, with leaf litter sampled approximately every

four weeks between April 1992 and July 2003 (Tibby et al., 2016). Leaf litter samples from 45 collection periods were used in this study, with a temporal resolution of approximately three months. Nine leaves from each of the collection periods were selected and homogenised under liquid nitrogen in a ceramic mortar and pestle.

2.2.2 South-east Queensland (SEQ) study

The SEQ study area is located in a humid subtropical climate zone (Fig. 1), as defined by the modified Köppen-Geiger climate classification (Peel et al., 2007). Sampling was undertaken at 21 sites across SEQ, with a cluster of small leaves (~15–20) from near the growing tip, assumed to be relatively young leaves, taken from one tree at each sampling site at a height of 1–2 m using pruning shears. Leaves were consistently taken from the northern side of trees in open sun to mitigate the influence of sun versus shade leaves (Suh and Diefendorf, 2018). From the cluster of leaves sampled, the nine smallest leaves were selected for homogenisation. After collection, leaves were stored in paper bags and subsequently oven dried at 50 ºC for 48 h, prior to homogenisation under liquid nitrogen in a ceramic mortar and pestle.

2.2.3 Cross-Queensland (QLD) study

The QLD study area encompasses the SEQ study area, along with four other sites on the Cape York Peninsula in far-north Queensland, located in a tropical savanna climate zone (Peel et al., 2007) and ~1500 km from the SEQ sites (Fig. 1). These sites were chosen to be sampled because of their distinct climate compared to the SEQ sample set. Leaves were collected and processed as per the SEQ samples.

2.3 Lipid extraction and purification

2.3.1 Time-series

Total lipid extraction (TLE) of homogenised leaf samples from the time-series study was undertaken at Newcastle University, UK. The method used dichloromethane (DCM):methanol (MeOH) (3:1, v/v) and a CEM MARS 5 microwave system that heated samples to 70 ºC over 5 min, holding them at 70 ºC for 5 min and then allowing them to cool for 30 min. Excess solvent was removed from the TLE by evaporating under a stream of N_2 (ultra-high purity; 99.999%). An internal standard of tetratriacontane was added to all samples, which were then passed through a preconditioned silica gel column (35–70 mesh size), with the non-polar fraction eluted using *n*-hexane (grade >99.8%). The non-polar fraction then underwent solid phase extraction using a Bond Elut SCX cartridge to separate saturated and unsaturated compounds.

n-Alkane (C18 to C33) concentrations were quantified using a HP 5890 Series 2 Gas Chromatograph-Flame Ionization Detector (GC-FID) with a HP1 column (50 m × 0.32 mm i.d. × 0.17 μm film thickness) with a flow rate of 2 mL/min of helium carrier gas. A 1 μL aliquot of sample was injected using a temperature programme that increased the temperature from 50 ºC to 300 ºC at a rate of 6 ºC/min. Compounds were identified using a Thermo Finnigan Trace gas chromatograph–mass spectrometer (GC–MS) with a HP1 column (50 m × 0.32 mm i.d. × 0.17 μm film thickness) with a flow rate of 2 mL/min in a helium carrier gas. A 1 μL aliquot of sample was injected into a programmable temperature vaporising injector system at 270 ºC in split-less mode with GC temperature ramped up from 50 ºC to 300 ºC at a rate of 6 ºC/min. Concentrations were normalised to total dry weight of leaf material extracted and are reported as μg/g dry leaf material.

2.3.2 Spatial studies: SEQ and QLD

Preparation of samples from SEQ and QLD took place at the University of Adelaide, Australia. Ground plant material from each sample was subjected to solvent extraction by being sonicated for 15 min in 7 mL of DCM:MeOH (9:1, v/v). The mixture was then decanted through ashed glass fibre filters. Sonication and filtration were conducted in triplicate on the same sample material, with extracts combined. Excess solvent was removed from the TLE by evaporating under a stream of N_2 (ultra-high purity; 99.999%). The total lipid extract (TLE) was fractionated using short column chromatography with ~0.5 g of activated silica gel (35–70 mesh size). The non-polar fraction, that included *n*-alkanes, was eluted with 4 mL of *n*-hexane (OptimaTM grade, Fisher Scientific), followed by elution of the polar fraction with 4 mL DCM:MeOH (1:1, v/v). The non-polar fraction was then evaporated under N_2 and redissolved in 100 µL of *n*-hexane spiked with 10 µg/mL of 1,1′- binaphthyl as internal standard. A quantitation standard was prepared by dilution of a Certified Reference Material (C7–C40 Saturated Alkanes Standard, Supelco 49452-U) to a concentration of 10 µg/mL and spiked with 10 µg/mL of 1,1′- binaphthyl internal standard for concurrent analysis with the sample batch.

n-Alkane characterisation was undertaken using a Perkin Elmer Clarus 500 GC–MS, with an SGE CPSil-5MS (30 m × 0.25 mm ID × 0.25 mm film thickness) capillary column with helium carrier gas with a flow rate of 1 mL/min. A 1 µL aliquot of sample was injected at a temperature of 300 ºC. The oven temperature program was 50 ºC, held for one min, prior to an 8 ºC/min ramp to 340 ºC and a final hold of 7.75 min. The mass spectrometer was scanned from 45 to 500 Da. Concentrations of *n*-alkane homologs from C25 to C33 were quantified using PerkinElmer TurboMass analytical software based on response factors of individual *n*-alkane homologs in the standard against the internal standard. The method was validated against a six-point linearity curve in triplicate with

reproducibility assessed by 10 times repeat injection ($R^2 > 0.98$, ±3% reproducibility). Concentrations were normalised as per the time-series data.

2.4 Time-averaged climate data

Climate data utilised in this study were derived from the SILO (Scientific Information for Land Owners) database (Jeffrey et al., 2001). Daily climate variables (total precipitation and maximum temperature) were interpolated for sample locations from daily climate observations at proximal observation sites using the Data-Drill system (Jeffrey et al., 2001). Growing season climate (June–November, inclusive) was calculated for both the temporal and spatial studies with a mean calculated for three full growing seasons prior to sample collection. Climate averages for three growing seasons were utilised for this study due to the leaf life span of the species – i.e. 2–4 years (Van et al., 2002) – and follows the approach of Tibby et al. (2016). Growing season precipitation at Carbrook Wetlands averaged for the three years prior to sample collection ranged from 280 mm to 543 mm, while maximum daily temperature averaged across the three previous growing seasons ranged from 22.8 ºC to 23.6 ºC. At SEQ sites, growing season precipitation ranged from 269 mm to 558 mm, with growing season temperature ranging from 22.3 ºC to 24.5 ºC. Growing season precipitation for QLD sites, where Cape York sites were included, ranged from 89 mm to 558 mm, with growing season temperature ranging from 22.3 ºC to 33.2 ºC (Fig. 2).

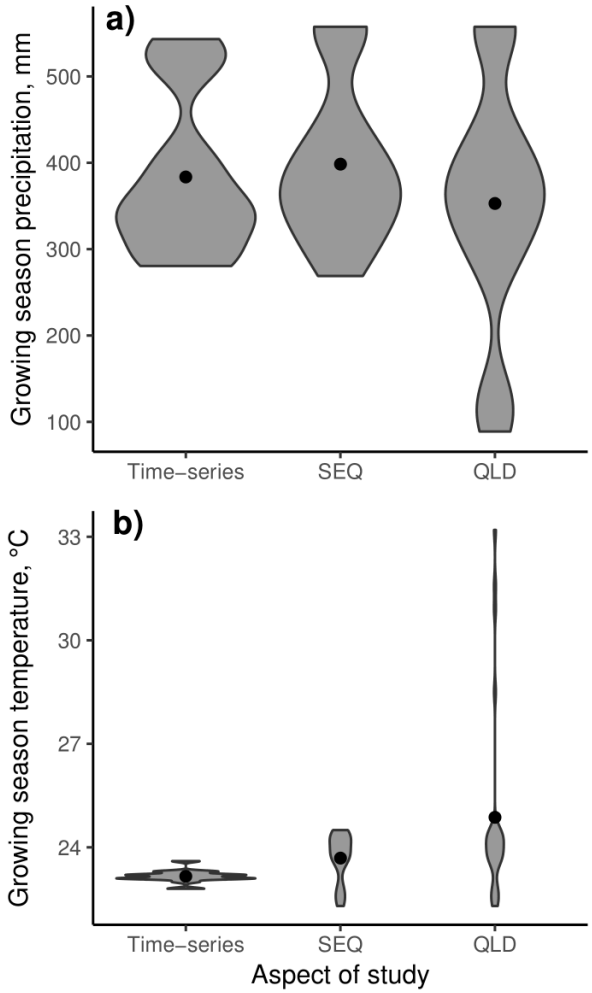

Figure 2. Violin plots showing the range of (a) growing season precipitation and (b) growing season temperature for each of the time-series, SEQ and QLD aspects of the study. Black symbols represent the mean for each range.

2.5 Leaf wax characteristic calculations and statistical analysis

Concentration, average chain length (ACL), Norm31 and dispersion were calculated for *n*-alkane chain lengths C25 to C33, inclusive. With the exception of concentration, all variables are dimensionless metrics of *n*-alkane distribution variability. ACL is the weighted mean of odd long-chain *n*-alkane concentrations and quantifies the dominant long chain *n*-alkane homolog in a sample (Bush and McInerney, 2013, 2015). Norm31 is the normalized ratio of the C31 *n*-alkane homolog to the C29 *n*-alkane homolog and is a parameter that is environmentally sensitive (Carr et al., 2014). Dispersion is a

measure of how narrowly distributed *n*-alkane chain lengths are around a mean (Dodd and Afzal-Rafii, 2000). Formulae for these metrics are as follows:

$$\mathrm{ACL} = \frac{\sum(n \times C_n)}{\sum(C_n)} \quad 1.$$

where *n* is the odd carbon chain length and C_n is the concentration of the *n*-alkane with *n* carbon atoms (Bush and McInerney, 2015).

$$\mathrm{Norm31} = \frac{C_{31}}{C_{29} + C_{31}} \quad 2.$$

where C31 and C29 are the concentrations of those *n*-alkane homologs (Carr et al. 2014).

$$\mathrm{Dispersion} = \sum[p_n(n - \mathrm{ACL})^2] \quad 3.$$

where, *n* is *n*-alkane chain length and p_n is the proportional concentration of that chain length relative to the total concentration of *n*-alkanes (Dodd and Afzal-Rafii, 2000).

We utilised redundancy analysis (RDA) in the 'Vegan' package (Oksanen et al., 2017) in R (R Core Team, 2016) to determine the extent to which our environmental variables (rainfall and temperature) explain patterns in the proportional concentration of *n*-alkanes (C25–C33) in the spatial studies. Redundancy analysis is a multivariate technique for examining species–environment relationships. It is equivalent to Principal Components Analysis with the important distinction being that the axes represent combinations of environmental variables (Lepš and Šmilauer, 2003). Redundancy analysis is an appropriate technique to use where the response of the objects (in this case the *n*-alkane characteristics) are linear in relation to the environmental variables. To determine whether a linear method was appropriate to use we undertook a detrended correspondence analysis in the 'Vegan' package in R (Oksanen et al., 2017), which showed the gradient length of the data set was

less than two, indicating linear-based RDA was an appropriate methodology (ter Braak and Prentice, 2004).

Statistical tests were utilised to determine the equality of variance between *n*-alkane characteristics from the SEQ and time-series studies, to compare variance through time at a single site and across space at a single time. The Shapiro-Wilk test in base R (R Core Team, 2016) was used to check for normality in the distributions of ACL, concentration, Norm31 and dispersion from each of the SEQ and time-series studies. In most cases, distributions were not normal; because of this it was decided to use Levene's test to determine homogeneity of variance. This was undertaken using the 'leveneTest' function in the 'Car' package (Fox and Weisberg, 2011) in R (R Core Team, 2016). Lastly, we undertook a series of linear regressions between climate and leaf wax *n*-alkane characteristics using $p < 0.05$ as our measure of statistical significance.

3 Results

3.1 Time-series

For samples from the time-series study (Table 1), total concentration of *n*-alkanes (C25 to C33 summed) ranged from 47.1 to 1170 μg/g dry leaf (mean: 182; σ: 169). ACL minima and maxima were 28.9 and 30.2 (mean: 29.7; σ: 0.27). Norm31 ranged from 0.50 to 0.77 (mean: 0.67; σ: 0.06). Dispersion varied between 2.4 and 5.6 (mean: 3.9; σ: 0.57). Total concentration, ACL and Norm 31 did not show statistically significant linear correlations with either of growing season precipitation or temperature (Fig. 3). Dispersion had a significant, though weak, linear correlation with growing season precipitation ($R = 0.33$, $p = 0.028$) and no correlation with growing season temperature (Fig. 3). Note that absolute values of results from this aspect of the study cannot be directly compared with

279 the SEQ and QLD datasets below, as a result of different sampling strategies and *n*-alkane
280 extraction methods used.

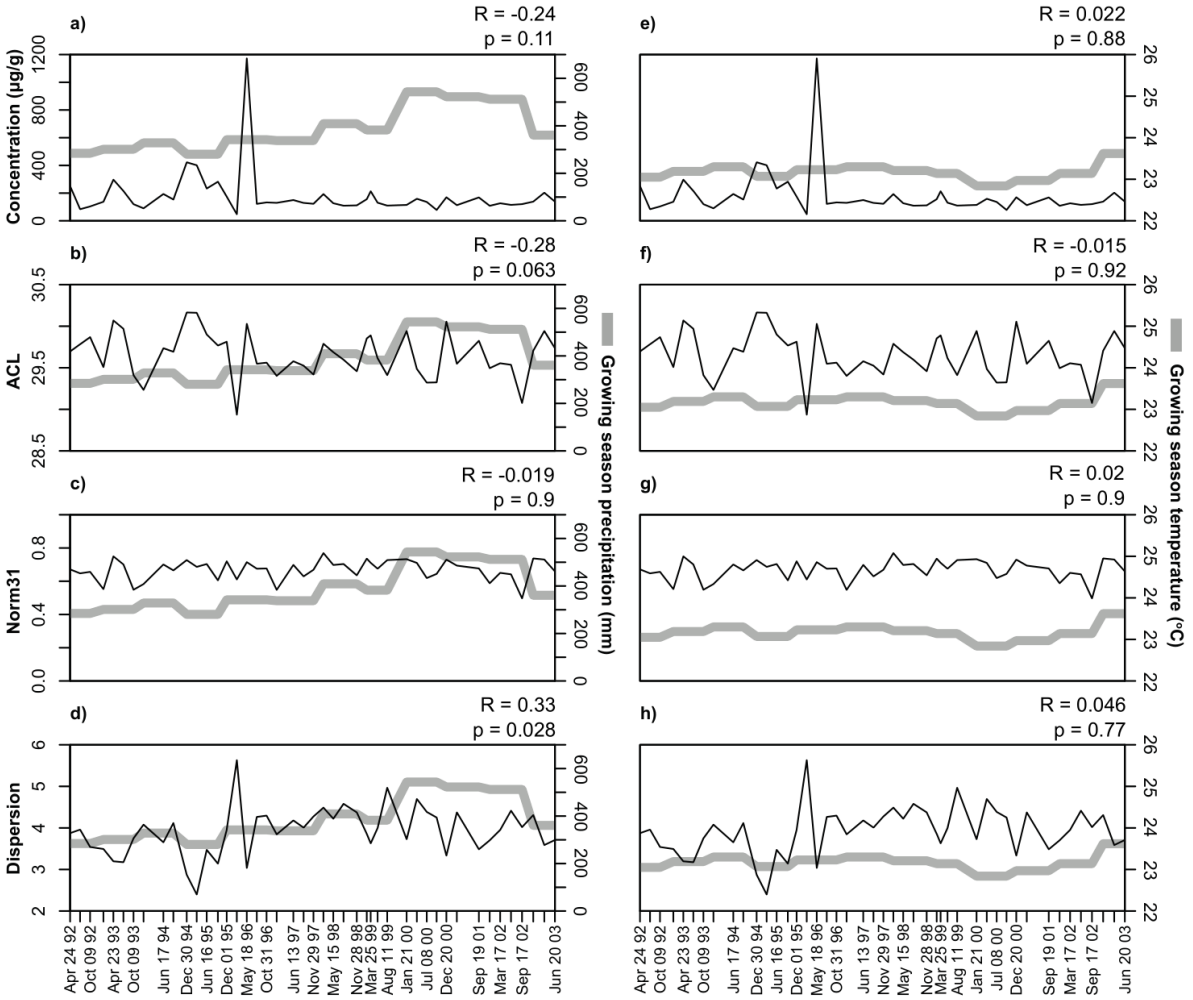

Figure 3. *n*-Alkane characteristics and growing season precipitation (a, b, c, d) and growing season temperature (e, f, g, h) through time from Carbrook Wetlands. Results of linear regression modelling between each *n*-alkane characteristic and precipitation or temperature is indicated at the top right of each panel. The thin black line represents the *n*-alkane characteristic data series, while the wide gray line represents climate variables.

Table 1. Dates of sample collection, climate variables and leaf wax *n*-alkane characteristics for samples in the time-series study at Carbrook Wetlands.

Date of sample collection	Mean growing season total precipitation (mm)	Mean daily growing season temperature (ºC)	ACL (C25-C33)	Concentration (µg/g dry leaf, C25-C33)	Norm 31	Dispersion (C25-C33)
24.4.92	284.4	23.1	29.7	250.6	0.7	3.9
17.7.92	284.4	23.1	29.8	83.6	0.6	4.0
9.10.92	284.4	23.1	29.9	103.7	0.7	3.5
29.1.93	301.2	23.2	29.5	137.5	0.6	3.5
23.4.93	301.2	23.2	30.1	297.0	0.7	3.2
16.7.93	301.2	23.2	30.0	215.6	0.7	3.2
9.10.93	301.2	23.2	29.4	120.1	0.5	3.8
1.1.94	328.3	23.3	29.2	90.1	0.6	4.1
17.6.94	328.3	23.3	29.7	193.5	0.7	3.7
9.9.94	328.3	23.3	29.7	153.6	0.7	4.1
30.12.94	280.5	23.1	30.2	422.3	0.7	2.9
24.3.95	280.5	23.1	30.2	401.1	0.7	2.4
16.6.95	280.5	23.1	29.9	233.0	0.7	3.5
18.9.95	280.5	23.1	29.8	282.3	0.6	3.1
1.12.95	341.7	23.2	29.8	174.7	0.7	4.0
24.2.96	341.7	23.2	28.9	47.1	0.6	5.6
18.5.96	341.7	23.2	30.0	1173.1	0.7	3.0
10.8.96	341.7	23.2	29.5	122.2	0.7	4.3
31.10.96	341.7	23.2	29.6	132.9	0.7	4.3
24.1.97	337.9	23.3	29.4	129.6	0.5	3.8
13.6.97	337.9	23.3	29.6	149.8	0.7	4.2
7.9.97	337.9	23.3	29.5	129.1	0.6	4.0
29.11.97	337.9	23.3	29.4	122.7	0.7	4.3
21.2.98	409.1	23.2	29.8	193.0	0.8	4.5
15.5.98	409.1	23.2	29.7	126.8	0.7	4.2
9.8.98	409.1	23.2	29.6	109.1	0.7	4.6
28.11.98	409.1	23.2	29.5	111.6	0.6	4.4
20.2.99	382.4	23.1	29.9	156.2	0.7	3.9
25.3.99	382.4	23.1	29.9	213.3	0.7	3.6

22.5.99	382.4	23.1	29.6	130.6	0.7	4.0
11.8.99	382.4	23.1	29.4	109.8	0.7	5.0
21.1.00	543.2	22.8	29.9	114.6	0.7	3.7
16.4.00	543.2	22.8	29.5	158.9	0.7	4.7
8.7.00	543.2	22.8	29.3	136.1	0.6	4.4
29.9.00	543.2	22.8	29.3	78.2	0.6	4.3
20.12.00	522.4	23.0	30.1	169.7	0.7	3.3
18.3.01	522.4	23.0	29.5	112.9	0.7	4.4
19.9.01	522.4	23.0	29.8	168.7	0.7	3.5
19.12.01	512.0	23.1	29.5	108.3	0.6	3.7
17.3.02	512.0	23.1	29.6	126.5	0.7	4.0
16.6.02	512.0	23.1	29.5	115.0	0.6	4.4
17.9.02	512.0	23.1	29.1	120.3	0.5	4.0
20.12.02	360.8	23.6	29.7	138.4	0.7	4.3
23.3.03	360.8	23.6	29.9	202.7	0.7	3.6
20.6.03	360.8	23.6	29.7	138.6	0.7	3.7

3.2 South-east Queensland (SEQ)

In samples from SEQ (Table 2), the total concentration of *n*-alkanes (C25 to C33 summed) ranged from 2.9 to 287 μg/g dry leaf (mean: 34.5; σ: 59.7). ACL ranged from 29.0 to 30.3 (mean: 29.7; σ: 0.32), and Norm31 from 0.52 to 0.81 (mean: 0.66; σ: 0.07). Values of dispersion varied from 1.0 to 6.2 (mean: 4.2; σ: 1.15). For SEQ sites, only Norm31 had statistically significant, but weak, linear correlations with both growing season precipitation and growing season temperature ($R = -0.45$, $p = 0.043$ and $R = 0.45$, $p = 0.041$, respectively) (Fig. 4). Redundancy analysis (Fig. S1 in Chapter 2 Appendix) indicated that variance in *n*-alkane characteristics of samples from SEQ sites was primarily explained by axis one (constrained to be a combination of the influence of growing season precipitation and temperature, and hence aridity), but the variance explained was low

292 (<10%). Axis 2 summarises the dominant hypothetical gradient unrelated to the measured
293 variables and explained less than 1% of the variance.

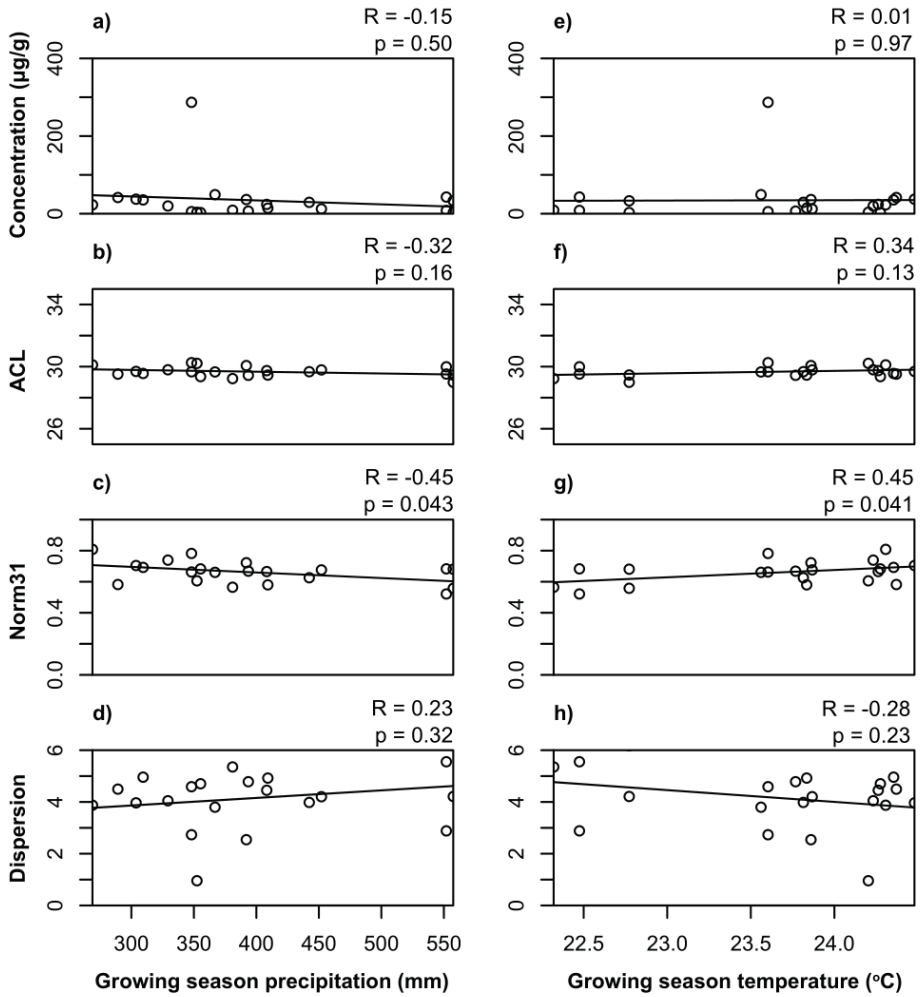

Figure 4. *n*-Alkane characteristics versus growing season precipitation (a, b, c, d) and growing season temperature (e, f, g, h) from our south-east Queensland study (SEQ), with summary statistics of linear regression modelling indicated.

294 **3.3 Cross-Queensland (QLD)**

295 For samples from the QLD sites (Table 2), the summed concentration of the suite
296 of *n*-alkane homologs from C25 to C33 ranged from 2.9 to 411 µg/g dry leaf (mean: 66.5;
297 σ: 102). ACL ranged from 29 to 31.5 (mean: 29.9; σ: 0.65). Norm31 ranged from 0.52 to

298 0.94 (mean: 0.7; σ: 0.12). Values of dispersion varied from 1 to 6.2 (mean: 3.7; σ: 1.43).
299 Redundancy analysis on spatial data across QLD sites (Fig. S2 in Chapter 2 Appendix)
300 showed that 44% of variance in the *n*-alkane characteristics was explained by axis one,
301 with this axis representing aridity. Axis 2, which summarises the dominant hypothetical
302 gradient unrelated to the measured variables, explained less than 1% of the variance.
303 Concentration, ACL, Norm31 and dispersion all displayed strong correlations with
304 growing season precipitation ($R = -0.61$, $p = 0.001$; $R = -0.78$, $p < 0.001$; $R = -0.8$, $p <$
305 0.001; $R = 0.64$, $p < 0.001$; respectively), and growing season temperature ($R = 0.62$, $p <$
306 0.001; $R = 0.86$, $p < 0.001$; $R = 0.83$, $p < 0.001$; $R = -0.68$, $p < 0.001$; respectively) (Fig.
307 5). When the Cape York samples (samples CY1, 2, 3, 4) in this aspect of the study are
308 considered alone, no significant linear correlations between *n*-alkane characteristics and
309 either of growing season precipitation or temperature are observed (Fig. 5).

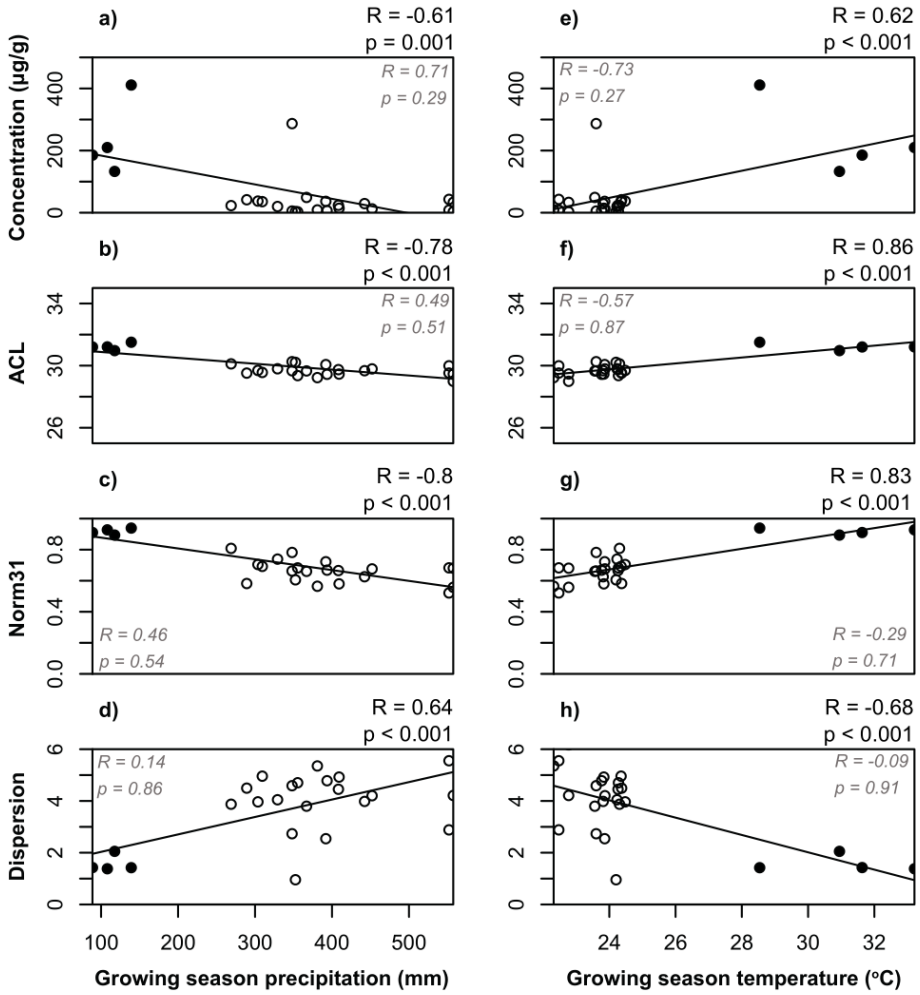

Figure 5. *n*-Alkane characteristics versus growing season precipitation (a, b, c, d) and growing season temperature (e, f, g, h) from the cross-Queensland study (QLD). Open symbols indicate samples from SEQ study, with closed symbols representing Cape York samples augmenting the SEQ data. Summary statistics from linear regressions (correlation coefficient and p-value) are indicated for all samples (black) and only Cape York samples (gray, italics).

Table 2. Geographic locations, climate variables and leaf wax *n*-alkane characteristics for samples in the SEQ and QLD studies.

Sample name	Longitude E (º)	Latitude S (º)	Mean growing season total precipitation (mm)	Mean daily growing season temperature (ºC)	ACL (C25-C33)	Concentration (µg/g dry leaf, C25-C33)	Norm31	Dispersion (C25-C33)
G1a	153.1	27.7	348.1	23.6	30.3	286.8	0.8	2.7
G2a	153.2	27.7	355.4	24.3	29.4	2.9	0.7	4.7
G3a	153.3	27.7	352.5	24.2	30.2	3.6	0.6	1.0
G4a	153.3	27.6	392.0	23.9	30.1	36.4	0.7	2.5
G5a	153.3	27.5	366.9	23.6	29.7	49.1	0.7	3.8
G6a	153.1	26.8	452.0	23.9	29.8	12.2	0.7	4.2
G7a	153.0	26.8	393.6	23.8	29.4	6.7	0.7	4.8
G8a	153.0	26.9	381.0	22.3	29.2	8.9	0.6	5.4
G9a	152.9	27.0	289.2	24.4	29.5	41.6	0.6	4.5
G10a	153.2	27.1	348.1	23.6	29.7	5.2	0.7	4.6
J1a	153.1	27.6	268.9	24.3	30.1	22.8	0.8	3.9
J2a	152.9	27.6	303.7	24.5	29.7	37.3	0.7	4.0
J3a	153.0	27.7	309.4	24.4	29.6	35.5	0.7	5.0
J4a	153.0	26.7	408.3	24.3	29.7	23.9	0.7	4.5
J5a	153.0	26.3	329.2	24.2	29.8	19.9	0.7	4.0
J6a	153.1	26.4	409.2	23.8	29.5	14.2	0.6	4.9
J7a	153.1	26.5	442.3	23.8	29.7	29.2	0.6	4.0
WL1a	153.4	27.4	557.5	22.8	29.0	2.9	0.6	6.2
WL2a	153.4	27.4	557.5	22.8	29.5	33.2	0.7	4.2
SL1a	153.5	27.5	552.0	22.5	30.0	42.9	0.7	2.9
BL1a	153.4	27.5	552.0	22.5	29.5	8.3	0.5	5.6
CY1a	141.7	14.8	88.8	31.6	31.2	185.4	0.9	1.4
CY2a	144.5	15.6	139.2	28.5	31.5	411.0	0.9	1.4
CY3a	144.1	14.8	117.6	30.9	31.0	132.9	0.9	2.1
CY4a	145.2	15.5	108.1	33.2	31.2	209.8	0.9	1.4

3.4 Levene's test of homogeneity of variance (SEQ and time-series)

Comparison of variance between the SEQ and time-series studies using Levene's test resulted in p-values for the *n*-alkane characteristics ACL, concentration and Norm31 of 0.71, 0.21 and 0.64, respectively. As such, homogeneity of variance of these *n*-alkane characteristics exists between the SEQ and time-series studies. Comparison of *n*-alkane dispersion variance between the SEQ and time-series studies using Levene's test resulted in a p-value of 0.01, indicating significant heterogeneity of variance.

4 Discussion

We measured *n*-alkane characteristics of modern *M. quinquenervia* leaves in a 11 year time-series, as well as across small- and large-scale climate transects, to explore the potential for calibration of these characteristics for novel single species palaeoclimatic reconstructions in south-east Queensland (Tibby et al., 2016; Barr et al., 2019). The single species approach undertaken in this study controlled for intrinsic differences in *n*-alkane production within plant communities that have the potential to significantly bias modern *n*-alkane characteristic-climate calibrations (Vogts et al., 2009; Diefendorf et al., 2011, 2015; Carr et al., 2014; Freeman and Pancost, 2014; Garcin et al., 2014; Diefendorf and Freimuth, 2017; Jansen and Wiesenberg, 2017; Howard et al., 2018). This was crucial for assessment of *n*-alkane characteristic responsiveness to climate, and to constrain whether leaf wax *n*-alkane characteristics in *M. quinquenervia* reflect plastic responses to short-term climate changes or whether they reflect fixed traits associated with different ambient climate conditions (Bender et al., 2017).

Most *n*-alkane characteristics of *M. quinquenervia* (concentration, ACL, Norm31) did not respond plastically to climate variability in the 11-year time-series from Carbrook Wetlands (Fig. 3). In the smaller regional sample set of south-east Queensland (SEQ) concentration, ACL, and dispersion are also not significantly correlated with climate (Fig. 4). Similarly, *n*-alkane characteristics of samples from the Cape York region, when considered alone as a regional sample set, do not correlate with climate, although the sample size is small (Fig. 5).

Concentration, ACL and Norm31 displayed homogenous variance between the time-series and SEQ datasets, suggesting that variation in these characteristics at the site level is as large as at the regional level. While most of the variation in the temporal and

SEQ data is not explained by climate, weak correlations were observed between dispersion and precipitation in the time-series as well as between Norm31 and both climate variables in SEQ. Therefore, overall *n*-alkane characteristics are unresponsive or only weakly responsive to climate variability in a plastic sense when examined in a time-series at one location, and across relatively small distances (~150 km). This lack of responsiveness of *n*-alkane characteristics to climate in the time-series and SEQ could be influenced by hydrological buffering in the wetland habitat of this species (Ireland et al., 2002). However, carbon isotope ratios of leaves from this same time-series show strong correlations with rainfall through the impact of water stress on carbon isotope fractionation (Tibby et al., 2016). The carbon isotope data demonstrates that these trees are sensitive to climatic fluctuations through time. Therefore, the lack of response in *n*-alkane characteristics observed here indicates a lack of plasticity.

In contrast, the QLD data show significant linear relationships between climate and all *n*-alkane characteristics measured. The linear relationships observed are largely a function of the addition of Cape York samples from sites with markedly lower growing season precipitation and higher growing season temperature than sites in SEQ. These samples display distinctly higher concentration, ACL, Norm31 and lower dispersion than samples from SEQ, and this is suggestive of two broad distinct groups of *M. quinquenervia* in terms of their *n*-alkane production. The assertion of geographic groupings of *n*-alkane characteristics in *M. quinquenervia* is further supported by redundancy analysis of samples from SEQ and QLD (Figs. S1 and S2 in Chapter 2 Appendix). When Cape York samples are included in the redundancy analysis, 44% of variance in *n*-alkane characteristics can be explained by aridity, compared to less than 10% for only SEQ samples.

The observations in the QLD aspect of the study are consistent with the functional role of leaf wax *n*-alkanes proposed by the barrier membrane model (Riederer and Schneider, 1990; Reynhardt and Riederer, 1994; Riederer and Schreiber, 1995; Jetter and Riederer, 2016). More abundant, longer and more narrowly distributed *n*-alkanes are observed at sites with lower growing season rainfall and higher temperatures, where mitigating non-stomatal water loss would be critical. Similar positive correlations have been observed between ACL and growing season temperature in a study that examined within-species variation in *Acer rubrum* and *Juniperus virginiana* from a spatial transect in North America (Tipple and Pagani, 2013).

Taken together, the data suggest that leaf wax *n*-alkane characteristics of *M. quinquenervia* do not respond plastically to climate, but instead appear fixed. Yet, *n*-alkane characteristics differ between south-east Queensland and Cape York in ways that are consistent with the barrier-membrane model. These fixed differences could reflect natural selection for less permeable cuticles in more arid regions. A number of studies have interpreted differences in *n*-alkane production in plants as a result of adaptation to different climates of populations of a single species, rather than a plastic response (Dodd et al., 1998; Dodd and Afzal-Rafii, 2000; Dodd and Poveda, 2003; Rajčević et al., 2014). Greenhouse and common garden experiments indicate that leaf wax compound profiles reflect genetic determination more strongly than short-term environmental influence (Gosney et al., 2016; Bender et al., 2017). To demonstrate that leaf wax *n*-alkane characteristics in *M. quinquenervia* are fixed through genetic control requires further research (e.g., genetic sequencing, common garden experiments). However, the evidence is suggestive that genetics could be the main control on *n*-alkane production in leaves of *M. quinquenervia*.

The results of this study have implications for approaches using *n*-alkane abundance and distributions for palaeoclimatic reconstructions. Any changes in *n*-alkane characteristics of sub-fossil leaves of *M. quinquenervia* would likely not reflect plastic responses to small-scale variations in climate, but instead could represent much larger and longer sustained climatological shifts. This distinction has important ramifications for the interpretation of *n*-alkane characteristics as a proxy for variation in climate through time, particularly in the context of the scale of climatological shifts able to be perceived from geological records.

5 Conclusions

Leaf wax *n*-alkane characteristics have been examined in leaves of *Melaleuca quinquenervia* on both spatial and temporal climate gradients. We observed weak or no correlation between both growing season precipitation and temperature and *n*-alkane characteristics in proximal samples from south-east Queensland and a time-series of one population, even though climate and *n*-alkane characteristics vary substantially in both cases. We observed longer and more narrowly distributed leaf wax *n*-alkanes in samples of *M. quinquenervia* from a markedly warmer and dryer growing season climate regime, which is consistent with the prevailing model for the function of leaf-wax *n*-alkanes in preventing water loss. We interpret our results as reflecting fixed responses to broad climate regimes as opposed to plastic responses to regional microclimate spatially and through time. These results have implications for interpreting *n*-alkane characteristics of sub-fossil leaves, with changes in these in sedimentary archives likely reflecting large climatological shifts, rather than short-term climate variability.

Acknowledgements

This study was funded through an Australian Research Council (ARC) Future Fellowship (FT110100793) awarded to F.A.M., an ARC Discovery project (DP150103875) led by J.T., and a NERC Life Sciences Mass Spectrometry Facility grant (LSMSFBRIS/071/0414) awarded to A.C.G.H. J.W.A. was supported by an Australian Government Research Training Program Scholarship and a University of Adelaide Faculty of Sciences Divisional Scholarship. C.B. was supported by ARC grant DP150103875 and a University of Adelaide Research Fellowship. The authors would like to thank Tim Page for his field and logistical support, and Kristine Nielson, Ian Bull and Stephanie Rankine for invaluable research assistance, laboratory and analytical support. Thank you to Aaron Diefendorf and one anonymous reviewer for their comments which significantly improved the paper. The authors declare no conflict of interest.

References

Baczynski, A.A., McInerney, F.A., Wing, S.L., Kraus, M.J., Morse, P.E., Bloch, J.I., Chung, A.H., Freeman, K.H., 2016. Distortion of carbon isotope excursion in bulk soil organic matter during the Paleocene-Eocene thermal maximum. Geological Society of America Bulletin 128, 1352–1366.

Barr, C., Tibby, J., Leng, M.J., Tyler, J.J., Henderson, A.G.C., Overpeck, J.T., Simpson, G.I., Cole, J.E., Phipps, S.J., Marshall, J.C., McGregor, G.B., Hua, Q., McRobie, F., 2019. Holocene El Niño-Southern Oscillation variability reflected in subtropical Australian precipitation. Scientific Reports 9.

Bender, A.L.D., Chitwood, D.H., Bradley, A.S., 2017. Heritability of the structures and ^{13}C fractionation in tomato leaf wax alkanes: a genetic model system to inform paleoenvironmental reconstructions. Frontiers in Earth Science 5, 1–13.

Boland, D.J., Brooker, M.I.H., Chippendale, G.M., Hall, N., Hyland, B.P.M., Johnston, R. D., Kleinig, D.A., McDonald, M.W., Turner, J.D., 2006. Forest Trees of Australia. CSIRO Publishing, Australia.

Bush, R.T., McInerney, F.A., 2013. Leaf wax *n*-alkane distributions in and across modern plants: implications for paleoecology and chemotaxonomy. Geochimica et Cosmochimica Acta 117, 161–179.

Bush, R.T., McInerney, F.A., 2015. Influence of temperature and C4 abundance on *n*-alkane chain length distributions across the central USA. Organic Geochemistry 79, 65–73.

Carr, A.S., Boom, A., Grimes, H.L., Chase, B.M., Meadows, M.E., Harris, A., 2014. Leaf wax *n*-alkane distributions in arid zone South African flora: environmental controls, chemotaxonomy and palaeoecological implications. Organic Geochemistry 67, 72–84.

Diefendorf, A.F., Freeman, K.H., Wing, S.L., Graham, H.V., 2011. Production of *n*-alkyl lipids in living plants and implications for the geologic past. Geochimica et Cosmochimica Acta 75, 7472–7485.

Diefendorf, A.F., Freimuth, E.J., 2017. Extracting the most from terrestrial plant-derived *n*-alkyl lipids and their carbon isotopes from the sedimentary record: a review. Organic Geochemistry 103, 1–21.

Diefendorf, A.F., Leslie, A.B., Wing, S.L., 2015. Leaf wax composition and carbon isotopes vary among major conifer groups. Geochimica et Cosmochimica Acta 170, 145–156.

Dodd, R.S., Afzal-Rafii, Z., 2000. Habitat-related adaptive properties of plant cuticular lipids. Evolution 54, 1438–1444.

458 Dodd, R.S., Poveda, M.M., 2003. Environmental gradients and population divergence
459 contribute to variation in cuticular wax composition in *Juniperus communis*.
460 Biochemical Systematics and Ecology 31, 1257–1270.
461 Dodd, R.S., Rafii, Z.A., Power, A.B., 1998. Ecotypic adaptation in *Austrocedrus chilensis*
462 in cuticular hydrocarbon composition. The New Phytologist 138, 699–708.
463 Eglinton, G., Hamilton, R.J., 1967. Leaf epicuticular waxes. Science 156, 1322–1335.
464 Eglinton, G., Hamilton, R.J., Raphael, R.A., 1962. Hydrocarbon constituents of the wax
465 coatings of plant leaves: a taxonomic survey. Nature 193, 739–742.
466 Fox, J., Weisberg, S., 2011. An R Companion to Applied Regression. SAGE, Thousand
467 Oaks, California.
468 Freeman, K.H., Pancost, R.D., 2014. Biomarkers for terrestrial plants and climate. In:
469 Holland, H.D., Turekian, K.K. (Eds.), Treatise on Geochemistry. second ed.
470 Elsevier, Oxford, pp. 395–416.
471 Garcin, Y., Schefuß, E., Schwab, V.F., Garreta, V., Gleixner, G., Vincens, A., Todou, G.,
472 Séné, O., Onana, J.-M., Achoundong, G., Sachse, D., 2014. Reconstructing C3 and
473 C4 vegetation cover using *n*-alkane carbon isotope ratios in recent lake sediments
474 from Cameroon, Western Central Africa. Geochimica et Cosmochimica Acta 142,
475 482–500.
476 Gosney, B.J., Potts, B.M., O'Reilly-Wapstra, J.M., Vaillancourt, R.E., Fitzgerald, H.,
477 Davies, N.W., Freeman, J.S., 2016. Genetic control of cuticular wax compounds in
478 *Eucalyptus globulus*. New Phytologist 209, 202–215.
479 Greenway, M., 1994. Litter accession and accumulation in a *Melaleuca quinquenervia*
480 (Cav.) S.T. Blake wetland in south-eastern Queensland. Marine and Freshwater
481 Research 45, 1509–1519.

Hoffman, B., Kahmen, A., Cernusak, L.A., Arndt, S.K., Sachse, D., 2013. Abundance and distribution of leaf wax *n*-alkanes in leaves of *Acacia* and *Eucalyptus* trees along a strong humidity gradient in northern Australia. Organic Geochemistry 62, 62–67.

Howard, S., McInerney, F.A., Caddy-Retalic, S., Hall, P.A., Andrae, J.W., 2018. Modelling leaf wax *n*-alkane inputs to soils along a latitudinal transect across Australia. Organic Geochemistry 121, 126–137.

Ireland, B.F., Hibbert, D.B., Goldsack, R.J., Doran, J.C., Brophy, J.J., 2002. Chemical variation in the leaf essential oil of *Melaleuca quinquenervia* (Cav.) S.T. Blake. Biochemical Systematics and Ecology 30, 457–470.

Jansen, B., Wiesenberg, G.L.B., 2017. Opportunities and limitations related to the application of plant-derived lipid molecular proxies in soil science. Soil 3, 211–234.

Jeffrey, S.J., Carter, J.O., Moodie, K.B., Beswick, A.R., 2001. Using spatial interpolation to construct a comprehensive archive of Australian climate data. Environmental Modelling & Software 16, 309–330.

Jetter, R., Kunst, L., Samuels, A.L., 2006. Composition of plant cuticular waxes. In: Riederer, M., Muller, C. (Eds.), Biology of the Plant Cuticle. Blackwell Publishing, Oxford, pp. 145–181.

Jetter, R., Riederer, M., 2016. Localization of the transpiration barrier in the epi- and intracuticular waxes of eight plant species: water transport resistances are associated with fatty acyl rather than alicyclic components. Plant Physiology 170, 921–934.

Koch, K., Ensikat, H.J., 2008. The hydrophobic coatings of plant surfaces: epicuticular wax crystals and their morphologies, crystallinity and molecular self-assembly. Micron 39, 759–772.

Kunst, L., Samuels, A.L., 2003. Biosynthesis and secretion of plant cuticular wax. Progress in Lipid Research 42, 51–80.

Leider, A., Hinrichs, K.-U., Schefuß, E., Versteegh, G.J.M., 2013. Distribution and stable isotopes of plant wax derived *n*-alkanes in lacustrine, fluvial and marine surface sediments along an eastern Italian transect and their potential to reconstruct the hydrological cycle. Geochimica et Cosmochimica Acta 117, 16–32.

Lepš, J., Šmilauer, P., 2003. Multivariate Analysis of Ecological Data Using CANOCO. Cambridge University Press, Cambridge.

Oksanen, J., Blanchet, F.G., Friendly, M., Kindt, R., Legendre, P., McGlinn, D., Minchin, P.R., O'Hara, R.B., Simpson, G.L., Solymos, P., Stevens, M.H.H., Szoecs, E., Wagner, H., 2017. Package 'vegan' (R).

Peel, M.C., Finlayson, B.L., McMahon, T.A., 2007. Updated world map of the Köppen-Geiger climate classification. Hydrology and Earth System Sciences 11, 1633–1644.

Pickett, S.T.A., 1989. Space-for-time substitution as an alternative to long-term studies. In: Likens, G.E. (Ed.), Long-Term Studies in Ecology: Approaches and Alternatives. Springer, New York, NY, pp. 110–135.

Core Team, R., 2016. R: A Language and Environment for Statistical Computing. R Foundation for Statistical Computing, Vienna, Austria.

Rajčević, N., Janaćković, P., Dodoš, T., Tešević, V., Marin, P.D., 2014. Biogeographic variation of foliar *n*-alkanes of *Juniperus communis* var. *saxatilis pallas* from the Balkans. Chemistry & Biodiversity 11, 1923–1938.

Reynhardt, E.C., Riederer, M., 1994. Structures and molecular dynamics of plant waxes. European Biophysics Journal 23, 59–70.

Riederer, M., Schneider, G., 1990. The effect of the environment on the permeability and composition of *Citrus* leaf cuticles. Planta 180, 154–165.

Riederer, M., Schreiber, L., 1995. Waxes – the transport barriers of plant cuticles. In: Hamilton, R.J. (Ed.), Waxes: Chemistry, Molecular Biology, and Functions. Oily Press, Dundee, pp. 130–156.

Riederer, M., Schreiber, L., 2001. Protecting against water loss: analysis of the barrier properties of plant cuticles. Journal of Experimental Botany 52, 2023–2032.

Rouillard, A., Greenwood, P.F., Grice, K., Skrzypek, G., Dogramaci, S., Turney, C., Grierson, P.F., 2016. Interpreting vegetation change in tropical arid ecosystems from sediment molecular fossils and their stable isotope compositions: a baseline study from the Pilbara region of northwest Australia. Palaeogeography, Palaeoclimatology, Palaeoecology 459, 495–507.

Schefuss, E., Ratmeyer, V., Stuut, J.-B.W., Jansen, J.H.F., Sinninghe Damsté, J.S., 2003. Carbon isotope analyses of *n*-alkanes in dust from the lower atmosphere over the central eastern Atlantic. Geochimica et Cosmochimica Acta 67, 1757–1767.

Schreiber, L., Riederer, M., 1996. Ecophysiology of cuticular transpiration: comparative investigation of cuticular water permeability of plant species from different habitats. Oecologia 107, 426–432.

Schuster, A.-C., Burghardt, M., Alfarhan, A., Bueno, A., Hedrich, R., Leide, J., Thomas, J., Riederer, M., 2016. Effectiveness of cuticular transpiration barriers in a desert plant at controlling water loss at high temperatures. AoB Plants 8, 1–14.

Serbesoff-King, K., 2003. *Melaleuca* in Florida: a literature review on the taxonomy, distribution, biology, ecology, economic importance and control measures. Journal of Aquatic Plant Management 41, 98–112.

Shepherd, T., Griffiths, D.W., 2006. The effects of stress on plant cuticular waxes. New Phytologist 171, 469–499.

Smith, F.A., Wing, S.L., Freeman, K.H., 2007. Magnitude of the carbon isotope excursion at the Paleocene-Eocene thermal maximum: the role of plant community change. Earth and Planetary Science Letters 262, 50–65.

Suh, Y.J., Diefendorf, A.F., 2018. Seasonal and canopy height variation in *n*-alkanes and their carbon isotopes in a temperate forest. Organic Geochemistry 116, 23–34.

ter Braak, C.J.F., Prentice, I.C., 2004. A theory of gradient analysis. *Advances in Ecological Research* 34, 235–282.

Tibby, J., Barr, C., McInerney, F.A., Henderson, A.C.G., Leng, M.J., Greenway, M., Marshall, J.C., McGregor, G.B., Tyler, J.J., McNeil, V., 2016. Carbon isotope discrimination in leaves of the broad-leaved paperbark tree, *Melaleuca quinquenervia*, as a tool for quantifying past tropical and sub-tropical rainfall. Global Change Biology 22, 3474–3486.

Tipple, B.J., Pagani, M., 2013. Environmental control on eastern broadleaf forest species' leaf wax distributions and D/H ratios. Geochimica et Cosmochimica Acta 111, 64–77.

Van, T.K., Rayachhetry, M.B., Center, T.D., Pratt, P., 2002. Litter dynamics and phenology of *Melaleuca quinquenervia* in south Florida. Journal of Aquatic Plant Management 40, 22–27.

Vogts, A., Moossen, H., Rommerskirchen, F., Rullkötter, J., 2009. Distribution patterns and stable carbon isotopic composition of alkanes and alkan-1-ols from plant waxes of African rain forest and savanna C3 species. Organic Geochemistry 40, 1037–1054.

Appendix

Variation in leaf wax *n*-alkane characteristics with climate in the broad-leaved paperbark (*Melaleuca quinquenervia*)*

*Originally published as Andrae, J.W., McInerney, F.A., Tibby, J., Henderson, Andrew C.G., Hall, P.A., Marshall, J.C., McGregor, G.B., Barr, C. and Greenway, M. (2019) Variation in leaf wax *n*-alkane characteristics with climate in the broad-leaved paperbark (*Melaleuca quinquenervia*), *Organic Geochemistry*, 130, 33-42

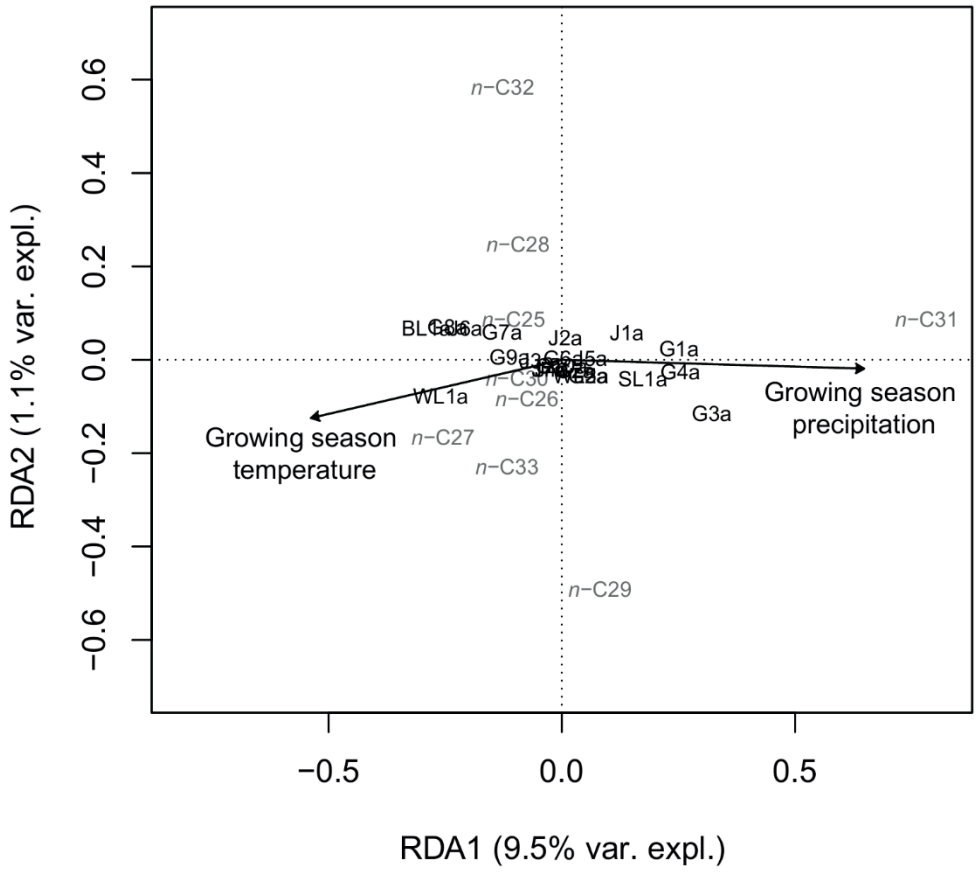

Figure S1. Redundancy analysis of sample *n*-alkane chain length distributions in the context of growing season precipitation and growing season temperature at sites in our south-east Queensland (SEQ). Arrows represent measured environmental gradient vectors.

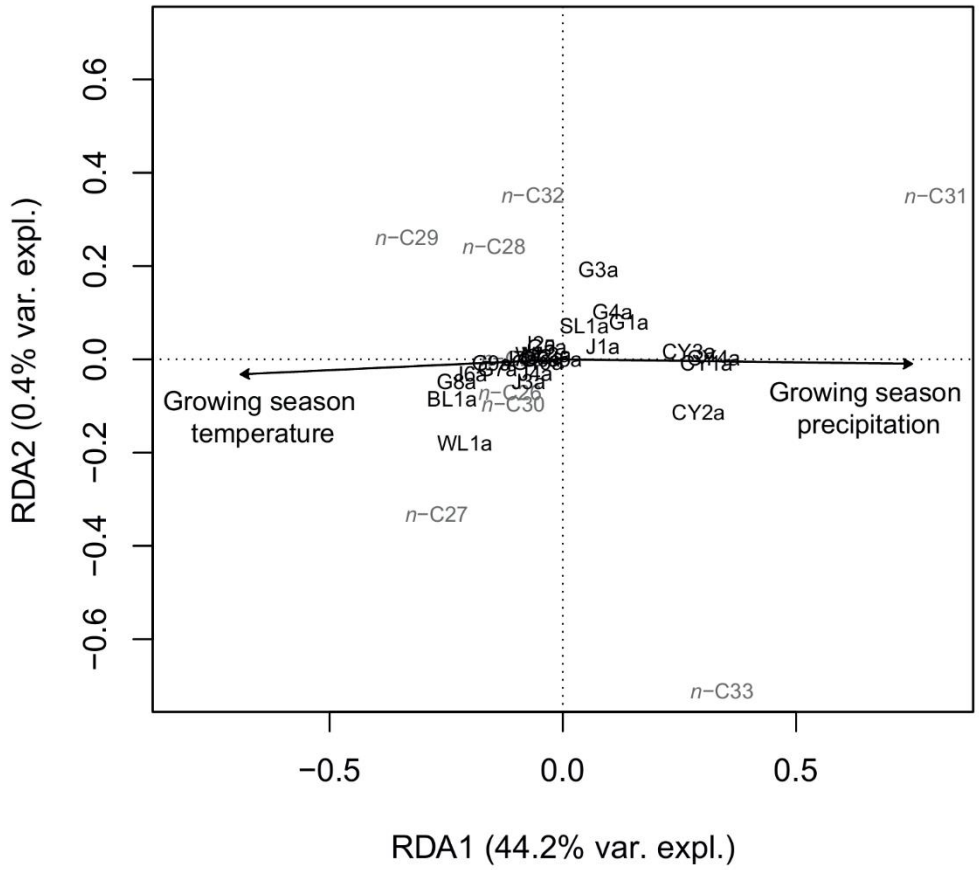

Figure S2. Redundancy analysis of sample *n*-alkane chain length distributions in the context of growing season precipitation and growing season temperature at sites in our cross-Queensland study (QLD). Arrows represent measured environmental gradient vectors.

Data Set S1

Time-series n-alkane quantitation

	Concentration of each n-alkane (µg/g)														
Sample	C18	C20	C21	C22	C23	C24	C25	C26	C27	C28	C29	C30	C31	C32	C33
Sample 1 (13/06/1997)	11.57	18.06	0.98	15.35	2.09	10.79	5.25	8.81	19.00	6.99	27.37	6.38	63.34	4.61	8.05
Sample 2 (08/07/2000)	6.23	16.80	N/A	18.88	3.80	14.33	6.89	10.24	15.00	9.07	29.65	6.49	48.13	4.31	6.36
Sample 3 (19/12/2001)	5.71	6.58	1.17	5.91	2.36	5.16	3.33	3.95	14.99	5.02	28.89	3.40	41.19	2.21	5.35
Sample 4 (29/09/2000)	2.92	8.18	0.74	8.96	2.05	6.61	2.95	5.01	12.31	4.56	15.85	3.08	28.71	2.17	3.57
Sample 5 (24/04/1992)	21.22	28.30	0.99	22.81	2.31	16.75	8.33	12.92	24.07	11.21	53.78	9.57	109.79	6.80	14.08
Sample 6 (25/03/1999)	5.30	6.71	1.11	5.80	2.92	5.44	5.80	6.19	24.06	5.58	42.85	5.16	105.30	3.88	14.46
Sample 7 (24/03/1995)	22.43	26.72	N/A	20.31	N/A	13.88	3.00	10.17	18.40	9.73	99.58	13.81	218.12	8.54	19.78
Sample 8 (29/01/1993)	6.43	8.05	N/A	6.92	1.09	5.44	3.14	5.98	15.68	8.93	38.63	6.98	47.67	3.54	6.90
Sample 9 (09/10/1992)	9.29	11.50	N/A	9.15	1.32	6.85	2.07	4.71	8.18	5.18	22.88	5.64	43.70	4.16	7.12
Sample 10 (31/10/1996)	19.69	31.16	N/A	27.24	3.73	19.03	3.66	12.50	10.64	10.25	23.52	8.43	49.26	7.24	7.40
Sample 11 (09/10/1993)	13.14	20.01	1.30	17.93	2.57	12.68	2.51	9.26	12.30	8.31	32.08	6.53	39.00	4.96	5.15
Sample 12 24/02/1996	17.17	27.67	N/A	23.00	N/A	16.89	0.88	11.84	1.52	8.54	3.10	7.10	4.86	6.35	2.91
Sample 13 21/02/1998	32.72	53.38	N/A	44.38	N/A	33.87	3.36	22.34	9.00	16.56	22.37	15.14	74.52	15.59	14.06
Sample 14 17/07/1992	10.48	14.77	N/A	11.87	N/A	8.67	2.13	5.45	5.63	5.35	17.51	4.75	32.15	4.53	6.06
Sample 15 10/08/1996	6.25	8.17	N/A	7.22	N/A	6.80	4.53	6.41	16.80	5.91	23.87	4.10	49.64	3.32	7.64
Sample 16 19/09/2001	7.12	9.09	N/A	7.84	N/A	6.99	4.87	6.36	15.05	5.38	38.38	5.51	80.37	4.20	8.57
Sample 17 20/06/2003	6.67	9.11	N/A	8.09	N/A	7.64	4.31	6.03	13.18	5.80	31.83	4.51	61.53	3.65	7.73
Sample 18 16/06/1995	11.56	13.61	N/A	11.81	N/A	9.62	5.89	9.41	19.53	7.96	48.15	8.36	114.22	6.35	13.18
Sample 19 23/03/2003	16.24	18.30	N/A	14.34	N/A	12.27	5.08	8.79	17.12	7.00	37.72	6.43	102.29	5.25	13.03
Sample 20 17/09/2002	6.84	7.77	N/A	8.16	N/A	8.19	5.78	7.15	19.86	6.52	35.23	3.65	34.75	2.71	4.65
Sample 21 23/04/1993	10.46	13.60	N/A	12.06	N/A	10.37	5.50	9.10	25.22	8.14	53.36	9.92	159.79	7.71	18.20
Sample 22 16/07/1993	8.70	12.87	N/A	11.56	N/A	9.28	4.63	7.69	15.21	7.36	46.84	7.34	109.78	5.54	11.18
Sample 23 18/09/1995	7.44	10.09	N/A	8.51	N/A	8.49	7.63	8.42	22.57	8.65	81.59	10.52	125.08	5.73	12.10
Sample 24 20/12/2000	7.49	10.27	N/A	9.78	N/A	7.76	2.94	6.14	13.58	5.80	32.00	5.52	86.62	4.71	12.37
Sample 25 07/09/1997	9.07	12.71	N/A	13.44	N/A	11.45	4.03	9.17	12.61	7.87	28.77	6.44	48.80	5.29	6.16
Sample 26 24/01/1997	11.32	14.61	N/A	13.20	N/A	10.39	4.11	9.02	13.50	6.98	35.95	6.22	43.56	4.76	5.51
Sample 27 01/12/1995	13.87	16.93	N/A	15.73	N/A	12.50	4.66	10.13	15.89	8.85	30.28	8.19	77.94	7.42	11.35
Sample 28 20/02/1999	11.43	14.67	N/A	13.44	N/A	10.48	4.43	7.60	15.15	6.36	26.97	5.73	75.13	4.75	10.04
Sample 29 11/08/1999	17.40	22.76	N/A	21.65	N/A	17.41	5.10	11.74	10.27	9.12	14.61	7.09	38.93	6.15	6.76
Sample 30 18/03/2001	12.00	14.10	N/A	12.43	N/A	10.13	3.97	7.33	14.72	5.92	20.12	4.43	45.63	3.70	7.07
Sample 31 28/11/1998	11.44	13.47	N/A	11.84	N/A	9.72	3.87	7.99	14.16	6.80	22.49	5.32	39.26	5.14	6.61
Sample 32 01/01/1994	6.34	8.15	N/A	7.37	N/A	6.28	3.34	5.63	14.54	5.40	21.39	3.56	29.88	2.79	3.53
Sample 33 21/01/2000	7.72	11.82	N/A	11.72	N/A	9.57	2.77	6.93	7.01	5.60	19.82	5.48	54.31	5.30	7.39
Sample 34 18/05/1996	24.56	34.79	N/A	34.29	N/A	32.34	22.97	32.62	87.44	35.34	247.36	38.91	619.95	25.63	62.91
Sample 35 09/09/1994	7.79	13.17	N/A	12.75	N/A	10.47	5.45	8.41	15.13	7.39	31.74	6.26	63.05	5.89	10.23
Sample 36 22/05/1999	17.82	18.56	N/A	13.86	N/A	9.89	3.69	7.16	16.35	6.29	26.02	5.46	54.09	4.36	7.20
Sample 37 15/05/1998	14.05	15.72	N/A	13.14	N/A	10.68	4.25	8.16	12.57	6.57	23.04	5.69	53.17	4.95	8.36
Sample 38 16/04/2000	27.57	30.01	N/A	24.24	N/A	18.86	6.31	13.51	18.59	10.55	24.20	8.62	59.30	7.77	10.03
Sample 39 17/03/2002	14.49	17.36	N/A	13.56	N/A	10.61	3.87	8.16	13.52	6.74	27.58	5.47	51.31	3.70	6.17
Sample 40 09/08/1998	13.18	20.73	N/A	18.85	N/A	14.39	3.52	10.40	9.11	7.84	17.18	6.66	40.78	6.14	7.45
Sample 41 30/12/1994	21.10	26.71	N/A	23.08	N/A	17.86	6.13	15.04	20.16	12.37	84.03	21.11	224.04	12.54	26.89
Sample 42 16/06/2002	11.62	17.51	N/A	15.65	N/A	12.58	3.02	9.32	12.92	8.05	22.07	6.14	39.51	5.63	8.37
Sample 43 17/06/1994	10.42	13.92	N/A	12.38	N/A	10.27	4.62	9.12	21.56	8.23	38.41	7.21	89.94	5.14	9.24
Sample 44 20/12/2002	13.42	21.28	N/A	19.15	N/A	14.21	3.13	10.46	15.02	8.74	20.58	6.59	57.76	6.10	9.96
Sample 45 29/11/1997	10.09	13.54	N/A	12.25	N/A	9.80	4.00	8.20	18.37	6.93	22.85	5.67	46.16	4.42	6.11

Data Set S2									
SEQ and QLD n-alkane quantitation									
	Concentration of each n-alkane (µg/g)								
Sample name	C25	C26	C27	C28	C29	C30	C31	C32	C33
G1a	5.636842105	4.83157895	18.4673684	5.69052632	48.3694737	7.51578947	173.507368	6.38842105	16.4273684
G2a	0.165015167	0.20626896	0.30940344	0.24752275	0.55692619	0	1.19635996	0	0.19595551
G3a	0	0	0	0	1.428	0	2.193	0	0
G4a	0.618876404	0.80224719	2.20044944	0.84808989	8.32044944	0.77932584	21.6148315	0	1.26067416
G5a	1.480645161	1.84258065	6.05419355	2.36903226	11.0554839	0.85548387	21.4858065	1.25032258	2.66516129
G6a	0.472847682	0.37634816	1.4474929	0.58864711	2.34493851	0.43424787	4.89252602	0.70444655	0.95534532
G7a	0.381003202	0.34834578	0.82732124	0.64226254	0.99060832	0.52251868	1.99210245	0.5660619	0.40277481
G8a	0.693877551	0.39319728	1.3877551	1.01768707	1.41088435	0.53197279	1.82721088	1.06394558	0.60136054
G9a	1.677631579	2.90789474	4.51842105	2.34868421	8.85789474	2.84078947	12.325	3.66842105	2.48289474
G10a	0.29766537	0.19844358	0.58540856	0.22821012	1.05175097	0.16867704	2.06381323	0.22821012	0.4266537
J1a	0.800382775	0.72229665	2.04	0.67349282	2.84038278	0.74181818	11.9666986	1.18105263	1.82526316
J2a	1.664048338	1.41752266	3.26646526	3.05075529	6.31722054	2.65015106	15.0380665	2.21873112	1.72567976
J3a	2.102177068	1.391582	5.16661829	1.9245283	5.72917271	1.64325109	12.8795356	1.36197388	3.3161103
J4a	1.028414299	0.74793767	2.96370302	1.2527956	4.57176902	0.98166819	9.08744271	0.87882676	2.37470211
J5a	0.580239521	0.8754491	2.42275449	0.83473054	3.19640719	0.90598802	9.0497006	0.5497006	1.45568862
J6a	0.77018393	1.06640852	1.13552759	1.6588577	2.29080348	1.56011617	3.15972894	1.53049371	1.05653437
J7a	1.123646724	0.77492877	3.86495726	1.09458689	6.48034188	1.61766382	10.819943	1.6951567	1.74358974
CY1a	0.362536023	0.27435159	2.74351585	0.26455331	12.4536023	1.48933718	126.30951	3.83112392	37.6253602
CY2a	0.8791381	0.36963761	3.59647405	0.37962782	16.1341822	2.9970617	247.417434	12.0481881	127.175318
CY3a	1.678606002	0.46408519	3.98915779	0.28635044	10.5060987	1.70822846	88.4032914	4.25575992	21.6342691
CY4a	0.867	0.3468	2.499	0.408	11.475	1.683	146.88	5.0082	40.6776
WL1a	0.266486486	0.19297297	0.61567568	0.18378378	0.45945946	0.18378378	0.57891892	0	0.4227027
WL2a	1.533834586	1.43157895	5.12130326	1.21854637	6.75739348	0.63909774	14.4010025	0.53684211	1.53383459
SL1a	0.816816817	0.72492492	3.67567568	1.04144144	10.4858859	0.7963964	22.5747748	0.68408408	2.05225225
BL1a	0.398091934	0.78733738	0.80503036	0.76964441	1.21196878	0.99080659	1.31812663	1.14119688	0.9111882

Statement of Authorship

Title of Paper	Carbon isotope systematics of leaf wax *n*-alkane compounds in a lacustrine depositional environment
Publication Status	☐ Published ☐ Accepted for Publication ☐ Submitted for Publication ☑ Unpublished and Unsubmitted work written in manuscript style
Publication Details	Formatted for submission to *Organic Geochemistry*

Principal Author

Name of Principal Author (Candidate)	Jake W. Andrae
Contribution to the Paper	Undertook research design, sample preparation and much of the sample analysis, statistical analysis and interpretation. Undertook a large portion of the development and drafting of the manuscript and produced all figures.
Overall percentage (%)	80%
Certification:	This paper reports on original research I conducted during the period of my Higher Degree by Research candidature and is not subject to any obligations or contractual agreements with a third party that would constrain its inclusion in this thesis. I am the primary author of this paper.

Signature Date 11/07/19

Co-Author Contributions

By signing the Statement of Authorship, each author certifies that:

iv. the candidate's stated contribution to the publication is accurate (as detailed above);

v. permission is granted for the candidate in include the publication in the thesis; and

vi. the sum of all co-author contributions is equal to 100% less the candidate's stated contribution.

Name of Co-Author	Francesca A. McInerney
Contribution to the Paper	Undertook research design, along with statistical analysis and data interpretation. Conceptualised figures 1-3. Provided extensive feedback and revisions on drafts and approved final manuscript.

Signature Date 01/08/19

Chapter 3: Carbon isotope systematics of leaf wax *n*-alkanes in a lacustrine depositional environment

Jake W. Andrae [1,2] and Francesca A. McInerney [1,2,3]

[1]University of Adelaide, School of Physical Sciences, Adelaide, South Australia 5005, Australia

[2]University of Adelaide, Sprigg Geobiology Centre, Adelaide, South Australia 5005, Australia

[3]Northwestern University, Department of Earth and Planetary Sciences, Evanston, IL, 60208, USA

Corresponding author: Jake W. Andrae (jake.andrae@adelaide.edu.au)

Highlights

- Lacustrine sediments incorporate mixed aquatic and terrestrial plant inputs.
- Mixing may influence *n*-alkane $\delta^{13}C$ values in lacustrine records.
- Varying degrees of isotopic mixing are observed for different homologs.
- Very long chain *n*-alkanes (≥ C31) show lowest degree of isotopic mixing.
- Long-chain *n*-alkane $\delta^{13}C$ values more robustly reflect photosynthetic pathway.

Abstract

The carbon isotope ratio ($\delta^{13}C$) of plant derived organic carbon preserved in geological archives can be a valuable proxy for past vegetation. Changes in the abundance of C3 and C4 terrestrial vegetation on the landscape through time can be quantified from $\delta^{13}C$ values of terrestrial plant derived carbon, as a result of mechanistic differences in CO_2 assimilation between these photosynthetic pathways. In certain sedimentary archives, however, plant derived carbon can be derived from complex mixtures of both terrestrial and aquatic vegetation. Non-emergent aquatic macrophytes (hereafter aquatic

macrophytes) are ^{13}C enriched compared to C3 terrestrial plant sources. Mixing of terrestrial C3 and aquatic macrophyte sourced carbon integrated in sedimentary archives will result in sedimentary organic matter (OM) $\delta^{13}C$ signatures that could be misinterpreted as shifts in the abundance of C3 and C4 vegetation. There is potential for this problem to be mitigated using leaf wax *n*-alkane compound specific $\delta^{13}C$ measurements due to *n*-alkane production differing between terrestrial vegetation and aquatic macrophytes. This however requires an increased understanding of how mixed inputs of terrestrial plant and aquatic macrophyte *n*-alkanes impacts $\delta^{13}C$ values of different *n*-alkane homologs. This study quantifies carbon isotope mixing dynamics for discrete leaf wax *n*-alkane compounds as a function of mixing of *n*-alkanes derived from terrestrial vegetation and aquatic macrophytes. We first estimated contributions of terrestrial vegetation and aquatic macrophytes to a temporally and spatially integrated lacustrine sedimentary record. To do this, we used leaf wax *n*-alkane molecular distributions and calculated the metric proportion aquatic (P_{aq}); the relative abundance of mid-chain *n*-alkanes to long-chain *n*-alkanes. $\delta^{13}C$ values of discrete *n*-alkane homologs were then measured and compared to P_{aq} for each sample. We find that in lacustrine systems, $\delta^{13}C$ values of mid- and some long-chain *n*-alkanes (C23-C29) are likely to be strongly impacted by mixing between C3 terrestrial and non-emergent aquatic macrophyte-derived *n*-alkanes. In contrast, $\delta^{13}C$ values of very long chain (C31, C35) *n*-alkanes integrated in sediments are found to be least affected by this isotopic mixing. In lacustrine geological archives where there is significant input of *n*-alkanes from aquatic macrophytes, $\delta^{13}C$ values of the very long chain *n*-alkanes will provide the most robust quantification of *n*-alkane inputs from C3 and C4 plants.

Key words

Leaf wax; *n*-alkane; compound-specific; isotopes; carbon; terrestrial; aquatic; vegetation

1 Introduction

$\delta^{13}C$ values of plant derived carbon preserved in sedimentary archives hold great potential as a tool for reconstructing past vegetation dynamics (Diefendorf et al., 2011; Diefendorf and Freimuth, 2017). Mixing of inputs from terrestrial vegetation using different photosynthetic pathways will affect the $\delta^{13}C$ signature of plant derived carbon in sedimentary record, as a result of C4 plants being enriched in ^{13}C (Collister et al., 1994). However, another possible control on the $\delta^{13}C$ signature of plant derived carbon in sediments is mixing of inputs from C3 terrestrial and non-emergent aquatic macrophytes (hereafter aquatic macrophytes) (Naafs et al., 2019). Aquatic macrophytes are generally enriched in ^{13}C, as a result of complexity in the carbon assimilation pathway of these plants. Many aquatic macrophytes have evolved the ability to assimilate carbon from dissolved HCO_3^- along with assimilation of CO_2 during photosynthesis, with HCO_3^- being more ^{13}C enriched than CO_2 by ~7-11 ‰ (Keeley, 1990). In addition, assimilation of carbon from CO_2 by aquatic macrophytes is likely to be affected by the greater diffusional resistance of an aquatic compared to an aerial environment, influencing the $\delta^{13}C$ signature of sedimentary *n*-alkanes derived from aquatic macrophytes (Keeley and Sandquist, 1992). As such, problems may arise in the interpretation of proportional changes in photosynthetic pathway from geological records where there is a significant contribution of plant derived carbon from aquatic macrophytes (Aichner et al., 2010; Liu and Liu, 2016).

There is potential for this problem to be overcome through measurement of $\delta^{13}C$ values from cuticular leaf wax compounds preserved in geological archives (Mead et al., 2005; Aichner et al., 2010). Among these organic compounds are highly recalcitrant and long-lived *n*-alkyl lipids including leaf wax *n*-alkanes (Eglinton and Logan, 1991; Diefendorf et al., 2011; Diefendorf and Freimuth, 2017). Mid- to long-chain (C21-C35)

leaf wax *n*-alkanes are biosynthesized by both terrestrial plants and aquatic macrophytes (Eglinton and Hamilton, 1967; Chikaraishi and Naraoka, 2003). There is however strong evidence to suggest variation in *n*-alkane distributions between these groups (Fig. 1). In general, terrestrial plants produce *n*-alkane distributions with long-chain (C29-C33) abundance maxima (Ficken et al., 2000; Chikaraishi and Naraoka, 2003; Bush and McInerney, 2013; Diefendorf and Freimuth, 2017). Conversely, aquatic macrophytes in lacustrine environments are found to produce *n*-alkane distributions with mid-chain (C21-C25) abundance maxima (Ficken et al., 2000; Aichner et al., 2010; Gao et al., 2011) (Fig. 1). Still, there is some crossover in *n*-alkane production between terrestrial plants and aquatic macrophytes (Liu and Liu, 2016; Pu et al., 2018).

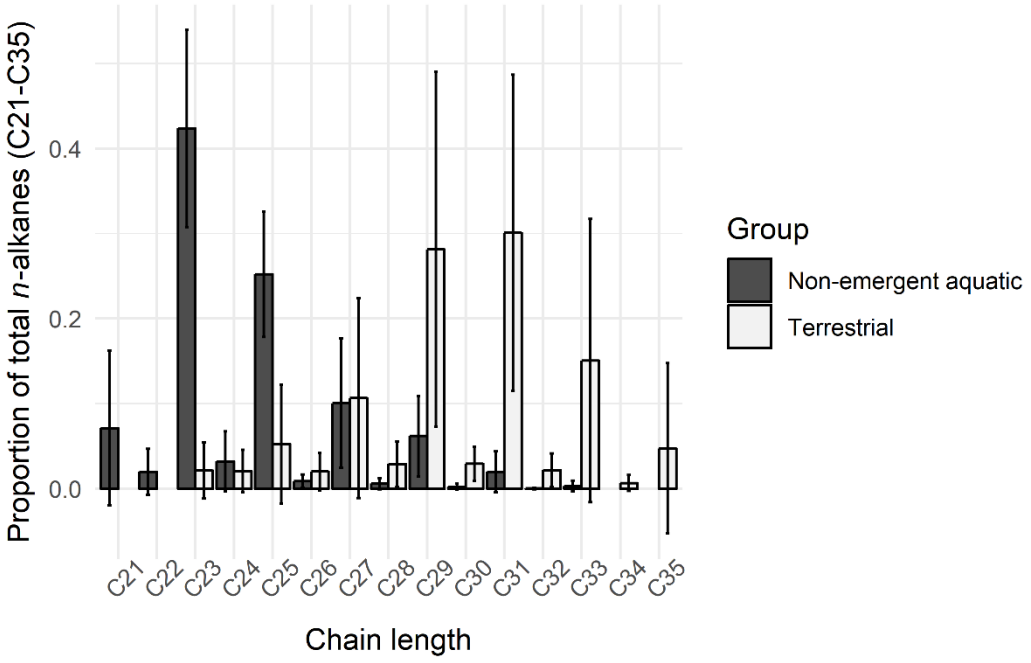

Figure 1. Individual *n*-alkane compounds as an average proportion of total *n*-alkane concentration (C21-C35) for non-emergent aquatic macrophytes (*n* = 58) and terrestrial plants (*n* = 383), illustrating the difference in dominant chain length production between these groups, with some crossover. Error bars reflect one standard deviation from the mean. Terrestrial plant data from Diefendorf and Freimuth (2017). non-emergent aquatic macrophyte data compiled from Aichner et al. (2010) and Liu and Liu (2016).

Total *n*-alkane production between terrestrial plants and aquatic macrophytes is found to be relatively similar on average (Fig. 2). As such, inputs to sedimentary records should be minimally biased by *n*-alkane production between these plant groups. The ratio of mid-chain (i.e. C23 and C25) to long-chain (i.e. C29 and C31) *n*-alkanes in sedimentary records can therefore be considered a robust proxy for quantifying the relative input of *n*-alkanes from terrestrial and aquatic macrophyte sources. Ficken et al. (2000) designated this ratio as proportion aquatic (P_{aq}).

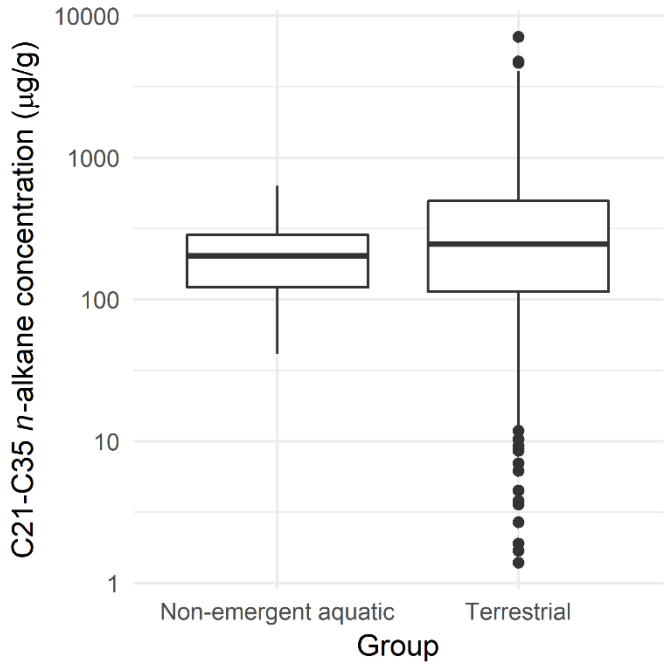

Figure 2. Box and whisker plots showing total *n*-alkane concentration (C21-C35) for non-emergent aquatic macrophytes (*n* = 58) and terrestrial plants (*n* = 383), illustrating similar total abundance of *n*-alkanes produced by each of the groups. Note, data is plotted on a logarithmic scale, with outliers indicated by black symbols. Terrestrial plant data from Diefendorf and Freimuth (2017), and non-emergent aquatic macrophyte data compiled from Aichner et al. (2010) and Liu and Liu (2016).

The distinct molecular distributions and $\delta^{13}C$ values of these different vegetation groups should result in different *n*-alkane homologs displaying different sensitivity to isotopic mixing in a sedimentary environment with mixed C3 terrestrial and aquatic

94 macrophyte derived *n*-alkane inputs. $\delta^{13}C$ values of mid-chain (C23,C25) *n*-alkanes in a
95 record of mixed inputs should predominantly reflect the aquatic macrophyte component.
96 As such, mid-chain *n*-alkanes should be systematically enriched in ^{13}C, even where C3
97 terrestrial vegetation derived *n*-alkane inputs to the sediment are high. Conversely, it can
98 be hypothesized that $\delta^{13}C$ values of long-chain (C29-C35) *n*-alkanes will predominantly
99 reflect C3 terrestrial vegetation inputs, with these homologs depleted in ^{13}C even where
100 aquatic macrophyte inputs are high. $\delta^{13}C$ values of the C27 *n*-alkane should display the
101 strongest isotopic mixing, given similar production by both aquatic macrophytes and C3
102 terrestrial vegetation (Fig. 3).

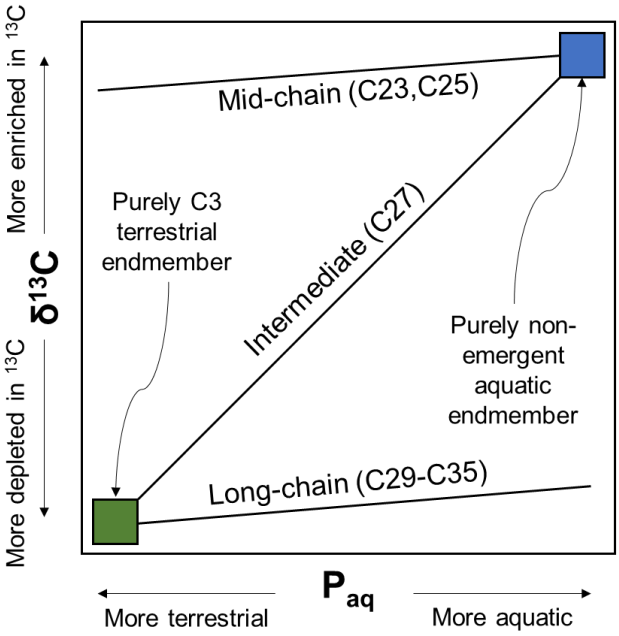

Figure 3. Schematic of relationships between P_{aq} and $\delta^{13}C$ values for different *n*-alkane homologs in a lacustrine sedimentary record, given differences in molecular distribution between C3 terrestrial plants and non-emergent aquatic macrophytes. Boxes indicate hypothetical end-members for purely non-emergent aquatic macrophyte and purely C3 terrestrial vegetation inputs.

103 This study uses a Pleistocene lacustrine sedimentary record from south-eastern

Australia to test these hypotheses at a single site through time in a natural laboratory framework. Here, we estimate terrestrial aquatic macrophyte inputs using *n*-alkane molecular distributions (P_{aq}). Values of $\delta^{13}C$ for discrete *n*-alkane homologs are quantified along with P_{aq} estimates of varying contributions of terrestrial plants and aquatic macrophytes in order to elucidate the degrees of carbon isotopic mixing for different *n*-alkane chain lengths.

2 Materials and methods

2.1 Site information

Garvoc palaeo-lake is a geomorphologically old volcanic maar crater infilled with semi-lithified organic rich (>20%) clays, sands and tuff beds, located in Victoria, Australia (Kershaw, 1997; Kershaw et al., 2014). The site was rotary drilled in 1992-1993, with ~100 m of sediment recovered (Kale Sniderman, pers. comm.). Fission track dating of zircons from volcanic tuff beds provided two preliminary ages of 840,000 ± 100,000 and 930,000 ± 120,000, suggesting the record was likely deposited through the middle Pleistocene (Kershaw et al., 2014).

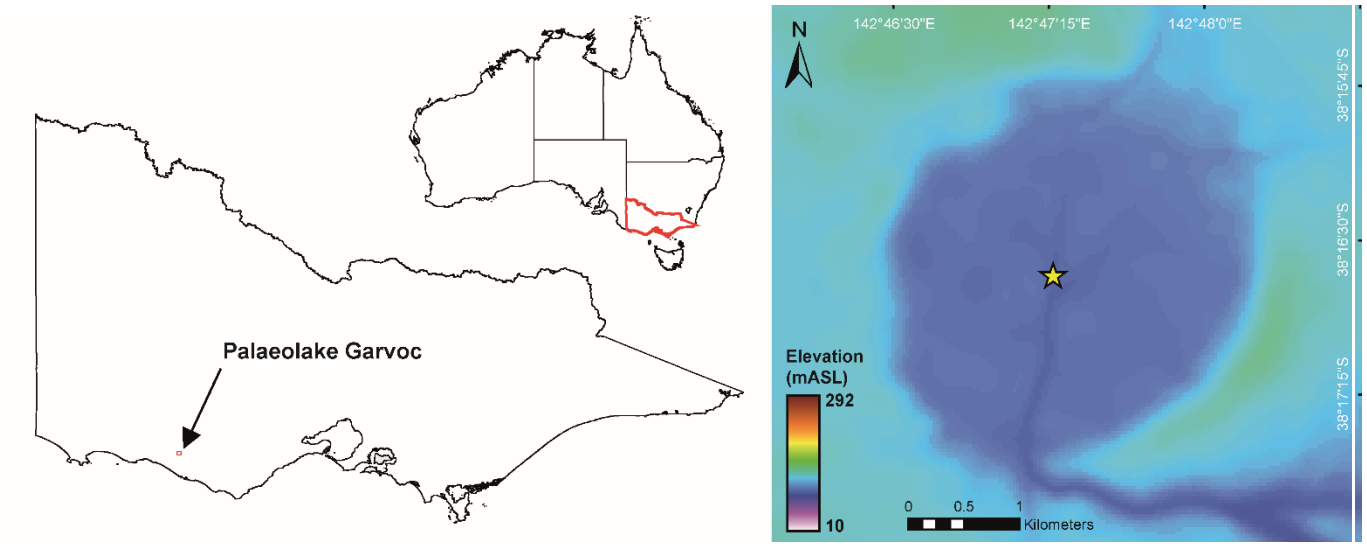

Figure 4. Map of study site Location of Garvoc palaeo-lake in Victoria, Australia (38°16'40.3" S, 142°47'16.25" E) with a digital elevation model indicating the maar crater extent. (Commonwealth of Australia (Geoscience Australia), 2018). The yellow star indicates the site of core collection (Kale Sniderman, pers. comm.).

2.2 Sample preparation

Thirty sample splits from the core were prepared for organic geochemical analysis. All utensils and apparatus that were in contact with samples during preparation were thoroughly cleaned or ashed (425 °C, 9hrs) between each sample. Cleaning consisted of washing with 10% Decon 90® in water followed by three rinses of reverse osmosis water, and three rinses each of methanol, dichloromethane (DCM) and *n*-hexane. Approximately 0.5 cm of the outer surface of each sample was removed to minimize contamination. Samples were lyophilized in ashed borosilicate glass containers, before homogenization in a Retsch MM 400 ball mill (15 sec mill time at 30 Hz).

Total lipids were extracted from between 4.56 g and 16.51 g of sedimentary material (mean: 10 g) using a Thermo Scientific™ Dionex™ ASE™ 350. Samples underwent five cycles of solvent rinse (five minute static rinse with 9:1 DCM:methanol)

and purge (two minutes) at a temperature of 100 ^{o}C and a pressure of ~110 bar. Solvents were evaporated from the total lipid extract (TLE) at 50 ^{o}C under ultra-high purity (99.999%, BOC) nitrogen gas (N_2) using a Biotage TurboVap® LV heated evaporator. For 16 of the 30 samples, TLE was quantitatively diluted by mass to ensure that columns were not overloaded during compound separation. TLE was separated into three compound classes (aliphatic, ketone/ester and polar), by short column solid phase extraction through 0.5 g of solvent cleaned and oven activated (100 ^{o}C, 24hrs) silica gel of 35 to 70 mesh size (Acros Organics; 240360010) using 4 mL each of *n*-hexane (F1), DCM (F2) and methanol (F3), respectively. A small amount of copper turnings was added to each aliphatic fraction (F1Cu) prior to separation of saturated and unsaturated aliphatic compounds to remove elemental sulfur. Saturated and unsaturated compounds in the aliphatic fraction were separated by short column solid phase extraction through 0.5 g of oven activated (100 ^{o}C, 8hrs) silver nitrate ($AgNO_3$) impregnated (10% w/w) silica gel of 230 mesh size (Sigma Aldrich; 248762-50G), using 4 mL of *n*-hexane and ethyl acetate, respectively. Prior to elution of samples, columns were rinsed with 4 mL *n*-hexane. Throughout dry packing, oven activation, and compound separation, $AgNO_3$ short columns were wrapped in ashed aluminum foil and the laboratory lights were dimmed to prevent silver photooxidation (methodology after Uno et al., 2016).

2.3 *n*-Alkane characterization and quantitation

n-Alkanes (C15 to C36) in the saturated aliphatic fraction were characterized and quantified on an Agilent 7890B GC with a 15m DB-5 HT column, coupled to an Agilent 5977B MSD. Samples were dissolved in 100 µL *n*-hexane spiked with 10 µg mL^{-1} 1-1' binaphthyl as internal standard. Quantitation standards were prepared by dilution of a Certified Reference Material (C7-C40 Saturated Alkanes Standard, Supelco 49452-U) to a concentration of 10 µg mL^{-1} with 10 µg mL^{-1} 1-1' binaphthyl as internal standard for

concurrent analysis with the sample batch. A 1 μL aliquot of sample was injected and split at a 10:1 ratio to avoid column saturation. Total helium carrier gas flow across the run was at a rate of 14 mL min^{-1}. Initial GC oven temperature was 50 ^{o}C, held for 1 min, prior to a temperature ramp of 10 ^{o}C min^{-1} to 320 ^{o}C, held for 7 min. Following a solvent delay of 8.5 min, data was collected in full scan mode from 45 Da to 600 Da at a scan speed of 5 scans sec^{-1}. *n*-Alkane concentrations were quantitatively adjusted for any dilution that took place prior to short column solid phase extraction. The concentration of each compound in a sample is reported as the total mass of that compound per gram of sample that underwent lipid extraction.

2.4 Calculation of *n*-alkane distribution indexes

Indexes of *n*-alkane distribution were calculated to examine the distribution of *n*-alkanes in samples, including carbon preference index (CPI), average chain length (ACL), Norm33 and proportion aquatic (P_{aq}). Carbon preference index (CPI) is the concentration weighted ratio of odd to even *n*-alkane chain lengths (C26-C36). It is utilized to quantify the source of long-chain *n*-alkanes (higher plant derived or other), as well as the possibility of post-depositional modification of *n*-alkanes in a sedimentary record, and is calculated as follows after Bray and Evans (1961):

$$\mathrm{CPI} = 0.5\left[\left[\frac{(\mathrm{C27} + \mathrm{C29} + \ldots + \mathrm{C35})}{(\mathrm{C26} + \mathrm{C28} + \ldots + \mathrm{C34})}\right] + \left[\frac{(\mathrm{C27} + \mathrm{C29} + \ldots + \mathrm{C35})}{(\mathrm{C28} + \mathrm{C30} + \ldots + \mathrm{C36})}\right]\right]$$

Where C*n* is the total mass of a given compound in a sample.

Average chain length (ACL) is the concentration weighted mean of long-chain *n*-alkanes (C27-C35), and is calculated as follows, after Bush and McInerney (2015):

$$\mathrm{ACL} = [(27 \times \mathrm{C27}) + (29 \times \mathrm{C29}) \ldots + (35 \times \mathrm{C35})]/[\mathrm{C27} + \mathrm{C29} + \ldots + \mathrm{C35}]$$

Where C*n* is the total mass of a given compound in a sample.

Norm33 is the normalized ratio of the concentration of the C33 to the C29 *n*-alkane homolog. Where CPI suggests a dominant higher plant source of long-chain *n*-alkanes in a sedimentary record, it is used as a proxy for the relative contributions of grass and tree leaf wax *n*-alkanes. Higher values indicate larger contributions of grass derived *n*-alkanes. It is calculated as follows, after Howard et al. (2018):

$$\text{Norm33} = \frac{\text{C33}}{\text{C29} + \text{C33}}$$

Where C*n* is the total mass of a given compound in a sample.

P_{aq} quantifies the relative contributions of aquatic macrophytes to terrestrial higher plant *n*-alkanes to a sedimentary record. It is calculated as follows (Ficken et al., 2000):

$$P_{aq} = \frac{\text{C23} + \text{C25}}{\text{C29} + \text{C31} + \text{C23} + \text{C25}}$$

Where C*n* is the total mass of a given compound in a sample.

2.5 Leaf wax *n*-alkane δ^{13}C analysis

Carbon isotope ratios were measured with gas chromatography-isotope ratio mass spectrometry (GC-IRMS) using a Thermo Trace GC Ultra coupled to a Thermo Scientific Delta V Plus IRMS through a GC-C III interface at Northwestern University. For carbon isotope measurements, samples were dissolved in 90-150 μL of *n*-hexane and injected at a volume of between 3 and 7 μL into a PTV inlet. The inlet was held split-less at 65 ºC during injection, before being ramped to 330 ºC during the transfer phase. Samples were chromatographically separated on a ZB-MS5 column (10 m, 0.1 μm film thickness) using

194 helium carrier gas at a flow rate of 1.4 mL/min, with the oven ramped from 65 ºC to 330
195 ºC at a rate of 6.3 ºC/min. GC effluent was combusted in a reactor consisting of two
196 strands each of 0.1 mm copper, nickel and platinum wire in a 0.58mm fused silica capillary
197 held at 940 ºC. Complete combustion of compounds was ensured with a trace O_2 bleed.
198 Samples were run in duplicate, and a standard mixture of *n*-alkanes with known $\delta^{13}C$
199 values (A6; acquired from Arndt Schimmelmann, Indiana University) was injected every
200 three samples at a volume of 1 μL for CO_2 tank calibration. Linearity of $\delta^{13}C$ across the
201 sample run was assessed by periodic injection of A6 in variable volume (0.6, 1, 2 and 4
202 μL). Average $\delta^{13}C$ values versus peak intensities of C21-C30 in A6 were used as
203 correction factors for peaks within the range <12V. Compound specific $\delta^{13}C$ values are
204 reported to the Vee Pee Dee Belemnite (VPDB) scale. Reported *n*-alkane $\delta^{13}C$ values are
205 means of replicates, with associated standard deviations from the mean.

206 **3 Results**

207 **3.1 *n*-Alkane quantification**

208 *n*-Alkanes are abundant throughout the record, with the summed concentration of
209 mid chain homologs (C23-C25) ranging from 0.098 to 9.31 μg/g dry sediment and that of
210 long-chain *n*-alkane homologs (C27-C35) ranging from 0.54 to 41.93 μg/g dry sediment.
211 Values of CPI are markedly high, ranging from 12.25 to 34.71, indicating a high odd-over-
212 even predominance of long-chain *n*-alkanes throughout the record. These values of CPI
213 indicate a predominantly higher vegetation source of *n*-alkanes in this record, as opposed
214 to petrogenic sources (Bray and Evans, 1961; Bush and McInerney, 2013). Values of ACL
215 range from 29.16 to 31.5, while those of Norm33 range from 0.22 to 0.8, with both
216 showing a generally decreasing pattern across the record. Values for P_{aq} range from 0.051
217 to 0.73 and generally increase in the upper part of the record (Fig. 2).

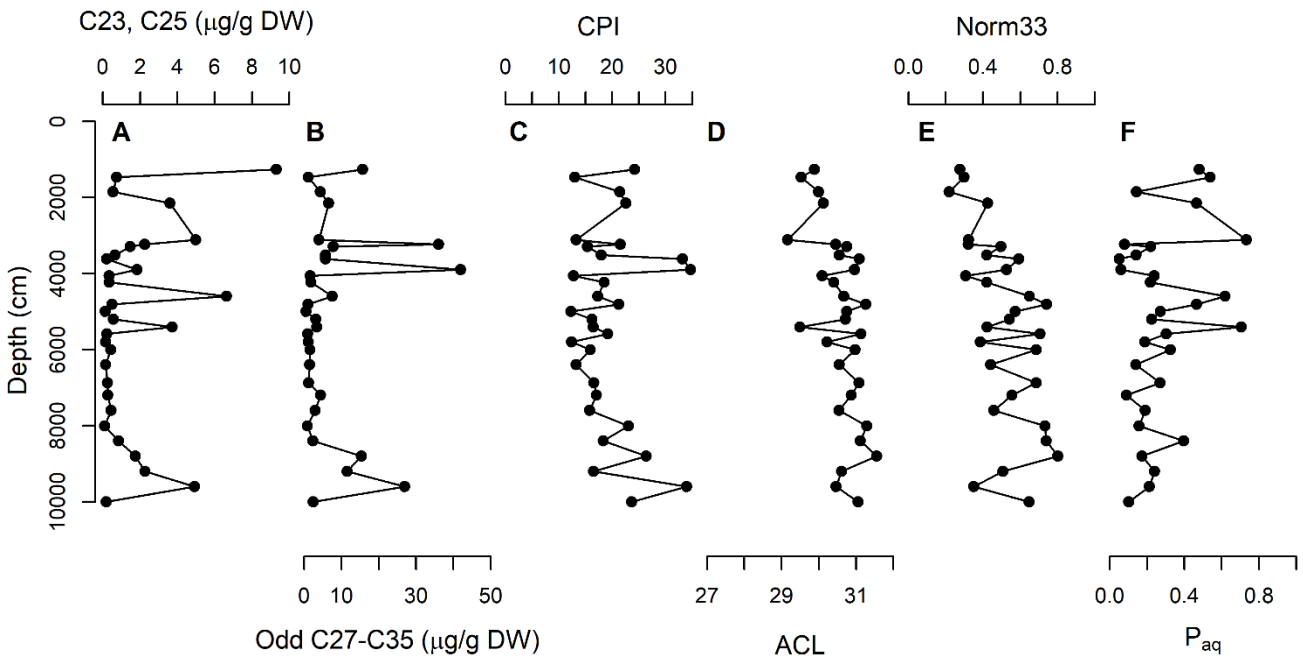

Figure 2. Garvoc palaeo-lake leaf wax *n*-alkane concentration and molecular distribution a) Summed concentration of C23 and C25 *n*-alkanes in samples, derived primarily from non-emergent aquatic macrophytes. b) Summed concentration of odd *n*-alkane homologs from C27 to C35 in samples, derived primarily from terrestrial higher plants. c) Carbon preference index indicating odd-over-even predominance of *n*-alkanes, d) average chain length, e) normalized ratio of the C33 to the C29 *n*-alkane, and f) proportion aquatic.

3.2 Leaf wax *n*-alkane $\delta^{13}C$

Leaf wax *n*-alkane $\delta^{13}C$ measurements are reported for odd *n*-alkane homologs from C23-C35 (Fig. 3). $\delta^{13}C_{C23}$ values range from -30.37 to -18.87‰, $\delta^{13}C_{C25}$ from -31.48 to -19.69‰, $\delta^{13}C_{C27}$ from -32.55 to -21.77‰, $\delta^{13}C_{C29}$ from -34.13 to -25.07‰, $\delta^{13}C_{C31}$ from -33.54 to -28.85‰, $\delta^{13}C_{C33}$ from -34.11 to -31.07‰ and $\delta^{13}C_{C35}$ from -34.74 to -30.66‰. Variability in $\delta^{13}C$ across the record generally decreases with increasing chain length.

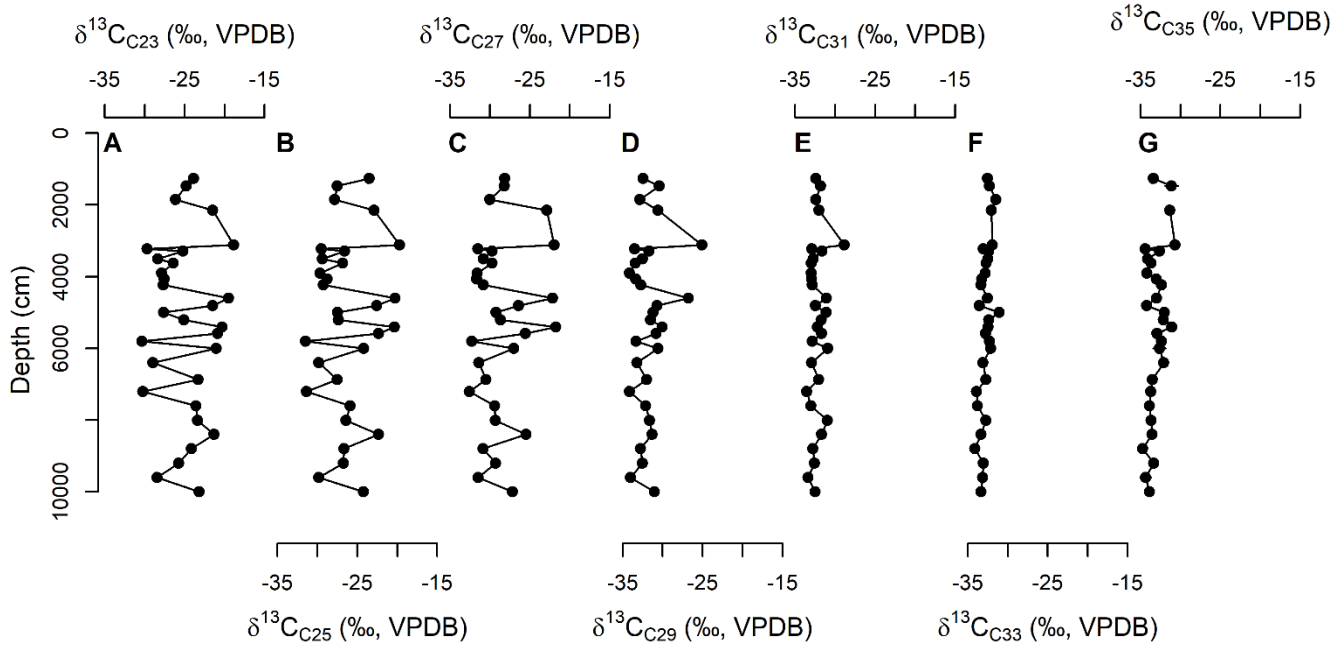

Figure 3. Depth series of $\delta^{13}C$ values measured for a) C23, b) C25, c) C27, d) C29, e) C31, f) C33 and g) C35 *n*-alkanes. Error bars reflect one standard deviation from the mean, and in many cases are smaller than the size of the symbol.

3.3 Relationship between P_{aq} and *n*-alkane $\delta^{13}C$

Statistically significant linear relationships between P_{aq} and $\delta^{13}C$ values are observed for all *n*-alkanes analyzed except for C33 (Fig. 4, Table 1). The relationships between P_{aq} and $\delta^{13}C$ values are strongest for the mid-chain *n*-alkanes chain lengths, generally becoming weaker for longer chain *n*-alkane homologs (Table 1).

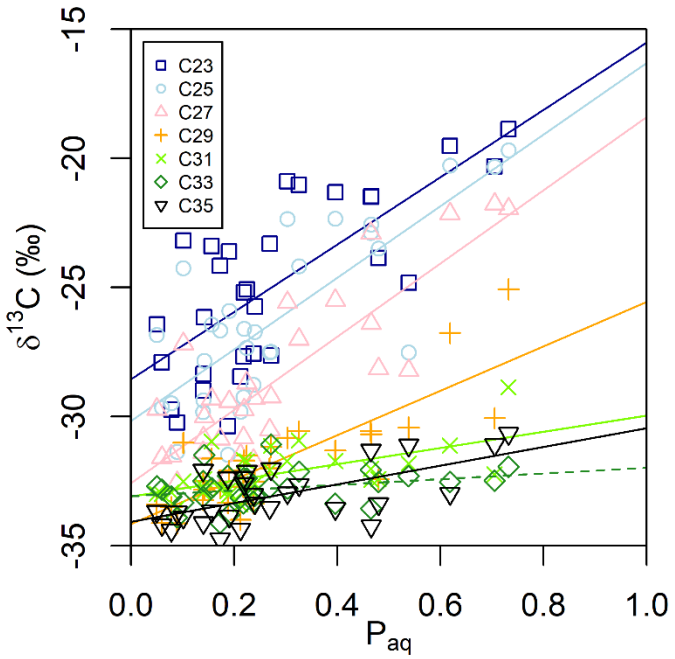

Figure 4. Least-square linear regressions of P_{aq} versus $\delta^{13}C$ values of odd *n*-alkane homologs (C23-C35). Solid lines represent statistically significant linear correlation between variables, while dashed represents a linear correlation that is not statistically significant.

Compound	Correlation coefficient	p-value	Linear equation
C23	0.73	<0.01	13x - 28.6
C25	0.78	<0.01	13.9x - 30.2
C27	0.84	<0.01	14.2x - 32.6
C29	0.81	<0.01	8.6x - 34.2
C31	0.61	<0.01	3.1x - 33.1
C33	0.3	0.11	1.1x - 33.1
C35	0.62	<0.01	3.6x - 34.1

Table 1. Correlation and least-square linear regression equations of relationships between P_{aq} and each odd *n*-alkane homolog from C23-C35 in samples from Garvoc palaeo-lake.

4 Discussion

n-Alkanes in lacustrine sediments can be derived from a complex mixture of terrestrial plants and aquatic macrophytes (Ficken et al., 2000; Aichner et al., 2010). C3 terrestrial vegetation and aquatic macrophytes show distinct *n*-alkane molecular distributions and $\delta^{13}C$ values (Keeley and Sandquist, 1992; Ficken et al., 2000; Liu and Liu, 2016). As such, mixing of *n*-alkanes derived from C3 terrestrial and aquatic

macrophytes should theoretically result in different *n*-alkane homologs reflecting varying degrees of isotopic mixing (Aichner et al., 2010). There is potential for this isotopic mixing to be misinterpreted in palaeo-vegetation reconstructions as a C4 vegetation signal, due to aquatic macrophytes and C4 plants being similarly enriched in ^{13}C. There has, however, been limited quantification of the degree to which this isotopic mixing varies across different *n*-alkane homologs in lake sediments, and whether specific *n*-alkanes are less likely to be impacted.

Here, we investigated the impact of mixing C3 terrestrial vegetation and aquatic macrophyte derived *n*-alkanes on $\delta^{13}C$ values of discrete *n*-alkane compounds in a lacustrine sedimentary record. Because terrestrial C4 vegetation and aquatic macrophytes are observed to be similarly enriched in ^{13}C (Keeley and Sandquist, 1992), a system that is dominated by C3 terrestrial vegetation inputs is required to test the hypotheses outlined. Terrestrial plant derived *n*-alkanes in this record appear to have been predominantly biosynthesized by vegetation using the C3 photosynthetic pathway. The longest chain length *n*-alkanes (C31, C33 and C35) in sediments of Garvoc palaeo-lake are all relatively depleted in ^{13}C, suggesting predominantly C3 terrestrial plant inputs (Collister et al., 1994). This interpretation is supported by consistency in $\delta^{13}C$ values for each of these *n*-alkane chain lengths. In a number of regions, grasses are found to produce higher proportions of longer chain lengths (C31, C33) than trees, which produce higher proportions of C29 (Bliedtner et al., 2018; Howard et al., 2018). As a large proportion of C4 plant species are grasses (Edwards et al., 2010), longer chain-lengths should be more sensitive to the presence of C4 on the landscape than C29 (Andrae et al., 2018). If terrestrial C4 vegetation derived *n*-alkanes were a significant contributor to the Garvoc palaeo-lake record, C33 should be substantially more enriched in ^{13}C than C29. Here, this pattern of ^{13}C enrichment is not observed. This interpretation is also reasonable given the location of the record, with

modern C4 plant abundance on the landscape minimal in south-eastern Australia (Hattersley, 1983; Murphy and Bowman, 2007; Andrae et al., 2018).

It was hypothesized that mid-chain *n*-alkanes would be consistently enriched in ^{13}C throughout the record, even for periods when C3 terrestrial plants dominate the *n*-alkane input (low P_{aq}), due to the dominant production of these homologs by aquatic macrophytes (Fig. 1). In contrast, long-chain (C29-C35) *n*-alkanes were hypothesized to be consistently depleted in ^{13}C, even for periods of high aquatic macrophyte input (high P_{aq}). $\delta^{13}C$ values of the C27 *n*-alkane were expected to display the strongest isotopic mixing, because of the similar production by both aquatic macrophytes and C3 terrestrial vegetation (Fig.1). The observed variations in carbon isotope ratios of *n*-alkanes in relation to P_{aq} is found to be generally consistent with the hypotheses of the study. The long-chain *n*-alkanes (C31-C35) are depleted in ^{13}C, even where inputs from aquatic macrophytes are high. However, the statistically significant linear correlations between P_{aq} and $\delta^{13}C$ values for most of these chain-lengths (except for C33) suggests that there is a small degree of carbon isotope mixing of *n*-alkanes derived from aquatic macrophytes, even for the longest chain *n*-alkane homologs. The slopes of the linear relationships generally decrease as chain length increases, suggesting aquatic macrophyte sourced *n*-alkanes minimally impact on the isotopic signature of the longest chain *n*-alkanes (i.e. C31, C35). Additional impacts of climatological factors like water stress on $\delta^{13}C$ variability of the long-chain *n*-alkanes cannot be discounted (Kohn, 2010), and could contribute to the observed variations in the longest chain-lengths. Though relatively stable, average chain length (ACL) and Norm33 each show a slight decrease toward to upper part of the record. These results are likely to reflect an increase in terrestrial *n*-alkane inputs from trees relative to grasses (Howard et al., 2018). While non-woody C3 plants can be slightly more enriched in ^{13}C than their

284 woody counterparts (Magill et al., 2013), there is little indication that variability in long-
285 chain *n*-alkane $\delta^{13}C$ values are systematically influenced by this here (Fig. 3).

286 Carbon isotopic mixing between aquatic macrophyte and terrestrial vegetation
287 sourced *n*-alkanes is observed to be most sensitive for the C27 homolog, as demonstrated
288 by the steepest linear relationship between P_{aq} and $\delta^{13}C$ values and highest correlation
289 coefficient (Table 1). The high degree of carbon isotopic mixing for the C27 *n*-alkane
290 supports our hypothesis, and reflects the significant production of this compound by both
291 terrestrial plants and aquatic macrophytes (Aichner et al., 2010; Liu and Liu, 2016;
292 Diefendorf and Freimuth, 2017). In contrast, the relatively steeply sloping linear
293 relationship between P_{aq} and values of $\delta^{13}C_{C29}$ is inconsistent with the C29 *n*-alkane being
294 produced predominantly by C3 terrestrial vegetation (Ficken et al., 2000; Chikaraishi and
295 Naraoka, 2003). Our results suggest that $\delta^{13}C_{C29}$ values may reflect significant isotopic
296 mixing between C3 terrestrial vegetation and aquatic macrophyte sources. Recent work has
297 indicated the potential for significant production of the C29 *n*-alkane by aquatic
298 macrophytes (Liu and Liu, 2016). Our results provide additional evidence that aquatic
299 macrophyte contributions of C29 *n*-alkanes to lacustrine sedimentary records could be
300 greater than previously estimated (e.g. Chikaraishi and Naraoka, 2003).

301 Linear correlations between P_{aq} and $\delta^{13}C$ values of the mid-chain *n*-alkanes (C23,
302 C25) are strong, statistically significant and show steep slopes. From this, a high degree of
303 isotopic mixing between C3 terrestrial plant and aquatic macrophyte derived C23 and C25
304 is interpreted. This is inconsistent with the hypothesis of mid-chain *n*-alkanes being
305 systematically ^{13}C enriched, even where aquatic macrophyte inputs are low. One
306 explanation for this discrepancy is higher production of ^{13}C depleted mid-chain *n*-alkanes
307 by terrestrial vegetation than previous studies have suggested (Fig. 1). Recent work has

demonstrated that in some cases, higher terrestrial plants can produce *n*-alkane distributions with mid-chain abundance maxima (Diefendorf and Freimuth, 2017; Pu et al., 2018; Struck et al., 2019). A lack of reporting of mid-chain *n*-alkane quantification from many studies examining terrestrial plant *n*-alkane distributions is likely to limit or bias our appreciation of this (Diefendorf and Freimuth, 2017). Another possible explanation for this discrepancy is variability in the carbon isotope ratios of dissolved inorganic carbon (DIC) related to variability in primary productivity, particularly by algae (Aichner et al., 2010). Periods of lower primary productivity in the lake are likely to create conditions of HCO_3^- excess (Leng and Marshall, 2004; Aichner et al., 2010). In this scenario, the DIC pool from which aquatic plants assimilate carbon (comprised primarily of HCO_3^-) will be relatively depleted in ^{13}C, resulting in more negative values of $\delta^{13}C$ for the mid-chain *n*-alkanes than for limiting conditions. More work is required to elucidate the exact mechanism for $\delta^{13}C$ variability of the sedimentary mid-chain *n*-alkanes. If mid-chain *n*-alkane $\delta^{13}C$ values strongly reflect DIC pool $\delta^{13}C$ variability, then $\delta^{13}C$ values of these homologs may prove an important tool for reconstructing primary productivity of lacustrine systems (Aichner et al., 2010; Castañeda and Schouten, 2011).

$\delta^{13}C$ values of long-chain *n*-alkanes (C29-C35) preserved in geological archives are regularly used for reconstructing proportions of photosynthetic pathway on the landscape (Eglinton and Eglinton, 2008; Castañeda and Schouten, 2011). The results of this study suggest that in lacustrine geological archives, ^{13}C enrichment observed for the C29 *n*-alkane is likely to reflect both *n*-alkane contributions from aquatic macrophytes and from terrestrial vegetation. Our results affirm the observations of Aichner et al. (2010), and have implications for the use of compound specific $\delta^{13}C$ values for vegetation reconstructions. In geological archives where significant input from aquatic macrophytes can be expected (e.g. lacustrine systems), care should be taken to assess the potential effects of mixing by

comparing $\delta^{13}C$ values of different homologues with P_{aq}, as done in this study. The practice of taking amount-weighted averages of *n*-alkane isotope data in lake records with mixed carbon sources is likely to obscure variable impacts of isotopic mixing on different chain-lengths and lead to spurious interpretations. Using $\delta^{13}C$ values of only the longest chain sedimentary *n*-alkanes ($\geq$ C31) should provide records with the least influence of aquatic vegetation and enable interpretation of changes in photosynthetic pathway abundance on the landscape. Building on previous work (Huang et al., 2004; Hou et al., 2007; Gao et al., 2011), our results also demonstrate the potential for δD values of mid- and even some long-chain leaf wax *n*-alkanes to more strongly reflect lake water than precipitation. This has significant implications for the interpretation of changes in precipitation isotopes using leaf wax *n*-alkane δD from lacustrine geological archives, particularly in the context of the use of homologs like C27 and C29. It is worth noting that these results have limited implications for depositional settings where terrestrial vegetation derived *n*-alkane inputs dominate, such as marine sedimentary archives. Our results reaffirm the benefit of sedimentary compound specific isotope analysis as a tool for disentangling and reconstructing vegetation structure and climate from records with complex mixing of organic matter sources.

5 Conclusions

Similar $\delta^{13}C$ signatures are found between aquatic macrophyte and C4 derived OM. As a result, problems may arise in the interpretation of proportion of photosynthetic pathway on the landscape from OM $\delta^{13}C$ values in records with significant aquatic macrophyte inputs. Because *n*-alkane distributions differ between aquatic macrophytes and terrestrial plants, compound specific $\delta^{13}C$ values of *n*-alkanes hold potential for overcoming this issue. Here, we find $\delta^{13}C$ values of most mid- and some long-chain *n*-alkanes (C23-C29) in the lacustrine sediments of our record indicate significant degrees of

isotopic mixing between C3 terrestrial plant and aquatic macrophyte derived *n*-alkanes. However, $\delta^{13}C$ values of mid-chain *n*-alkanes in lacustrine systems could also reflect variability in DIC pool $\delta^{13}C$ values. $\delta^{13}C$ values of the longest chain ($\geq$ C31) *n*-alkanes biosynthesized by plants and integrated in sediments will be least affected by isotopic mixing between vegetation groups or DIC pool $\delta^{13}C$ variability. These results have implications for the application of *n*-alkane compound specific $\delta^{13}C$ measurements for reconstructing aspects of palaeo-vegetation and palaeo-climate. The use of the longest chain *n*-alkanes (≥ C31) preserved in lacustrine sedimentary records will provide the most robust reconstructions of terrestrial vegetation and climate, particularly proportions of photosynthetic pathway on the landscape and isotope ratios of precipitation.

Acknowledgements

The authors declare no conflict of interest. Funding for this research was provided by a Royal Society of South Australia Small Research Grant awarded to J.W.A. and F.A.M., an Australian Research Council Future Fellowship (FT110100100793) awarded to F.A.M., and Australian Government Research Training Program and University of Adelaide Faculty of Sciences Divisional scholarships awarded to J.W.A. Thank you to Kale Sniderman (University of Melbourne) for providing access to samples. We sincerely thank Andrew L. Masterson (Northwestern University) for leaf wax *n*-alkane compound specific carbon isotope analysis. The authors declare no competing interests. All data required to understand and assess the conclusions of this study are available in the main text and supplementary materials.

References

Aichner, B., Herzschuh, U., Wilkes, H., 2010. Influence of aquatic macrophytes on the stable carbon isotopic signatures of sedimentary organic matter in lakes on the Tibetan Plateau. Organic Geochemistry 41, 706-718.

Andrae, J.W., McInerney, F.A., Polissar, P.J., Sniderman, J.M.K., Howard, S., Hall, P.A., Phelps, S.R., 2018. Initial expansion of C4 vegetation in Australia during the late Pliocene. Geophysical Research Letters 45, 4831-4840.

Bliedtner, M., Schäfer, I.K., Zech, R., von Suchodoletz, H., 2018. Leaf wax *n*-alkanes in modern plants and topsoils from eastern Georgia (Caucasus) – implications for reconstructing regional paleovegetation. Biogeosciences 15, 3927-3936.

Bray, E.E., Evans, E.D., 1961. Distribution of *n*-paraffins as a clue to recognition of source beds. Geochimica et Cosmochimica Acta 22, 2-15.

Bush, R.T., McInerney, F.A., 2013. Leaf wax *n*-alkane distributions in and across modern plants: implications for paleoecology and chemotaxonomy. Geochimica et Cosmochimica Acta 117, 161-179.

Bush, R.T., McInerney, F.A., 2015. Influence of temperature and C4 abundance on *n*-alkane chain length distributions across the central USA. Organic Geochemistry 79, 65-73.

Castañeda, I.S., Schouten, S., 2011. A review of molecular organic proxies for examining modern and ancient lacustrine environments. Quaternary Science Reviews 30, 2851-2891.

Chikaraishi, Y., Naraoka, H., 2003. Compound-specific δD–δ^{13}C analyses of *n*-alkanes extracted from terrestrial and aquatic plants. Phytochemistry 63, 361-371.

Collister, J.W., Rieley, G., Stern, B., Eglinton, G., Fry, B., 1994. Compound-specific δ^{13}C analyses of leaf lipids from plants with differing carbon dioxide metabolisms. Organic Geochemistry 21, 619-627.

Commonwealth of Australia (Geoscience Australia), 2018. Elevation Information System (ELVIS).

Diefendorf, A.F., Freeman, K.H., Wing, S.L., Graham, H.V., 2011. Production of *n*-alkyl lipids in living plants and implications for the geologic past. Geochimica et Cosmochimica Acta 75, 7472-7485.

Diefendorf, A.F., Freimuth, E.J., 2017. Extracting the most from terrestrial plant-derived *n*-alkyl lipids and their carbon isotopes from the sedimentary record: a review. Organic Geochemistry 103, 1-21.

Edwards, E.J., Osborne, C.P., Stromberg, C.A.E., Smith, S.A., 2010. The origins of C4 grasslands: integrating evolutionary and ecosystem science. Science 328, 587-591.

Eglinton, G., Hamilton, R.J., 1967. Leaf epicuticular waxes. Science 156, 1322-1335.

Eglinton, G., Logan, G.A., 1991. Molecular preservation. Philosophical Transactions - Royal Society of London B 333, 315-328.

Eglinton, T.I., Eglinton, G., 2008. Molecular proxies for paleoclimatology. Earth and Planetary Science Letters 275, 1–16.

Ficken, K.J., Li, B., Swain, D.L., Eglinton, G., 2000. An *n*-alkane proxy for the sedimentary input of submerged/floating freshwater aquatic macrophytes. Organic Geochemistry 31, 745-749.

Gao, L., Hou, J., Toney, J., MacDonald, D., Huang, Y., 2011. Mathematical modeling of the aquatic macrophyte inputs of mid-chain *n*-alkyl lipids to lake sediments: implications for interpreting compound specific hydrogen isotopic records. Geochimica et Cosmochimica Acta 75, 3781-3791.

Hattersley, P.W., 1983. The distribution of C3 and C4 grasses in Australia in relation to climate. Oecologia 57, 113-128.

Hou, J., Huang, Y., Oswald, W.W., Foster, D.R., Shuman, B., 2007. Centennial-scale compound-specific hydrogen isotope record of Pleistocene–Holocene climate transition from southern New England. Geophysical Research Letters 34.

Howard, S., McInerney, F.A., Caddy-Retalic, S., Hall, P.A., Andrae, J.W., 2018. Modelling leaf wax *n*-alkane inputs to soils along a latitudinal transect across Australia. Organic Geochemistry 121, 126-137.

Huang, Y., Shuman, B., Wang, Y., Webb, T., 2004. Hydrogen isotope ratios of individual lipids in lake sediments as novel tracers of climatic and environmental change: a surface sediment test. Journal of Paleolimnology 31, 363-375.

Keeley, J.E., 1990. Photosynthetic pathways in freshwater aquatic plants. Trends in Ecology & Evolution 5, 330-333.

Keeley, J.E., Sandquist, D.R., 1992. Carbon: freshwater plants. Plant, Cell & Environment 15, 1021-1035.

Kershaw, A.P., 1997. The potential for production of high resolution palynological records from the Early Pleistocene of Australia in: Leroy, S., Ravazzi, C. (Eds.), INTER-INQUA Colloquium, Ankara, Turkey.

Kershaw, A.P., Wagstaff, B.E., O'Sullivan, P.B., Sniderman, J.M.K., 2014. Nature, causes and impacts of the Mid-Pleistocene Transition in southeastern Australia AQUA Biennial Meeting, Mildura, Australia.

Kohn, M.J., 2010. Carbon isotope compositions of terrestrial C3 plants as indicators of (paleo)ecology and (paleo)climate. Proceedings of the National Academy of Sciences 107, 19691-19695.

Leng, M.J., Marshall, J.D., 2004. Palaeoclimate interpretation of stable isotope data from lake sediment archives. Quaternary Science Reviews 23, 811-831.

Liu, H., Liu, W., 2016. *n*-Alkane distributions and concentrations in algae, submerged plants and terrestrial plants from the Qinghai-Tibetan Plateau. Organic Geochemistry 99, 10-22.

Magill, C.R., Ashley, G.M., Freeman, K.H., 2013. Ecosystem variability and early human habitats in eastern Africa. Proceedings of the National Academy of Sciences 110, 1167-1174.

Mead, R., Xu, Y., Chong, J., Jaffé, R., 2005. Sediment and soil organic matter source assessment as revealed by the molecular distribution and carbon isotopic composition of *n*-alkanes. Organic Geochemistry 36, 363-370.

Murphy, B.P., Bowman, D.M.J.S., 2007. Seasonal water availability predicts the relative abundance of C3 and C4 grasses in Australia. Global Ecology and Biogeography 16, 160-169.

Naafs, B.D.A., Inglis, G.N., Blewett, J., McClymont, E.L., Lauretano, V., Xie, S., Evershed, R.P., Pancost, R.D., 2019. The potential of biomarker proxies to trace climate, vegetation, and biogeochemical processes in peat: a review. Global and Planetary Change 179, 57-79.

Pu, Y., Cao, J., Jia, J., Shao, X., Han, Y., 2018. Unusual hydrocarbon waxes detected in *Salix oritrepha* leaf from Nianbaoyeze Mountains, eastern Qinghai-Tibetan Plateau. Journal of Mountain Science 15, 2445-2452.

Struck, J., Bliedtner, M., Strobel, P., Schumacher, J., Bazarradnaa, E., Zech, R., 2019. Leaf wax *n*-alkane pattern and compound-specific $\delta^{13}C$ of plants and topsoils from semi-arid Mongolia. Biogeosciences Discuss.

Uno, K.T., Polissar, P.J., Jackson, K.E., deMenocal, P.B., 2016. Neogene biomarker record of vegetation change in eastern Africa. Proceedings of the National Academy of Sciences 113, 6355-6363.

Appendix

Carbon isotope systematics of leaf wax *n*-alkane compounds in a lacustrine depositional environment

Table S1. *n*-Alkane quantification data

Sample ID	Depth (cm)	C15 (ng/g sed.)	C16 (ng/g sed.)	C17 (ng/g sed.)	C18 (ng/g sed.)	C19 (ng/g sed.)	C20 (ng/g sed.)	C21 (ng/g sed.)	C22 (ng/g sed.)	C23 (ng/g sed.)	C24 (ng/g sed.)	C25 (ng/g sed.)	C26 (ng/g sed.)	C27 (ng/g sed.)	C28 (ng/g sed.)	C29 (ng/g sed.)	C30 (ng/g sed.)	C31 (ng/g sed.)	C32 (ng/g sed.)	C33 (ng/g sed.)	C34 (ng/g sed.)	C35 (ng/g	C36 (ng/g sed.)
Garvoc 1 F1 CuS	1265	0.00	37.54	0.00	34.84	41.17	0.00	789.91	333.89	6195.05	414.66	3117.77	438.44	3210.41	315.61	5241.94	0.00	4844.32	181.30	1996.67	0.00	426.82	0.00
Garvoc 2 F1 CuS	1470	0.00	7.30	0.00	0.00	0.00	3.21	39.05	32.05	340.11	57.72	398.81	56.62	339.13	29.54	284.57	23.22	348.31	12.56	121.27	0.00	13.30	0.00
Garvoc 3 F1 CuS	1850	0.00	6.11	0.00	0.00	0.00	0.00	17.41	18.68	153.63	47.27	388.80	45.80	481.80	64.93	1819.21	64.00	1444.60	51.59	511.47	0.00	47.83	0.00
Garvoc 4 F1 CuS	2150	0.00	0.00	0.00	0.00	0.00	8.86	74.72	60.22	1257.07	159.06	2345.12	141.24	1346.29	81.19	1360.47	70.87	2777.94	85.12	1011.21	0.00	82.94	0.00
Garvoc 5 F1 CuS	3230	0.00	0.00	0.00	0.00	0.00	0.00	108.07	73.28	1014.47	181.82	1238.59	291.59	2838.64	428.84	12147.45	589.00	14199.65	408.73	5763.06	114.26	1117.97	0.00
Garvoc 6 F1 CuS	3115	0.00	0.00	0.00	0.00	26.00	26.99	359.66	396.00	2637.28	518.53	2347.87	291.66	1670.93	125.49	830.47	52.21	993.88	28.49	397.50	6.27	68.10	0.00
Garvoc 7 F1 CuS	3290	8.04	6.68	0.00	0.00	5.69	4.65	31.49	89.26	608.76	142.52	854.84	123.25	710.87	128.69	1629.98	184.14	3572.98	103.77	1612.82	27.93	228.33	10.91
Garvoc 8 F1 CuS	3510	0.00	0.00	0.00	0.00	0.00	0.00	20.83	31.53	189.19	57.63	465.95	64.20	588.78	77.71	1342.62	108.21	2653.53	102.15	974.96	0.00	135.05	0.00
Garvoc 9 F1 CuS	3620	0.00	0.00	0.00	0.00	0.00	0.00	0.00	7.20	68.81	16.56	136.51	24.33	282.24	32.59	965.34	66.43	2875.74	46.34	1405.02	15.18	181.37	0.00
Garvoc 10 F1 CuS	3900	0.00	0.00	0.00	0.00	0.00	0.00	92.23	34.75	448.41	202.29	1379.15	213.31	2397.62	301.55	8621.50	429.85	19932.41	379.17	9542.89	0.00	1435.05	0.00
Garvoc 11 F1 CuS	4063	0.00	0.00	3.98	0.00	2.08	2.46	6.26	9.01	99.94	27.64	241.10	40.74	267.92	49.65	544.26	40.51	548.72	21.52	241.44	0.00	44.12	0.00
Garvoc 12 F1 CuS	4230	0.00	0.88	0.00	0.00	0.00	2.66	24.40	13.80	149.81	33.48	182.05	37.02	239.79	48.43	517.27	35.55	669.86	0.00	374.02	0.00	37.08	0.00
Garvoc 13 F1 CuS	4600	0.00	5.69	4.66	4.33	19.30	20.51	208.50	326.83	3025.42	729.57	3611.42	378.33	1236.75	147.18	1084.13	89.07	3010.81	78.19	2011.93	0.00	150.62	0.00
Garvoc 14 F1 CuS	4810	0.00	0.00	0.00	0.00	0.00	2.65	10.33	13.34	258.42	50.80	229.64	19.11	73.01	11.46	111.26	12.34	448.08	14.83	319.63	0.00	32.20	0.00
Garvoc 15 F1 CuS	5000	0.00	0.00	0.00	0.97	0.00	1.02	14.39	10.11	64.67	14.28	61.20	11.21	63.39	13.09	93.77	13.51	243.28	10.14	125.82	2.45	13.71	0.00
Garvoc 16 F1 CuS	5205	0.00	0.00	0.00	0.00	4.72	6.13	51.39	41.48	264.84	54.60	296.69	62.41	350.50	63.36	663.11	60.09	1272.05	43.54	784.34	0.00	66.61	0.00
Garvoc 17 F1 CuS	5405	0.00	0.00	0.00	5.10	7.77	15.24	289.00	146.07	2054.75	219.64	1668.56	154.07	1238.46	75.23	644.66	40.90	912.74	35.30	471.29	0.00	69.31	0.00
Garvoc 18 F1 CuS	5590	0.00	1.16	0.00	1.69	0.00	3.35	26.95	9.50	118.65	15.47	106.68	13.07	89.83	12.11	122.61	15.24	394.47	15.71	294.41	0.00	33.33	0.00
Garvoc 19 F1 CuS	5800	0.00	0.00	0.00	0.00	0.00	0.00	5.10	7.47	52.75	19.76	104.35	26.40	176.51	29.70	313.58	27.12	364.48	18.95	197.07	0.00	24.99	0.00
Garvoc 20 F1 CuS	6000	0.00	1.49	0.97	1.42	3.01	4.90	57.58	40.85	269.74	31.17	163.19	24.92	170.72	26.65	200.39	24.99	694.69	26.28	437.91	8.11	40.27	0.00
Garvoc 21 F1 CuS	6400	0.00	0.00	0.00	0.00	0.00	1.41	7.17	12.17	60.83	21.64	93.03	28.06	152.59	34.94	421.78	39.18	521.11	22.54	333.54	0.00	31.46	2.54
Garvoc 22 F1 CuS	6870	0.00	0.00	0.00	0.00	0.89	3.12	32.46	20.33	132.51	23.57	123.75	19.96	106.27	14.75	159.58	18.74	535.71	20.43	349.05	8.13	33.93	1.31
Garvoc 23 F1 CuS	7200	0.00	0.00	0.00	0.00	0.00	2.77	14.41	15.31	81.78	38.02	191.22	48.94	372.28	86.04	918.61	69.22	1853.68	61.38	1148.75	19.01	111.21	0.00
Garvoc 24 F1 CuS	7600	0.00	0.00	0.00	0.00	0.00	2.31	12.77	14.07	130.47	45.77	310.72	55.91	351.06	58.87	729.54	45.96	1144.42	44.58	617.72	9.09	72.80	3.28
Garvoc 25 F1 CuS	8005	0.00	0.00	0.00	1.55	0.00	0.00	34.42	6.39	57.14	7.25	40.69	6.92	36.55	7.87	86.34	12.83	439.96	11.63	236.79	0.00	19.07	0.00
Garvoc 26 F1 CuS	8400	0.00	2.23	1.12	1.52	4.20	6.52	65.37	63.97	408.44	86.85	426.81	47.35	232.09	28.04	254.77	32.44	1016.56	33.89	725.50	11.22	60.00	0.00
Garvoc 27 F1 CuS	8800	0.00	4.05	6.35	9.82	23.59	43.45	399.43	158.58	918.42	166.86	832.79	104.44	604.80	122.32	1438.78	164.25	6934.11	179.49	5841.84	68.10	528.54	0.00
Garvoc 28 F1 CuS	9200	0.00	0.00	5.05	9.89	6.76	8.60	46.93	56.29	712.53	251.34	1556.88	230.77	1453.13	207.00	2491.01	191.63	4675.57	142.83	2570.85	49.73	291.79	11.24
Garvoc 29 F1 CuS	9600	0.00	0.00	0.00	0.00	0.00	0.00	308.56	180.57	3338.21	258.61	1581.09	261.06	2860.95	300.85	8555.74	381.68	9668.59	0.00	4630.02	0.00	1216.30	0.00
Garvoc 30 F1 CuS	10000	0.00	4.87	0.00	3.18	0.00	3.80	4.92	6.22	48.23	19.04	131.01	19.73	170.53	34.51	325.54	23.33	1252.99	35.25	596.83	0.00	66.59	0.00

Table S2. *n*-Alkane carbon isotope data

Sample ID	Depth (cm)	C23 (‰)	C25 (‰)	C27 (‰)	C29 (‰)	C31 (‰)	C33 (‰)	C35 (‰)	C23 (1 sd)	C25 (1 sd)	C27 (1 sd)	C29 (1 sd)	C31 (1 sd)	C33 (1 sd)	C35 (1 sd)
Garvoc_1_F1_CuS	1265	-23.87	-23.49	-28.14	-32.42	-32.42	-32.52	-33.37	0.03	0.05	0.05	0.10	0.08	0.08	0.21
Garvoc_2_F1_CuS	1470	-24.82	-27.52	-28.21	-30.42	-31.82	-32.30	-31.10	0.06	0.09	0.04	0.10	0.06	0.07	0.82
Garvoc_3_F1_CuS	1850	-26.16	-27.84	-30.01	-32.83	-32.41	-31.48		0.04	0.01	0.10	0.08	0.13	0.45	
Garvoc_4_F1_CuS	2150	-21.49	-22.89	-22.90	-30.56	-32.01	-32.06	-31.30	0.03	0.03	0.14	0.10	0.03	0.10	0.18
Garvoc_5_F1_CuS	3230	-29.72	-29.48	-31.52	-33.50	-32.93	-33.09	-34.40	0.05	0.14	0.08	0.09	0.06	0.23	0.30
Garvoc_6_F1_CuS	3115	-18.87	-19.69	-21.96	-25.07	-28.85	-31.94	-30.66	0.03	0.02	0.04	0.03	0.17	0.22	0.27
Garvoc_7_F1_CuS	3290	-25.19	-26.59	-29.73	-31.70	-31.68	-32.38	-32.60	0.02	0.01	0.04	0.23	0.14	0.02	0.19
Garvoc_8_F1_CuS	3510	-28.35	-29.37	-30.82	-32.50	-32.74	-32.49	-34.11	0.16	0.04	0.07	0.01	0.04	0.05	0.11
Garvoc_9_F1_CuS	3620	-26.42	-26.83	-29.71	-33.40	-32.99	-32.68	-33.67	0.06	0.01	0.03	0.08	0.08	0.01	0.24
Garvoc_10_F1_CuS	3900	-27.90	-29.66	-31.57	-34.11	-32.99	-32.82	-34.18	0.09	0.08	0.17	0.02	0.04	0.09	0.29
Garvoc_11_F1_CuS	4063	-27.56	-28.76	-31.68	-33.36	-32.95	-33.29	-33.01	0.14	0.01	0.09	0.00	0.01	0.35	0.29
Garvoc_12_F1_CuS	4230	-27.67	-29.24	-30.81	-32.71	-32.89	-33.35	-32.35	0.04	0.08	0.05	0.09	0.12	0.05	0.26
Garvoc_13_F1_CuS	4600	-19.52	-20.29	-22.15	-26.77	-31.11	-32.53	-32.98	0.07	0.01	0.01	0.06	0.04	0.11	0.14
Garvoc_14_F1_CuS	4810	-21.47	-22.57	-26.39	-30.69	-32.45	-33.55	-34.24	0.01	0.09	0.05	0.08	0.15	0.05	0.05
Garvoc_15_F1_CuS	5000	-27.63	-27.48	-29.24	-31.17	-31.13	-31.07	-32.02	0.11	0.04	0.12	0.07	0.04	0.04	0.18
Garvoc_16_F1_CuS	5205	-25.08	-27.34	-28.69	-31.51	-31.73	-32.38	-32.12	0.10	0.21	0.02	0.08	0.07	0.06	0.12
Garvoc_17_F1_CuS	5405	-20.31	-20.33	-21.77	-30.06	-32.23	-32.47	-31.09	0.01	0.02	0.05	0.05	0.09	0.05	0.29
Garvoc_18_F1_CuS	5590	-20.88	-22.35	-25.58	-30.82	-31.72	-32.78	-32.95	0.03	0.05	0.06	0.12	0.06	0.10	0.01
Garvoc_19_F1_CuS	5800	-30.37	-31.48	-32.27	-33.34	-32.87	-32.29	-32.38	0.01	0.07	0.07	0.00	0.07	0.10	0.06
Garvoc_20_F1_CuS	6000	-21.03	-24.18	-27.00	-30.56	-30.91	-32.12	-32.63	0.09	0.05	0.03	0.11	0.03	0.12	0.80
Garvoc_21_F1_CuS	6400	-28.99	-29.82	-31.38	-33.22	-32.93	-33.10	-32.08	0.01	0.02	0.05	0.05	0.02	0.01	0.12
Garvoc_22_F1_CuS	6870	-23.31	-27.51	-30.50	-31.99	-32.06	-32.74	-33.52	0.09	0.07	0.01	0.04	0.10	0.02	0.21
Garvoc_23_F1_CuS	7200	-30.23	-31.36	-32.55	-34.13	-33.54	-33.90	-33.70	0.01	0.11	0.01	0.06	0.06	0.17	0.25
Garvoc_24_F1_CuS	7600	-23.60	-25.91	-29.42	-32.09	-33.03	-33.79	-33.85	0.12	0.08	0.04	0.05	0.03	0.05	0.26
Garvoc_25_F1_CuS	8005	-23.39	-26.43	-29.31	-31.62	-30.95	-32.76	-33.66	0.02	0.00	0.24	0.10	0.01	0.02	0.16
Garvoc_26_F1_CuS	8400	-21.32	-22.33	-25.50	-31.31	-31.72	-33.36	-33.56	0.04	0.05	0.06	0.09	0.04	0.11	0.33
Garvoc_27_F1_CuS	8800	-24.16	-26.66	-30.87	-32.77	-32.79	-34.11	-34.74	0.02	0.14	0.11	0.00	0.02	0.04	0.10
Garvoc_28_F1_CuS	9200	-25.73	-26.72	-29.30	-32.51	-32.60	-33.06	-33.34	0.03	0.11	0.12	0.02	0.02	0.15	0.22
Garvoc_29_F1_CuS	9600	-28.45	-29.80	-31.48	-33.99	-33.40	-33.13	-34.36	0.09	0.01	0.02	0.05	0.04	0.07	0.69
Garvoc_30_F1_CuS	10000	-23.18	-24.25	-27.18	-31.01	-32.50	-33.33	-33.89	0.17	0.20	0.06	0.05	0.03	0.09	0.15

Statement of Authorship

Title of Paper	Initial expansion of C_4 vegetation in Australia during the late Pliocene
Publication Status	☑ Published ☐ Accepted for Publication ☐ Submitted for Publication ☐ Unpublished and Unsubmitted work written in manuscript style
Publication Details	Published in Geophysical Research Letters: Andrae, J.W., McInerney, F.A., Polissar, P.J., Sniderman, J.M.K., Howard, S., Hall, P.A. and Phelps, S.R. (2018) Initial Expansion of C4 Vegetation in Australia During the Late Pliocene, *Geophysical Research Letters*, 45, 4831-4840

Principal Author

Name of Principal Author (Candidate)	Jake W. Andrae
Contribution to the Paper	Undertook research design, sample acquisition, sample preparation and much of the data analysis, processing and interpretation. Led the development and drafting of the manuscript, produced all figures, and acted as the corresponding author. Along with Francesca McInerney, acquired the funding that enabled the research reported in the paper to be undertaken.
Overall percentage (%)	70%
Certification:	This paper reports on original research I conducted during the period of my Higher Degree by Research candidature and is not subject to any obligations or contractual agreements with a third party that would constrain its inclusion in this thesis. I am the primary author of this paper.

Signature Date 08/05/2018

Co-Author Contributions

By signing the Statement of Authorship, each author certifies that:

vii. the candidate's stated contribution to the publication is accurate (as detailed above);

viii. permission is granted for the candidate in include the publication in the thesis; and

ix. the sum of all co-author contributions is equal to 100% less the candidate's stated contribution.

Name of Co-Author	Dr Francesca A. McInerney
Contribution to the Paper	Undertook research design and sample acquisition and contributed extensively to data interpretation. Edited and provided feedback on drafts. Along with Jake Andrae, acquired the funding that enabled the research reported in the paper to be undertaken. Approved final manuscript.

Signature Date 04/07/19

Name of Co-Author	Dr Pratigya J. Polissar
Contribution to the Paper	Undertook research design and isotopic data analysis and contributed extensively to data processing and data interpretation. Provided input in isotopic analysis methods section, edited and provided feedback on drafts, and approved final manuscript.

Signature Date 25/06/19

Name of Co-Author	Dr J.M. Kale Sniderman
Contribution to the Paper	Undertook palynological sample preparation as well as analysis and data interpretation in this regard. Wrote palynology methods and results section. Edited and provided feedback on drafts and approved final manuscript.

Signature Date 28/06/19

Name of Co-Author	Sian Howard
Contribution to the Paper	Contributed extensively to geochemical analyses and data interpretation, particularly regarding leaf wax *n*-alkane compound distributions. Edited and provided feedback on drafts and approved final manuscript.

Signature Date 03/07/19

Name of Co-Author	Dr P. Anthony Hall
Contribution to the Paper	Contributed extensively to geochemical sample analysis, data processing and data interpretation in the context of leaf wax *n*-alkane compound distributions. Edited and provided feedback on drafts and approved final manuscript.

Signature Date 25/06/19

Name of Co-Author	Samuel R. Phelps
Contribution to the Paper	Contributed extensively to isotopic data analysis, data processing and data interpretation. Edited and provided feedback on drafts and approved final manuscript.

Signature Date 03/07/19

Chapter 4: Initial expansion of C4 vegetation in Australia during the late Pliocene*

*Originally published as Andrae, J.W., McInerney, F.A., Polissar, P.J., Sniderman, J.M.K., Howard, S., Hall, P.A. and Phelps, S.R. (2018) Initial expansion of C4 vegetation in Australia during the late Pliocene, *Geophysical Research Letters*, 45, 4831-4840.

Key points

- Carbon isotope ratios of leaf waxes reveal the onset of C4 expansion during the late Pliocene in Australia, later than other geographic regions
- Palynological analysis reveals increasingly open landscapes in the lead-up to C4 expansion
- Northern Australian monsoon initiation linked to East Asian winter monsoon intensification is hypothesized as a driver

Abstract

Since the late Miocene, plants using the C4 photosynthetic pathway have increased to become major components of many tropical and subtropical ecosystems. However, the drivers for this expansion remain under debate, in part because of the varied histories of C4 vegetation on different continents. Australia hosts the highest dominance of C4 vegetation of all continents, but little is known about the history of C4 vegetation there. Carbon isotope ratios of leaf waxes from scientific ocean drilling sediments off north-western Australia reveal the onset of Australian C4 expansion at ~3.5 Ma, later than in many other regions. Pollen analysis from the same sediments reveals increasingly open C3-dominated biomes preceding the shift to open C4-dominated biomes by several million years. We hypothesize that the development of a summer monsoon climate beginning in the late

Pliocene promoted a highly seasonal precipitation regime favorable to the expansion of C4 vegetation.

Plain language summary

This study documents for the first time that C4 vegetation initially expanded on the Australian continent in the late Pliocene, several million years later than in Asia, Africa, North America, and South America. The expansion of C4 plants displaced C3 open habitat vegetation. Understanding the timing and sequence of expansion of C4-dominated biomes enables us to better constrain the key environmental and evolutionary factors in their development and provides a basis for future conservation of these widespread and important biomes.

1 Introduction

Vegetation utilizing the C4 photosynthetic pathway is an important component of modern ecosystems globally, comprising ~23% of global gross primary productivity (Still et al., 2003). Biomes dominated by C4 plants are mainly "open" habitats, that is, with sparse tree canopy density. Australia has the highest proportional area dominated by C4 vegetation of all continents (Murphy & Bowman, 2007; Still et al., 2003). The majority of the continent is dominated by C4 rather than C3 grasses, and the relative abundance of C4 species within grass communities is closely related to seasonal water availability (Murphy & Bowman, 2007). Survey data on modern Australian vegetation compiled in this study further support a close association between warm-season precipitation and C4 dominance (Figure 1 and Text S1.1 in Chapter 4 Appendix). Australian biomes with significant C4 taxa include arid and tropical to subtropical grasslands and savannas, dominating in the north, and chenopod shrublands, dominating in the south (Hattersley, 1983; Leigh, 1994; Murphy & Bowman, 2007).

On many continents, C4 vegetation began to proliferate by the late Miocene, with this expansion recorded as shifts in carbon isotope ratios of plant-fixed carbon stored within a wide range of terrestrial and marine sediments and palaeosols, as well as in fossil tooth enamel (Cerling et al., 1997; Strömberg, 2011; Tipple & Pagani, 2007). C4 expansion on these continents occurred as the final stage in what has been inferred as a stepwise progression of ecosystem transformation in which C3 forest transitioned to C3 open landscapes, and then to C4 open landscapes (Cerling et al., 1997; Edwards et al., 2010; Strömberg, 2011). Despite being the most C4-dominated continent today, little is known about the timing and pattern of C4 expansion in Australia. Evidence exists for open habitat vegetation increasing in abundance in the late Miocene (e.g., Locker & Martini, 1986; Macphail, 1997; Martin, 2006; Martin & McMinn, 1994; Sniderman et al., 2016). However, it is unknown whether late Miocene Australian grasses and chenopods employed the C3 or C4 photosynthetic pathway. Reconstructing changes in the dominant photosynthetic pathway has been limited by the spatial and temporal discontinuity of Australian terrestrial geological records (Kershaw et al., 1994; Macphail, 1997).

In this paper, we present ~10 Myr records of leaf wax *n*-alkane carbon isotopes and pollen abundances from sediments of Ocean Drilling Program (ODP) Hole 763A (hereafter ODP 763A), off north-western Australia, to determine when, how, and why C4 vegetation expanded on the Australian continent.

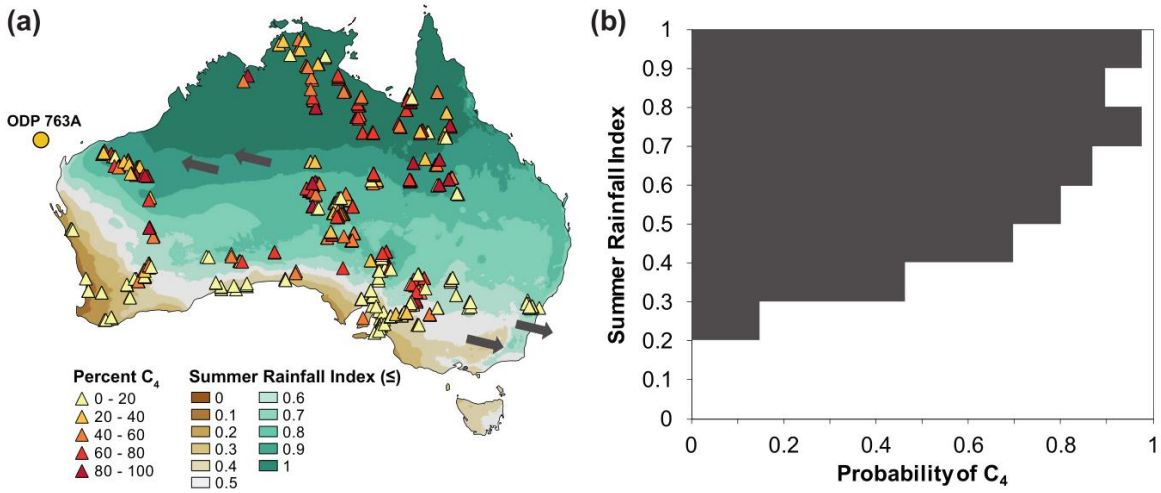

Figure 1. Study site in the context of modern Australian C4 vegetation and climate. (a) Location of ODP 763A, with mapped Summer Rainfall Index (SRI) and surveyed percent C4 plant cover (Kattge et al., 2011; Lowrey, 2015; Osborne et al., 2014; White et al., 2012, see Text S1.1 in Chapter 4 Appendix for details). SRI calculated as the proportion of summer rainfall (December, January, and February) out of summed summer (December, January, and February) and winter (June, July, and August) rainfall (Australian Government Bureau of Meteorology, 2016). The arrows indicate modern dust transport pathways (Hesse & McTainsh, 2003). (b) The probability that C4 vegetation is present for a given range of SRI based on survey data.

2 Materials and methods

2.1 ODP 763 sample preparation

Samples constitute 26 portions of foraminifera to nanno-fossil ooze or foraminifera-bearing nanno-fossil chalk (Haq et al., 1990) from ODP 763A (collected August 1988). To minimize contamination, 0.5 cm of all exposed faces of the samples was removed and all tools and equipment were thoroughly cleaned (washed with dilute Decon 90® decontaminant solution followed by three rinses of reverse osmosis water, and three rinses each of methanol, dichloromethane [DCM], and *n*-hexane). Samples were lyophilized in ashed borosilicate glass containers, prior to homogenization using a mortar and pestle. Total lipids were extracted from 9.5 to 18.9 g of each sample (mean: 13.9 g) using a Thermo Scientific™ Dionex™ ASE™ 350. Samples underwent five cycles of

solvent rinse (5-min static rinse with 9:1 DCM:methanol) and purge (2 min) at a temperature of 100 °C and a pressure of ~11,000 kPa. Solvents were evaporated from the total lipid extract under N_2 on a FlexiVap™ heated evaporator. Non-polar and polar components were separated by solid phase extraction through ~0.5 g of solvent-cleaned activated silica gel of 0.035 to 0.070 mm size using 4 mL of *n*-hexane and 4 mL 1:1 DCM:methanol, respectively. Elemental sulfur was removed using copper shavings activated in hydrochloric acid.

2.2 Biomarker quantitation and compound-specific carbon isotope analysis

n-Alkanes (C16 to C35) were characterized and quantified on a Perkin Elmer Clarus 580 gas chromatograph-mass spectrometer (GC-MS) fitted with a PE Elite 5MS capillary column. Samples were dissolved in 100 μL *n*-hexane with 1 μg/mL 1-1' binaphthyl as internal standard. Quantitation standards were prepared by dilution of a Certified Reference Material (C7-C40 Saturated Alkanes Standard, Supelco 49452-U) with 1-1' binaphthyl as internal standard for concurrent analysis with the sample batch (see Text S1.2 in Chapter 4 Appendix for full GC-MS instrument setup specifications).

Compound-specific $\delta^{13}C$ measurements were performed for *n*-alkanes (C25-C35) using a Thermo Delta V isotope ratio MS coupled to a Thermo Trace GC Ultra and Isolink through a ConFlo IV interface. Samples were injected into a PTV injector with 2 mm i.d. silicosteel liner packed with glass wool. The inlet was held splitless at 60 °C during injection and then ramped ballistically to 320 °C where it was held for 1.5 min during the transfer phase. Compounds were separated on an HP-5MS column (30 m length, 0.25 mm i.d., and 0.25 μm phase thickness) with a constant helium flow of 1.0 mL/min. The GC oven was held at 60 °C for 1.5 min, ramped at 15 °C/min to 150 °C and then at 4 °C/min to 320 °C, and held for 10 min. The GC effluent was connected to a custom-made

combustion reactor consisting of 1 strand each of 0.1 mm nickel, copper, and platinum wires inside a 0.5 mm i.d. fused alumina tube held at 1000 °C. Continued oxidation and complete combustion of compounds were ensured with the introduction of a trickle of 1% O_2 in helium. Water was removed from the combustion effluent with a custom-built cryotrap consisting of a 20-cm loop of 0.25 mm i.d. deactivated fused silica capillary immersed in an ethanol bath at -85 °C. The trap was periodically thawed and purged to prevent plugging from the buildup of ice. Standard mixtures of *n*-alkanes with known $\delta^{13}C$ values (Mixes B4 and A5 purchased from Arndt Schimmelmann, Indiana University) were interspersed between sample measurements to calibrate the isotopic measurements. Measurement uncertainties (standard error of the mean), including both analytical uncertainty and uncertainty in realizing the Vienna Pee Dee Belemnite reporting scale, were calculated after Polissar and D'Andrea (2014).

2.3 ODP 763A age model

Sample ages were calculated using linear interpolations between tie-points in an age-depth model established in Karas et al. (2011), complemented by palaeo-magnetic reversal event datum tie-points established in Tang (1992) and updated to Hilgen et al. (2012). See Data Set S4 in Chapter 4 Appendix.

2.4 Adjustment for preindustrial atmospheric $\delta^{13}C$ and modeling percent C4

The sedimentary *n*-alkane $\delta^{13}C$ values were normalized to preindustrial atmospheric CO_2 $\delta^{13}C$ by applying the offset between $\delta^{13}C$ of atmospheric CO_2 for a given sample age estimated from a 3 Myr moving average benthic foraminifera record and $\delta^{13}C$ of atmospheric CO_2 of -6.5‰ (Tipple et al., 2010; Uno et al., 2016). Fraction of C4 vegetation was calculated from the carbon isotopic composition of C31 in the sediments using a linear two end-member mixing model incorporating the mean carbon isotopic

composition of C31 in a calibration set of modern C3 (n = 106) and C4 (n = 45) plants, also normalized to preindustrial atmospheric CO_2 $\delta^{13}C$ of -6.5‰ (Garcin et al., 2014). The C31 alkane was used to minimize leaf wax production biases related to plant functional type (Garcin et al., 2014).

2.5 Pollen

Fossil pollen was extracted from 12 sample splits using palynological methods adapted from Moore et al. (1991). Samples were digested in cold HCl, followed by treatment with hot 10% KOH, acetolysis (a 9:1 mixture of acetic anhydride and concentrated sulfuric acid), and overnight immersion in concentrated HF, followed by heavy liquid separation using a Na-polytungstate liquid of specific gravity 2.0 (Munsterman & Kerstholt, 1996). The acid- and alkali-resistant residues were then dehydrated in ethanol and mounted on glass slides in glycerol. Pollen was counted along transects at 300X and 600X magnification on a Zeiss AxioScope A.1 with EC Plan Neofluar objectives, until at least 100 pollen grains were counted. Pollen was identified by comparison with modern reference collections and with images stored in the Australasian Pollen and Spore Atlas (APSA Members, 2007).

3 Results

3.1 Leaf wax *n*-alkane distributions and carbon isotope ratios

Sedimentary *n*-alkanes in samples from 8.8 to 1.0 Ma display unimodal homolog distributions, peaking at C29, C31, or C33, with a strong odd-over-even predominance (carbon preference index > 2; Data Set S1 in Chapter 4 Appendix) that is indicative of a higher plant origin (Bush & McInerney, 2013). The oldest sample, at 9.5 Ma, has a bimodal distribution with peaks at C26 and C29 and a weak odd-over-even predominance (carbon preference index < 2; Data Set S1 in Chapter 4 Appendix), suggestive of

petrogenic hydrocarbons from unknown sources that obscure plant-derived $\delta^{13}C$ and chain-length distributions. Thus, we disregard the oldest sample as it is likely not of terrestrial plant origin. The proportional abundance of C33 compared to C29 *n*-alkanes increases significantly throughout the record (Figure 2 and Data Set S1 in Chapter 4 Appendix). From 8.8 to 3.6 Ma, carbon isotope ratios of C29, C31, and C33 are stable with values indicative of predominantly C3 vegetation. Beginning at 3.5 Ma, $\delta^{13}C$ values progressively increase, becoming more enriched in ^{13}C (Figure 2 and Data Set S1 in Chapter 4 Appendix). In addition, at 3.5 Ma, the $\delta^{13}C$ values of C29, C31, and C33 *n*-alkanes begin to diverge, causing an increasing difference between $\delta^{13}C$ values of C33 and C29 after that time (Figure 2 and Data Set S1 in Chapter Appendix).

The fraction of the source vegetation that is C4 plants is estimated from the carbon isotopic composition of the sedimentary C31 *n*-alkane (Figures 2 and 3). Estimated C4 fraction from 8.8 to 3.6 Ma is low, ranging from 9.2 $^{+27.5}_{-9.2}$ % to 19.2 $^{+26.5}_{-19.2}$ % (modern plant end-member 1-sigma calculation uncertainty). At ~3.5 Ma, the estimated C4 fraction begins progressively increasing, save for one sample at 2.8 Ma. Percent C4 reaches a maximum of 59.2 ± 22.4% at 1.0 Ma (Figures 2 and 3 and Data Set S1 in Chapter 4 Appendix). It must be noted that the uncertainties in calculations of fraction C4 vegetation are likely overestimated, due to the geographically and climatically broad modern plant calibration set used (Garcin et al., 2014). Variability in the isotopic composition of the C31 *n*-alkane in modern C3 and C4 plant end-members from any one region is likely to be less than the calibration set.

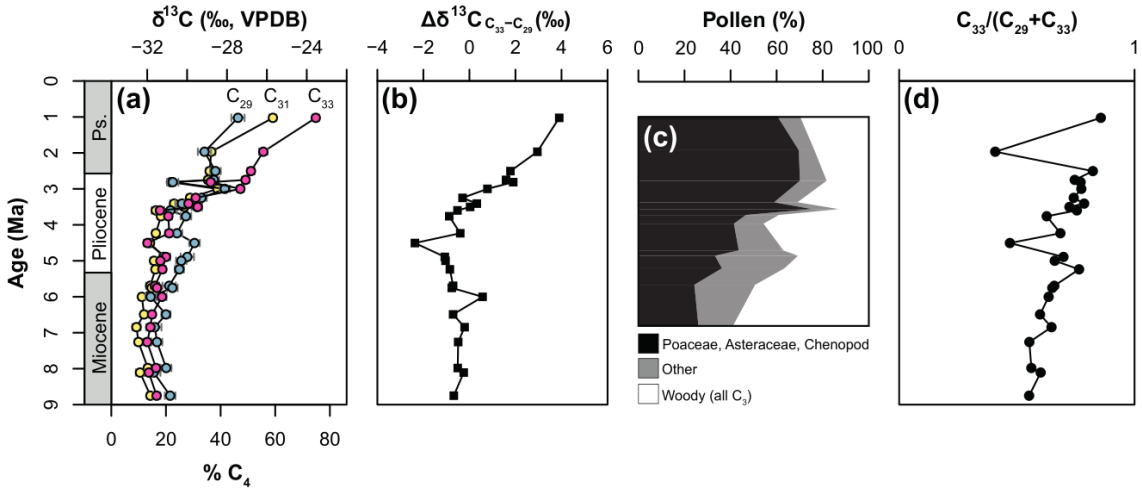

Figure 2. Organic geochemical and palynological data derived from sediments of ODP 763A. (a) Compound specific carbon isotope ratios of *n*-alkane homologs: C29 (blue), C31 (yellow), and C33 (pink), with percent C4 based on the C31 homolog. The error bars represent plus and minus one standard error of the mean. (b) The difference between the carbon isotope ratio of C33 and that of C29. (c) Grouped pollen percentages indicating relative proportions of herbaceous, woody, and other taxa. (d) The proportional concentration of C33 relative to C29 + C33.

3.2 Palynological results

Pollen analysis was undertaken on samples ranging in age from 6.8 to 1.0 Ma, and results are presented as a summary pollen percentage diagram (Figure 2). During the latest Miocene, Gyrostemonaceae, Casuarinaceae, *Acacia*, and *Dodonaea* are important components of the pollen sum. Poaceae, Asteraceae, and Eucalyptus pollen are also present in substantial proportions during the latest Miocene. Across the Miocene-Pliocene boundary, values of Gyrostemonaceae, Casuarinaceae, *Acacia*, and *Dodonaea* decline, while those for Restionaceae, indeterminate Myrtaceae pollen, Cyperaceae, and ferns (Polypodiaceae and *Cyathea*) increase steadily until collapsing at ~4.9 Ma. Poaceae, Asteraceae, and chenopods maintain steady or increasing values through the Early Pliocene. Around the early-late Pliocene boundary (3.5–3.6 Ma), the vegetation becomes strongly dominated by Poaceae and Asteraceae, with varying contributions from

178 *Eucalyptus*, Myrtaceae, and chenopods, which persists with little subsequent change for the
179 remainder of the record (note, the full pollen data are presented in Figure S3 and Data Set
180 S2 in Chapter 4 Appendix).

181 **4 Discussion and conclusions**

182 **4.1 Pliocene expansion of C4 vegetation**

183 The carbon isotope ratios of leaf wax *n*-alkanes begin to become enriched in ^{13}C at
184 ~3.5 Ma (Figure 2) implying an expansion of C4 vegetation in north-western Australia. In
185 addition, beginning at ~3.5 Ma, the $\delta^{13}C$ of the C33 *n*-alkane becomes increasingly
186 enriched in ^{13}C compared to the other shorter chain lengths (Figure 2). Modern Australian
187 grasses produce a higher proportion of C33 than trees or shrubs (Howard et al., 2018,
188 Figure S2, Table S1, Text S1.3, and Data Set S3 in Chapter 4 Appendix). This pattern is
189 mirrored in North America and Africa, where grasses have higher abundances of longer
190 chain *n*-alkanes (C33 and C35) than trees that show higher abundances of shorter chain *n*-
191 alkanes (C27 and C29; Bush & McInerney, 2013; Garcin et al., 2014; Rommerskirchen et
192 al., 2006; Vogts et al., 2009). C33 is therefore proposed to be more sensitive to the
193 presence of C4 grasses on the landscape (Uno et al., 2016), while C29 is less influenced by
194 grasses. Carbon-13 enrichment and the beginning of isotopic divergence between C29 and
195 C33 in our sedimentary record at ~3.5 Ma mark the onset of the expansion of C4
196 vegetation.

197 Phylogenetic evidence suggests that the moderately diverse C4 grass tribe
198 Triodiinae, characteristic of central Australian arid vegetation today, radiated in the
199 Australian interior during the late Miocene (Toon et al., 2015). Nonetheless, any late
200 Miocene C4 vegetation must have been sparse, as it is not detectable in our C29 to C33 *n*-
201 alkane record. However, ^{13}C enrichment of the C35 *n*-alkanes relative to C29, C31 and

202 C33 (Figure S1 in Chapter 4 Appendix) could be an indication of trace amounts of C4
203 vegetation on the landscape prior to 3.5 Ma. The significant expansion in C4 vegetation
204 beginning at 3.5 Ma indicated by the inflection in our carbon isotope record reflects
205 widespread biologically productive C4 vegetation like that supported in the Australian
206 monsoon tropics today (Williams et al., 2017). This timing postdates the onset of most C4
207 expansions in Asia, Africa, North America, and South America, which occurred across the
208 middle to late Miocene (Cerling et al., 1997; Dupont et al., 2013; Feakins et al., 2013; Fox
209 et al., 2012; Fox & Koch, 2004; Ghosh et al., 2017; Hoetzel et al., 2013; MacFadden et al.,
210 1996; Passey et al., 2002; Passey et al., 2009; Quade & Cerling, 1995; Uno et al., 2016).

211 **4.2 Late Miocene/Early Pliocene opening of the landscape**

212 Substantial Poaceae, Asteraceae, and *Eucalyptus* pollen suggest that north-west
213 Australia was dominated by open woodland or shrubland in the latest Miocene. The
214 prominence of Gyrostemonaceae and Casuarinaceae suggests that this vegetation may have
215 had similarities to contemporaneous late Miocene open shrubland recorded on the
216 Nullarbor Plain in the south of the continent, which was dominated palynologically by
217 these two families (Sniderman et al., 2016). Increases in Restionaceae pollen percentages
218 across the late Miocene/early Pliocene transition suggest an increase in effective
219 precipitation, based on the preference of Restionaceae for seasonally moist wetland
220 habitats (Briggs, 2001). Peaks in representation of Myrtaceae, Cyperaceae, and ferns are
221 consistent with a peak in moisture at ~4.9 Ma, just before these taxa decline abruptly.
222 Rising values of Poaceae, Asteraceae, and chenopod pollen during the early Pliocene imply
223 the increasing dominance of very open vegetation, in which grass and chenopods were
224 more important than previously. Increasing relative abundance of the C33 compared to
225 C29 *n*-alkane homolog beginning between 7 and 6 Ma also suggests increasing
226 contributions from grasses (Figure 2). Our carbon isotope record indicates that C4

vegetation did not begin to compose a significant fraction of the increasingly open landscape until ~3.5 Ma. From these data, we interpret an initial late Miocene expansion of C3 grasses and/or chenopods, followed by a shift to C4 grasses and/or chenopods near the early/late Pliocene boundary. Fossil marsupial tooth enamel isotope data showing mixed C3 and C4 diets from the bio-stratigraphically dated late Pliocene Chinchilla Sands of south-eastern Queensland are consistent with this timing (Montanari et al., 2013). We infer from our record a pattern of ecosystem changes on the Australian continent not dissimilar to other geographic regions (Edwards et al., 2010; Strömberg, 2011), though delayed by several million years.

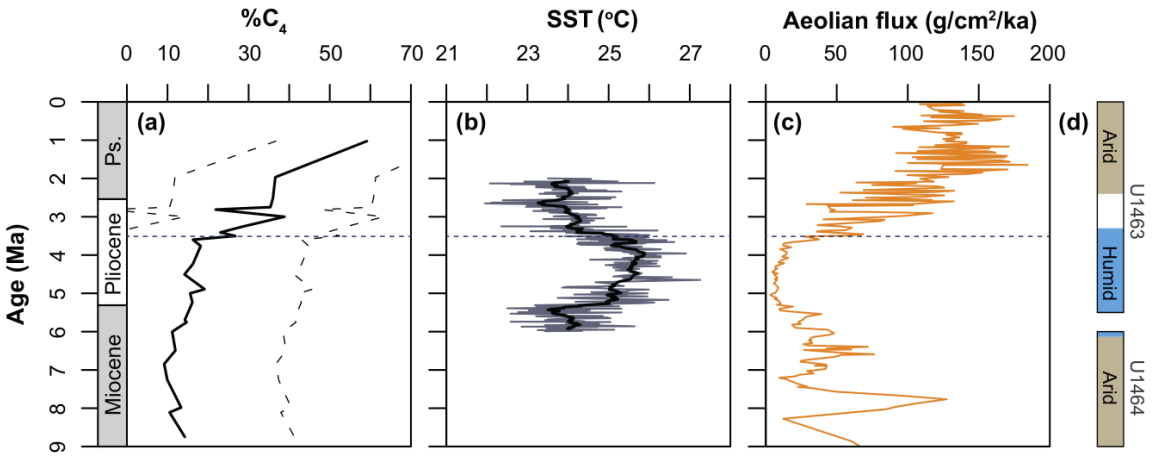

Figure 3. Australian record of C4 expansion in the context of contemporaneous climate records and interpretations. (a) Percent C4 reconstructed from the carbon isotope ratio of the C31 *n*-alkane homolog, with modern plant end-member 1-sigma calculation uncertainty shown as dashed black lines. (b) Mg/Ca sea surface temperature reconstruction from ODP 763A (the black line is a 15-point simple moving average, calculated using the "TTR" package; Ulrich, 2018, in R; R Core Team, 2016). Data from Karas et al. (2011). (c) Mass accumulation rates from ODP Sites 885/886 in the central North Pacific Ocean (Rea et al., 1993, 1998; Snoeckx et al., 1995), interpreted as increasing aeolian flux into sediments resulting from intensification of the East Asian winter monsoon (Data Set S5 in Chapter 4 Appendix, see Text S1.4 in Chapter 4 Appendix for methods used to calculate mass accumulation rate and to update timescale). (d) Arid (tan) and humid (blue)

intervals interpreted from potassium abundance in wireline logs from IODP U1463 and U1464 off north-west Australia (Christensen et al., 2017; Groeneveld et al., 2017). The dashed lines on all panels indicate approximate alignment between a SST change point at 3.44 Ma (Sniderman et al., 2016), the increase observed in percent C4 at ~3.5 Ma, and increased aeolian dust flux into the central North Pacific Ocean.

4.3 Drivers of late C4 expansion on the Australian continent

Environmental conditions that tend to promote C4 over C3 photosynthesis are low atmospheric pCO_2, high temperature, aridity, warm-season precipitation, high irradiance, and fire (Ehleringer, 2005; Keeley & Bond, 2001; Knapp & Medina, 1999; Long, 1999). Decreased pCO_2 has been postulated as a major control on the onset of C4 expansion globally (Cerling et al., 1993; Cerling et al., 1997; Ehleringer et al., 1991), with new developments in atmospheric pCO_2 reconstruction suggesting a significant decrease through the late Miocene (Bolton et al., 2016; Mejía et al., 2017). However, heterogeneous timing of C4 expansion across the globe (Figure S4 in Chapter 4 Appendix) indicates that decreased pCO_2 cannot be the only driving factor. This assertion is supported by models showing that while changes in pCO_2 have the potential to transform global vegetation states, the timing of transformation will vary due to regional differences in the timing and rates of change of temperature, rainfall amount and seasonality, and fire severity (Higgins & Scheiter, 2012). We argue that the relative importance of pCO_2 and environmental factors will likely vary by region.

The timing of the expansion of C4 vegetation documented here coincides closely with evidence for cooling and aridification in north-west Australia. Sea surface temperatures cool significantly in the region at 3.44 Ma (Karas et al., 2011; Sniderman et al., 2016; Figure 3), while at 3.3 Ma, there is evidence for the beginning of a transition from a humid to a more arid and/or more seasonal climate (Christensen et al., 2017; Figure

3). On the Nullarbor Plain, Sniderman et al. (2016) found no pollen in Pliocene speleothems younger than 3.4 Ma, suggesting that increasing aridity slowed speleothem growth after this time. The drivers of Australian aridification are debated; restriction of the Indonesian Throughflow (ITF) has been hypothesized as the driver of changes in precipitation in north-western Australia during the Pliocene (Christensen et al., 2017; Krebs et al., 2011). Krebs et al. (2011) simulated a constricted ITF based on Pliocene ocean bathymetry, finding that this could have caused a precipitation decrease of up to 30% over the eastern Indian Ocean. Conversely, other modeling experiments have indicated that ITF restriction was not associated with a decrease in precipitation over the eastern Indian Ocean, nor was it associated with significant globally pervasive impact on climate (Brierley & Fedorov, 2016; Jochum et al., 2009). Regardless of the driver of late Pliocene aridification, there is also evidence for aridity in north-western Australia during the late Miocene, from ~16 to 6 Ma (Groeneveld et al., 2017), that did not lead to an expansion of C4 vegetation (Figure 3). This suggests that aridity by itself was not the primary driver of the Australian late Pliocene C4 expansion, an inference that is substantiated by globally inconsistent relationships between C4 plant distributions and modern climate (Sage et al., 1999).

Opening of the landscape, increased seasonality of precipitation, and increased incidence of fire are suggested to have played significant roles in promoting the expansion of C4 vegetation on other continents (Beerling & Osborne, 2006; Edwards et al., 2010; Osborne, 2008; Scheiter et al., 2012; Zhou et al., 2017). Our pollen record suggests that Australian vegetation structure was already open by the late Miocene/early Pliocene. Our record of C4 expansion also coincides very closely with evidence of increased east Asian dust flux into marine sediments, at ~3.5 Ma (Figure 3; Rea et al., 1993, 1998; Snoeckx et al., 1995), widely interpreted as marking the initial intensification of the East Asian winter

monsoon (EAWM) or Siberian High (An et al., 2001; Guo et al., 2004; Rea et al., 1998; Sun et al., 1998; Zheng et al., 2004). Controls governing the Australian monsoon over late Neogene to Quaternary timescales are complex (Z. Liu et al., 2003; Wyrwoll & Valdes, 2003), but are dominated by two opposed influences: within-hemisphere insolation forcing (Wyrwoll et al., 2007; Wyrwoll & Valdes, 2003), that is comparatively weak because of the relatively small, low relief land surface of northern Australia; and remote forcing driven by cross-equatorial thermal and pressure gradients between Australia and East Asia (An, 2000). The persistence of an east Asian-Australian precipitation teleconnection, in which northern cooling leads to southward migration of the Intertropical Convergence Zone, has been indicated at a range of Quaternary timescales from centennial-millennial (Denniston et al., 2013; Eroglu et al., 2016) to orbital (Y. Liu et al., 2015) and has been observed in sedimentary records from the Holocene (Eroglu et al., 2016), the last deglaciation (Yancheva et al., 2007), and as far back as the mid-Pleistocene (Y. Liu et al., 2015). The sensitivity of the cross-equatorial meridional circulation linking the EAWM and the Australian monsoon to orbital obliquity has been explored using climate model simulations (Shi et al., 2011).

The abrupt increase in the abundance of C4 plants at ~3.5 Ma is most easily explained as a vegetation response to the onset of the Australian monsoon regime. In this interpretation, the intensification of the EAWM (Figure S4 in Chapter 4 Appendix), itself thought to be related to ongoing late Cenozoic global cooling (Herbert et al., 2016; Ge et al., 2013; Lu et al., 2010; Raymo, 1994), for the first time pushed the Intertropical Convergence Zone far enough southward to develop a substantial summer monsoon in northern Australia, characterized by a strong seasonal precipitation contrast and potentially greater incidence of fire. The relatively late appearance of a distinctly monsoonal moisture regime in northern Australia may help to explain the Plio-Pleistocene evolution of animal

clades confined to the Australian monsoon tropics today that are nested within lineages more typical of inland, arid Australia (Laver et al., 2017; Nielsen et al., 2016). The establishment of this new climatic regime would have provided the ecological opportunities necessary for the expansion of C4 vegetation in Australia beginning at ~3.5 Ma. This supports the hypothesis that the heterogeneous rise of C4 ecosystems globally reflects variations in the environmental factors providing competitive advantages to C4 vegetation.

Acknowledgments

The authors declare no conflict of interest. Data can be found in Data Sets S1 though S5 in Chapter 4 Appendix. Supplementary text and figures can be found in Chapter 4 Appendix. This research utilized samples and data provided by the International Ocean Discovery Program (IODP). Funding for this research was provided by an Australian IODP Office Special Post-Cruise Analytical Funding grant awarded to J. W. A and F. A. M., an Australian Research Council Future Fellowship (FT110100100793) awarded to F. A. M., an Australian Government Research Training Program Scholarship and University of Adelaide Faculty of Sciences Divisional Scholarship awarded to J. W. A. and S. H., and an NSF Graduate Research Fellowship to S. R. P (DGE 16-44869). Isotopic analyses were supported by the Climate Center at LDEO. Thank you to David Fox and one anonymous reviewer for their helpful comments. We acknowledge the Terrestrial Ecosystems Research Network for provision of plant survey data and samples. Thank you to Kristine Nielson, Emrys Leitch, Stefan Caddy-Retalic, and Nicole deRoberts for research support.

References

An, Z. (2000). The history and variability of the east Asian paleomonsoon climate. *Quaternary Science Reviews*, 19(1), 171–187.

An, Z., Kutzbach, J. E., Prell, W. L., & Porter, S. C. (2001). Evolution of Asian monsoons and phased uplift of the Himalaya–Tibetan plateau since late Miocene times. *Nature*, 411, 62–66.

APSA Members (2007). The Australasian Pollen and Spore Atlas V1.0. Retrieved from http://apsa.anu.edu.au/

Australian Government Bureau of Meteorology. (2016). Gridded climate datasets. Retrieved from http://www.bom.gov.au/climate/averages/climatology/gridded-data-info/gridded-climate-data.shtml

Beerling, D. J., & Osborne, C. P. (2006). The origin of the savanna biome. *Global Change Biology*, 12(11), 2023–2031.

Bolton, C. T., Hernandez-Sanchez, M. T., Fuertes, M.A., Gonzalez-Lemos, S., Abrevaya, L., Mendez-Vicente, A., et al. (2016). Decrease in coccolithophore calcification and CO_2 since the middle Miocene. *Nature Communications*, 7.

Brierley, C. M., & Fedorov, A. V. (2016). Comparing the impacts of Miocene–Pliocene changes in inter-ocean gateways on climate: Central American seaway, Bering Strait, and Indonesia. *Earth and Planetary Science Letters*, 444, 116–130.

Briggs, B. G. (2001). The restiads invade the north: The diaspora of the Restionaceae. In I Metcalfe, et al. (Eds.), Faunal and Floral Migration and Evolution in SE Asia-Australasia (pp. 237–241). Boca Raton, FL: CRC Press.

Bush, R., & McInerney, F. A. (2013). Leaf wax *n*-alkane distributions in and across modern plants: implications for paleoecology and chemotaxonomy. *Geochimica et Cosmochimica Acta*, 117, 161–179.

Cerling, T. E., Harris, J. M., MacFadden, B. J., Leakey, M. G., Quade, J., Eisenmann, V., & Ehleringer, J. R. (1997). Global vegetation change through the Miocene/Pliocene boundary. *Nature*, 389, 153–158.

Cerling, T. E., Wang, Y., & Quade, J. (1993). Expansion of C4 ecosystems as an indicator of global ecological change in the late Miocene. *Letters to Nature*, 361, 344–345.

Christensen, B. A., Renema, W., Henderiks, J., De Vleeschouwer, D., Groeneveld, J., Castañeda, I. S., et al. (2017). Indonesian Throughflow drove Australian climate from humid Pliocene to arid Pleistocene. *Geophysical Research Letters*, 44, 6914–6925.

Core Team, R. (2016). R: A language and environment for statistical computing. Vienna, Austria: R Foundation for Statistical Computing. Retrieved from https://www.r-project.org/

Denniston, R. F., Wyrwoll, K.-H., Asmerom, Y., Polyak, V. J., Humphreys, W. F., Cugley, J., et al. (2013). North Atlantic forcing of millennial-scale indo-Australian monsoon dynamics during the last glacial period. *Quaternary Science Reviews*, 72, 159–168.

Dupont, L. M., Rommerskirchen, F., Mollenhauer, G., & Schefuß, E. (2013). Miocene to Pliocene changes in south African hydrology and vegetation in relation to the expansion of C4 plants. *Earth and Planetary Science Letters*, 375, 408–417.

Edwards, E. J., Osborne, C. P., Stromberg, C. A. E., & Smith, S. A. (2010). The origins of C4 grasslands: integrating evolutionary and ecosystem science. *Science*, 328, 587–591.

Ehleringer, J. R. (2005). The influence of atmospheric CO_2, temperature, and water on the abundance of C3/C4 taxa. In I. T. Baldwin, M. M. Caldwell, G. Heldmaier, R. B. Jackson, O. L. Lange, H. A. Mooney, et al. (Eds.), A history of atmospheric CO_2 and its effects on plants, animals, and ecosystems, (pp. 214–231). New York, NY: Springer.

Ehleringer, J. R., Sage, R. F., Flanagan, L. B., & Pearcy, R. W. (1991). Climate change and the evolution of C4 photosynthesis. *Trends in Ecology & Evolution*, 6(3), 95–99.

Eroglu, D., McRobie, F. H., Ozken, I., Stemler, T., Wyrwoll, K.H., Breitenbach, S. F. M., et al. (2016). See–saw relationship of the Holocene East Asian–Australian summer monsoon. *Nature Communications*, 7.

Feakins, S. J., Levin, N. E., Liddy, H. M., Sieracki, A., Eglinton, T. I., & Bonnefille, R. (2013). Northeast African vegetation change over 12 m.y. *Geology*, 41(3), 295–298.

Fox, D. L., Honey, J. G., Martin, R. A., & Peláez-Campomanes, P. (2012). Pedogenic carbonate stable isotope record of environmental change during the Neogene in the southern Great Plains, southwest Kansas, USA: carbon isotopes and the evolution of C4-dominated grasslands. *GSA Bulletin*, 124(3–4), 444–462.

Fox, D. L., & Koch, P. L. (2004). Carbon and oxygen isotopic variability in Neogene paleosol carbonates: constraints on the evolution of the C4-grasslands of the Great Plains, USA. *Palaeogeography, Palaeoclimatology, Palaeoecology*, 207(3), 305–329.

Garcin, Y., Schefuß, E., Schwab, V. F., Garreta, V., Gleixner, G., Vincens, A., et al. (2014). Reconstructing C3 and C4 vegetation cover using *n*-alkane carbon isotope ratios in recent lake sediments from Cameroon, Western Central Africa. *Geochimica et Cosmochimica Acta*, 142, 482–500.

Ge, J., Dai, Y., Zhang, Z., Zhao, D., Li, Q., Zhang, Y., et al. (2013). Major changes in east Asian climate in themid-Pliocene: Triggered by the uplift of the Tibetan plateau or global cooling? *Journal of Asian Earth Sciences*, 69, 48–59.

Ghosh, S., Sanyal, P., & Kumar, R. (2017). Evolution of C4 plants and controlling factors: insight from *n*-alkane isotopic values of NW Indian Siwalik paleosols. *Organic Geochemistry*, 110, 110–121.

Groeneveld, J., Henderiks, J., Renema, W., McHugh, C. M., De Vleeschouwer, D., Christensen, B. A., et al. (2017). Australian shelf sediments reveal shifts in Miocene Southern Hemisphere westerlies. *Science Advances*, 3(5).

406 Guo, Z., Peng, S., Hao, Q., Biscaye, P. E., An, Z., & Liu, T. (2004). Late Miocene–
407 Pliocene development of Asian aridification as recorded in the red-earth formation
408 in northern China. *Global and Planetary Change*, 41(3), 135–145.
409 Haq, B. U., von Rad, U., O'Connell, S., Bent, A., Blome, C. D., Borella, P. E., et al.
410 (1990). Proceedings of the ODP Initial Reports, 122.
411 Hattersley, P. W. (1983). The distribution of C3 and C4 grasses in Australia in relation to
412 climate. *Oecologia*, 57(1-2), 113–128.
413 Herbert, T. D., Lawrence, K. T., Tzanova, A., Peterson, L. C., Caballero-Gill, R., & Kelly,
414 C. S. (2016). Late Miocene global cooling and the rise of modern ecosystems.
415 *Nature Geoscience*, 9(11), 843–847.
416 Hesse, P. P., & McTainsh, G. H. (2003). Australian dust deposits: modern processes and
417 the Quaternary record. *Quaternary Science Reviews*, 22(18-19), 2007–2035.
418 Higgins, S. I., & Scheiter, S. (2012). Atmospheric CO_2 forces abrupt vegetation shifts
419 locally, but not globally. *Nature*, 488, 209–212.
420 Hilgen, F. J., Lourens, L. J., Van Dam, J. A., Beu, A. G., Boyes, A. F., Cooper, R. A., et al.
421 (2012). Chapter 29—The Neogene Period. In The Geologic Time Scale, (pp. 923–
422 978). Boston: Elsevier.
423 Hoetzel, S., Dupont, L., Schefuß, E., Rommerskirchen, F., & Wefer, G. (2013). The role of
424 fire in Miocene to Pliocene C4 grassland and ecosystem evolution. *Nature*
425 *Geoscience*, 6(12), 1027–1030.
426 Howard, S., McInerney, F. A., Caddy-Retalic, S., Hall, P. A., & Andrae, J. W. (2018).
427 Modelling leaf wax *n*-alkane inputs to soils along a latitudinal transect across
428 Australia. *Organic Geochemistry*, 121, 126–137.
429 Jochum, M., Fox-Kemper, B., Molnar, P. H., & Shields, C. (2009). Differences in the
430 Indonesian seaway in a coupled climate model and their relevance to Pliocene
431 climate and El Niño. *Paleoceanography*, 24(1).

Karas, C., Nürnberg, D., Tiedemann, R., & Garbe-Schönberg, D. (2011). Pliocene Indonesian Throughflow and Leeuwin Current dynamics: Implications for Indian Ocean polar heat flux. *Paleoceanography*, 26(2).

Kattge, J., Díaz, S., Lavorel, S., Prentice, I. C., Leadley, P., Bönisch, G., et al. (2011). TRY—A global database of plant traits. *Global Change Biology*, 17(9), 2905–2935.

Keeley, J. E., & Bond, W. J. (2001). On incorporating fire into our thinking about natural ecosystems: a response to Saha and Howe. *The American Naturalist*, 158(6), 664–670.

Kershaw, A. P., Martin, H. A., & McEwen-Mason, J. R. C. (1994). The Neogene: A period of transition. In R. S. Hill (Ed.), History of the Australian Vegetation: Cretaceous to Recent (Chapter 13, pp. 299–327). New York: Cambridge University Press.

Knapp, A. K., &Medina, E. (1999). Success of C4 photosynthesis in the field: Lessons from communities dominated by C4 plants. In R. F. Sage, & R. K. Monson (Eds.), C4 Plant Biology (Chapter 8, pp. 251–283). London: Academic Press.

Krebs, U., Park, W., & Schneider, B. (2011). Pliocene aridification of Australia caused by tectonically induced weakening of the Indonesian throughflow. *Palaeogeography, Palaeoclimatology, Palaeoecology*, 309(1), 111–117.

Laver, R. J., Nielsen, S. V., Rosauer, D. F., & Oliver, P. M. (2017). Trans-biome diversity in Australian grass-specialist lizards (Diplodactylidae: Strophurus). *Molecular Phylogenetics and Evolution*, 115, 62–70.

Leigh, J. H. (1994). Chenopod shrublands. In R. H. Groves (Ed.), Australian Vegetation (Chapter 12, pp. 345–368). Cambridge: Cambridge University Press.

Liu, Y., Lo, L., Shi, Z., Wei, K.-Y., Chou, C.-J., Chen, Y.-C., et al. (2015). Obliquity pacing of the western Pacific Intertropical Convergence Zone over the past 282,000 years. *Nature Communications*, 6(1).

457 Liu, Z., Otto-Bliesner, B., Kutzbach, J., Li, L., & Shields, C. (2003). Coupled climate
458 simulation of the evolution of global monsoons in the Holocene. *Journal of*
459 *Climate*, 16(15), 2472–2490.
460 Locker, S., & Martini, E. (1986). Phytoliths from the Southwest Pacific, Site 591. *Initial*
461 *Reports of the Deep Sea Drilling Project*, 90, 1079–1084.
462 Long, S. P. (1999). Environmental responses. In R. F. Sage, & R. K. Monson (Eds.), C4
463 Plant Biology (Chapter 7, pp. 215–249). London: Academic Press.
464 Lowrey, T. (2015). Master plant species information database for the Sevilleta National
465 Wildlife Refuge, New Mexico (1989-1996). Retrieved from:
466 http://sev.lternet.edu/data/sev-51
467 Lu, H., Wang, X., & Li, L. (2010). Aeolian sediment evidence that global cooling has
468 driven late Cenozoic stepwise aridification in central Asia. In P. D. Clift, R. Tada,
469 & H. Zheng (Eds.), Monsoon Evolution and Tectonics-Climate Linkage in Asia,
470 (Vol. 342, pp. 29–44). London: Geological Society.
471 MacFadden, B. J., Cerling, T. E., & Prado, J. (1996). Cenozoic terrestrial ecosystem
472 evolution in Argentina: evidence from carbon isotopes of fossil mammal teeth.
473 *PALAIOS*, 11(4), 319–327.
474 Macphail, M. K. (1997). Late Neogene climates in Australia: fossil pollen- and spore-
475 based estimates in retrospect and Prospect. *Australian Journal of Botany*, 45(3),
476 425–464.
477 Martin, H. A. (2006). Cenozoic climatic change and the development of the arid vegetation
478 in Australia. *Journal of Arid Environments*, 66(3), 533–563.
479 Martin, H. A., & McMinn, A. (1994). Late Cainozoic vegetation history of North-Western
480 Australia, from the palynology of a deep sea core (ODP site 765). *Australian*
481 *Journal of Botany*, 42(1), 95–102.

Mejía, L. M., Méndez-Vicente, A., Abrevaya, L., Lawrence, K. T., Ladlow, C., Bolton, C., et al. (2017). A diatom record of CO_2 decline since the late Miocene. Earth and Planetary Science Letters, 479, 18–33.

Montanari, S., Louys, J., & Price, G. J. (2013). Pliocene paleoenvironments of southeastern Queensland, Australia inferred from stable isotopes of marsupial tooth enamel. *PLoS One*, 8(6).

Moore, P. D., Webb, J. A., & Collinson, M. E. (1991). Pollen analysis, (2nd ed.). London: Blackwell Scientific Publications. Munsterman, D., & Kerstholt, S. (1996). Sodium polytungstate, a new non-toxic alternative to bromoform in heavy liquid separation. Review of Palaeobotany and Palynology, 91(1), 417–422.

Murphy, B. P., & Bowman, D. M. J. S. (2007). Seasonal water availability predicts the relative abundance of C3 and C4 grasses in Australia. *Global Ecology and Biogeography*, 16(2), 160–169.

Nielsen, S. V., Oliver, P. M., Laver, R. J., Bauer, A. M., & Noonan, B. P. (2016). Stripes, jewels and spines: further investigations into the evolution of defensive strategies in a chemically defended gecko radiation (Strophurus, Diplodactylidae). *Zoologica Scripta*, 45(5), 481–493.

Osborne, C. P. (2008). Atmosphere, ecology and evolution: what drove the Miocene expansion of C4 grasslands? *Journal of Ecology*, 96(1), 35–45.

Osborne, C. P., Salomaa, A., Kluyver, T. A., Visser, V., Kellogg, E. A., Morrone, O., et al. (2014). A global database of C4 photosynthesis in grasses. *New Phytologist*, 204(3), 441–446.

Passey, B. H., Ayliffe, L. K., Kaakinen, A., Zhang, Z., Eronen, J. T., Zhu, Y., et al. (2009). Strengthened East Asian summer monsoons during a period of high-latitude warmth? Isotopic evidence from Mio-Pliocene fossil mammals and soil carbonates from northern China. *Earth and Planetary Science Letters*, 277(3-4), 443–452.

508 Passey, B. H., Cerling, T. E., Perkins, M. E., Voorhies, M. R., Harris, J. M., & Tucker, S.
509 T. (2002). Environmental change in the Great Plains: an isotopic record from fossil
510 horses. *The Journal of Geology*, 110(2), 123–140.
511 Polissar, P. J., & D'Andrea, W. J. (2014). Uncertainty in paleohydrologic reconstructions
512 from molecular δD values. *Geochimica et Cosmochimica Acta*, 129, 146–156.
513 Quade, J., & Cerling, T. E. (1995). Expansion of C4 grasses in the late Miocene of
514 northern Pakistan: evidence from stable isotopes in paleosols. *Palaeogeography,*
515 *Palaeoclimatology, Palaeoecology*, 115(1-4), 91–116.
516 Raymo, M. E. (1994). The initiation of northern hemisphere glaciation. *Annual Review of*
517 *Earth and Planetary Sciences*, 22(1), 353–383.
518 Rea, D. K., Basov, I. A., Janecek, T. R., Arnold, E., Barron, J. A., Beaufort, L., et al.
519 (1993). Sites 885/886. *Proceedings of Ocean Drilling Program*, Initial Report 145,
520 303.
521 Rea, D. K., Snoeckx, H., & Joseph, L. H. (1998). Late Cenozoic eolian deposition in the
522 North Pacific: Asian drying, Tibetan uplift, and cooling of the northern hemisphere.
523 *Paleoceanography*, 13, 215–224.
524 Rommerskirchen, F., Plader, A., Eglinton, G., Chikaraishi, Y., & Rullkötter, J. (2006).
525 Chemotaxonomic significance of distribution and stable carbon isotopic
526 composition of long-chain alkanes and alkan-1-ols in C4 grass waxes. *Organic*
527 *Geochemistry*, 37(10), 1303–1332.
528 Sage, R. F., Wedin, D. A., & Li, M. (1999). The biogeography of C4 photosynthesis:
529 Patterns and controlling factors. In R. F. Sage, & R. K. Monson (Eds.), C4 Plant
530 Biology (Chapter 10, pp. 313–373). London: Academic Press.
531 Scheiter, S., Higgins, S. I., Osborne, C. P., Bradshaw, C., Lunt, D. J., Ripley, B. S., et al.
532 (2012). Fire and fire-adapted vegetation promoted C4 expansion in the late
533 Miocene. *New Phytologist*, 195(3), 653–666.

534 Shi, Z. G., Liu, X. D., Sun, Y. B., An, Z. S., Liu, Z., & Kutzbach, J. (2011). Distinct
535 responses of East Asian summer and winter monsoons to astronomical forcing.
536 *Climate of the Past*, 7(4), 1363–1370.
537 Sniderman, J. M. K., Woodhead, J. D., Hellstrom, J., Jordan, G. J., Drysdale, R. N., Tyler,
538 J. J., & Porch, N. (2016). Pliocene reversal of late Neogene aridification.
539 *Proceedings of the National Academy of Sciences*, 113(8), 1999–2004.
540 Snoeckx, H., Rea, D. K., Jones, C. E., & Ingram, B. L. (1995). Eolian and silica deposition
541 in the Central North Pacific: results from Sites 885/886. *Proceedings of the Ocean*
542 *Drilling Program*, Scientific Results, 145.
543 Still, C. J., Berry, J. A., Collatz, G. J., & DeFries, R. S. (2003). Global distribution of C3
544 and C4 vegetation: carbon cycle implications. *Global Biogeochemical Cycles*,
545 17(1), 1006.
546 Strömberg, C. A. E. (2011). Evolution of grasses and grassland ecosystems. *Annual Review*
547 *of Earth and Planetary Sciences*, 39(1), 517–544.
548 Sun, D., Shaw, J., An, Z., Cheng, M., & Yue, L. (1998). Magnetostratigraphy and
549 paleoclimatic interpretation of a continuous 7.2 Ma late Cenozoic eolian sediments
550 from the Chinese Loess Plateau. *Geophysical Research Letters*, 25, 85–88.
551 Tang, C. (1992). Paleomagnetism of Cenozoic sediments in holes 762B and 763A, central
552 Exmouth Plateau, Northwest Australia. *Proceedings of the ODP*, 122, 717–733.
553 Tipple, B. J., Meyers, S. R., & Pagani, M. (2010). Carbon isotope ratio of Cenozoic CO_2: a
554 comparative evaluation of available geochemical proxies. *Paleoceanography*, 25(3).
555 Tipple, B. J., & Pagani, M. (2007). The early origins of terrestrial C4 photosynthesis.
556 *Annual Review of Earth and Planetary Sciences*, 35(1), 435–461.
557 Toon, A., Crisp, M. D., Gamage, H., Mant, J., Morris, D. C., Schmidt, S., & Cook, L. G.
558 (2015). Key innovation or adaptive change? A test of leaf traits using Triodiinae in
559 Australia. *Scientific Reports*, 5(1).

560 Ulrich, J. (2018). TTR: Technical Trading Rules. Retrieved from https://cran.r-
561 project.org/package=TTR
562 Uno, K. T., Polissar, P. J., Jackson, K. E., & deMenocal, P. B. (2016). Neogene biomarker
563 record of vegetation change in eastern Africa. *Proceedings of the National Academy*
564 *of Sciences*, 113(23), 6355–6363.
565 Vogts, A., Moossen, H., Rommerskirchen, F., & Rullkötter, J. (2009). Distribution patterns
566 and stable carbon isotopic composition of alkanes and alkan-1-ols from plant waxes
567 of African rain forest and savanna C3 species. *Organic Geochemistry*, 40(10),
568 1037–1054.
569 White, A., Sparrow, B., Leitch, E., Foulkes, J., Filitton, R., Lowe, A. J., & Caddy-Retalic,
570 S. (2012). AusPlots Rangelands Survey Protocol Manual. Adelaide: Adelaide
571 University Press.
572 Williams, R. J., Cook, G. D., Liedloff, A. C., & Bond, W. J. (2017). Australia's tropical
573 savannas: Vast, ancient and rich landscapes. In D. A. Keith (Ed.), Australian
574 Vegetation, (pp. 368–388). Cambridge: Cambridge University Press.
575 Wyrwoll, K.-H., Liu, Z., Chen, G., Kutzbach, J. E., & Liu, X. (2007). Sensitivity of the
576 Australian summer monsoon to tilt and precession forcing. *Quaternary Science*
577 *Reviews*, 26(25), 3043–3057.
578 Wyrwoll, K.-H., & Valdes, P. (2003). Insolation forcing of the Australian monsoon as
579 controls of Pleistocene mega-lake events. *Geophysical Research Letters*, 30(24),
580 2279.
581 Yancheva, G., Nowaczyk, N. R., Mingram, J., Dulski, P., Schettler, G., Negendank, J. F.
582 W., et al. (2007). Influence of the intertropical convergence zone on the East Asian
583 monsoon. *Nature*, 445, 74–77.

584 Zheng, H., Powell, C. M., Rea, D. K., Wang, J., & Wang, P. (2004). Late Miocene and
585 mid-Pliocene enhancement of the East Asian monsoon as viewed from the land and
586 sea. *Global and Planetary Change*, 41(3), 147–155.
587 Zhou, B., Bird, M., Zheng, H., Zhang, E., Wurster, C. M., Xie, L., & Taylor, D. (2017).
588 New sedimentary evidence reveals a unique history of C4 biomass in continental
589 East Asia since the Early Miocene. *Scientific Reports*, 7(1), 170–178.

Appendix

Initial expansion of C4 vegetation in Australia during the late Pliocene*

*Originally published as Andrae, J.W., McInerney, F.A., Polissar, P.J., Sniderman, J.M.K., Howard, S., Hall, P.A. and Phelps, S.R. (2018) Initial expansion of C4 vegetation in Australia during the late Pliocene, *Geophysical Research Letters*, 45, 4831-4840.

Introduction

This document consists of supporting information detailing methods used to generate supporting data used for interpretation of records. Supplementary figures are visual representations of either full datasets, or data used exclusively for interpretation purposes that does not warrant inclusion in the main text. This includes: isotope data of all *n*-alkane homologs, including those that are not ubiquitous throughout the record, and as such are not included in the main text figures; and pollen diagrams of all taxa individually, summarized in the main text figures. A supplementary table details Kolmogorov-Smirnoff statistical results from modern plant *n*-alkane distribution comparisons. Captions for full datasets are also included.

Text S1.

Text S1.1 Construction of C4 distribution map and C4 probability calculations

C4 proportion at sites across Australia was estimated based on vegetation surveys (n=521) undertaken by the Terrestrial Ecosystems Research Network (TERN) and made available through the TERN AEKOS data portal (www.aekos.org.au). The surveys were conducted following the Austplots Rangeland Survey Protocol in which vegetation occurrences are documented at each of 1010 survey point across a one hectare plot (White et al., 2012). Each species was assigned, when possible, to the C3, C4 or CAM photosynthetic pathway by cross-referencing species names in the Ausplots surveys with

those in several photosynthetic pathway databases; TRY (Kattge et al., 2011), Osborne et al. (2014) and Sevilleta LTER (Lowrey, 2015). Proportion C4 was calculated for a given site by dividing the C4 species' occurrences by the total occurrences of C3 and C4 species. Taxa that could not be assigned a photosynthetic pathway were excluded from the calculations. Probability of the presence of C4 for a given Summer Rainfall Index (SRI) was calculated using this survey data. SRI was calculated as total summer precipitation (December, January, February) divided by the sum of summer (December, January February) and winter (June, July, August) precipitation, using Australian Bureau of Meteorology 1 km resolution gridded climate datasets (Australian Government Bureau of Meteorology, 2016) (Figure 1a). SRI values were extracted for each TERN site. Sites where any C4 was present were assigned a value of 1, and sites with no C4 assigned a value of 0. Sites were binned by SRI in intervals of 0.1, with the binary presence/absence values for a given bin averaged.

Text S1.2 GC-MS specifications for sedimentary *n*-alkane characterization

Samples were injected into a PSS injector in split-less mode at an initial temperature and flow rate of 225 ^{o}C and 5 mL min^{-1} respectively. The injector was then ramped immediately to 325 ^{o}C (0.6 min hold). Flow rate was reduced to 1 mL min^{-1} with a split ratio of 30:1 at 0.5 min and increased to 3mL min^{-1} at a rate of 1mL min^{-1} after 32.4 min, remaining at this rate until completion. Oven temperature was held for 1 min at 50 ^{o}C then ramped at 8 ^{o}C min^{-1} up to 310 ^{o}C and held for 16.5 minutes. Following a solvent delay (3.5 minutes), data was collected in full scan mode from 45Da to 500Da at 3 scans sec^{-1}.

636 **Text S1.3 Analysis of modern Australian plant *n*-alkanes**

637 Quantitation of long-chain (C27 to C35) *n*-alkanes was undertaken on leaf waxes
638 extracted from samples of plants collected in Australia by the Terrestrial Ecosystems
639 Research Network (TERN). *n*-Alkanes were extracted using sonication in 9:1
640 DCM:methanol, and purified using silica gel chromatography, with 4 mL of hexane
641 followed by 4 mL of 1:1 DCM:methanol. The *n*-alkanes were characterized and quantified
642 using the GC-MS methodology described above. The proportional abundance of each of
643 the odd *n*-alkane homologs (C27-C35) was calculated. This data was subset based on broad
644 plant growth habits (trees, shrubs (including forbs) and grasses). Distributions of *n*-alkane
645 homologs for different plant growth habits were subject to two-sample Kolmogorov-
646 Smirnov (K-S) tests, conducted using base R (R Core Team, 2016), to assess the
647 frequentist statistical significance of differences between these distributions. Please note
648 that these methods and data are published in Howard et al., 2018.

649 **Text S1.4 Mass Accumulation Rate (MAR) Recalculations**

650 MAR data from ODP cores 885A and 886B (Snoeckx et al., 1995) was recalculated
651 based on updated palaeo-magnetic reversal event ages, with those from Rea et al. (1993)
652 updated to Hilgen et al. (2012). These event ages were used as tie-points to create linearly
653 interpolated age-depth models for each core. MAR was recalculated using sedimentation
654 rates based on the updated age-depth models, as well as dry bulk density and weight
655 percent aeolian values from Snoeckx et al. (1995).

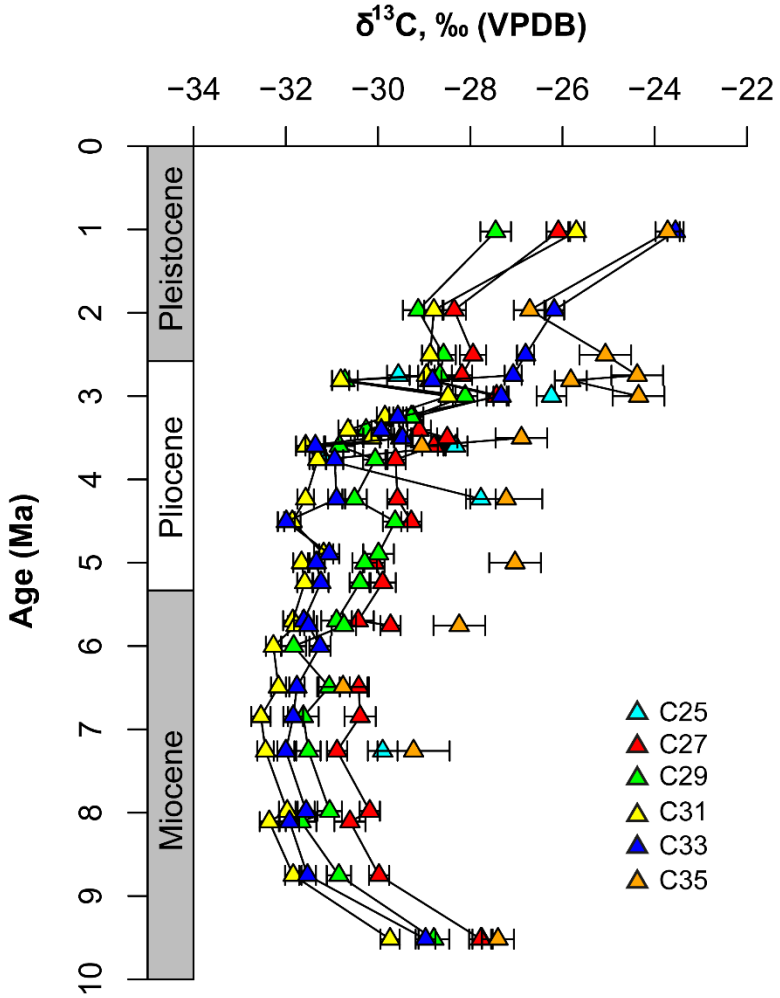

Figure S1. Compound specific carbon isotope ratios of all *n*-alkane homologs measured (odd C25-C35). Note that some carbon isotope ratios could not be measured in all samples due to either low abundance or co-elution with other compounds (those presented in the main text are ubiquitous through the record). Error bars represent plus and minus one standard error of the mean.

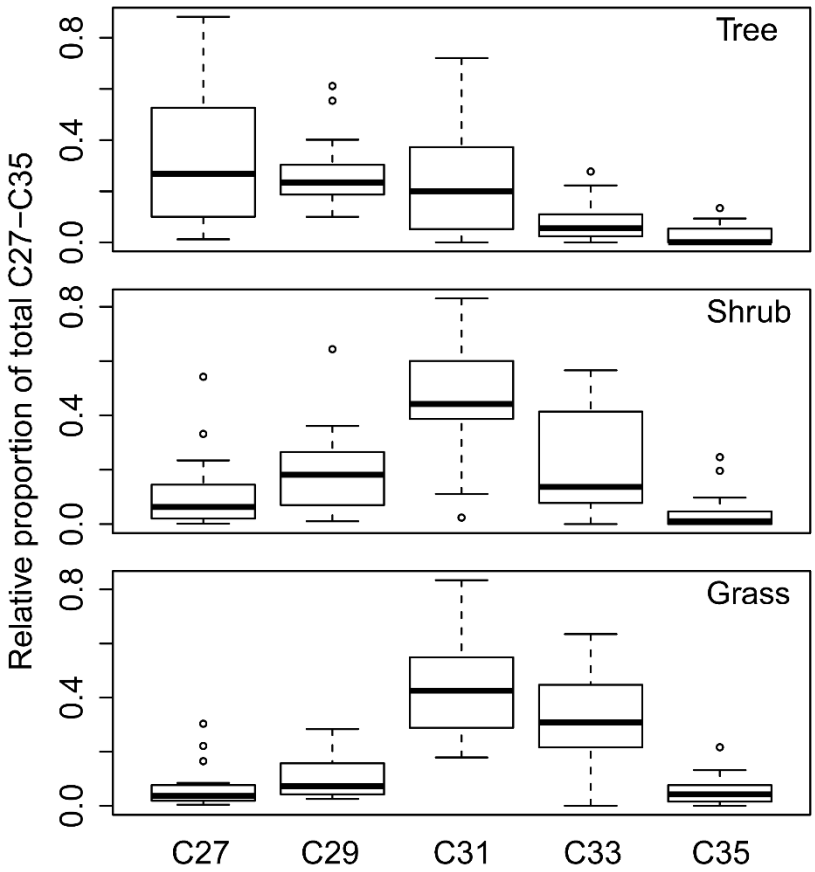

Figure S2. Odd *n*-alkane concentrations (C27-C35) as a proportion of the sum of total concentration for Australian trees, shrubs and grasses (Howard et al., 2018).

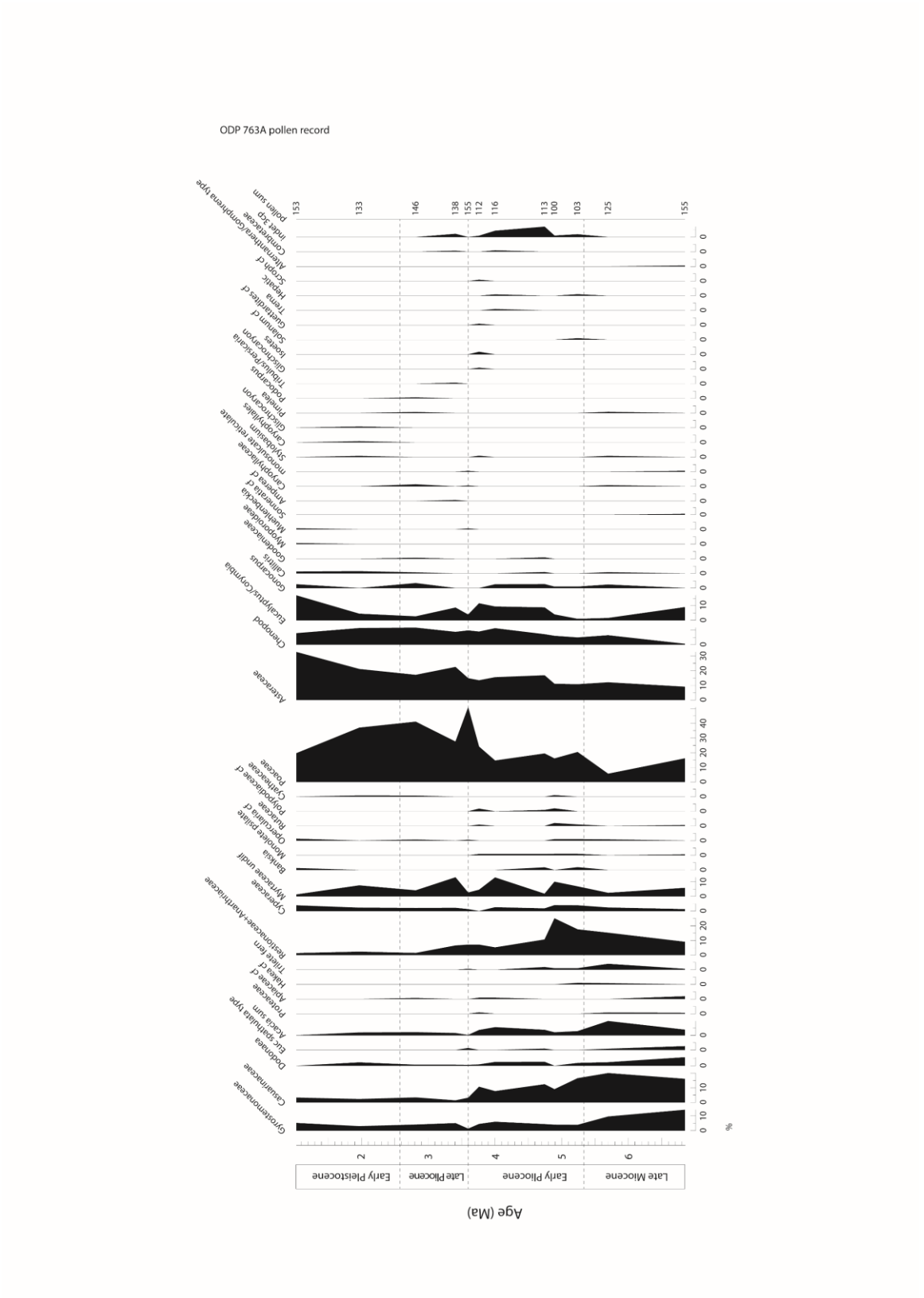

Figure S3. Complete pollen diagram showing proportional abundances of taxa and total pollen counts for ODP 763A.

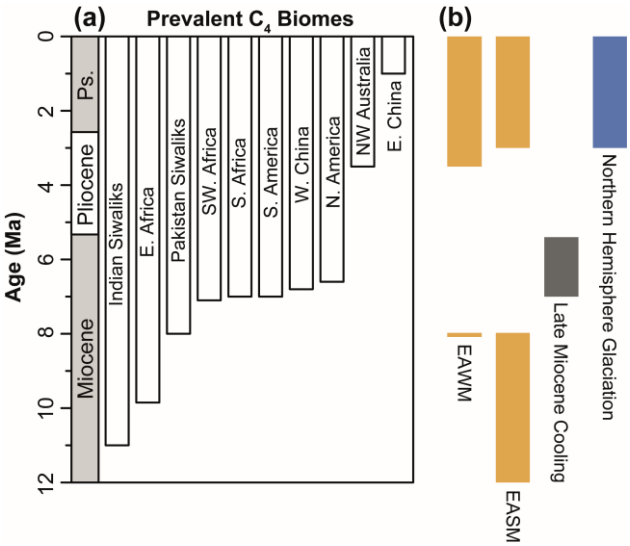

Figure S4. The timing of onsets of C4 expansion from different geographic regions, in the context of contemporaneous key global climate and environment changes. (a) Timing of onsets in order of oldest to youngest; Indian Siwaliks (Ghosh et al., 2017), East Africa (Uno et al., 2016), Pakistan Siwaliks (Quade & Cerling, 1995), South-Western Africa (Hoetzel et al., 2013), South Africa (Dupont et al., 2013), South America (Cerling et al., 1997; MacFadden et al., 1996), Western China (Passey et al., 2009), North America (Cerling et al., 1997; Passey et al., 2002), NW Australia (this study), Eastern China (Zhou et al., 2017). (b) Timings of significant climate and environmental changes that may have contributed to promoting the conditions necessary for C4 expansion on the Australian continent. Orange bars indicate periods of East Asian Winter monsoon (EAWM) and East Asian Summer monsoon (EASM) intensification (Rea et al., 1998; Snoeckx et al., 1995; Zhou et al., 2017). Grey and blue bars show periods of cooling, specifically the Late Miocene Cooling (Herbert et al., 2016) and the period of Northern Hemisphere glaciation (Raymo, 1994).

Kolmogorov-Smirnov D value

	C27 Tree	C27 Shrub	C27 Grass
C27 Tree		0.502	0.696
C27 Shrub	0.502		0.326
C27 Grass	0.696	0.326	
	C29 Tree	C29 Shrub	C29 Grass
C29 Tree		0.333	0.646
C29 Shrub	0.333		0.324
C29 Grass	0.646	0.324	
	C31 Tree	C31 Shrub	C31 Grass
C31 Tree		0.608	0.492
C31 Shrub	0.608		0.186
C31 Grass	0.492	0.186	
	C33 Tree	C33 Shrub	C33 Grass
C33 Tree		0.436	0.719
C33 Shrub	0.436		0.464
C33 Grass	0.719	0.464	

	C35 Tree	C35 Shrub	C35 Grass
C35 Tree		0.187	0.465
C35 Shrub	0.187		0.321
C35 Grass	0.465	0.321	

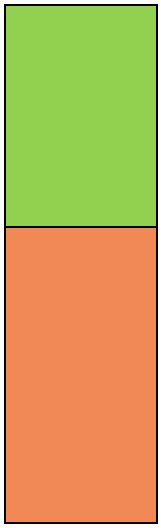

Significant difference ($p < 0.05$)

No significant difference ($p > 0.05$)

Table S1. KS statistics for modern Australian vegetation *n*-alkane distribution comparisons (Howard et al., 2018).

For supplementary Data Sets S1 through S5, the reader is directed to the online version of the article: https://doi.org/10.1029/2018GL077833

Additionally, Data Sets S1 and S2 can be found archived with the PANGAEA Data Publisher for Earth and Environmental Sciences: https://doi.pangaea.de/10.1594/PANGAEA.903716

Statement of Authorship

Title of Paper	Expansion of C4 vegetation in north-western Australia driven by increased seasonality of precipitation
Publication Status	☐ Published ☐ Accepted for Publication ☐ Submitted for Publication ☑ Unpublished and Unsubmitted work written in manuscript style
Publication Details	Formatted for submission to *Paleoceanography and Paleoclimatology*

Principal Author

Name of Principal Author (Candidate)	Jake W. Andrae
Contribution to the Paper	Undertook research design, sample acquisition, sample preparation and much of the data analysis, processing and interpretation. Led the development and drafting of the manuscript, produced all figures, and acted as the corresponding author. Along with Francesca McInerney, acquired the funding that enabled the research reported in the paper to be undertaken.
Overall percentage (%)	70%
Certification:	This paper reports on original research I conducted during the period of my Higher Degree by Research candidature and is not subject to any obligations or contractual agreements with a third party that would constrain its inclusion in this thesis. I am the primary author of this paper.
Signature	Date 04/07/19

Co-Author Contributions

By signing the Statement of Authorship, each author certifies that:

i. the candidate's stated contribution to the publication is accurate (as detailed above);
ii. permission is granted for the candidate in include the publication in the thesis; and
iii. the sum of all co-author contributions is equal to 100% less the candidate's stated contribution.

Name of Co-Author	Dr Francesca A. McInerney
Contribution to the Paper	Undertook research design and sample acquisition and contributed extensively to data interpretation. Edited and provided feedback on drafts. Along with Jake Andrae, acquired the funding that enabled the research reported in the paper to be undertaken.
Signature	Date 01/08/19

Name of Co-Author	Dr Pratigya J. Polissar
Contribution to the Paper	Undertook research design and isotopic data analysis and contributed extensively to data processing and data interpretation. Edited and provided feedback on manuscript drafts.

Signature Date 31/07/19

Name of Co-Author	Samuel R. Phelps
Contribution to the Paper	Contributed extensively to hydrogen isotope data analysis, along with data processing and interpretation. Edited and provided feedback on manuscript drafts.

Signature Date 31/07/19

Name of Co-Author	Dr Jonathan J. Tyler
Contribution to the Paper	Contributed extensively to modern climate data analysis and interpretation. Edited and provided feedback on manuscript drafts.

Signature Date 23/07/19

Name of Co-Author	J.M. Kale Sniderman
Contribution to the Paper	Undertook pollen data analysis and wrote pollen methods section. Edited and provided feedback on manuscript drafts.

Signature Date 08/07/19

Chapter 5: Expansion of C4 vegetation in north-western Australia driven by increased seasonality of precipitation

Jake W. Andrae [1,2], Francesca A. McInerney [1,2], Pratigya J. Polissar [3], Samuel R. Phelps [4,5], Jonathan J. Tyler [1,2], J.M. Kale Sniderman [6]

[1]University of Adelaide, School of Physical Sciences, Adelaide, South Australia, Australia

[2]University of Adelaide, Sprigg Geobiology Centre, Adelaide, South Australia, Australia

[3]University of California Santa Cruz, Ocean Sciences Department, Santa Cruz, CA, USA

[4]Lamont-Doherty Earth Observatory of Columbia University, Biology and Paleo Environment, Palisades, NY, USA

[5]Columbia University, Department of Earth and Environmental Sciences, New York, NY, USA

[6]University of Melbourne, School of Earth Sciences, Parkville, Victoria, Australia

Corresponding author: Jake Andrae (jake.andrae@adelaide.edu.au)

Key points

- Late Cenozoic palaeo-hydrology of north-west Australia is quantified using leaf wax hydrogen isotopes from a marine sedimentary record.
- Increasingly negative δD values of precipitation are observed since the late Pliocene in north-western Australia.
- This coincides with the onset of C4 expansion in this region and suggests a potential hydrological driver for this ecological change.

Abstract

The asynchronous expansion of C4 vegetation during the late Cenozoic between different continents was likely the result of regionally differing interplay between climate and other environmental factors, including atmospheric CO_2 concentration. The onset of C4 vegetation expansion in north-western Australia occurred several million years later than many other geographic regions, at ~3.5 Ma. In Australia today, C4 vegetation is prevalent in areas dominated by warm season precipitation, and previous work hypothesized that increased dominance of warm season precipitation may have been a strong regional tipping point for this ecological shift. Here, we measure sedimentary *n*-alkane hydrogen isotope ratios (δD_{wax}) from an Ocean Drilling Program core (ODP 763A) off north-western Australia to reconstruct precipitation dynamics across the interval of C4 expansion in Australia. We observe increasingly negative leaf wax *n*-alkane δD values from ~4 Ma, and from this interpret an increase in warm season precipitation since the late Pliocene, despite a general trend towards progressive aridification in many regions of the Australian continent since this time. Our data finds that the expansion of C4 vegetation in north-western Australia since the late Pliocene was likely to have been strongly controlled by northern Australian hydrological change.

1 Introduction

1.1 Timing and drivers of C4 expansion

The expansion of ecosystems dominated by C4 vegetation is observed across much of the globe during the late Cenozoic through the ^{13}C-enrichment of plant-fixed carbon preserved in marine and terrestrial sediments (Cerling et al., 1997; Stromberg, 2011; Tipple & Pagani, 2007). Expansion of C4 vegetation is argued to have been the final stage in a stepwise progression toward more open landscapes across this period of time, transitioning from C3 forests to C3 open-canopied vegetation and then finally C4 open-

canopied vegetation (Edwards et al., 2010; Stromberg, 2011). The expansion of C4 vegetation in Australia is recorded as ^{13}C-enrichment of leaf wax *n*-alkane compounds preserved in marine sediments off the north-west coast, with an onset of expansion during the latest Pliocene (~3.5 Ma) (Andrae et al., 2018). In Africa and Asia, carbon isotope ratios of various plant derived substrates record an onset of C4 expansion between ~6-10 Ma (Freeman & Colarusso, 2001; Polissar et al., 2019; Uno et al., 2016). In North and South America, this onset is recorded between 4-6 Ma (Cerling et al., 1997; Fox et al., 2012; Passey et al., 2009). The relative asynchronicity in the global proliferation of these now widespread ecosystems has led to debate over the drivers of these major ecological changes (Edwards et al., 2010; Fox et al., 2018; Stromberg, 2011; Zhou et al., 2018). Decreasing atmospheric CO_2 concentration (pCO_2) across the late Cenozoic had been postulated as a dominant driver for C4 expansion globally (Cerling et al., 1997; Cerling et al., 1993; Ehleringer et al., 1991) due to the competitive advantage of C4 photosynthesis over C3 photosynthesis under low pCO_2 conditions. However, the observed asynchronicity in the timing of onset of C4 expansions in different regions suggests that a global decrease in pCO_2 was not the sole cause. Work using the adaptive Dynamic Global Vegetation Model (aDGVM) shows that while pCO_2 changes have the potential to transform vegetation states, the timing of vegetation shifts globally is likely to be strongly influenced by regional differences in other climatic and environmental factors including temperature, rainfall (amount and seasonality) and fire severity (Higgins & Scheiter, 2012; Lehmann et al., 2014; Zhou et al., 2018).

One of the dominant settings in which C4 plants maintain a competitive advantage over C3 plants is where vegetation growing season is warm, with precipitation confined primarily to the warmest part of the year (Ehleringer, 2005). This is related to C4 plants not photorespiring at high temperatures, due to their using the Hatch-Slack biochemical

pathway of atmospheric CO_2 fixation (Long, 1999). The modern hydroclimate of the northern Australian tropics and sub-tropics, where C4 plants dominate today (Hattersley, 1983; Murphy & Bowman, 2007), is strongly influenced by the Indo-Australian Monsoon climate system and is characterised by a highly seasonal distribution of precipitation (Wheeler & McBride, 2005). The annual distribution of precipitation on the Australian continent clearly shows that most rainfall in northern Australia falls during the Austral summer months (December, January, February; DJF) (Fig. 1). Given modern relationships between summer-dominated precipitation and the distribution of C4 vegetation in Australia, Andrae et al. (2018) proposed that the onset of C4 expansion in Australia at ~3.5 Ma could have been driven by the onset and/or intensification of the Indo-Australian Monsoon. In this scenario, restriction of rainfall to the warmer months and reduction of winter precipitation would have increasingly confined growing season to the warmest months of the year (Austral Summer; DJF). This would have resulted in C4 plants gaining a competitive advantage over C3 plants in this region at that time. This scenario is supported by evidence for intensification of the East Asian Winter Monsoon during this time in conjunction with evidence for the existence of a cross-hemispherical relationship between the East Asian Winter and Indo-Australian Summer Monsoon systems that is observed back to at least the mid-Pleistocene (Eroglu et al., 2016; Liu et al., 2015; Rea et al., 1998; Yancheva et al., 2007). In addition, several published records suggest a link between the proliferation of C4 vegetation to regional hydrological change (e.g. Dupont et al., 2013; Huang et al., 2007). Several north-western Australian proxy records capture significant hydrological variability across the late Cenozoic (Christensen et al., 2017; Groeneveld et al., 2017; Martin, 2006; Stuut et al., 2019). Still, constraints on warm-season precipitation variability through this interval are lacking, and this hampers our ability to test this as a control on the expansion of C4 vegetation in Australia.

1.2 Reconstruction of hydrological variability using sedimentary δD_{wax}

While the annual distribution of rainfall is difficult to constrain from most proxy records, hydrogen isotope ratios of sedimentary leaf wax *n*-alkanes (sedimentary δD_{wax}) from tropical regions show promise for reconstructing warm season precipitation amount (Collins et al., 2013; Kuechler et al., 2013). Higher precipitation is correlated with increased terrestrial biomass and leads to increased net primary productivity and net carbon sequestration in terrestrial ecosystems (Chen et al., 2009; Wu et al., 2011). Production and transport of leaf wax lipids increases with increased terrestrial primary production (Conte & Weber, 2002). Today, precipitation during the Austral summer dominates the northern Australian region and plant biomass is highest during this time (Chen et al., 2003). Under these conditions, vegetation δD_{wax} transported to northern Australian sedimentary records should be biased toward reflecting growing season (warm season) precipitation δD values (Collins et al., 2013). Values of δD of precipitation in the global subtropics have been demonstrated to correlate with the amount of seasonal precipitation (Liu et al., 2010; Rozanski et al., 1993). Consequently, sedimentary δD_{wax} values in time-series from this region should primarily reflect variability in warm season precipitation amount. There is great potential for the use of sedimentary δD_{wax} to investigate precipitation dynamics across the late Cenozoic in Australia, with implications for understanding warm season precipitation variability through this time.

1.3 Study aims

In this study, we investigate key controls on modern δD values of precipitation at a local scale and develop an interpretative framework for sedimentary δD_{wax} for northern Australia using recent Global Network of Isotopes in Precipitation (GNIP) observational data. We then use this framework to infer warm season precipitation amount across the interval of C4 expansion in north-west Australia. This is undertaken through measurement

of δD_{wax} values from sediments of Ocean Drilling Program (ODP) Site 763A (Fig. 1) and development of a time-series reconstruction of ancient precipitation δD (δD_P) values, with calculations incorporating leaf wax *n*-alkane $\delta^{13}C$ values and molecular distributions to account for vegetation change. Interpretation of this reconstruction in undertaken the context of modern precipitation dynamics of northern Australia.

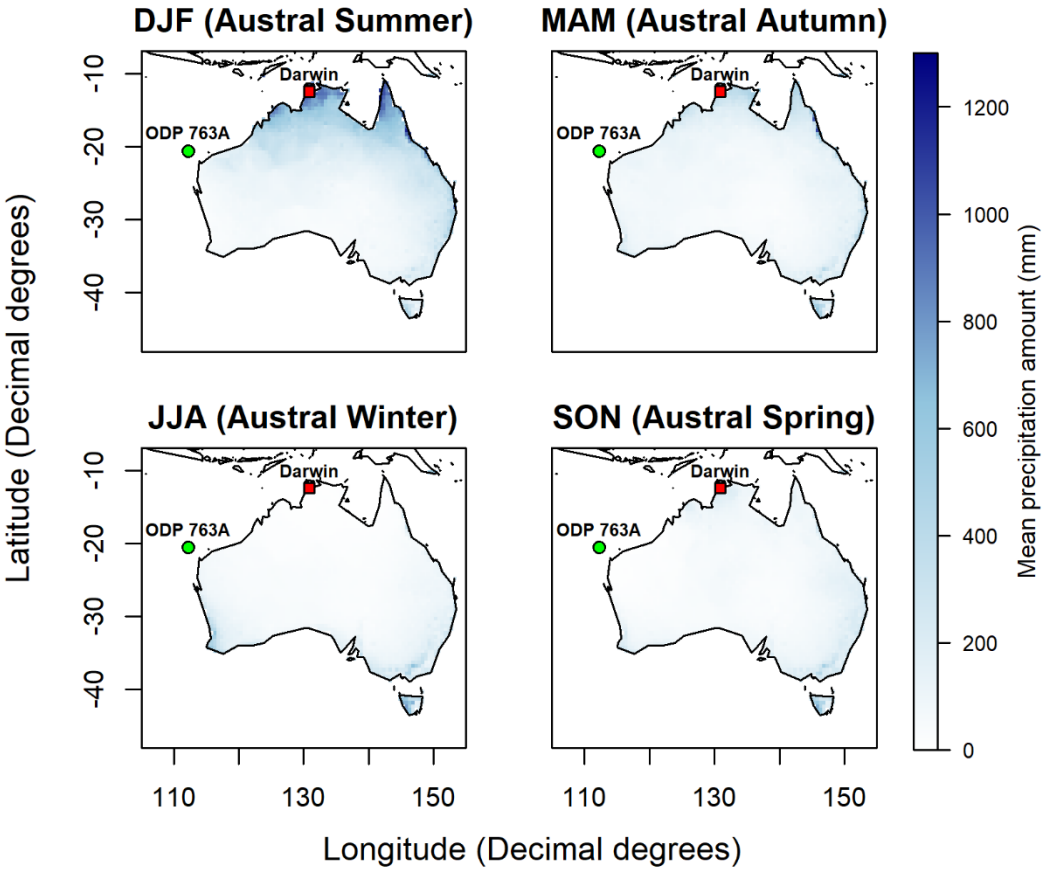

Figure 1. Total precipitation amount by season for Australia Summed precipitation amount of the Austral seasons (months indicated) across Australia interpolated for the period 1900-2014. Localities of study site (ODP 763A) and the Darwin GNIP field station are indicated. Precipitation data derived from Matsuura and Willmott (2015), with derivation and plotting of seasonal 0.5 × 0.5 degree grids undertaken using the R package 'raster' (Hijmans et al., 2019).

2 Materials and methods

2.1 Modern northern Australian precipitation characterization

Interpolated gridded monthly precipitation amount data (Matsuura & Willmott, 2015) was averaged across the period 1900 to 2014 (Matsuura & Willmott, 2015) and output as new gridded rasters using the R package 'raster' (Hijmans et al., 2019). Monthly rasters were summed to estimate total mean precipitation by Austral seasons (Summer, Autumn, Winter, Spring). In addition, means and standard error of means were calculated for observations of air temperature, precipitation amount and precipitation δD for each month of the year for the period 1962-2002 from cumulatively integrated observational data of the Darwin GNIP Darwin field station (12°25′47.99″S, 130°52′12″E; Fig. 1) (IAEA/WMO, 2019), using the 'dplyr' package (Wickham et al., 2019) in R.

2.2 Sample preparation

Samples utilized in this study comprise portions of foraminifera to nanno-fossil ooze and foraminifera bearing nanno-fossil chalk (Haq et al., 1990) from Ocean Drilling Program Hole 763A, hereafter ODP 763A. All glass apparatus in contact with samples during preparation was thoroughly cleaned with 10% Decon 90® decontaminant solution in reverse osmosis (RO) water followed by three rinses of Milli-Q water, before being ashed (425 ºC, 9hrs). Other apparatus was cleaned as above before being rinsed with three times each of methanol (MeOH), dichloromethane (DCM) and *n*-hexane. A 0.5 cm portion of all exposed surfaces of the samples was removed with a scalpel to minimize contamination by allochthonous lipid material. Samples were lyophilized in ashed borosilicate glass containers for 48 hrs prior to homogenization in a Retsch MM 400 ball mill (5 sec mill time at 30 Hz). Total lipids were extracted from sediments using a Thermo Scientific™ Dionex™ ASE™ 350. Samples underwent five cycles of solvent rinse (five minute static rinse with 9:1 DCM:methanol) and purge (two minutes) at a temperature of

100 ºC and a pressure of ~110 bar. Solvents were evaporated from the total lipid extract (TLE) at 30 ºC under ultra-high purity (99.999%, BOC) N_2 using a Biotage TurboVap® LV heated evaporator. The TLE was separated into three fractions (aliphatic, ketone/ester and polar) by solid phase extraction through ~0.5 g of solvent cleaned and oven activated (100 ºC, 24 hours) silica gel of 35 to 70 mesh size using 4 mL each of *n*-hexane, DCM and methanol, respectively. A small quantity of solvent cleaned copper turnings activated in hydrochloric acid was added to each aliphatic fraction to remove elemental sulfur prior to analysis. For sample age calculations, the published age-depth model for ODP 763A was utilized (Karas et al., 2011). Linear interpolations between palaeo-magnetic reversal datum tie-points established in Tang (1992) and updated to Hilgen et al. (2012) were utilized for periods where data was not available in the published model (after Andrae et al., 2018).

2.3 Sedimentary *n*-alkane quantification

n-Alkanes (C14 to C36) in the aliphatic fraction were characterized and quantified on an Agilent 7890B GC coupled to an Agilent 5977B MSD. Samples were dissolved in 100 μL *n*-hexane and spiked with an internal standard of 1-1' binaphthyl at a concentration of 10 μg/mL. An *n*-alkane quantitation standard was prepared by dilution of a Certified Reference Material (C7-C40 Saturated Alkanes Standard, Supelco 49452-U) to a concentration of 10 μg/mL, also with an internal standard of 1-1′ binaphthyl at a concentration of 10 μg/mL for concurrent analysis with the sample batch. From quantification data, *n*-alkane distribution metrics were calculated, including carbon preference index (CPI) and the ratio of C33 to C29 *n*-alkanes (Norm33). Formulae are as follows:

$$CPI = 0.5\left[\left[\frac{(C25 + C27 + \ldots + C35)}{(C24 + C26 + \ldots + C34)}\right] + \left[\frac{(C25 + C27 + \ldots + C35)}{(C26 + C28 + \ldots + C36)}\right]\right] \quad \text{Equation 1.}$$

Where C*n* is the total mass of a given compound in a sample (Bray & Evans, 1961).

$$\text{Norm33} = \frac{C33}{C29 + C33} \qquad \text{Equation 2.}$$

Where C*n* is the total mass of a given compound in a sample (modified from Carr et al., 2014).

2.4 Sedimentary *n*-alkane δD analysis

δD values were measured for odd *n*-alkane homologs from C25 to C35 using a Thermo Trace gas chromatograph (GC) Ultra and Isolink coupled to a Thermo Delta V isotope ratio mass spectrometer (IRMS) through a ConFlo IV interface. Samples were quantitatively diluted in *n*-hexane and injected into a PTV injector with 2 mm i.d. silicosteel liner packed with glass wool. The inlet was held splitless at 60 °C during injection and then ramped ballistically to 320 °C where it was held for 1.5 min during the transfer phase. Compounds were separated on an HP-5MS column (30 m length, 0.25 mm i.d., and 0.25 μm phase thickness) with a constant helium flow of 1.0 mL/min. The GC oven was held at 60 °C for 1.5 min, ramped at 15 °C/min to 150 °C and then at 4 °C/min to 320 ºC, and held for 10 min. The GC effluent was connected to a Thermo Scientific High Temperature Conversion (HTC) reactor held at 1430 °C. A standard mixture of *n*-alkanes (C16 to C30) with known δD values (Mix A7 purchased from Arndt Schimmelmann, Indiana University) was interspersed between sample measurements to calibrate the isotopic measurements. Measurement uncertainties (standard error of the mean), including both analytical uncertainty and uncertainty in realizing the Vienna Standard Mean Ocean Water (VSMOW) reporting scale, were calculated after Polissar and D'Andrea (2014). Data presented here are reported as means and standard error of replicates.

2.5 Sedimentary *n*-alkane $\delta^{13}C$ analysis

$\delta^{13}C$ values were measured for odd *n*-alkane homologs from C25 to C35 following the methodology reported in Andrae et al. (2018), with the exception of a Nafion membrane being used in place of a custom built cryotrap. The offset between the $\delta^{13}C$ ratio of atmospheric CO_2 for a given sample age (estimated from a high-resolution benthic CO_2 $\delta^{13}C$ record; Tipple et al. (2010)) and the pre-industrial $\delta^{13}C$ ratio of atmospheric CO_2 (-6.5‰) was applied to normalize the sedimentary $\delta^{13}C$ values (Andrae et al., 2018). A two end-member mixing model incorporating mean $\delta^{13}C$ values of the C31 *n*-alkane in modern C3 (-33.8 ‰; n = 106) and C4 (-20.1 ‰; n = 45) plants was used to calculate percent C4 from sedimentary $\delta^{13}C_{C31}$, after Garcin et al. (2014). Data presented here are reported as means and standard error of replicates.

2.6 Fossil pollen assemblage analysis

A protocol adapted from Moore et al. (1991) was utilised for fossil pollen extraction, which consisted of digesting samples in cold HCl, followed by treatment with hot 10% KOH, acetolysis (a 9:1 mixture of acetic anhydride and concentrated sulfuric acid) and overnight immersion in concentrated HF. Heavy liquid separation using a Na-polytungstate liquid of specific gravity 2.0 (Munsterman & Kerstholt, 1996) was used to isolate the acid- and alkali-resistant residues which were then dehydrated in ethanol and mounted on glass slides in glycerol. Pollen was counted using a Zeiss AxioScope A.1 with EC Plan Neofluar objectives along transects at 300X and 600X magnification until at least 100 grains were counted for most samples. Pollen type was identified by comparison with modern reference collections and with images stored in the Australasian Pollen and Spore Atlas (APSA Members, 2007).

2.7 Sample specific $\varepsilon_{C31/P}$ ($\varepsilon_{C31corr}$) calculations

Sample specific $\varepsilon_{C31/P}$ ($\varepsilon_{C31Corr}$) was calculated for each sample using a 3 end-member mixing model similar to Feakins (2013), to estimate values of δD_P from δD_{wax} through time. This calculation for each sample incorporated modern mean $\varepsilon_{C31/P}$ values of different plant growth habits (trees, C3 grasses, C4 grasses) from a compilation dataset (Sachse et al., 2012) in conjunction with estimates of fractions of these plant growth habits and photosynthetic pathway for each sample estimated using mean $\delta^{13}C_{C31}$ (see section 2.4) and Norm33. $\varepsilon_{C31Corr}$ was calculated as follows:

$$\varepsilon_{C31Corr} = [f_{grass} \times f_{C3} \times \varepsilon_{C3grass}] + [f_{grass} \times f_{C4} \times \varepsilon_{C4grass}] + [f_{tree} \times \varepsilon_{tree}] \quad \text{Equation 3.}$$

3 Results

3.1 Modern northern Australian precipitation

Observational data of precipitation amount, temperature and precipitation δD values from the Darwin, Australia GNIP field station (IAEA/WMO, 2019) was utilized to explore recent northern Australian climate and precipitation isotope dynamics (Fig. 2). Results indicate that in Darwin, most rainfall occurs during the Austral Summer (December, January, February) and the first month of Austral Autumn (March) (range of 258.86 to 463.55 mm), with moderate to low rainfall across the rest of the year (range of 7.12 to 132.74 mm) (Fig. 2a). Average mean temperatures are relatively stable between months, though the Austral winter months are somewhat cooler than DJFM. Temperatures for the winter months range between 23.71 and 25.08ºC, compared to between 28.27 and 29.04 ºC for DJFM (Fig. 2b). Average mean precipitation δD values vary considerably between months, ranging across the year from -34 to 3 ‰ (Fig. 2c).

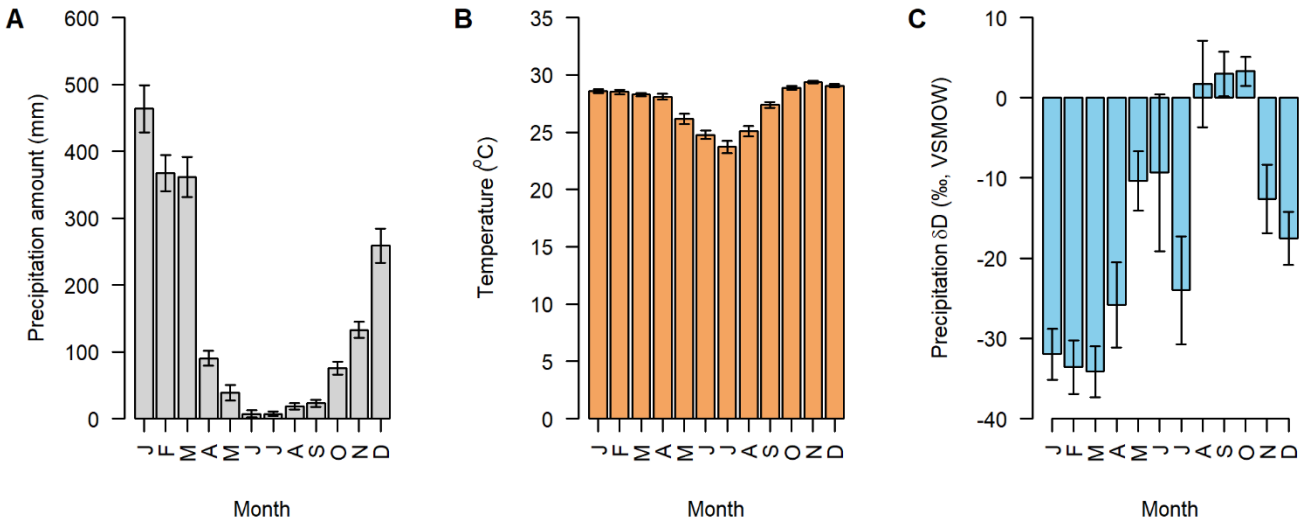

Figure 2. Average monthly mean precipitation amount, air temperature and precipitation δD for Darwin, Australia a) Aggregated mean precipitation amount of each month for the period 1962 – 2002, b) aggregated mean temperature of each month for the same period and c) aggregated mean precipitation δD of each month. Data are cumulatively integrated monthly observations from the Darwin GNIP field station (Northern Territory, Australia) (IAEA/WMO, 2019). Error bars represent one standard error of the mean.

Regression analysis of precipitation δD values and both precipitation amount and air temperature observations for 1962-2002 was undertaken using cumulatively integrated monthly observations from the Darwin GNIP field station (IAEA/WMO, 2019). This was done to understand environmental controls on modern precipitation δD values in northern Australia, particularly in relation to the temperature and amount effects (after Liu et al., 2010). No significant linear correlation exists between air temperature and precipitation δD values for all observational data across the period 1962-2002 (Fig. S1). A weak but statistically significant positive linear correlation exists, however, for observational data from only the wettest months (December, January, February, March; DJFM) across the period 1962 – 2002 (Fig. 3a). Strong and statistically significant negative linear correlations are observed between precipitation amount and precipitation δD values for all observations and DJFM observations across 1962 – 2002 (Fig. S1b, Fig. 3b).

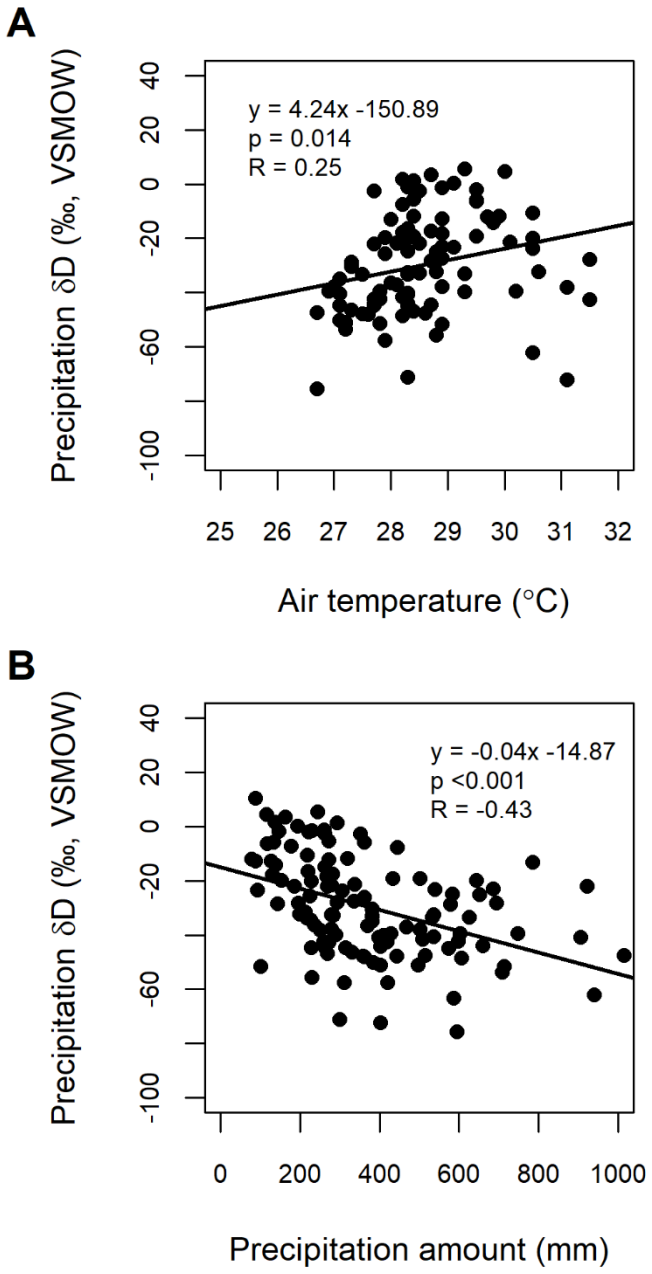

Figure 3. Linear regressions of December, January, February and March climate and precipitation δD observations for Darwin, Australia a) Relationship between air temperature and precipitation δD values for December, January, February and March observations across the period 1962 – 2002. b) Relationship between precipitation amount and precipitation δD values for December, January, February and March across the same period. Data are cumutively integrated monthly observations from the Darwin GNIP field station (IAEA/WMO, 2019).

3.2 Sedimentary δD and $\delta^{13}C$

Sedimentary δD_{wax} values are reported for *n*-alkanes extracted from 19 sediment sections of ODP 763A, ranging in age from 0.0052 to 6.75 Ma (Fig. 4a, Data Set S1). δD_{C29} values range from -133 to -106 ‰, δD_{C31} values range from -132 to -108 ‰, and δD_{C33} values range from -137 to -91 ‰. δD_{C31} values were measured for all samples, with all other chain lengths measured whenever possible. In some cases, chromatographic co-elution with the C25, C27, C29 and C35 *n*-alkane peaks occurred at the concentrations required for δD measurements, impeding reliable measurement of δD values. In these cases, the data are not presented. δD_{C31} values therefore provide the longest, highest resolution and most reliable record. The minimal bias in the production of the C31 *n*-alkane by different plant functional types (PFTs) compared to other long-chain *n*-alkane compounds (Bush & McInerney, 2013; Garcin et al., 2014; Howard et al., 2018; Vogts et al., 2009) is favourable for interpretation. No systematic size effect was found for δD_{wax} measured from compounds where peak area is above 25 Vs. For peak areas between 10 and 25 Vs, δD_{wax} bias related to peak size is ~1-2 ‰, and within the uncertainty of reference gas realization.

Sedimentary $\delta^{13}C_{wax}$ values from 19 new core levels in ODP 763A are reported here and compiled with those reported in Andrae et al. (2018), to produce a time-series of observations ranging in age from 0.0052 to 8.82 Ma (Fig. 4b, Data Set S2). Carbon isotope ratios of C29, C31 and C33 *n*-alkanes are reported for all samples. Values of $\delta^{13}C_{wax}$ adjusted for values of atmospheric CO_2 $\delta^{13}C$ range from -33.8 to -25.32 ‰ for C29, -32.8 to -24.73 ‰ for C31, and -33.8 to -23.07 ‰ for C33. $\delta^{13}C_{wax}$ values become more positive across the record for C29, C31 and C33. The expanded dataset significantly increases the resolution and length of the record and ensures complementary measurements of $\delta^{13}C_{C31}$ and δD_{C31} from the same sample. Percent C4 calculated from sedimentary $\delta^{13}C_{C31}$ values

275 ranges from 7.32 to 66.2% (see section 2.4, Fig. 4b, Data Set S2).

276 **3.3 Leaf wax *n*-alkane distributions and fossil pollen**

277 Summed concentrations of the C29, C31 and C33 *n*-alkanes in sediments of ODP
278 763A measured in this study and compiled with those from Andrae et al. (2018) range
279 from 17.6 to 314.9 ng/g dry sediment. *n*-Alkane molecular distribution metrics CPI and
280 Norm33 (see section 2.2) are reported for 19 new core levels of ODP 763A and compiled
281 with those reported in Andrae et al. (2018) (Fig. 4c, Data Set S3). In several cases,
282 measurements of CPI and Norm33 reported for previous work from this site were
283 recalculated using updated *n*-alkane quantification data from the same core levels. Overall,
284 CPI values are high throughout the record, ranging from 3.97 to 15.41. Norm33 is
285 relatively variable throughout the record, ranging from 0.41 to 0.87. Data from nine new
286 core levels are compiled with those presented in Andrae et al. (2018) to produce a time-
287 series of pollen observations ranging in age from 1.03 to 8.14 Ma (Fig. 4d, Data Set S4).
288 Pollen as a percentage of total pollen counts (between 57 to 163 grains) from the families
289 Poaceae, Asteraceae and Chenopodiaceae ranges from 24 to 75.4%, and generally
290 increases across the record. Pollen of swamp, wetland and wet heath taxa (Cyperaceae,
291 Restionaceae, Anathriaceae families, plus isoetes), as a percentage of total pollen counts,
292 ranges from 3.5 to 39.1%, with a significant decrease beginning between 4-5 Ma.

293 **3.4 Source of sedimentary *n*-alkanes in ODP 763A**

294 High CPI throughout the record is indicative of leaf wax *n*-alkanes preserved in
295 sediments of ODP 763A being derived primarily from terrestrial vegetation (Bush &
296 McInerney, 2013). In addition, the presence of substantial terrestrial vegetation pollen in
297 the record (Fig. 4d) affirms the transport and deposition of terrestrially derived plant
298 material to sediments of ODP 763A. Compound specific isotope measurements therefore

299 reflect the plant physiology and environmental variability as experienced by plants.
300 Complementary measurements of $\delta^{13}C_{wax}$, Norm 33 and δD_{wax} from the same samples
301 enable the estimation of the contribution of leaf wax *n*-alkanes from plants using different
302 photosynthetic pathways (C3 and C4) and PFT to each sample. *n*-Alkanes preserved in
303 sediments of ODP 763A are likely to be integrated from a large spatial extent of the north-
304 west Australian region and to have been transported by predominantly aeolian processes
305 given the ~300 km offshore site locality (Schreuder et al., 2018; Stuut et al., 2019).

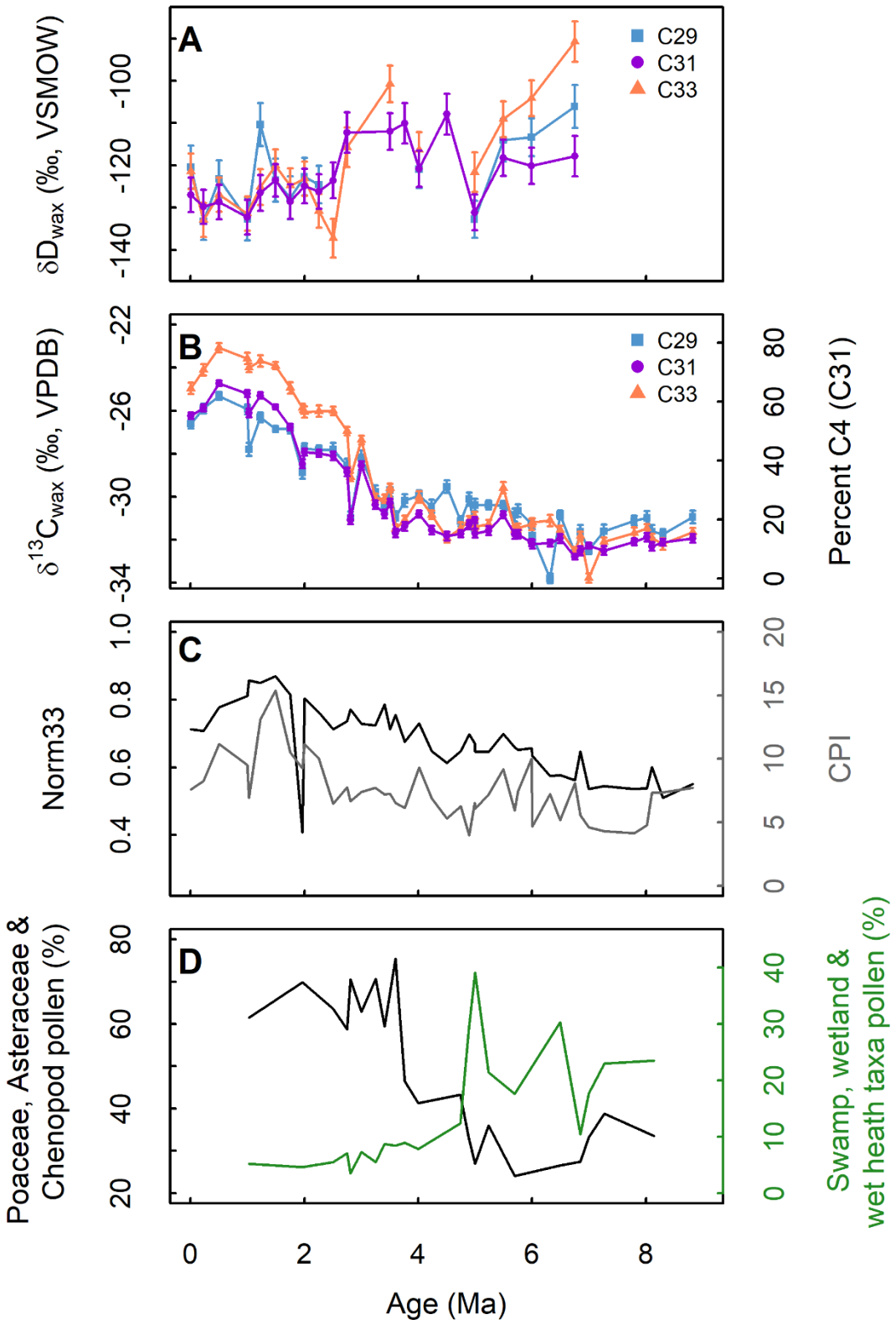

Figure 4. Sedimentary δD_{wax}, $\delta^{13}C_{wax}$, *n*-alkane molecular distribution and pollen results a) δD_{wax} values measured for the three most ubiquitous long-chain *n*-alkane compounds in the record; C29,C31,C33. b) $\delta^{13}C_{wax}$ values measured for the same compounds. c) *n*-Alkane molecular

distribution metrics Norm33 (black) and carbon preference index (grey). d) Pollen of the Poaceae, Asteraceae and Chenpodiaceae families (black) and pollen of swamp, wetland and wet heath taxa (Cyperaceae, Restionaceae and Anarthriaceae families plus isoetes; green) as percentages of total counts. Error bars for carbon and hydrogen isotope measurements represent one standard error of the mean, as calculated after Polissar and D'Andrea (2014). $\delta^{13}C_{wax}$, Norm33 and CPI include data from this study and Andrae et al. (2018); see Data Set S1 for data source.

4 Discussion

4.1 Modern northern Australian precipitation δD and sedimentary δD_{wax}

Analysis of modern observational data from the wettest months (DJFM) indicates a strong correlation between precipitation δD values and precipitation amount in the tropical wet and dry (monsoonal) climate region of northern Australia (Peel et al., 2007). There is indication of a limited temperature control on precipitation δD values for this region, consistent with the findings of Liu et al. (2010). Similar climate-isotope relationships are also observed for other tropical to sub-tropical regions, including central Africa (Collins et al., 2013) and East Asia (Vuille et al., 2005). These relationships are consistent with the amount effect being dominant where large-scale moisture convergence is the primary source of atmospheric moisture over surface evaporation (Moore et al., 2014).

Based on a study of transport dynamics of leaf wax lipids to the western North Atlantic (Conte & Weber, 2002), we assume that production, ablation and transport of leaf wax *n*-alkanes to sediments increases proportionally with biomass in northern Australia. Given this, it can be argued that sedimentary δD_{wax} in ODP 763A will be weighted towards predominantly reflecting the isotopic composition of precipitation during DJFM. As the dominant control on precipitation δD values in the north-west Australian region is found to be the amount effect, variability in sedimentary δD_{wax} values in ODP 763A should strongly reflect variability in warm season precipitation amount through time. In this interpretive

framework, more negative values of δD_{wax} will reflect periods of greater warm season precipitation. For ODP 763A, sedimentary δD_{wax} values for samples in the interval from ~4 Ma to recent show a strong trend toward more negative values, suggesting increasingly greater amount of warm season precipitation through this interval. Prior to ~4 Ma, δD_{wax} values are more variable and display higher isotopic spread. This is contrasts with samples younger than ~4 Ma, where δD_{wax} values show relatively low isotopic spread among homologs. In general, the earlier part of our record shows *n*-alkanes with more positive δD values relative to the later part of the record, suggesting that warm season precipitation dominance in northern Australia was low until the late Pliocene.

4.2 Estimates of δD_P from δD_{wax}

A series of hydrogen isotope fractionations occur in plants between source water uptake and biosynthesis of *n*-alkanes, with a resultant net apparent fractionation between values of precipitation δD and plant δD_{wax} ($\varepsilon_{wax/P}$) (Sachse et al., 2012). Significant variability is found in $\varepsilon_{wax/P}$ between different plant functional type and photosynthetic pathway. For δD_{C31} in modern plants, respective $\varepsilon_{C31/P}$ values for C3 grass, C4 grass, shrubs and trees are found to be -157 ± 4 ‰, -136 ± 3 ‰, -99 ± 4 ‰ and -113 ± 3 ‰ (Sachse et al., 2012). The $\varepsilon_{C31/P}$ value used to estimate δD_P from sedimentary δD_{C31} through time is therefore likely to be dependent on different vegetation contributions to the record. In an effort to account for this, $\varepsilon_{C31corr}$ was calculated using PFT and photosynthetic pathway fraction estimates in conjunction with a mixing model incorporating values of $\varepsilon_{C31/P}$ for different PFT and photosynthetic pathway (see Equation 3, section 2.6) (Feakins, 2013). By considering the differences in apparent fractionation between vegetation type as well as photosynthetic pathway, values of δD_{C31} were normalized to remove physiological influences that may obscure climatological signals.

Ancient δD_P values reconstructed using $\varepsilon_{C31Corr}$ are high compared to values of modern values of precipitation δD in northern Australia, which are relatively negative even in the driest months of the year (Fig. 5a). This could reflect the assumed $\varepsilon_{C31/P}$ for different plant functional type and photosynthetic pathway not being appropriate for the catchment area of ODP 763A, because the values derive from a global compilation of plants that mostly reflects regions other than Australia (Sachse et al., 2012). While Australian $\varepsilon_{C31/P}$ values estimates would be preferable for calculating $\varepsilon_{C31Corr}$ for this study, this was not possible given that of the derived $\varepsilon_{C31/P}$ values from Sachse et al. (2012) (n=331), only a small fraction (n=9) were calculated from Australian plant samples. As such, values of $\varepsilon_{C31Corr}$ used to calculate ancient δD_P values may not be realistic in the context of the Australian flora. In addition, sample-specific apparent fractionation ($\varepsilon_{C31corr}$) values applied to values of δD_{wax} varied by only ~6 ‰ throughout the record, and thus had a relatively minor impact on the range of estimated δD_P values. As such, interpretations of changing warm season rainfall amount from values of δD_P derived by applying constant apparent fractionation may be justified, as suggested by Feakins and Sessions (2010) and Vogts et al. (2016).

For modern data that encompasses various plant functional types and regions, mean apparent fractionation and one standard error of the mean for the C31 *n*-alkane ($\varepsilon_{C31/P}$) is -123 ± 2 ‰ (Sachse et al., 2012). In a survey of plants living in the arid ecosystems of southern California, Feakins and Sessions (2010) found a mean apparent fractionation of -94 ± 3 ‰, for all compounds ($\varepsilon_{wax/P}$). These values are applied as a constant apparent fractionation to values of δD_{C31} and result in values of δD_P that are much more consistent with modern estimates of northern Australian precipitation δD range (Fig 5b,c). Application of the arid ecosystem derived value of apparent fractionation of Feakins and Sessions (2010) (Fig. 5c) is realistic in the context of the relatively arid environment of the

374 Australian continent inferred across the record interval (Christensen et al., 2017; Macphail,

375 1997; Martin & McMinn, 1994) .

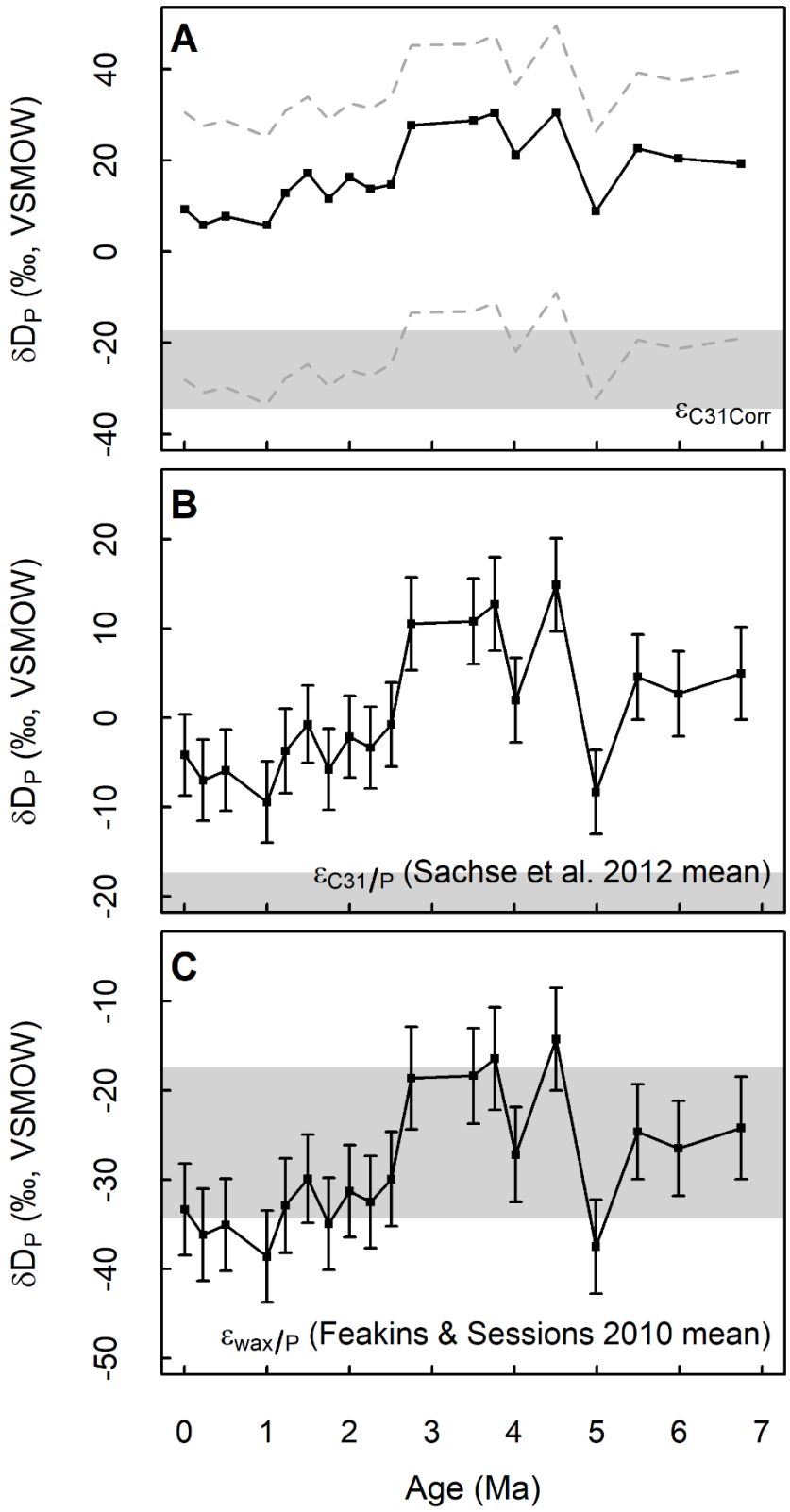

Figure 5. δD_P derivations from values of sedimentary δD_{C31} using different apparent fractionation values a) Values of δD_P derived using sample specific values of $\varepsilon_{C31Corr}$. Grey dashed lines represent δD_P derived by applying apparent fractionation values assuming 100% C3 grass and shrub input to the record, respectively (Sachse et al., 2012). b) Values of δD_P derived

using a constant value of apparent fractionation for the C31 *n*-alkane (ε_{C31}) of -123 ± 2 ‰, the mean of the global dataset of Sachse et al. (2012). Error bars reflect propagated standard error incorporating sedimentary δD measurement and modern $\varepsilon_{C31/P}$ standard error. c) Values of δD_P derived using a constant value of apparent fractionation for C25-C33 (ε_{wax}) of -94 ± 3 ‰, the mean of the arid ecosystem dataset of Feakins and Sessions (2010). Error bars reflect propagated standard error incorporating sedimentary δD measurement uncertainty and modern $\varepsilon_{wax/P}$ standard error. Grey bars reflect the range of mean values of modern precipitation δD from the months of DJFM in Darwin, Australia (from Fig. 2c).

Regardless of the apparent fractionation factor applied, after ~4 Ma, values of δD_P become increasingly negative. From this, we interpret an increase in the amount of warm season precipitation in north-western Australia, coincident with expansion of C4 vegetation in the region (Andrae et al., 2018). Several contemporaneous proxy records suggest progressive drying in north-west Australia since the late Pliocene (Christensen et al., 2017; Macphail, 1997; Martin & McMinn, 1994), and seem at first glance to be at odds with increasing warm season precipitation. However, a scenario of increasing warm season precipitation contemporaneous with greater seasonality and increasing aridity in north-west Australia is supported by climate modelling of the north-west Australian region for the Last Glacial Maximum (LGM) (Yan et al., 2018). Thus, a trend toward greater warm season precipitation in north-western Australia since ~4 Ma is interpreted from our record in the context of increasing aridification. Cool months would have become increasingly dry, while warm months would have become much wetter. This interpretation is corroborated by changes in the percentage of swamp, wetland and wet heath taxa pollen quantified from the record (Fig. 4d). High abundances of these taxa, particularly Restionaceae, prior to ~4 Ma implies perennially moist soils and suggests relatively high and uniformly distributed precipitation across north-western Australia (Briggs, 2001; Linder et al., 2003), perhaps higher than other palaeo-climatological studies have estimated

for this time (e.g. Christensen et al., 2017; Groeneveld et al., 2017). In this context, relatively negative values of δD_P in the early part of the record may reflect high and uniformly distributed precipitation in north-western Australia, rather than high warm-season precipitation. The significant decrease in these swamp, wetland and wet heath taxa pollen in sediments of ODP 763A since ~4 Ma suggests an onset of hydroclimatic conditions that were unable to support this flora, likely increasingly seasonally arid conditions.

4.3 Mechanisms for late Cenozoic hydrological change in northern Australia

Recent work by Auer et al. (2019) suggests that hydrological change in the northern Australian region could have been driven by local-scale tectonic changes. Prior to ~3.54 Ma, water transport between the Indian and Pacific Oceans was connected equatorially. At this time, tectonic uplift is thought to have caused restriction of the Indonesian Throughflow (ITF) (Auer et al., 2019; Christensen et al., 2017; Karas et al., 2011). This, in turn, caused the source region of water being transported to eastern Indian Ocean to shift from the warm tropical Pacific to the cool northern Pacific. The resultant eastern Indian Ocean cooling led to the establishment of an Indian Ocean Dipole-like mechanism, with associated changes in sea surface temperature (SST) and atmospheric circulation forcing aridification of northern Australia after ~3.3 Ma (Auer et al., 2019; Stuut et al., 2019). Experimental model results support this mechanism, indicating that ITF restriction could have reduced precipitation over the eastern Indian Ocean by as much as 30% (Krebs et al., 2011).

ITF restriction accounts for the late Cenozoic aridification observed in a number of northern Australian and other distal Australian palaeo-climatic proxy records (Christensen et al., 2017; Miller et al., 2012; Sniderman et al., 2016; Stuut et al., 2019), but it does not

account for the evolution of a summer dominated precipitation regime in northern Australia suggested by the data reported in this study. Increased aeolian dust flux into the north Pacific marine sedimentary record since the late Pliocene (Rea et al., 1998; Snoeckx et al., 1995) is interpreted as the onset of East Asian winter Monsoon (EAWM) intensification (An et al., 2001; Guo et al., 2004; Sun et al., 1998; Zheng et al., 2004). The Indo-Australian Monsoon climate system is suggested to be predominantly controlled by cross-equatorial thermal and pressure gradients between Australia and East Asia (An, 2000). Southward migration of the Intertropical convergence zone (ITCZ) related to northern hemisphere cooling has been observed on centennial–millennial to orbital time-scales in a range of late Cenozoic sedimentary records (Denniston et al., 2013; Eroglu et al., 2016; Liu et al., 2015; Yancheva et al., 2007). Stuut et al. (2019) attributed increased incidence of precipitation variance and frequency of large rainfall events after 3.8 Ma to increased summer monsoon activity linked to changes in SST. The onset of late Pliocene EAWM intensification that could have pushed the ITCZ far enough southward to drive significantly higher warm season precipitation across northern Australia (Andrae et al., 2018). The resultant seasonally wet/dry climatic conditions would have been advantageous to C4 vegetation, resulting in proliferation of C4 dominated ecosystems since that time. There is potential for these climatic conditions to have promoted environmental feedbacks such as wildfire (Osborne 2008), with these potentially further influencing the expansion of C4 vegetation in the Australian region.

5 Conclusions

Using recent climate and precipitation isotope data from Darwin, Australia, we find that the dominant control on northern Australian precipitation is the amount effect at both annual and warm season scales (DJFM). From this observation, we developed an interpretive framework for the sedimentary δD_{wax} record of ODP 763A that incorporated

leaf wax *n*-alkane production and transport dynamics. We concluded that sedimentary δD_{wax} values will be biased toward reflecting warm season precipitation for this region. As such, values of sedimentary δD_{wax} across the ODP 763A record will reflect changes in the amount of warm season precipitation through time, with D-depletion in δD_{wax} indicating increased warm season rainfall. To derive ancient values of δD_P, we applied several apparent fractionation values to δD_{C31}. Sample specific apparent fractionation incorporating PFT and photosynthetic pathway differences resulted in unrealistic values of δD_P in the context of values for modern precipitation δD values in northern Australia. We instead applied a constant value of apparent fractionation measured from a survey of arid land plants and found that values of δD_P were more consistent with the range in recent northern Australian values of precipitation δD. In ODP 763A, we observe δD_P values becoming more negative by up to ~20 ‰ since ~4 Ma. We interpret this as increasing amount of warm season precipitation across north-western Australia through this interval. This is coincident with the expansion of C4 vegetation in this region through the last ~3.5 Ma and suggests a strong hydrological control on this ecological shift. Our results reaffirm the importance of regional controls on the promotion of C4 expansion across different regions of the globe.

Acknowledgements, samples and data

This research utilized samples and data provided by the International Ocean Discovery Program (IODP). Funding for this research was provided by an Australian IODP Office Special Post-Cruise Analytical Funding grant. ANZIC is supported by the Australian Government through the Australian Research Council's (ARC) LIEF funding scheme (LE160100067) and the Australian and New Zealand consortium of universities and government agencies. Additional funding was provided by an Australian Research Council Future Fellowship (FT110100100793), an Australian Government Research

Training Program Scholarship, a University of Adelaide Faculty of Sciences Divisional Scholarship and an Elsevier Research Scholarship. Isotopic analyses were supported by the Climate Center at LDEO. The authors thank Tony Hall for technical expertise. All data required to understand and assess the conclusions of this study are available in the main text and supplementary materials. The authors declare no competing interests.

References

An, Z. (2000). The history and variability of the East Asian paleomonsoon climate. *Quaternary Science Reviews, 19*(1), 171-187.

An, Z., Kutzbach, J. E., Prell, W. L., & Porter, S. C. (2001). Evolution of Asian monsoons and phased uplift of the Himalaya–Tibetan plateau since Late Miocene times. *Nature, 411*, 62-66.

Andrae, J. W., McInerney, F. A., Polissar, P. J., Sniderman, J. M. K., Howard, S., Hall, P. A., & Phelps, S. R. (2018). Initial expansion of C4 vegetation in Australia during the late Pliocene. *Geophysical Research Letters*, *10*, 4831-4840.

APSA Members. (2007). The Australasian Pollen and Spore Atlas V1.0. Retrieved from http://apsa.anu.edu.au/

Auer, G., De Vleeschouwer, D., Smith, R. A., Bogus, K., Groeneveld, J., Grunert, P., et al. (2019). Timing and pacing of Indonesian Throughflow Restriction and its connection to late Pliocene climate shifts. *Paleoceanography and Paleoclimatology, 34*, 635-657.

Bray, E. E., & Evans, E. D. (1961). Distribution of *n*-paraffins as a clue to recognition of source beds. *Geochimica et Cosmochimica Acta, 22*(1), 2-15.

Briggs, B. G. (2001). The restiads invade the north: the diaspora of the Restionaceae. CRC Press.

Bush, R. T., & McInerney, F. A. (2013). Leaf wax *n*-alkane distributions in and across modern plants: implications for paleoecology and chemotaxonomy. *Geochimica et Cosmochimica Acta, 117*, 161-179.

Carr, A. S., Boom, A., Grimes, H. L., Chase, B. M., Meadows, M. E., & Harris, A. (2014). Leaf wax *n*-alkane distributions in arid zone South African flora: environmental controls, chemotaxonomy and palaeoecological implications. *Organic Geochemistry, 67*, 72-84.

Cerling, T. E., Harris, J. M., MacFadden, B. J., Leakey, M. G., Quade, J., Eisenmann, V., & Ehleringer, J. R. (1997). Global vegetation change through the Miocene/Pliocene boundary. *Nature, 389*, 153-158.

Cerling, T. E., Wang, Y., & Quade, J. (1993). Expansion of C4 ecosystems as an indicator of global ecological change in the late Miocene. *Letters to Nature, 361*, 344-345.

Chen, S., Lin, G., Huang, J., & Jenerette, G. D. (2009). Dependence of carbon sequestration on the differential responses of ecosystem photosynthesis and respiration to rain pulses in a semiarid steppe. *Global Change Biology, 15*(10), 2450-2461.

Chen, X., Hutley, L. B., & Eamus, D. (2003). Carbon balance of a tropical savanna of northern Australia. *Oecologia, 137*(3), 405-416.

Christensen, B. A., Renema, W., Henderiks, J., De Vleeschouwer, D., Groeneveld, J., Castañeda, I. S., et al. (2017). Indonesian Throughflow drove Australian climate from humid Pliocene to arid Pleistocene. *Geophysical Research Letters, 44*(13), 6914-6925.

Collins, J. A., Schefuß, E., Mulitza, S., Prange, M., Werner, M., Tharammal, T., et al. (2013). Estimating the hydrogen isotopic composition of past precipitation using leaf-waxes from western Africa. *Quaternary Science Reviews, 65*, 88-101.

517 Conte, M. H., & Weber, J. C. (2002). Long-range atmospheric transport of terrestrial
518 biomarkers to the western North Atlantic. *Global Biogeochemical cycles, 16*(4).
519 Denniston, R. F., Wyrwoll, K.-H., Asmerom, Y., Polyak, V. J., Humphreys, W. F., Cugley,
520 J., et al. (2013). North Atlantic forcing of millennial-scale Indo-Australian
521 monsoon dynamics during the Last Glacial period. *Quaternary Science Reviews,*
522 *72*, 159-168.
523 Dupont, L. M., Rommerskirchen, F., Mollenhauer, G., & Schefuß, E. (2013). Miocene to
524 Pliocene changes in South African hydrology and vegetation in relation to the
525 expansion of C4 plants. *Earth and Planetary Science Letters, 375*, 408-417.
526 Edwards, E. J., Osborne, C. P., Stromberg, C. A. E., & Smith, S. A. (2010). The origins of
527 C4 grasslands: integrating evolutionary and ecosystem science. *Science, 328*, 587-
528 591.
529 Ehleringer, J. R. (2005). The Influence of Atmospheric CO_2, Temperature, and Water on
530 the Abundance of C3/C4 Taxa. In I. T. Baldwin, M. M. Caldwell, G. Heldmaier, R.
531 B. Jackson, O. L. Lange, H. A. Mooney, E. D. Schulze, U. Sommer, J. R.
532 Ehleringer, M. D. Dearing, & T. E. Cerling (Eds.), *A History of Atmospheric CO_2*
533 *and Its Effects on Plants, Animals, and Ecosystems* (pp. 214-231). New York, NY:
534 Springer.
535 Ehleringer, J. R., Sage, R. F., Flanagan, L. B., & Pearcy, R. W. (1991). Climate change and
536 the evolution of C4 photosynthesis. *Trends in Ecology of Evolution, 6*, 95-99.
537 Eroglu, D., McRobie, F. H., Ozken, I., Stemler, T., Wyrwoll, K.-H., Breitenbach, S. F. M.,
538 et al. (2016). See–saw relationship of the Holocene East Asian–Australian summer
539 monsoon. *Nature Communications, 7*.
540 Feakins, S. (2013). Pollen-corrected leaf wax D/H reconstructions of northeast African
541 hydrological changes during the late Miocene, *Palaeogeography,*
542 *Palaeoclimatology, Palaeoecology, 374*, 62-71.

543 Feakins, S. J., & Sessions, A. L. (2010). Controls on the D/H tatios of plant leaf waxes in
544 an arid ecosystem. *Geochimica et Cosmochimica Acta, 74*, 2128-2141.
545 Fox, D. L., Honey, J. G., Martin, R. A., & Peláez-Campomanes, P. (2012). Pedogenic
546 carbonate stable isotope record of environmental change during the Neogene in the
547 southern Great Plains, southwest Kansas, USA: carbon isotopes and the evolution
548 of C4-dominated grasslands. *GSA Bulletin, 124*(3-4), 444-462.
549 Fox, D. L., Pau, S., Taylor, L., Strömberg, C. A. E., Osborne, C. P., Bradshaw, C., et al.
550 (2018). Climatic Controls on C4 grassland distributions during the Neogene: a
551 model-data comparison. *Frontiers in Ecology and Evolution, 6*(147).
552 Freeman, K. H., & Colarusso, L. A. (2001). Molecular and isotopic records of C4
553 grassland expansion in the late Miocene. *Geochimica et Cosmochimica Acta, 65*(9),
554 1439–1454.
555 Garcin, Y., Schefuß, E., Schwab, V. F., Garreta, V., Gleixner, G., Vincens, A., et al.
556 (2014). Reconstructing C3 and C4 vegetation cover using *n*-alkane carbon isotope
557 ratios in recent lake sediments from Cameroon, Western Central Africa.
558 *Geochimica et Cosmochimica Acta, 142*, 482-500.
559 Groeneveld, J., Henderiks, J., Renema, W., McHugh, C. M., De Vleeschouwer, D.,
560 Christensen, B. A., et al. (2017). Australian shelf sediments reveal shifts in
561 Miocene Southern Hemisphere westerlies. *Science Advances, 3*(5).
562 Guo, Z., Peng, S., Hao, Q., Biscaye, P. E., An, Z., & Liu, T. (2004). Late Miocene–
563 Pliocene development of Asian aridification as recorded in the Red-Earth
564 Formation in northern China. *Global and Planetary Change, 41*(3), 135-145.
565 Haq, B. U., von Rad, U., O'Connell, S., Bent, A., Blome, C. D., Borella, P. E., et al.
566 (1990). Site 763. *Proceedings of the ODP Initial Reports, 122*.
567 Hattersley, P. W. (1983). The distribution of C3 and C4 grasses in Australia in relation to
568 climate. *Oecologia, 57*, 113-128.

Higgins, S. I., & Scheiter, S. (2012). Atmospheric CO_2 forces abrubt vegetation shifts locally, but not globally. *Nature, 488*, 209-213.

Hijmans, R. J., van Etten, J., Sumner, M., Cheng , J., Bevan, A., Bivand, R., et al. (2019). Package 'raster' (R).

Hilgen, F. J., Lourens, L. J., Van Dam, J. A., Beu, A. G., Boyes, A. F., Cooper, R. A., et al. (2012). Chapter 29 - The Neogene Period *The Geologic Time Scale* (pp. 923-978). Boston: Elsevier.

Howard, S., McInerney, F. A., Caddy-Retalic, S., Hall, P. A., & Andrae, J. W. (2018). Modelling leaf wax *n*-alkane inputs to soils along a latitudinal transect across Australia. *Organic Geochemistry, 121*, 126-137.

Huang, Y., Clemens, S. C., Liu, W., Wang, Y., & Prell, W. L. (2007). Large-scale hydrological change drove the late Miocene C4 plant expansion in the Himalayan foreland and Arabian Peninsula. *Geology, 35*(6), 531–534.

IAEA/WMO. (2019). Global Network of Isotopes in Precipitation. The GNIP Database. Retrieved from https://nucleus.iaea.org/wiser

Karas, C., Nürnberg, D., Tiedemann, R., & Garbe-Schönberg, D. (2011). Pliocene Indonesian Throughflow and Leeuwin Current dynamics: implications for Indian Ocean polar heat flux. *Paleoceanography, 26*(2).

Krebs, U., Park, W., & Schneider, B. (2011). Pliocene aridification of Australia caused by tectonically induced weakening of the Indonesian throughflow. *Palaeogeography, Palaeoclimatology, Palaeoecology, 309*(1), 111-117.

Kuechler, R. R., Schefuß, E., Beckmann, B., Dupont, L., & Wefer, G. (2013). NW African hydrology and vegetation during the Last Glacial cycle reflected in plant-wax-specific hydrogen and carbon isotopes. *Quaternary Science Reviews, 82*, 56-67.

593 Lehmann, C. E. R., Anderson, T. M., Sankaran, M., Higgins, S. I., Archibald, S.,
594 Hoffmann, W. A., et al. (2014). Savanna vegetation-fire-climate relationships differ
595 among continents. *Science, 343*, 548.
596 Linder, H. P., Eldenas, P., & Briggs, B. G. (2003). Contrasting patterns of radiation in
597 African and Australian Restionaceae. *Evolution, 57*(12), 2688-2702.
598 Liu, J., Fu, G., Song, X., Charles, S. P., Zhang, Y., Han, D., & Wang, S. (2010). Stable
599 isotopic compositions in Australian precipitation. *Journal of Geophysical*
600 *Research: Atmospheres, 115*.
601 Liu, Y., Lo, L., Shi, Z., Wei, K.-Y., Chou, C.-J., Chen, Y.-C., et al. (2015). Obliquity
602 pacing of the western Pacific Intertropical Convergence Zone over the past 282,000
603 years. *Nature Communications, 6*.
604 Long, S. P. (1999). Environmental Responses. In R. F. Sage & R. K. Monson (Eds.), *C4*
605 *Plant Biology*. London: Academic Press.
606 Macphail, M. K. (1997). Late Neogene Climates in Australia: fossil pollen- and spore-
607 based estimates in retrospect and prospect. *Australian Journal of Botany, 45*(3),
608 425-464.
609 Martin, H. A. (2006). Cenozoic climatic change and the development of the arid vegetation
610 in Australia. *Journal of Arid Environments, 66*(3), 533-563.
611 Martin, H. A., & McMinn, A. (1994). Late Cainozoic vegetation history of North-Western
612 Australia, from the palynology of a deep sea core (ODP site 765). *Australian*
613 *Journal of Botany, 42*, 95-102.
614 Matsuura, K., & Willmott, C. J. (2015). Terrestrial Precipitation: 1900-2014 Gridded
615 Monthly Time Series (Version 4.01) Retrieved from
616 http://climate.geog.udel.edu/~climate/html_pages/download.html#P2014

617 Miller, C. R., James, N. P., & Bone, Y. (2012). Prolonged carbonate diagenesis under an
618 evolving late cenozoic climate; Nullarbor Plain, southern Australia. *Sedimentary*
619 *Geology, 261*, 33-49.
620 Moore, M., Kuang, Z., & Blossey, P. N. (2014). A moisture budget perspective of the
621 amount effect. *Geophysical Research Letters, 41*(4), 1329-1335.
622 Moore, P. D., Webb, J. A., & Collinson, M. E. (1991). *Pollen Analysis* (2nd ed.). London:
623 Blackwell Scientific Publications.
624 Munsterman, D., & Kerstholt, S. (1996). Sodium polytungstate, a new non-toxic
625 alternative to bromoform in heavy liquid separation. *Review of Palaeobotany and*
626 *Palynology, 91*(1), 417-422.
627 Murphy, B. P., & Bowman, D. M. J. S. (2007). Seasonal water availability predicts the
628 relative abundance of C3 and C4 grasses in Australia. *Global Ecology and*
629 *Biogeography, 16*, 160-169.
630 Osborne, C. P. (2008). Atmosphere, ecology and evolution: what drove the Miocene
631 expansion of C4 grasslands? J*ournal of Ecology, 96*¸ 35-45.
632 Passey, B. H., Ayliffe, L. K., Kaakinen, A., Zhang, Z., Eronen, J. T., Zhu, Y., et al. (2009).
633 Strengthened East Asian summer monsoons during a period of high-latitude
634 warmth? Isotopic evidence from Mio-Pliocene fossil mammals and soil carbonates
635 from northern China. *Earth and Planetary Science Letters, 277*, 443-452.
636 Peel, M. C., Finlayson, B. L., & McMahon, T. A. (2007). Updated world map of the
637 Köppen-Geiger climate classification. *Hydrology and Earth System Sciences,*
638 *11*(5), 1633-1644.
639 Polissar, P. J., & D'Andrea, W. J. (2014). Uncertainty in paleohydrologic reconstructions
640 from molecular δD values. *Geochimica et Cosmochimica Acta, 129*, 146-156.

641 Polissar, P. J., Rose, C., Uno, K. T., Phelps, S. R., & deMenocal, P. (2019). Synchronous
642 rise of African C4 ecosystems 10 million years ago in the absence of aridification.
643 *Nature Geoscience, 12*, 588–589.
644 Rea, D. K., Snoeckx, H., & Joseph, L. H. (1998). Late Cenozoic Eolian deposition in the
645 North Pacific: Asian drying, Tibetan uplift, and cooling of the northern hemisphere.
646 *Paleoceanography, 13*(3), 215-224.
647 Rozanski, K., Araguas-Araguas, L., & Gonfiantini, R. (1993). Isotopic patterns in modern
648 global precipitation. In P. K. Swart, K. C. Lohmann, J. McKenzie, & S. Savin
649 (Eds.), *Climate Change in Continental Isotopic Records Geophysical Monograph*
650 (Vol. 78, pp. 1-36): American Geophysical Union.
651 Sachse, D., Billault, I., Bowen, G. J., Chikaraishi, Y., Dawson, T. E., Feakins, S. J., et al.
652 (2012). Molecular paleohydrology: interpreting the hydrogen-isotopic composition
653 of lipid biomarkers from photosynthesizing organisms. *Annual Review of Earth and*
654 *Planetary Sciences, 40*, 221-249.
655 Schreuder, L. T., Stuut, J.-B. W., Korte, L. F., Sinninghe Damsté, J. S., & Schouten, S.
656 (2018). Aeolian transport and deposition of plant wax *n*-alkanes across the tropical
657 North Atlantic Ocean. *Organic Geochemistry, 115*, 113-123.
658 Sniderman, J. M. K., Woodhead, J. D., Hellstrom, J., Jordan, G. J., Drysdale, R. N., Tyler,
659 J. J., & Porch, N. (2016). Pliocene reversal of late Neogene aridification.
660 *Proceedings of the National Academy of Sciences, 113*(8), 1999-2004.
661 Snoeckx, H., Rea, D. K., Jones, C. E., & Ingram, B. L. (1995). Eolian and Silica
662 Deposition in the Central North Pacific: Results from Sites 885/886. *Proceedings of*
663 *the Ocean Drilling Program, Scientific Results, 145*.
664 Stromberg, C. A. E. (2011). Evolution of grasses and grassland ecosystems. *Annual Review*
665 *of Earth and Planetary Sciences, 39*, 517–544.

Stuut, J.B. W., De Deckker, P., Saavedra-Pellitero, M., Bassinot, F., Drury, A. J., Walczak, M. H., et al. (2019). A 5.3-million-year history of monsoonal precipitation in northwestern Australia. *Geophysical Research Letters, 46,* 6946– 6954.

Sun, D., Shaw, J., An, Z., Cheng, M., & Yue, L. (1998). Magnetostratigraphy and paleoclimatic interpretation of a continuous 7.2 Ma Late Cenozoic Eolian sediments from the Chinese Loess Plateau. *Geophysical Research Letters, 25*(1), 85-88.

Tang, C. (1992). Paleomagnetism of Cenozoic sediments in holes 762B and 763A, central Exmouth Plateau, Northwest Australia. *Proceedings of the ODP, 122,* 717-733.

Tipple, B. J., Meyers, S. R., & Pagani, M. (2010). Carbon isotope ratio of Cenozoic CO_2: a comparative evaluation of available geochemical proxies. *Paleoceanography, 25*(3).

Tipple, B. J., & Pagani, M. (2007). The early origins of terrestrial C4 photosynthesis. *Annual Review of Earth and Planetary Sciences, 35,* 435–461.

Uno, K. T., Polissar, P. J., Jackson, K. E., & deMenocal, P. B. (2016). Neogene biomarker record of vegetation change in eastern Africa. *Proceedings of the National Academy of Sciences, 113*(23), 6355-6363.

Vogts, A., Badewien, T., Rullkötter, J., & Schefuß, E. (2016). Near-constant apparent hydrogen isotope fractionation between leaf wax *n*-alkanes and precipitation in tropical regions: evidence from a marine sediment transect off SW Africa. *Organic Geochemistry, 96,* 18-27.

Vogts, A., Moossen, H., Rommerskirchen, F., & Rullkötter, J. (2009). Distribution patterns and stable carbon isotopic composition of alkanes and alkan-1-ols from plant waxes of African rain forest and savanna C3 species. *Organic Geochemistry, 40*(10), 1037-1054.

691 Vuille, M., Werner, M., Bradley, R. S., & Keimig, F. (2005). Stable isotopes in
692 precipitation in the Asian monsoon region. *Journal of Geophysical Research:*
693 *Atmospheres, 110*.
694 Wheeler, M. C., & McBride, J. L. (2005). Australian-Indonesian monsoon. In W. K. M.
695 Lau & D. E. Waliser (Eds.), *Intraseasonal Variability in the Atmosphere-Ocean*
696 *Climate System* (pp. 125-173). Berlin: Springer Berlin Heidelberg.
697 Wickham, H., Romain, F., Henry, L., & Müller, K. (2019). dplyr: A Grammar of Data
698 Manipulation (Version 0.8.0.1). Retrieved from https://CRAN.R-
699 project.org/package=dplyr
700 Wu, Z., Dijkstra, P., Koch, G. W., Peñuelas, J., & Hungate, B. A. (2011). Responses of
701 terrestrial ecosystems to temperature and precipitation change: a meta-analysis of
702 experimental manipulation. *Global Change Biology, 17*(2), 927-942.
703 Yan, M., Wang, B., Liu, J., Zhu, A., Ning, L., & Cao, J. (2018). Understanding the
704 Australian Monsoon change during the Last Glacial Maximum with a multi-model
705 ensemble. *Climate of the Past, 14*(12), 2037-2052.
706 Yancheva, G., Nowaczyk, N. R., Mingram, J., Dulski, P., Schettler, G., Negendank, J. F.
707 W., et al. (2007). Influence of the intertropical convergence zone on the East Asian
708 monsoon. *Nature, 445*, 74-77.
709 Zheng, H., Powell, C. M., Rea, D. K., Wang, J., & Wang, P. (2004). Late Miocene and
710 mid-Pliocene enhancement of the East Asian monsoon as viewed from the land and
711 sea. *Global and Planetary Change, 41*(3), 147-155.
712 Zhou, H., Helliker, B. R., Huber, M., Dicks, A., & Akçay, E. (2018). C4 photosynthesis
713 and climate through the lens of optimality. *Proceedings of the National Academy of*
714 *Sciences, 115*(47), 12057-12062.

Appendix

Expansion of C4 vegetation in north-west Australia driven by increased seasonality of precipitation

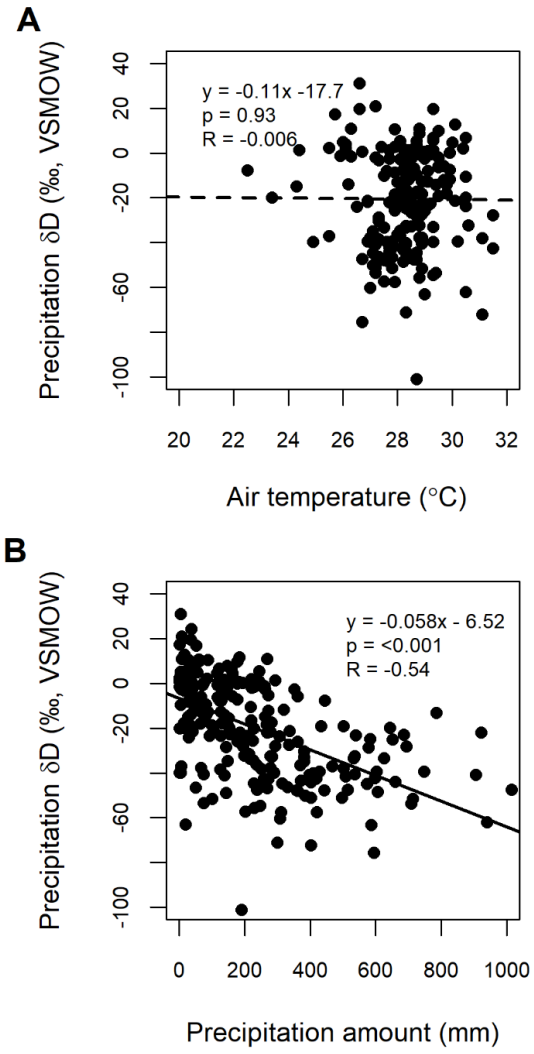

Figure S1. Linear regressions of climate and precipitation δD observations for Darwin a) Relationship between air temperature and precipitation δD observations across the period 1962 – 2002. b) Relationship between precipitation amount and precipitation δD observations for the same period. Data are cumutively integrated monthly observations from the Darwin GNIP field station (IAEA/WMO, 2019).

For supplementary Data Sets S1 through S5, the reader is directed to

https://adelaide.figshare.com/s/65e9f5bb25fec0448f8f

Chapter 6: Research outcomes, limitations and future directions

Research presented in this thesis was undertaken to address two separate groups of aims relating to the understanding and application of *n*-alkane molecular and isotopic proxy systems for palaeo-environmental reconstructions. The first group of aims related to addressing significant knowledge gaps in our understanding of key aspects of leaf wax *n*-alkane molecular distribution and isotopic proxy systems that have inhibited robust palaeo-environmental interpretations under certain circumstances. The second group of aims related to the application of more well constrained aspects of *n*-alkane molecular and isotopic proxy systems as tools to address key questions surrounding the development of the modern Australian flora and climate since the late Cenozoic. Each research chapter in the thesis discusses and summarises research findings individually. In this chapter, I undertake a broad synthesis of the research outcomes of this thesis in the context of the specific research aims and highlight some implications of these outcomes for future work in the field. I also briefly outline some limitations of the research and discuss ways in which these limitations may be addressed with further work.

Research outcomes, implications and limitations

For a single species, do leaf wax n-alkane molecular distributions respond plastically to climate variability, or are they fixed for distinct climate regimes?

Chapter 2 significantly increases our understanding of the scale at which leaf wax *n*-alkane molecular distributions reflect climate, particularly aridity. A single-species study was developed to mitigate any influence of phylogeny or plant functional type on leaf wax *n*-alkane distribution and ensure climatic control could be constrained to a greater extent than previous studies that used climate transects with high species turnover. *n*-Alkane molecular distributions in *Melaleuca quinquenervia* likely reflect fixed population level

responses to distinct climate regimes as opposed to plastic responses to local climate variability in space and time. These results have important implications for how sedimentary leaf wax *n*-alkane molecular distributions are interpreted from geological records. Where ancient *n*-alkanes can be derived from this species, *n*-alkane molecular distribution variability through time will likely reflect population responses to large climatological shifts. One limitation of the research in Chapter 2 is the study design only incorporated one species. This study design was largely motivated by the preservation of sub-fossil leaves of this species in Holocene sedimentary records from eastern Australia (Barr et al., 2019; Tibby et al., 2016), and the potential for application leaf wax *n*-alkane molecular distributions as a proxy system to these records. As such, the results of this work are limited, and implications for application of *n*-alkane molecular distributions as a proxy system to other species-specific records will need to be similarly tested. Additionally, a somewhat disjunct sampling regime limits the ability to determine whether changes in *n*-alkane characteristics between the two study regions occurred suddenly or gradually. Nevertheless, the work does suggest that leaf wax *n*-alkane production does not respond plastically to climate variability, at least in this species.

How do carbon isotope ratios of different n-alkanes in lacustrine sediments reflect mixing of n-alkanes derived from terrestrial and aquatic vegetation?

Chapter 3 constrains how mixing of *n*-alkane inputs from different vegetation type impacts $\delta^{13}C$ values of discrete *n*-alkane compounds preserved in lacustrine sedimentary archives, using a natural laboratory approach. Results suggest that sensitivity to vegetation change will vary between different *n*-alkane homologs. This includes both changes in proportions of photosynthetic pathway on the landscape as well as changes in non-emergent aquatic plant inputs to sedimentary records. This has important implications for how and in what circumstance aspects of leaf wax *n*-alkane proxy systems can be applied,

particularly from an isotopic perspective. The optimal *n*-alkane chain lengths for reconstructions of proportion of photosynthetic pathway on the landscape are found to be the longest biosynthesised by plants; those with greater than 31 carbon atoms. The results of Chapter 3 suggest that significant care should be taken in interpreting changes in the proportion of photosynthetic pathway on the landscape from other *n*-alkanes preserved in lacustrine sedimentary records. A significant limitation to the conclusions that could be attained in Chapter 3 is a lack of constraint on changes in $\delta^{13}C$ of the DIC pool in the Garvoc palaeo-lake record through time. As a result of this, it is unclear whether the variable $\delta^{13}C$ values for mid-chain *n*-alkanes could have resulted from high levels of mid-chain *n*-alkane production by C3 terrestrial vegetation or from DIC pool $\delta^{13}C$ variability through time. To follow this up, future research could undertake seasonal monitoring of lake systems, including analysis of contemporary DIC isotopes. Alternatively, analysis of lake sediments containing a mixture of both organic and inorganic carbonates, where the latter can be used as a proxy for lake DIC isotopes, would provide stronger constraints on the system.

What was the timing of C4 vegetation expansion on the Australian continent and was regional hydrology an important control on the expansion of C4 vegetation on the Australian continent?

In Chapter 4, the timing of C4 expansion onset on the Australian continent was constrained for the first time. Carbon isotope analysis of leaf wax *n*-alkanes in an offshore marine sedimentary record showed that the onset of C4 expansion in north-western Australia was at ~3.5 Ma, much later than most other geographic regions (Polissar et al., 2019). This record provides strong evidence for regional controls on the proliferation of C4 dominated ecosystems globally. Asynchronicity in timing of onsets points towards regional climate and environmental factors acting as tipping points for these significant ecological

shifts, as postulated by Higgins and Scheiter (2012). Chapter 5 provides evidence that changes in the seasonality of precipitation are likely to have been a primary driver for C4 expansion on the Australian continent. A trend toward globally declining pCO_2 is observed since the Miocene and seems to have been critical to the expansion of C4 vegetation in a number of other regions (Polissar et al., 2019). However, the expansion of C4 vegetation in Australia does not exhibit a correlation with global pCO_2 records and work presented in this chapter provides evidence substantiating the assertion that regional controls in association with global factors drove onsets of C4 expansions globally (Higgins & Scheiter, 2012). It is likely that globally declining pCO_2 was a prerequisite for C4 expansion globally, but that regional results presented indicate that asynchronous C4 vegetation expansions likely reflect the crossing of regional thresholds of atmospheric, climatic and environmental conditions in combination that afforded C4 vegetation a significant competitive advantage. It could be postulated that the more seasonal rainfall extremes interpreted for the Australian continent at this time may have influenced environmental factors like fire occurrence, and this may have further contributed to ecosystem change (Osborne 2008). These results and interpretations have significant implications for understanding the sensitivity of ecosystems to future impacts of changes to Earth's atmosphere and climate.

There are limitations in the spatial and temporal resolution of leaf wax *n*-alkane proxy systems as tools for palaeo-environmental reconstructions from marine deposits as presented in Chapters 4 and 5. In many cases, leaf wax *n*-alkanes preserved in deep-time marine geological archives will be highly spatially integrated as a result of a primarily aeolian transport pathway (Conte & Weber, 2002; Diefendorf & Freimuth, 2017; Uno et al., 2016). In these cases, leaf wax *n*-alkane molecular and isotopic properties will reflect an array of different vegetation biomes and climate regimes, with potential for muting of

important spatial variability. There is also great potential for temporal integration of leaf wax *n*-alkanes in marine sedimentary records as a result of low sedimentation rates and sediment turbidity (Uno et al., 2016), along with re-mobilisation of significantly pre-aged fossil *n*-alkanes from other geological successions (Douglas et al., 2014). It is suggested that for deep-sea marine sediment records, *n*-alkane molecular distribution and isotope signals representative of palaeo-vegetation and climate may be muted or obscured by factors including bioturbation and coring induced disturbance (Uno et al., 2016).

Additionally, vegetation and climate reconstructions may also be impacted by biases in the transport of leaf wax *n*-alkanes from plants to sediments (Freeman & Pancost, 2014; Howard et al., 2018). Conte and Weber (2002) found seasonal trends in the long-range transport of leaf wax lipids to marine sediments and demonstrated that the potential for episodic transport was high. This potential for seasonal bias has positive and negative aspects. On one hand, we demonstrate in Chapter 5 how this bias allows for investigation of seasonal aspects of hydrology that other proxies are unable to constrain. In this case, leaf wax production and transport will be maximised during the wet season in northern Australia, and leaf wax δD values in sediments will thus predominantly reflect wet season precipitation δD values. On the other hand, this bias may lead to leaf wax *n*-alkanes preserved in marine sediments not reflecting vegetation on the landscape to its full annual extent. Possible solutions to these issues are described in the section below, detailing future research directions.

Future research directions

The various limitations found in the course of this research may be addressed through additional work, including but not limited to:

- Further studies examining molecular distribution-climate relationships for other species with known preservation in geological archives of importance, to test whether the relationships observed for *Melaleuca quinquenervia* hold true for other species. Whole leaf preservation with the potential for species-specific *n*-alkane preservation may provide new opportunities for reconstructing past aridity. Controlling for vegetation turnover using species-specific *n*-alkane molecular distribution reconstructions should allow for primary interpretations of climate variability from *n*-alkane molecular distributions that had not been thoroughly explored previously.

- Factoring in DIC pool $\delta^{13}C$ variability to studies constraining the impact of *n*-alkane source mixing on $\delta^{13}C$ values of lacustrine sedimentary *n*-alkanes. This would aid in discerning whether variability in $\delta^{13}C$ values of sedimentary mid-chain *n*-alkanes in lacustrine systems results from DIC pool $\delta^{13}C$ variability or from significant production of mid-chain *n*-alkanes by terrestrial vegetation. A feasible way to achieve this may be through studies of lacustrine systems with significant inorganic carbonate precipitation through time. In addition, complementary work to constrain hydrogen isotope variability as a function of terrestrial and non-emergent aquatic vegetation inputs would be of importance. This would allow for the development of more nuanced hydrological interpretations from *n*-alkane δD values measured in lacustrine geological archives. One application of this could be development of complementary lake water dynamic and precipitation reconstructions.

- The development of late Cenozoic Australian palaeo-environmental reconstructions at higher spatial and temporal resolution than in the research undertaken here.

Higher spatial and temporal resolution *n*-alkane proxy records may provide local to regional scale insights and hold greater potential for robust time-series analysis than the marine sedimentary records presented in this thesis. Geological archives that may be used for this purpose are thought to be somewhat limited on the Australian continent (Kershaw et al., 1994), but there are several avenues that could be explored. Analysis of organic rich fluvial or lacustrine deposits (i.e. palaeo-channel deposits) where *n*-alkanes may be preserved could be viable options for these types of reconstructions. In addition, recent work has demonstrated potential for analysis of *n*-alkyl biomarkers preserved in speleothems and other cave deposits to provide reconstructions of vegetation and climatic at a range of spatial and temporal scales (Blyth et al., 2016; Blyth et al., 2010; Wang et al., 2019). In these cases, splicing of multiple records from a region may be required to produce reconstructions that are long enough to examine long-term palaeo-ecological and palaeo-climatic trends.

Research summary

Overall, the work presented in this thesis represents a significant advance in our understanding of leaf wax *n*-alkane proxy systems, particularly in an Australian context. It provides important new insights into how physiological and ecological processes are reflected by *n*-alkane molecular distributions and stable carbon and hydrogen isotope ratios. The results emphasise the importance of understanding *n*-alkane proxy systems at the compound level, with nuances in how different landscape processes are reflected by different *n*-alkane chain-lengths. The work also extensively contributes to the global understanding of late Cenozoic vegetation change. The novel reconstructions of vegetation and climate for the Australian continent presented here give insight into ecosystem responses to environmental change through an important period of Earth history, with

significant implications for understanding ecological impacts of future environmental change.

References

Barr, C., Tibby, J., Leng, M. J., Tyler, J. J., Henderson, A. G. C., Overpeck, J. T., et al. (2019). Holocene El Niño-Southern Oscillation variability reflected in subtropical Australian precipitation. *Scientific Reports, 9*.

Blyth, A. J., Hartland, A., & Baker, A. (2016). Organic proxies in speleothems – New developments, advantages and limitations. *Quaternary Science Reviews, 149*, 1-17.

Blyth, A. J., Watson, J. S., Woodhead, J., & Hellstrom, J. (2010). Organic compounds preserved in a 2.9 million year old stalagmite from the Nullarbor Plain, Australia. *Chemical Geology, 279*(3), 101-105.

Conte, M. H., & Weber, J. C. (2002). Long-range atmospheric transport of terrestrial biomarkers to the western North Atlantic. *Global Biogeochemical cycles, 16*(4).

Diefendorf, A. F., & Freimuth, E. J. (2017). Extracting the most from terrestrial plant-derived *n*-alkyl lipids and their carbon isotopes from the sedimentary record: a review. *Organic Geochemistry, 103*, 1-21.

Douglas, P. M. J., Pagani, M., Eglinton, T. I., Brenner, M., Hodell, D. A., Curtis, J. H., et al. (2014). Pre-aged plant waxes in tropical lake sediments and their influence on the chronology of molecular paleoclimate proxy records. *Geochimica et Cosmochimica Acta, 141*, 346-364.

Freeman, K. H., & Pancost, R. D. (2014). Biomarkers for terrestrial plants and climate. In H. D. Holland & K. K. Turekian (Eds.), *Treatise on Geochemistry* (2nd ed., pp. 395-416). Oxford: Elsevier.

Higgins, S. I., & Scheiter, S. (2012). Atmospheric CO_2 forces abrubt vegetation shifts locally, but not globally. *Nature, 488*, 209-213.

Howard, S., McInerney, F. A., Caddy-Retalic, S., Hall, P. A., & Andrae, J. W. (2018). Modelling leaf wax *n*-alkane inputs to soils along a latitudinal transect across Australia. *Organic Geochemistry, 121*, 126-137.

Kershaw, A. P., Martin, H. A., & McEwen-Mason, J. R. C. (1994). The Neogene: a period of transition. In R. S. Hill (Ed.), *History of the Australian vegetation: Cretaceous to recent*. New York: Cambridge University Press.

Osborne, C. P. (2008). Atmosphere, ecology and evolution: what drove the Miocene expansion of C4 grasslands? *Journal of Ecology*, *96*, 35-45.

Polissar, P. J., Rose, C., Uno, K. T., Phelps, S. R., & deMenocal, P. (2019). Synchronous rise of African C4 ecosystems 10 million years ago in the absence of aridification. *Nature Geoscience*, *12*, 588-589.

Tibby, J., Barr, C., McInerney, F. A., Henderson, A. C. G., Leng, M. J., Greenway, M., et al. (2016). Carbon isotope discrimination in leaves of the broad-leaved paperbark tree, *Melaleuca quinquenervia*, as a tool for quantifying past tropical and sub-tropical rainfall. *Global Change Biology*, *22*(10), 3474–3486

Uno, K. T., Polissar, P. J., Jackson, K. E., & deMenocal, P. B. (2016). Neogene biomarker record of vegetation change in eastern Africa. *Proceedings of the National Academy of Sciences, 113*(23), 6355-6363.

Wang, C., Bendle, J. A., Greene, S. E., Griffiths, M. L., Huang, J., Moossen, H., et al. (2019). Speleothem biomarker evidence for a negative terrestrial feedback on climate during Holocene warm periods. *Earth and Planetary Science Letters, 525*.

Chapter 7: Appendices

Appendix 1. Additional peer-reviewed publication authored during candidature*

*Originally published as Howard, S., McInerney, F.A., Caddy-Retalic, S., Hall, P.A., Andrae, J.W. (2018). Modelling leaf wax *n*-alkane inputs to soils along a latitudinal transect across Australia. *Organic Geochemistry* 121, pp. 126-137.

Organic Geochemistry 121 (2018) 126–137

Contents lists available at ScienceDirect

Organic Geochemistry

journal homepage: www.elsevier.com/locate/orggeochem

Modelling leaf wax *n*-alkane inputs to soils along a latitudinal transect across Australia

S. Howard [a,*], F.A. McInerney [a], S. Caddy-Retalic [b,c], P.A. Hall [a], J.W. Andrae [a]

[a] University of Adelaide, Sprigg Geobiology Centre and School of Physical Sciences, Australia
[b] University of Adelaide, School of Biological Sciences, Australia
[c] University of Sydney, School of Life and Environmental Sciences, Australia

ARTICLE INFO

Article history:
Received 26 September 2017
Received in revised form 23 March 2018
Accepted 25 March 2018
Available online 29 March 2018

Keywords:
Leaf wax
n-Alkanes
Average chain length
Carbon preference index
Soils
Palaeoecology
Vegetation reconstruction

ABSTRACT

Leaf wax *n*-alkanes provide a valuable palaeoecological proxy, but their interpretation requires an understanding of the scale of temporal and spatial integration in soils. Leaf wax *n*-alkanes are continually deposited into soils directly from local plants as well as from more distant plants via wind or water transport. In addition, *n*-alkanes can persist in soils for thousands of years, and tend to decrease in age with shallower depth. To explore whether the uppermost soils reflect recent leaf fall inputs we compared surface soils and modern vegetation from 20 sites along a transect across Australia. At each site, the three most dominant plant species and a soil sample from the top 3 cm were analysed for *n*-alkane concentration, average chain length (ACL), proportional abundance of C_{33} and C_{29} (Norm33) and carbon preference index (CPI). Chain length distributions differ between trees and grasses, with a higher proportion of C_{29} in trees and C_{33} in grasses. Norm33 in soils correlates with proportional grass to tree cover across the transect. To model *n*-alkane inputs for each site, we calculated a predicted ACL, Norm33 and CPI using the dominant plants at that site, weighted by proportional species cover and *n*-alkane concentration. Predicted ACL, Norm33 and CPI inputs were generally higher than the soils, demonstrating that recent and local inputs do not dominate soil *n*-alkanes at our study sites. Thus, *n*-alkane distributions in surface soils do not correlate with local, current vegetation, but do correlate with proportional grass and tree cover, suggesting they provide a faithful record of large scale ecosystem structure.

1. Introduction

Plant waxes provide critical protection for leaves by limiting non-stomatal water loss from the leaf surface (Eglinton and Hamilton, 1967; Dodd and Poveda, 2003; Jetter and Riederer, 2016), protecting against damage from UV radiation (Shepherd and Wynne Griffiths, 2006; Koch et al., 2009), and resisting fungal infection and herbivory (Eigenbrode and Espelie, 1995; Banthorpe, 2006). Plant waxes contain a range of compounds, including long chain *n*-alkanes, which are non-polar, unbranched, straight-chain hydrocarbons (Eglinton and Hamilton, 1967; Banthorpe, 2006). Long chain-odd-numbered *n*-alkanes (C_{25}–C_{35}) are produced nearly exclusively as part of the waxes of terrestrial plants (Eglinton and Hamilton, 1967). Plants generally produce greater quantities of odd than even chain lengths due to synthesis by sequential elongation or condensation of a C_2 primer, where even-numbered fatty acid chains become decarboxylated to produce odd chain length alkanes (Khan and Kolattukudy, 1974; Shepherd and Wynne Griffiths, 2006). Higher plants produce different distributions of chain lengths that range from C_{25} to C_{35} (Sachse et al., 2004; Pu et al., 2011; Bush and McInerney, 2013). The majority of plant wax *n*-alkanes in soils and sediments should derive from leaves due to the high proportional biomass of leaves, and the high concentrations of *n*-alkanes in leaves relative to other plant organs (Gamarra and Kahmen, 2015). Roots can contribute *n*-alkanes to the soil directly, but their concentration is one or two orders of magnitude less than leaves and thus they are unlikely to be the dominant source of *n*-alkane signals in surface soils (Gamarra and Kahmen, 2015; Angst et al., 2016; Jansen and Wiesenberg, 2017). There is some evidence that insects also produce long-chain *n*-alkanes with an odd-over-even predominance, however their biomass is orders of magnitude less than that of terrestrial plants and their annual *n*-alkane production rate is unquantified, so their contribution to soils and sediments is considered negligible in comparison to plants (Chikaraishi et al., 2012).

Plant lipid biomarkers, such as leaf wax *n*-alkanes, are very common in the sedimentary record, compared to macrofossils

* Corresponding author.
E-mail address: sian.howard@adelaide.edu.au (S. Howard).

https://doi.org/10.1016/j.orggeochem.2018.03.013
0146-6380/

which are comparatively rare. Leaf wax *n*-alkanes are valuable recorders of past vegetation (Eglinton and Eglinton, 2008; Diefendorf and Freimuth, 2017) and can be distinguished from petroleum sources by their odd-over-even predominance (Eglinton and Hamilton, 1967; Yamamoto and Kawamura, 2010). However, to interpret the signatures preserved in sediments, we must understand how sedimentary leaf wax *n*-alkanes reflect the vegetation both temporally and spatially (Diefendorf and Freimuth, 2017).

Direct ^{14}C dating suggests that leaf wax *n*-alkanes can be pre-aged in soils for hundreds to thousands of years prior to remobilisation and transport to lacustrine and marginal marine sediments (Smittenberg et al., 2006; Drenzek et al., 2007; Douglas et al., 2014; Gierga et al., 2016), frequently resulting in highly time-averaged *n*-alkane accumulations. Once buried in sediments, *n*-alkanes can persist for millions of years and have been extracted from sediments from the Cretaceous–Paleogene boundary (Yamamoto et al., 2010), Paleocene–Eocene (Smith et al., 2007), Miocene (Huang et al., 2001) and Holocene (Schwark et al., 2002).

Although *n*-alkanes can persist for thousands of years in deeper subsoils and millions of years in buried sediments, analyses of modern soils demonstrates that more recent *n*-alkane inputs dominate near the soil surface (Angst et al., 2016). Direct ^{14}C dating of *n*-alkanes and soil organic carbon in soils and lake sediments shows increasing age with depth (Huang et al., 1996; Angst et al., 2016; Gierga et al., 2016). Makou et al. (2018) found ^{14}C dating of long, odd-chain *n*-alkanes in a surface soil indicated a pool of pre-aged *n*-alkanes attributed to erosional inputs from adjacent slopes, however the dominant chain length present in the soil, C_{27}, was modern in age and attributed to inputs of fresh leaf waxes from nearby beech trees. Therefore, surface soils appear to be the least time-averaged, and predominantly represent the most recent *n*-alkane inputs.

Leaf fall and breakdown of leaf litter represents direct *n*-alkane deposition to soils (Cranwell, 1981; Lichtfouse et al., 1998), resulting in soil *n*-alkane signatures representative of local sources. Previous work examining the relationship between chain length and biome type showed that the chain length distributions associated with the plants were similar to those in the soils of those respective biomes (Carr et al., 2014). However, leaf wax *n*-alkanes are also readily ablated and wind-dispersed, which would lead soil deposits to represent a regional catchment area (van Gardingen et al., 1991; Gao et al., 2012). Wind-blown *n*-alkanes can travel as far as between continents (Bendle et al., 2007; Yamamoto and Kawamura, 2010; Nelson et al., 2017) and are primarily deposited with particulate matter scrubbed from the atmosphere by precipitation (Meyers and Hites, 1982; Diefendorf and Freimuth, 2017). Similarly, water can transport leaf wax *n*-alkanes long distances via streams, rivers and runoff, either by moving fallen leaves or deposited particulate matter (Rouillard et al., 2016; Diefendorf and Freimuth, 2017). The relative importance of these processes in delivering *n*-alkanes to soils will determine whether soil records represent a regional or more localised vegetation sample (Jansen and Wiesenberg, 2017).

Here, we test the hypothesis that *n*-alkane distributions in surface soils correlate with *n*-alkane distributions of current local vegetation. We sampled a latitudinal transect across Australia to capture a climatically and ecologically diverse set of sites (Fig. 1). The continent-wide transect spans from monsoonal tropics in the north to arid desert in the centre, to the winter-wet Mediterranean climate zone in the south. The biomes sampled include tropical and subtropical grasslands, savannas and shrublands in the north; desert and xeric shrublands in the centre; and Mediterranean shrublands and woodlands in the south (Supplementary Table S1). At each site, we characterised the *n*-alkane abundance and distribution from the three most dominant plant species. At the vast majority of sites, the three dominant species represent the majority of the plant cover (Table 1). While it does not equate directly to biomass, dominant coverage provides us with a reasonable estimate of the dominant *n*-alkane contributors to the surface soils and improves on previous studies that sample plants without respect to their coverage in the landscape. Using the concentration and distribution of *n*-alkanes of the dominant vegetation to account for differences in production, we modelled their inputs to surface soils and compared them to the distributions measured from the soils (top 3 cm). The degree to which local and recent vegetation contributes to soil *n*-alkane signatures will determine how well our modelled inputs match our measured soil *n*-alkane distributions. This comparison provides a direct test of the hypothesis that the leaf wax *n*-alkane signals in surface soils are dominated by local and recent inputs rather than regional and/or long-term inputs. We also examined whether soil *n*-alkane distributions broadly reflect plant cover growth form (e.g., grasses vs trees) at each site. The results constrain the nature of delivery and turnover of *n*-alkane soils across a large and diverse transect, and provide bounds on the range of possible paradigms for the development of *n*-alkane records in soils.

2. Methods

2.1. Sample collection

Soil and plant samples were collected from 20 sites on a north-south transect across Australia (Fig. 1), using the AusPlots Rangelands survey methodology (White et al., 2012). These samples were collected by Australia's Terrestrial Ecosystem Research Network (TERN) and made available for this research. The sites monitored by TERN are permanent plots where baseline surveys of soils and vegetation are conducted as a source of ongoing and long-term ecosystem data for research (White et al., 2012). Sites analysed here were distributed through seven Australian bioregions (See Supplementary Table S1 for descriptions). A single surface soil sample from the middle of each site, taken from a maximum of 3 cm depth (total n = 20), was selected for analysis after having been air dried and stored in calico. Soils were sieved with 1000 and 250 μm sieves to remove large plant material, such as leaves, bark and roots. Particle size percentages were determined using mid-infrared particle size analysis.

Proportional plant species cover and growth form cover was determined from point intercept data obtained from the online Soils2Satellites portal (www.soils2satellites.org.au). At each one hectare site, 1010 points were assessed and all vegetation occurrences were recorded (White et al., 2012). The total number of occurrences for each species and growth form was divided by the total number of vegetation occurrences per site to determine the proportional species cover and growth form (trees, grasses, forbs and shrubs, inclusive of chenopods) cover at each site.

$$\text{Proportional species cover} = \frac{\text{number of species occurrences}}{\text{total vegetation occurrences}} \quad (1)$$

$$\text{Proportional growth form cover} = \frac{\text{number of growth form occurrences}}{\text{total vegetation occurrences}} \quad (2)$$

Leaves from the three most dominant plant species, in terms of proportional species cover, were selected for analysis from each site, except for one site from which the two most dominant were available (total n = 59). The leaves were placed in gauze bags and dried on silica gel. The total proportional species cover that the three most dominant plant species represent ranges from 42 to 99% (Table 1).

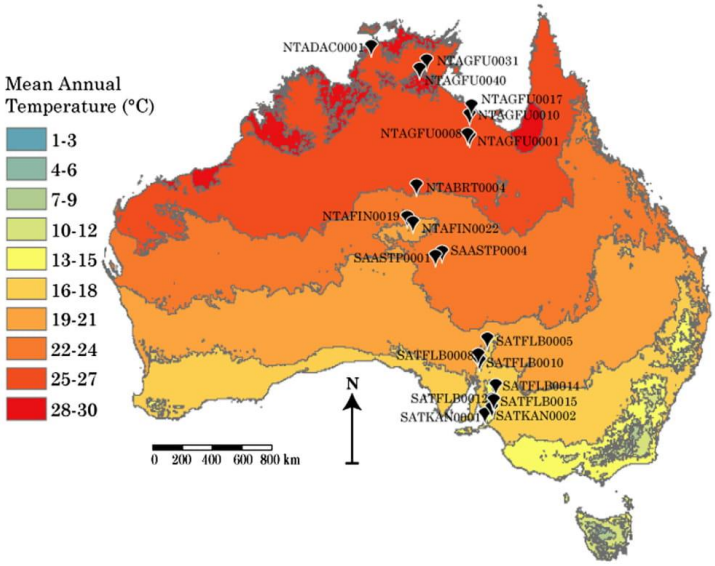

Fig. 1. Location map of selected AusPlots sites (black pins) across Australia with mean annual temperature shown as context. Climate data based on a standard 30-year climatology (1961–1990) and reproduced with permission from Bureau of Meteorology (© Commonwealth of Australia).

2.2. Lipid extraction from plants

Dried plant samples were ground to a fine powder with a mortar and pestle in liquid nitrogen. Lipids were extracted from the ground plant samples in dichloromethane:methanol (DCM:MeOH; 9:1; v:v) in a Soniclean 250TD sonicator. Sample weights ranged from 5.8 to 52.3 mg; with 51 of the 59 plant samples ≥50 mg. Excess solvent was evaporated from the total lipid extract (TLE) under nitrogen gas using a FlexiVap nitrogen blow-down station.

2.3. Lipid extraction from soils

Lipid extraction of the <250 μm soil fraction was conducted using a Thermo Scientific Dionex Accelerate Solvent Extractor (ASE) 350 using DCM:MeOH (9:1, v:v). Samples weights ranged from 4.5 to 26.6 g, with 15 of the 20 soils samples ≥10 mg. The ASE sequence was set to 100 °C with a 12 min preheat, three static cycles of five min, and a rinse volume of 60%. Excess solvent was evaporated from the TLE under nitrogen gas.

2.4. n-Alkane purification

The polar and non-polar fractions of both the plant and the soil TLEs were separated through a short glass column containing silica gel by eluting them with 4 ml of hexane to collect the non-polar, aliphatic hydrocarbon fraction, followed by DCM:MeOH (4 ml, 1:1, v:v) to collect the polar fraction, (modified from Bastow et al., 2007). The aliphatic hydrocarbon fraction was dried under nitrogen gas.

2.5. GC–MS lipid quantification

Quantification of *n*-alkanes was conducted using gas chromatography–mass spectrometry (GC–MS) analysis of the non-polar lipid fraction. Analysis was performed on a Perkin Elmer Clarus 500 GC–MS with the following specifications: The capillary was an SGE CPSil-5MS, 30 m (length) × 0.25 mm (i.d.) × 0.25 μm (phase thickness). The carrier gas was helium with a 1 ml/min constant flow. The injection temperature was 300 °C, with a temperature program of 50 °C (hold 1 min), ramped at 8 °C/min to 340 °C (hold for 7.75 min). Injection was set to 1 μl in either split mode, with a 50:1 split for higher concentration samples, or pulsed splitless for low sample concentrations. Perkin Elmer Turbomass software was used for data interpretation and quantification of *n*-alkane homologues (C_{25} to C_{35}). 1,1′-binaphthyl internal standard was added to each sample at a concentration of 1 μg/mL for quantification. Concentrations of *n*-alkanes were calculated from the response factor of each homologue against the internal standard plotted against a seven point calibration curve prepared and analysed in triplicate using known concentrations of a homologous suite of *n*-alkanes (C_7 to C_{40}) with the same 1 μg/mL 1-1′-binaphthyl internal standard concentration ($r^2 > 0.96$).

2.6. Calculations

Relative abundances of *n*-alkane chain lengths were characterised by calculating average chain length (ACL) (Eglinton and Hamilton, 1967):

$$\mathrm{ACL} = \frac{(25C_{25} + 27C_{27} + 29C_{29} + 31C_{31} + 33C_{33} + 35C_{35})}{(C_{25} + C_{27} + C_{29} + C_{31} + C_{33} + C_{35})} \quad (3)$$

where C_x is the total concentration of each *n*-alkane with *x* carbon atoms.

Carbon preference index (CPI) for each sample was calculated using the equation. Modified from Marzi et al. (1993):

$$\mathrm{CPI} = \frac{\left[\sum_{\mathrm{odd}}(C_{25-33}) + \sum_{\mathrm{odd}}(C_{27-35})\right]}{2\left(\sum_{\mathrm{even}}C_{26-34}\right)} \quad (4)$$

Table 1
Plant species sampled from each site, proportional species cover at each site, *n*-alkane concentration, ACL.

Site	Latitude	Longitude	Dominant plant species 1	Growth form	% Cover	Total μg/mg (C_{25}–C_{35})	ACL	Dominant plant species 2	Growth form	% Cover	Total μg/mg (C_{25}-C_{35})	ACL	Dominant plant species 3	Growth form	% Cover	Total μg/mg (C_{25}-C_{35})	ACL	Total site plant cover (%)
NTABRT 0004	−22.29	133.616	*Acacia aptaneura*	Shrub	54.9	11.84	32.1	*Aristida holathera*	Grass	24	1.33	32.4	*Triodia schinzii*	Grass	7.2	0.38	30.4	85.7
NTADAC 0001	−13.16	130.778	*Sorghum plumosum*	Grass	57.1	0.09	31.8	*Eucalyptus tetrodonta*	Tree	19	0.49	30.3	*Eucalyptus miniata*	Tree	7.8	0.38	29.9	84.3
NTAFIN 0019	−24.36	132.936	*Cenchrus ciliaris*	Grass	67.3	1.98	31.9	*Acacia estrophiolata*	Tree	19	5.63	30.4	*Enchylaena tomentosa*	Grass	2.3	1.37	29.3	88.4
NTAFIN 0022	−24.63	133.452	*Eremophila freelingii*	Shrub	49.6	50.88	30.2	*Enneapogon polyphyllus*	Grass	15	1.58	32.1	*Aristida contorta*	Grass	7.6	1.18	31.7	72
NTAGFU 0001	−18.91	137.069	*Aristida pruinosa*	Grass	16.7	0.58	30.8	*Enneapogon polyphyllus*	Grass	13	0.08	32.1	*Eucalyptus pruinosa*	Tree	13	0.04	27.6	42.22
NTAGFU 0008	−18.79	136.865	*Triodia pungens*	Grass	44.8	1.43	30.8	*Aristida contorta*	Grass	19	7.08	28.5	*Fimbristylis dichotoma*	Grass	14	0.5	32.1	78.2
NTAGFU 0010	−17.9	137.101	*Triodia pungens*	Grass	62.6	1.37	31.1	*Eucalyptus leucophloia*	Tree	36	0.33	30.7	N/A	N/A	N/A	N/A	N/A	99
NTAGFU 0017	−17.35	137.158	*Melaleuca viridiflora*	Shrub	31.2	0.08	28.2	*Chrysopogon fallax*	Grass	9.4	1	30.5	*Schizachyrium fragile*	Grass	7	0.09	31.5	47.6
NTAGFU 0031	−14.13	134.387	*Melaleuca viridiflora*	Shrub	29.9	0.71	31.1	*Schizachyrium pachyarthron*	Grass	28	0.13	31.1	*Petalostigma banksii*	Shrub	9.1	0.05	29.8	66.7
NTAGFU 0040	−14.67	133.845	*Acacia dimidiata*	Shrub	26.7	0.74	31.3	*Heteropogon contortus*	Grass	16	0.27	31.3	*Eucalyptus tectifica*	Tree	9.7	0.06	28.1	52.2
SAASTP 0001	−26.28	134.999	*Maireana aphylla*	Shrub	31	0.66	28.6	*Eragrostis setifolia*	Grass	12	0.25	31.1	*Acacia aneura* var. *tenuis*	Shrub	7.7	3.67	31.7	50.6
SAASTP 0004	−26.09	135.452	*Malvastrum americanum* var. *americanum*	Forb	25.6	1.72	29.6	*Rutidosis helichrysoides* subsp. *helichrysoides*	Forb	19	10.13	31.7	*Sida fubulifera*	Forb	12	5.06	32.2	55.8
SATFLB 0005	−31.32	138.566	*Dodonaea viscosa* subsp. *angustissima*	Shrub	21.8	20.02	28.9	*Eucalyptus flindersii*	Tree	19	0.48	26.7	*Chrysocephalum semipapposum*	Forb	13	5.08	30.5	53.6
SATFLB 0008	−32.32	137.954	*Triodia scariosa*	Grass	45.1	0.13	30.2	*Cassinia laevis*	Shrub	23	1.3	30.3	*Casuarina pauper*	Shrub	12	2.51	31.3	79.6
SATFLB 0010	−32.83	138.033	*Eucalyptus odorata*	Tree	65.1	0.21	26.8	*Rhagodia paradoxa*	Shrub	9.9	0.33	30.2	*Enchylaena tomentosa* var. *tomentosa*	Shrub	6	0.3	30.5	81
SATFLB 0012	−34.88	138.708	*Allocasuarina muelleriana* subsp. *Muelleriana*	Shrub	42	6.16	31.1	*Hibbertia crinita*	Shrub	16	0.14	30.0	*Eucalyptus fasciculosa*	Tree	13	0.04	28.3	70.2
SATFLB 0014	−34.01	138.959	*Eucalyptus odorata*	Tree	32.5	0.32	29.8	*Xanthorrhoea quadrangulata*	Shrub	18	0.22	30.3	*Allocasuarina verticillata*	Shrub	14	4.96	31.0	64.5
SATFLB 0015	−34.93	138.727	*Eucalyptus obliqua*	Tree	60	1.1	28.2	*Lepidosperma semiteres*	Grass	8.3	0.49	31.1	*Hibbertia crinita*	Shrub	6.5	0.6	28.3	74.8
SATKAN 0001	−35.61	138.261	*Eucalyptus baxteri*	Tree	42.5	1.41	29.9	*Lepidosperma semiteres*	Grass	11	0.09	31.5	*Pultenaea involucrata*	Shrub	10	0.37	31.8	63.9
SATKAN 0002	−35.27	138.690	*Eucalyptus obliqua*	Tree	54.7	0.07	29.1	*Lepidosperma semiteres*	Grass	9.1	0.2	31.9	*Hakea rostrata*	Shrub	8.2	0.48	30.4	72

where $\Sigma_{odd}C_{x-y}$ indicates the sum of all concentrations of *n*-alkanes with an odd carbon chain length from *x* to *y* inclusive and $\Sigma_{even}C_{a-b}$ is the sum of concentrations of *n*-alkanes with an even number of carbon chain lengths from *a* to *b* inclusive. Values where CPI > 1.5 were considered to represent an *n*-alkane source of primarily plant origin (Bush and McInerney, 2013).

Predicted soil ACL was calculated as an average of the three dominant plant species' (i = 1, 2, 3) ACL, weighted by both proportional species cover (% cover$_i$) and total concentration from C_{25}–C_{35} (conc$_i$) for each species:

$$\text{Predicted ACL} = \frac{\sum_{i=1}^{3}(\%\ \text{cover}_i \times \text{conc}_i \times \text{ACL}_i)}{\sum_{i=1}^{3}(\%\ \text{cover}_i \times \text{conc}_i)} \quad (5)$$

Predicted soil CPI was calculated as an average of the three dominant plant species' (i = 1, 2, 3) CPI, weighted by both species proportion (% cover$_i$) and concentration (conc$_i$) for each species:

$$\text{Predicted CPI} = \frac{\sum_{i=1}^{3}(\%\ \text{cover}_i \times \text{conc}_i \times \text{CPI}_i)}{\sum_{i=1}^{3}(\%\ \text{cover}_i \times \text{conc}_i)} \quad (6)$$

The proportional abundance of the C_{33} and C_{29} *n*-alkanes, termed Norm33, was calculated modified from Carr et al. (2014):

$$\text{Norm33} = \frac{C_{33}}{(C_{29} + C_{33})} \quad (7)$$

where C_x is the total concentration of each *n*-alkane with *x* carbon atoms.

2.7. Statistical analysis

Welch's t-tests were conducted using KaleidaGraph to examine the differences between the average ACL and Norm33 of the different plant growth forms and the soil. Least squares regression analysis was used to determine the strength of the relationships between the measured *n*-alkanes signals and plant growth form coverage, climate and particle size. Two-sided Kolmogorov-Smirnov tests were conducted using the ks.test function in base R (R Core Team, 2018) and used to compare the relative proportions of different chain lengths in association with different plant growth forms.

2.8. Climate data

Long-term site values for mean annual temperature (MAT), mean annual precipitation (MAP) and annual moisture index (MI), lowest quarter mean MI, highest period radiation and maximum temperature of the hottest month were extracted from ANUCLIM 6.1 layers of a 1960–2014 long term average (Xu and Hutchinson, 2013) through the Atlas of Living Australia (www.ala.org.au).

3. Results

In the plants, C_{31} had the highest concentration in the majority of samples (Fig. 2a, Supplementary Table S2). The ACL for plant samples ranged from 26.7 to 32.4, with a mean value of 30.4 ± 1.4 standard deviation (SD; Table 1). Concentrations of total *n*-alkanes in plants were generally less than <10 μg/mg dry wt, with the exception of three shrubs that ranged up to 50.9 μg/g dry wt (Supplementary Fig. S1).

In the soils, C_{29} had the highest concentration in the majority of samples (Fig. 2b, Supplementary Table S3). The measured ACL in the soils ranged from 27.4 to 30.9, with a mean value of 28.8 ± 0.9 (Table 2).

The average ACL of trees was 28.9 ± 1.4 (n = 13) and was lower and significantly different to that of forbs (31.0 ± 1.2, n = 4, p = 0.02), grasses (31.2 ± 0.9, n = 22, p < 0.0001), and shrubs (30.3 ± 1.2, n = 20, p = 0.005) (Fig. 3a). No other pair-wise comparisons between plant growth form and between plants and soils were statistically distinguishable (p > 0.5) (Fig. 3a).

From north to south, tree cover increased and grass cover decreased (Fig. 4). The measured soil ACL showed a weak but statistically significant positive correlation with grass cover (R^2 = 0.27, p = 0.02) and no relationship with tree cover (R^2 = 0.04, p = 0.4) (Fig. 5a and b).

The average Norm33 of trees was 0.21 ± 0.18 (n = 13) and was lower and significantly different to that of grasses (0.71 ± 0.24, n = 22, p < 0.0001), and shrubs (0.47 ± 0.47, n = 20, p = 0.007), but not distinguishable from that of forbs (0.60 ± 0.28, n = 4, p = 0.2) (Fig. 3b). The Norm33 of grasses was statistically different from shrubs (p = 0.01). No other pairwise comparisons showed statistical difference (p > 0.05) (Fig. 3b).

The measured soil Norm33 showed a weak but statistically significant positive relationship with grass cover (R^2 = 0.21, p = 0.04) and a weak but statistically significant negative relationship with tree cover (R^2 = 0.23, p = 0.03) (Fig. 5c and d).

Kolmogorov-Smirnov tests of leaf wax *n*-alkane distributions indicated that grasses (n = 20) contain significantly higher proportions of C_{33} than trees (n = 13) and shrubs (n = 21); trees contain a significantly higher proportion of C_{29} than grasses; and shrubs are indistinguishable from grasses or trees in terms of the proportion of C_{29} (Fig. 2. and Supplementary Fig. S2).

Plant CPI values ranged from 0.6 to 106.6, with all but one plant showing an odd-over-even carbon number preference (CPI > 1). The one sample that did not have an odd-over-even predominance was *Rhagodia paradoxa*, a chenopod, with a CPI of 0.6. The CPI for the soils ranged from 2.2 to 12.5. This strong odd-over-even predominance indicates that the source of the *n*-alkanes in the soils was from terrestrial higher plants.

In most cases, the predicted soil ACL and Norm33 was higher than the measured soil ACL and Norm33 (Fig. 6a and b). The degree of offset (measured soil-predicted soil) did not correlate with any climate variables (p > 0.05) (Fig. 4 and Supplementary Fig. S3) suggesting that model performance does not vary as a function of climate. Similarly, predicted soil CPI was higher than the measured soil CPI for the majority of sites (Fig. 6c). Particle size analysis revealed no relationship between *n*-alkane concentration, ACL or Norm33 and percentage clay, silt or sand of the soils (Supplementary Fig. S4).

4. Discussion

Long-chain *n*-alkanes extracted from sedimentary archives derived from ancient soils are routinely used as biomarkers for plants, therefore it is vital to understand what these archives represent. Cave sediments, such as Naracoorte Caves in SE Australia, represent a major archive derived largely from terrestrial soils (Macken et al., 2013). Similarly, tectonically active settings, such as the Bighorn Basin and the Siwalik Group preserve paleosols across key intervals of geologic history, such as the Paleocene–Eocene Thermal Maximum and Miocene, respectively (Zaleha, 1997; Smith et al., 2007; Ghosh et al., 2017). To better characterise the nature of these records, we compared *n*-alkane distributions in plants and soils along a transect across Australia to examine whether *n*-alkanes in surface soils are dominated by inputs from the current, local vegetation. We used point intercept data to approximate the proportional species cover of each of the three most dominant species present at a site. We then measured the concentration and distribution of long-chain *n*-alkanes from each of these species and from the surface soils at each site. *n*-Alkane inputs from vegetation are modelled as the cover- and

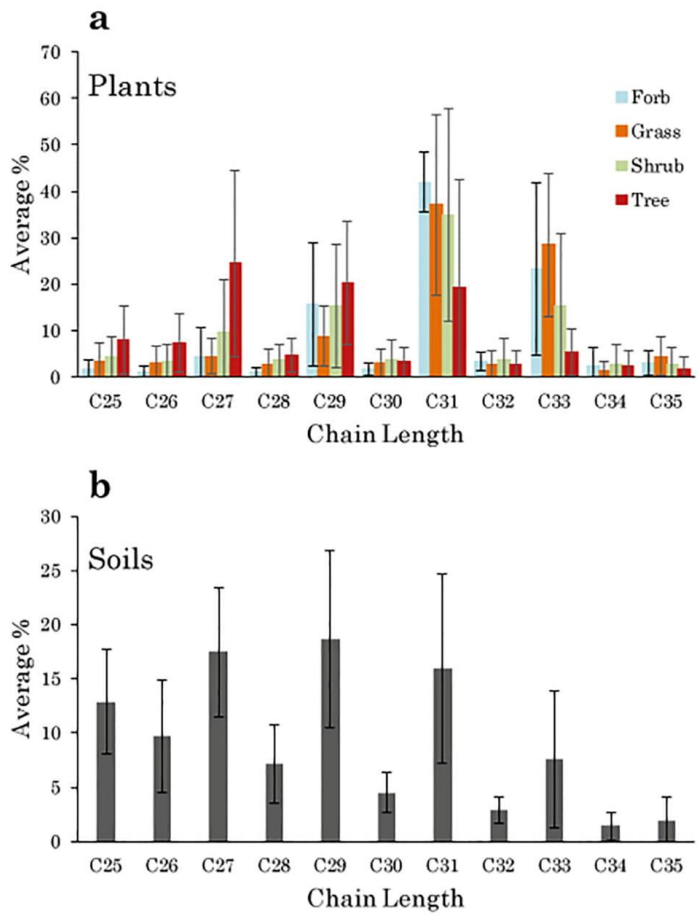

Fig. 2. Relative abundance of *n*-alkanes from (a) plants, separated into their different growth forms, and (b) soils. Distributions displayed as average percentage for each chain length relative to total *n*-alkanes (C_{25}–C_{35}). Error bars represent one standard deviation.

concentration-weighted average of the three most dominant taxa at each site. If local and recent vegetation were the dominant component of surface soil *n*-alkanes, we would expect the modelled *n*-alkane distributions to match those measured in soils. However, the modelled values of both ACL and Norm33 are offset from observed *n*-alkane characteristics, with measured values generally lower than the modelled ones (Fig. 6a and b). The offset between our modelled and observed distributions could be the result of integration of records over larger spatial scales/longer temporal scales than represented by the surveys, could reflect unaccounted fluxes of leaf waxes to soils, or could reflect post-depositional modification. These possibilities are evaluated below.

4.1. Regional vegetation inputs to soils

The modern vegetation survey used here encompasses one hectare plots (0.01 km^2), however, soils may accumulate *n*-alkanes from further afield. Aerosol samples collected from a mid-latitude forest in Germany have shown that their distribution of leaf wax *n*-alkane δD values differs significantly from that of local plants, suggesting that wind dispersal can transport *n*-alkanes across long-distances ranging from hundreds to thousands of kilometres (Nelson et al., 2017). Furthermore, Conte et al. (2003) demonstrated that the isotopic composition of ablated waxes in aerosols collected above a prairie canopy in southern Alberta, Canada, represented a regional scale catchment. Air mass trajectories have shown that wind-blown *n*-alkanes can travel as far as between continents, as well as having a regional or local source (Bendle et al., 2007; Yamamoto and Kawamura, 2010; Nelson et al., 2017). While *n*-alkanes in the atmosphere necessarily represent wind-blown aerosols, it is unclear whether in soils the aerosol deposition represents a significant contribution in comparison to local direct leaf fall. The offset observed here between measured and modelled *n*-alkane distributions may indicate that the signals recorded in the surface soils are integrating across a larger area than the one hectare survey plot.

Table 2
Soil samples from each site. Predicted CPI and ACL modelled from the plants.

Site	Total μg/mg (C_{25}-C_{35})	Measured CPI	Predicted CPI	Measured ACL	Predicted ACL
NTABRT 0004	0.017	6.0	14.6	30.9	32.1
NTADAC 0001	0.341	1.3	3.3	27.8	30.7
NTAFIN 0019	0.0004	5.8	23.9	29.6	31.2
NTAFIN 0022	0.224	1.1	1.9	27.9	30.2
NTAGFU 0001	0.006	3.6	3.1	30.0	30.8
NTAGFU 0008	0.003	3.6	14.3	29.8	29.4
NTAGFU 0010	0.028	6.1	42.8	29.9	31.1
NTAGFU 0017	0.044	3.4	4.7	28.1	30.1
NTAGFU 0031	0.002	2.2	2.1	29.3	31.1
NTAGFU 0040	0.022	4.5	4.7	29.4	31.3
SAASTP 0001	0.125	1.4	13.2	27.4	30.4
SAASTP 0004	0.002	1.2	8.2	28.2	31.5
SATFLB 0005	0.16	2.1	3.3	28.2	29.0
SATFLB 0008	0.113	1.9	4.6	28.5	30.8
SATFLB 0010	0.141	1.9	2.2	28.2	27.7
SATFLB 0012	0.001	1.8	31.6	28.2	31.1
SATFLB 0014	0.005	2.5	48.7	29.0	30.8
SATFLB 0015	0.005	4.9	4.8	27.8	28.4
SATKAN 0001	0.339	6.4	5.6	28.6	30.0
SATKAN 0002	0.007	3.3	36.3	28.1	30.1

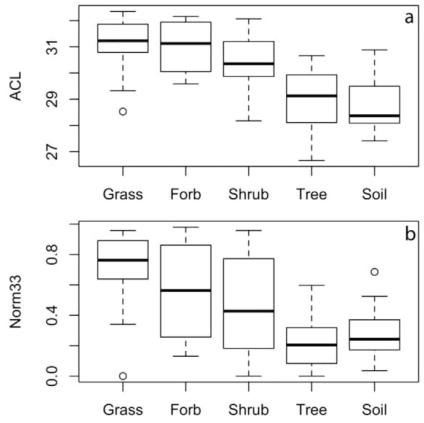

Fig. 3. (a) Boxplots of ACL values for plants, grouped by plant growth form, and soils. (b) Boxplots of Norm33 values for plants, grouped by plant growth form, and soils. Boxes represent 50% of the data, with the median shown by the line. Whiskers indicate lower and upper quartiles.

We observe a systematically shorter chain length distribution in the surface soils than that of the local plant community, which could result if regional aerosol or water borne inputs have shorter chain length distributions. Our results show that of all the growth forms, trees have the shortest average chain length (Fig. 3a). Therefore, if trees from outside of the hectare plots are contributing significantly to soils, this would explain the systematic offset between the local plant community and the surface soils. We hypothesize that trees may be overrepresented in the surface soils relative to other plant types due to their height in the landscape making them more susceptible to ablation by wind as compared to plants lower in stature, such as small shrubs and grasses.

4.2. Time averaging of n-alkane distributions in soils

The model uses the plants surveyed at the time of soil collection as the basis for the vegetation inputs to examine whether leaf waxes in surface soils are dominated by recent vegetation. However, *n*-alkanes can accumulate in soils over hundreds or thousands of years and then be re-mobilised and deposited with younger lacustrine and marine sediments (Smittenberg et al., 2006; Drenzek et al., 2007; Douglas et al., 2014; Gierga et al., 2016). If the *n*-alkanes in the surface soils accumulated over thousands of years, the standing plant community would be a poor predictor of soil *n*-alkane distributions because the dominant vegetation and climate across Australia have changed radically over this time (Hope, 2017). Over the course of the Late Pleistocene into the Holocene, variable but increasing aridity has resulted in a shift from forested to herbaceous vegetation in the Western Plains of Victoria (Edney et al., 1990) and an increase in the dominance of eucalypt dominated grassy woodlands in the last 5000 years in mainland SE Australia (Kershaw et al., 1991). More recently, vegetation has changed since European settlement. Australia's vegetation prior to European settlement had greater plant cover than today, with forests and woodlands in greater abundance (COAG Standing Council on Environment and Water, 2012). Past ecosystems with different *n*-alkane contributors would have produced different *n*-alkane distributions in soils. Environmental changes over the lifetime of the soil would cause a difference between the modern plant community and the temporally integrated soils. This would prevent soils from providing annual or decadal records, but not impact on using soils as recorders of long-term vegetation over centuries to millennia.

4.3. Unconstrained fluxes from plants to soils

Despite accounting for the relative abundances of the plants and differences in *n*-alkane concentration among the plants, we are unable to quantify the actual flux of *n*-alkanes from the plants to the surface soils. The flux can vary with the rate of litter fall, which is a function of leaf lifespan (Wright and Cannon, 2001), or with wax turnover rates within leaves due to physical removal (e.g., by wind ablation and herbivore removal and subsequent deposition) and regeneration of waxes (Koch et al., 2004). Leaf lifespan represents the duration of photosynthetic return to the plant and is balanced against the cost of producing greater leaf mass area (Wright et al., 2004). A global study of leaf economics has shown that in general plants that grow in arid conditions with higher mean annual temperature tend to have longer leaf lifespans (Wright et al., 2004). Our transect represents a broad range of climatic conditions, ranging from monsoonal tropics in the north, to

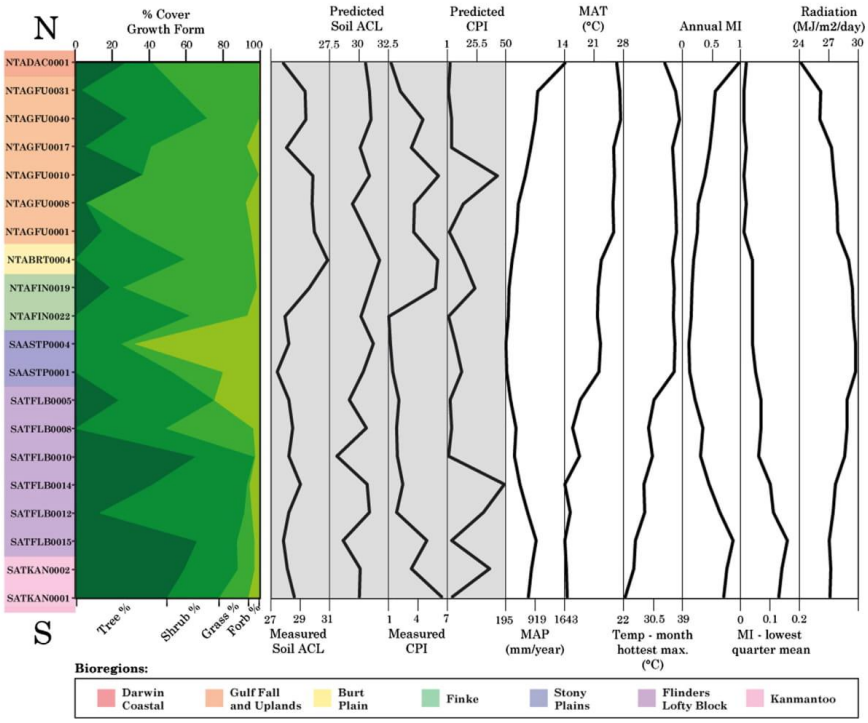

Fig. 4. Proportional coverage of the plant growth forms at each site compared to the measured and predicted soil ACL (unitless), the measured and predicted soil CPI (unitless), MAP, MAT, maximum temperature of the hottest month, annual and lowest quarter mean MI (unitless) and highest period of radiation for each site. Site bioregions (see Supplementary Table S1 for descriptions) indicated by colour bar.

arid central deserts, to winter rainfall in the south. These climatic differences are likely to contribute to variations in both leaf lifespan and the flux of litter to surface soils across the transect. Furthermore, the seasonal dominance of some annual species (e.g., *Sorghum* spp.) would lead to intra-annual variability in both local and regional *n*-alkane inputs. Similarly, differences in the rate of wax production and replacement within a leaf, particularly in rarer species, would result in inputs to surface soils that are not proportional to the standing vegetation composition and concentration. Our inability to constrain fluxes from plants to surface soils would contribute to the spread in the offset between modelled and measured values. However, it is unlikely to explain the systematic overestimates in modelled ACL and CPI.

4.4. Post-depositional modification

Our model tests the local, modern day inputs of *n*-alkanes, but does not measure the fate of these compounds once they have been deposited in the soils. In theory, post-depositional modification to the *n*-alkanes could alter the chain length distributions in soils. In Australian soils, carbon content of soils is positively correlated with precipitation and negatively correlated with temperature; high pH and high clay content also facilitate preservation (Oades, 1988; Carvalhais et al., 2014). Soil particle size is considered to play an important role in turnover of carbon, with decreasing carbon content and increasing carbon turnover rates in soils of increasing particle size (Cayet and Lichtfouse, 2001; Quenea et al., 2004; Quénéa et al., 2006). However, our study finds no correlation between particle size and *n*-alkane concentration or distribution (Supplementary Fig. S4).

At a global scale, organic matter turnover times vary across different biomes with shorter turnover times in tropical forests, savannahs and grasslands and longer turnover times in temperate forests, grasslands and shrublands (Carvalhais et al., 2014). We expect that variation in edaphic conditions could result in differential preservation potential of lipids. Bull et al. (2000) found an increase in *n*-alkane concentrations in soils with a higher pH and Pisani et al. (2015) found that soil warming resulted in a decrease in aliphatic lipid concentrations in the soil mineral horizon. Wang et al. (2017a) similarly find a decrease in concentration of *n*-alkanes with experimental heating at diagenetic temperatures ranging from 60 to 300 °C, as well as a decrease in ACL over time. However, due to our use of surface soils at a depth of only 3 cm, we expect temperatures to be significantly lower than in this experiment, and thus diagenetic effects to be minimised. Validated modelling of soil temperatures across Australia at 5 cm depths, a depth at which air temperature is the primary driver of the subsequent soil temperature, showed that even at extreme maximum temperatures of the year and day, soil temperature did not exceed 40 °C (Horton, 2012). In addition, if variations in climate controlled the degree of post-depositional modification, we would expect the offset between modelled and measured values to vary with climate. However, we find the degree of offset between our modelled and measured ACL does not correlate with temperature or precipitation

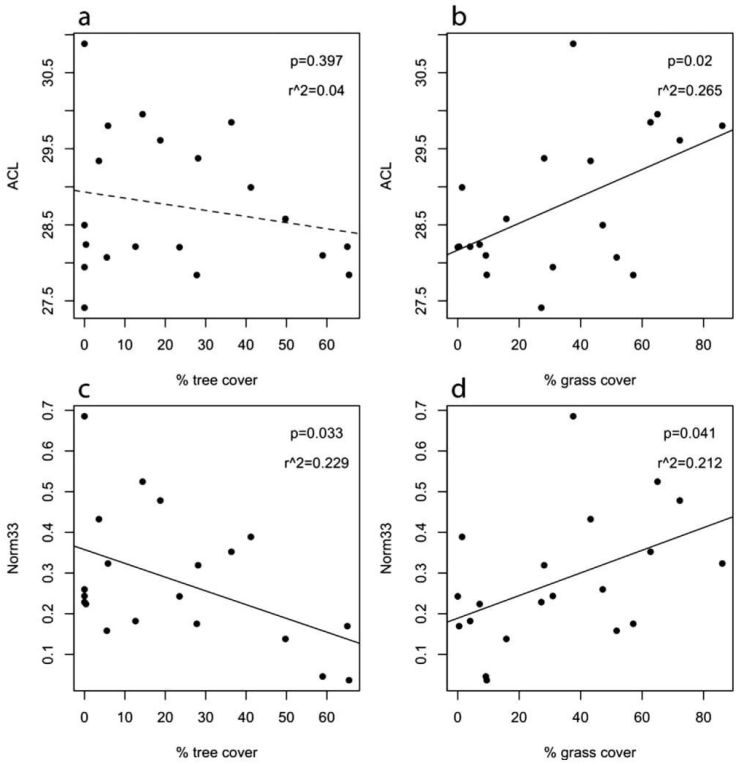

Fig. 5. Plots showing the relationship between ACL measured in the soils vs (a) the percentage of tree cover and, (b) the percentage of grass cover; plots showing the relationship between Norm33 measured in the soils vs (c) the percentage of tree cover and, (d) the percentage of grass cover. Black solid trend lines indicate a significant relationship ($p < 0.05$), a dashed trendline indicates a non-significant relationship ($p > 0.05$).

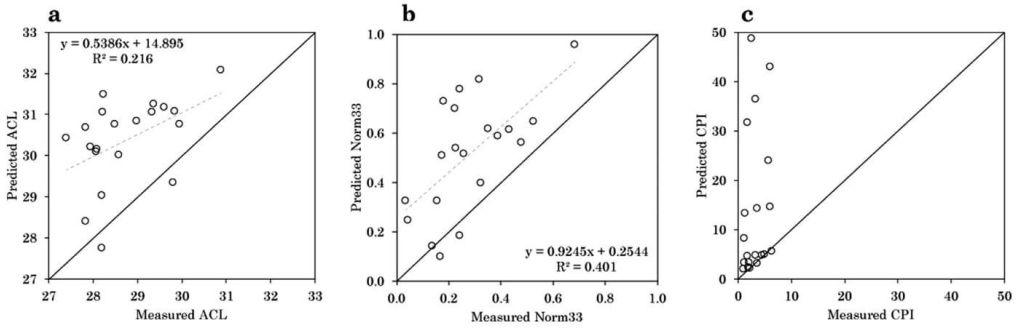

Fig. 6. Predicted vs measured soil (a) ACL, (b) Norm33 and (c) CPI. Prediction represents a concentration- and cover-weighted average of three most dominant plants at each site. The grey dashed line represents the trend. The black 1:1 line is shown for comparison.

(Supplementary Fig. S3). Thus, there is no evidence for climate-driven differences in post-depositional processing in our dataset.

Litterbag studies have explored the effects of microbial degradation on leaf waxes, but the effects varied among studies. Zech et al. (2011) find a decrease in concentration of odd, long-chain *n*-alkanes, as well a decrease in their odd-over-even predominance in a leaf litter bag experiment over 27 months which they interpret as a degradation signal. Similarly, our results show that overall the soils have a lower CPI than do the modelled plant inputs (Fig. 6c), which may indicate that degradation processes impact *n*-alkane

signals in the soil. In contrast, Nguyen Tu et al. (2017) noted that degradation processes resulted in a decrease in concentration of *n*-alkanes in a two-year litterbag study of beech leaves submerged in a pond, but did not result in a change to CPI, nor ACL. Additionally, Celerier et al. (2009) found that the longer chain lengths were not preferentially removed with depth in a soil profile of a long-term field experiment in France and show high resistance to microbial degradation. There is some evidence that differences in soil conditions may have an effect, where Li et al. (2017) found a small change to ACL of buried leaves at one of sites, but not at the other, with a different soil type. This evidence suggests that the ACL is not drastically altered by degradation processes in the soils, but that instead the odd-over-even predominance may vary in soils significantly as a result of degradation. As such, post-depositional modification is not a likely explanation for the ACL offset between the plants and surface soils.

4.5. Vegetation type and climatic effects on n-alkane distribution

A meta-analysis of plants from around the globe showed that in general grasses do not have longer ACL than woody vegetation (Bush and McInerney, 2013). However, within Africa, C4 monocots (grasses and sedges) produce more C_{33} than C3 plants, and C3 plants tend to produce more C_{29} than C4 monocots (Garcin et al., 2014). Similarly, in Australia, the grasses, which are predominantly C4, produce proportionally more C_{33} and had significantly longer ACL than trees (Fig. 3); trees produced statistically more C_{29}, and had a shorter ACL than grasses (Fig. 3). Shrubs and forbs produced a widely varying range of chain lengths (Fig. 3). Plant coverage effects are also evident in the soils. We find statistically significant ($p < 0.05$) correlations between percent grass cover with both Norm33 and ACL and between percent tree cover and Norm33 (Fig. 5). Similarly variations between biomes are seen in sediments from the southwest African continental margin, with longer chain lengths associated with savannahs, compared to shorter chain lengths in rainforests (Rommerskirchen et al., 2006). Carr et al. (2014) found that although there was considerable individual plant variability in the succulent karoo and fynbos biomes of South Africa, the succulent karoo was associated with longer maximum chain lengths than the fynbos, and these longer chain lengths were mirrored in the soils.

An alternative hypothesis for the cause of plant type differences observed here is that chain length distributions could be directly influenced by climate (Bush and McInerney, 2013, 2015). Evidence of correlations between ACL and climate (e.g., temperature, relative humidity) have been found in North America (Tipple and Pagani, 2013; Bush and McInerney, 2015), Italy (Leider et al., 2013), on the Tibetan Plateau (Jia et al., 2016) and in Australia (Hoffmann et al., 2013). We found no relationship between any climate variables and the ACL of plants or soils, testing both climatic extremes and annual means of both temperature and precipitation (Fig. 4, Supplementary Figs. S5 and S6). This is similar to the findings of Wang et al. (2017b), who did not find a strong relationship with temperature and ACL in soils across a >1000 km transect in SW China. Plant type appears to be a greater determinant of ACL than climate in this study. Carr et al. (2014), found that climate was only very weakly correlated with ACL, while there were clear differences between growth forms. Phylogenetic constraints on leaf wax concentration and distribution was shown among conifers (Diefendorf et al., 2015) and may play a role in constraining responses to climate in other groups as well.

4.6. Evaluation of factors influencing soil n-alkane signatures

Our results suggest that soil *n*-alkanes are not dominantly from local and recent vegetation at the sites examined in this study. Moreover, a greater influence of trees from more distant, or previous plant communities could cause shorter ACL in the soils than that observed in modern, local vegetation. Our inability to account for the flux of waxes from the local plants into the soils is noteworthy, but unlikely to result in systematic overestimates by the models. Post-depositional microbial modification may contribute to the reduction in CPI in soils compared to plants, but is unlikely to affect ACL. The offsets between the modelled and measured ACL and Norm33 most likely reflect that soils integrate over larger spatial and/or temporal scales than those sampled by our plant survey. The correspondence between plant cover type (percent grass or percent trees) and *n*-alkane distributions (Norm33, ACL) in soils suggests that soil *n*-alkanes faithfully record larger scale ecosystem features, rather than localised plant communities.

4.7. Implications for palaeoecology

Our results show that while we can be confident that the *n*-alkanes found in the surface soils are of a terrestrial plant origin due to their odd-over-even predominance. We suggest that the leaf waxes in the soils represent a spatially and/or temporally integrated signal. A distinct benefit for palaeoecology is that *n*-alkanes in soils should not be susceptible to microclimates, spatial heterogeneity of vegetation, or short term changes in vegetation due to interannual variability. The correspondence of *n*-alkane distributions in soils with plant cover type (grass or tree) suggests that information on vegetation structure is preserved in soils. Although we detect degradation processes occurring in the soils, with a decrease in soil CPI relative to the vegetation, we do not expect that the ACL of the soils is affected by degradation based on the results of previous studies, however further work to investigate this at greater depth is necessary.

5. Conclusions

Characterising the temporal and spatial scale of inputs of *n*-alkanes from plants to surface soils allows us to better understand what we are measuring when analysing these compounds. Our results show an offset between the modelled signals based on current and local vegetation, and the measured signals in the soils. This offset allows us to reject the hypothesis of recent and local source, and indicates spatial and/or temporal averaging of inputs into the soils. We further suggest that trees are the likely source of the shorter ACL observed in the soils, due to their elevation in the landscape, making them potentially more susceptible to wind ablation than lower-statured species, and due to their greater presence in Australia's pre-European settlement as compared to today. Vegetation cover type (percent grass or percent tree) correlates with surface soil *n*-alkane distributions (Norm33), suggesting that large-scale features of vegetation structure are preserved in soil *n*-alkanes. The signals we observe in sedimentary records are likely to reflect a regional, time-averaged signal that is not heavily susceptible to short-term variability or small-scale spatial heterogeneity in climate.

Acknowledgements

The authors thank the Terrestrial Ecosystem Research Network, for providing the samples and vegetation cover data used in this study. Thanks also to Kristine Nielson for assistance in the lab, Emrys Leitch for help with vegetation data and David McInerney for statistical advice. We also wish to thank three anonymous reviewers for their helpful comments. Funding was provided by the Australian Research Council to FAM (FT110100793, DP130104314). This research is also supported by Australian

Government Research Training Program (RTP) Scholarships to SH, SC-R and JWA.

Appendix A. Supplementary material

Supplementary data associated with this article can be found, in the online version, at https://doi.org/10.1016/j.orggeochem.2018.03.013.

Associate Editor—**Myrna Simpson**

References

Angst, G., John, S., Mueller, C.W., Kögel-Knabner, I., Rethemeyer, J., 2016. Tracing the sources and spatial distribution of organic carbon in subsoils using a multi-biomarker approach. Scientific Reports 6. https://doi.org/10.1038/srep29478.

Banthorpe, D.V., 2006. Natural Occurrence, Biochemistry and Toxicology, Alkanes and Cycloalkanes. John Wiley & Sons, Ltd, pp. 895–926.

Bastow, T.P., van Aarssen, B.G.K., Lang, D., 2007. Rapid small-scale separation of saturate, aromatic and polar components in petroleum. Organic Geochemistry 38, 1235–1250.

Bendle, J., Kawamura, K., Yamazaki, K., Niwai, T., 2007. Latitudinal distribution of terrestrial lipid biomarkers and *n*-alkane compound-specific stable carbon isotope ratios in the atmosphere over the western Pacific and Southern Ocean. Geochimica et Cosmochimica Acta 71, 5934–5955.

Bull, I.D., van Bergen, P.F., Nott, C.J., Poulton, P.R., Evershed, R.P., 2000. Organic geochemical studies of soils from the Rothamsted classical experiments—V. The fate of lipids in different long-term experiments. Organic Geochemistry 31, 389–408.

Bush, R.T., McInerney, F.A., 2013. Leaf wax *n*-alkane distributions in and across modern plants: implications for paleoecology and chemotaxonomy. Geochimica et Cosmochimica Acta 117, 161–179.

Bush, R.T., McInerney, F.A., 2015. Influence of temperature and C4 abundance on *n*-alkane chain length distributions across the central USA. Organic Geochemistry 79, 65–73.

Carr, A.S., Boom, A., Grimes, H.L., Chase, B.M., Meadows, M.E., Harris, A., 2014. Leaf wax *n*-alkane distributions in arid zone South African flora: environmental controls, chemotaxonomy and palaeoecological implications. Organic Geochemistry 67, 72–84.

Carvalhais, N., Forkel, M., Khomik, M., Bellarby, J., Jung, M., Migliavacca, M., Mu, M., Saatchi, S., Santoro, M., Thurner, M., Weber, U., Ahrens, B., Beer, C., Cescatti, A., Randerson, J.T., Reichstein, M., 2014. Global covariation of carbon turnover times with climate in terrestrial ecosystems. Nature 514, 213–217.

Cayet, C., Lichtfouse, E., 2001. $\delta^{13}C$ of plant-derived *n*-alkanes in soil particle-size fractions. Organic Geochemistry 32, 253–258.

Celerier, J., Rodier, C., Favetta, P., Lemee, L., Ambles, A., 2009. Depth-related variations in organic matter at the molecular level in a loamy soil: reference data for a long-term experiment devoted to the carbon sequestration research field. European Journal of Soil Science 60, 33–43.

Chikaraishi, Y., Kaneko, M., Ohkouchi, N., 2012. Stable hydrogen and carbon isotopic compositions of long-chain (C_{21}–C_{33}) *n*-alkanes and *n*-alkenes in insects. Geochimica et Cosmochimica Acta 95, 53–62.

COAG Standing Council on Environment and Water, 2012. Australia's Native Vegetation Framework. Australian Government, Department of Sustainability, Environment, Water, Population and Communities, Canberra.

Conte, M.H., Weber, J.C., Carlson, P.J., Flanagan, L.B., 2003. Molecular and carbon isotopic composition of leaf wax in vegetation and aerosols in a northern prairie ecosystem. Oecologia 135, 67–77.

Cranwell, P.A., 1981. Diagenesis of free and bound lipids in terrestrial detritus deposited in a lacustrine sediment. Organic Geochemistry 3, 79–89.

Diefendorf, A.F., Freimuth, E.J., 2017. Extracting the most from terrestrial plant-derived *n*-alkyl lipids and their carbon isotopes from the sedimentary record: a review. Organic Geochemistry 103, 1–21.

Diefendorf, A.F., Leslie, A.B., Wing, S.L., 2015. Leaf wax composition and carbon isotopes vary among major conifer groups. Geochimica et Cosmochimica Acta 170, 145–156.

Dodd, R.S., Poveda, M.M., 2003. Environmental gradients and population divergence contribute to variation in cuticular wax composition in Juniperus communis. Biochemical Systematics and Ecology 31, 1257–1270.

Douglas, P.M.J., Pagani, M., Eglinton, T.I., Brenner, M., Hodell, D.A., Curtis, J.H., Ma, K. F., Breckenridge, A., 2014. Pre-aged plant waxes in tropical lake sediments and their influence on the chronology of molecular paleoclimate proxy records. Geochimica et Cosmochimica Acta 141, 346–364.

Drenzek, N.J., Montluçon, D.B., Yunker, M.B., Macdonald, R.W., Eglinton, T.I., 2007. Constraints on the origin of sedimentary organic carbon in the Beaufort Sea from coupled molecular ^{13}C and ^{14}C measurements. Marine Chemistry 103, 146–162.

Edney, P.A., Kershaw, A.P., De Deckker, P., 1990. A late Pleistocene and Holocene vegetation and environmental record from Lake Wangoom, Western Plains of Victoria, Australia. Palaeogeography, Palaeoclimatology, Palaeoecology 80, 325–343.

Eglinton, G., Hamilton, R.J., 1967. Leaf epicuticular waxes. Science 156, 1322–1335.

Eglinton, T.I., Eglinton, G., 2008. Molecular proxies for paleoclimatology. Earth and Planetary Science Letters 275, 1–16.

Eigenbrode, S.D., Espelie, K.E., 1995. Effects of plant epicuticular lipids on insect herbivores. Annual Review of Entomology 40, 171–194.

Gamarra, B., Kahmen, A., 2015. Concentrations and δ^2H values of cuticular *n*-alkanes vary significantly among plant organs, species and habitats in grasses from an alpine and a temperate European grassland. Oecologia 178, 981–998.

Gao, L., Burnier, A., Huang, Y., 2012. Quantifying instantaneous regeneration rates of plant leaf waxes using stable hydrogen isotope labeling. Rapid Communications in Mass Spectrometry 26, 115–122.

Garcin, Y., Schefuß, E., Schwab, V.F., Garreta, V., Gleixner, G., Vincens, A., Todou, G., Séné, O., Onana, J.-M., Achoundong, G., Sachse, D., 2014. Reconstructing C3 and C4 vegetation cover using *n*-alkane carbon isotope ratios in recent lake sediments from Cameroon, Western Central Africa. Geochimica et Cosmochimica Acta 142, 482–500.

Ghosh, S., Sanyal, P., Kumar, R., 2017. Evolution of C4 plants and controlling factors: insight from *n*-alkane isotopic values of NW Indian Siwalik paleosols. Organic Geochemistry 110, 110–121.

Gierga, M., Hajdas, I., van Raden, U.J., Gilli, A., Wacker, L., Sturm, M., Bernasconi, S. M., Smittenberg, R.H., 2016. Long-stored soil carbon released by prehistoric land use: evidence from compound-specific radiocarbon analysis on Soppensee lake sediments. Quaternary Science Reviews 144, 123–131.

Hoffmann, B., Kahmen, A., Cernusak, L.A., Arndt, S.K., Sachse, D., 2013. Abundance and distribution of leaf wax *n*-alkanes in leaves of Acacia and Eucalyptus trees along a strong humidity gradient in northern Australia. Organic Geochemistry 62, 62–67.

Hope, G.S., 2017. Quaternary vegetation. In: Hill, R.S. (Ed.), History of the Australian Vegetation: Cretaceous to Recent. University of Adelaide Press, pp. 368–389.

Horton, B., 2012. Models for estimation of hourly soil temperature at 5 cm depth and for degree-day accumulation from minimum and maximum soil temperature. Soil Research 50, 447–454.

Huang, Y., Bol, R., Harkness, D.D., Ineson, P., Eglinton, G., 1996. Post-glacial variations in distributions, ^{13}C and ^{14}C contents of aliphatic hydrocarbons and bulk organic matter in three types of British acid upland soils. Organic Geochemistry 24, 273–287.

Huang, Y., Street-Perrott, F.A., Metcalfe, S.E., Brenner, M., Moreland, M., Freeman, K. H., 2001. Climate change as the dominant control on glacial-interglacial variations in C3 and C4 plant abundance. Science 293, 1647–1651.

Jansen, B., Wiesenberg, G.L.B., 2017. Opportunities and limitations related to the application of plant-derived lipid molecular proxies in soil science. Soil 3, 211–234.

Jetter, R., Riederer, M., 2016. Localization of the transpiration barrier in the epi- and intracuticular waxes of eight plant species: water transport resistances are associated with fatty acyl rather than alicyclic components. Plant Physiology 170, 921–934.

Jia, Q., Sun, Q., Xie, M., Shan, Y., Ling, Y., Zhu, Q., Tian, M., 2016. Normal alkane distributions in soil samples along a Lhasa-Bharatpur transect. Acta Geologica Sinica – English Edition 90, 738–748.

Kershaw, A.P., D'Costa, D.M., McEwen Mason, J.R.C., Wagstaff, B.E., 1991. Palynological evidence for Quaternary vegetation and environments of mainland southeastern Australia. Quaternary Science Reviews 10, 391–404.

Khan, A.A., Kolattukudy, P.E., 1974. Decarboxylation of long chain fatty acids to alkanes by cell free preparations of pea leaves (*Pisum sativum*). Biochemical and Biophysical Research Communications 61, 1379–1386.

Koch, K., Dommisse, A., Niemietz, A., Barthlott, W., Wandelt, K., 2009. Nanostructure of epicuticular plant waxes: self-assembly of wax tubules. Surface Science 603, 1961–1968.

Koch, K., Neinhuis, C., Ensikat, H.J., Barthlott, W., 2004. Self assembly of epicuticular waxes on living plant surfaces imaged by atomic force microscopy (AFM). Journal of Experimental Botany 55, 711–718.

Leider, A., Hinrichs, K.-U., Schefuß, E., Versteegh, G.J.M., 2013. Distribution and stable isotopes of plant wax derived *n*-alkanes in lacustrine, fluvial and marine surface sediments along an Eastern Italian transect and their potential to reconstruct the hydrological cycle. Geochimica et Cosmochimica Acta 117, 16–32.

Li, R., Fan, J., Xue, J., Meyers, P.A., 2017. Effects of early diagenesis on molecular distributions and carbon isotopic compositions of leaf wax long chain biomarker n-alkanes: comparison of two one-year-long burial experiments. Organic Geochemistry 104, 8–18.

Lichtfouse, É., Chenu, C., Baudin, F., Leblond, C., Da Silva, M., Behar, F., Derenne, S., Largeau, C., Wehrung, P., Albrecht, P., 1998. A novel pathway of soil organic matter formation by selective preservation of resistant straight-chain biopolymers: chemical and isotope evidence. Organic Geochemistry 28, 411–415.

Macken, A.C., McDowell, M.C., Bartholomeusz, D.N., Reed, E.H., 2013. Chronology and stratigraphy of the Wet Cave vertebrate fossil deposit, Naracoorte, and relationship to paleoclimatic conditions of the Last Glacial Cycle in south-eastern Australia. Australian Journal of Earth Sciences 60, 271–281.

Makou, M., Eglinton, T., McIntyre, C., Montluçon, D., Antheaume, I., Grossi, V., 2018. Plant wax *n*-alkane and *n*-alkanoic acid signatures overprinted by microbial contributions and old carbon in meromictic lake sediments. Geophysical Research Letters 45, 1049–1057.

Marzi, R., Torkelson, B.E., Olson, R.K., 1993. A revised carbon preference index. Organic Geochemistry 20, 1303–1306.

Meyers, P.A., Hites, R.A., 1982. Extractable organic compounds in midwest rain and snow. Atmospheric Environment 16, 2169–2175.

Nelson, D.B., Knohl, A., Sachse, D., Schefuß, E., Kahmen, A., 2017. Sources and abundances of leaf waxes in aerosols in central Europe. Geochimica et Cosmochimica Acta 198, 299–314.
Nguyen Tu, T.T., Egasse, C., Anquetil, C., Zanetti, F., Zeller, B., Huon, S., Derenne, S., 2017. Leaf lipid degradation in soils and surface sediments: a litterbag experiment. Organic Geochemistry 104, 35–41.
Oades, J.M., 1988. The retention of organic matter in soils. Biogeochemistry 5, 35–70.
Pisani, O., Frey, S.D., Simpson, A.J., Simpson, M.J., 2015. Soil warming and nitrogen deposition alter soil organic matter composition at the molecular-level. Biogeochemistry 123, 391–409.
Pu, Y., Zhang, H., Wang, Y., Lei, G., Nace, T., Zhang, S., 2011. Climatic and environmental implications from *n*-alkanes in glacially eroded lake sediments in Tibetan Plateau: an example from Ximen Co. Chinese Science Bulletin 56, 1503–1510.
Quenea, K., Derenne, S., Largeau, C., Rumpel, C., Mariotti, A., 2004. Variation in lipid relative abundance and composition among different particle size fractions of a forest soil. Organic Geochemistry 35, 1355–1370.
Quénéa, K., Largeau, C., Derenne, S., Spaccini, R., Bardoux, G., Mariotti, A., 2006. Molecular and isotopic study of lipids in particle size fractions of a sandy cultivated soil (Cestas cultivation sequence, southwest France): sources, degradation, and comparison with Cestas forest soil. Organic Geochemistry 37, 20–44.
R Core Team, 2018. R: A Language and Environment for Statistical Computing. R Foundation for Statistical Computing, Vienna, Austria. <https://www.R-project.org/>.
Rommerskirchen, F., Eglinton, G., Dupont, L., Rullkötter, J., 2006. Glacial/interglacial changes in southern Africa: compound-specific $\delta^{13}C$ land plant biomarker and pollen records from southeast Atlantic continental margin sediments. Geochemistry, Geophysics, Geosystems 7. https://doi.org/10.1029/2005GC001223.
Rouillard, A., Greenwood, P.F., Grice, K., Skrzypek, G., Dogramaci, S., Turney, C., Grierson, P.F., 2016. Interpreting vegetation change in tropical arid ecosystems from sediment molecular fossils and their stable isotope compositions: a baseline study from the Pilbara region of northwest Australia. Palaeogeography, Palaeoclimatology, Palaeoecology 459, 495–507.
Sachse, D., Radke, J., Gleixner, G., 2004. Hydrogen isotope ratios of recent lacustrine sedimentary *n*-alkanes record modern climate variability. Geochimica et Cosmochimica Acta 68, 4877–4889.
Schwark, L., Zink, K., Lechterbeck, J., 2002. Reconstruction of postglacial to early Holocene vegetation history in terrestrial Central Europe via cuticular lipid biomarkers and pollen records from lake sediments. Geology 30, 463–466.
Shepherd, T., Wynne Griffiths, D., 2006. The effects of stress on plant cuticular waxes. New Phytologist 171, 469–499.
Smith, F.A., Wing, S.L., Freeman, K.H., 2007. Magnitude of the carbon isotope excursion at the Paleocene-Eocene thermal maximum: the role of plant community change. Earth and Planetary Science Letters 262, 50–65.
Smittenberg, R.H., Eglinton, T.I., Schouten, S., Sinninghe Damsté, J.S., 2006. Ongoing buildup of refractory organic carbon in boreal soils during the Holocene. Science 314, 1283–1286.
Tipple, B.J., Pagani, M., 2013. Environmental control on eastern broadleaf forest species' leaf wax distributions and D/H ratios. Geochimica et Cosmochimica Acta 111, 64–77.
van Gardingen, P.R., Grace, J., Jeffree, C.E., 1991. Abrasive damage by wind to the needle surfaces of *Picea sitchensis* (Bong.) Carr. and *Pinus sylvestris* L. Plant, Cell & Environment 14, 185–193.
Wang, C., Eley, Y., Oakes, A., Hren, M., 2017a. Hydrogen isotope and molecular alteration of n-alkanes during heating in open and closed systems. Organic Geochemistry 112, 47–58.
Wang, C., Hren, M.T., Hoke, G.D., Liu-Zeng, J., Garzione, C.N., 2017b. Soil *n*-alkane δD and glycerol dialkyl glycerol tetraether (GDGT) distributions along an altitudinal transect from southwest China: evaluating organic molecular proxies for paleoclimate and paleoelevation. Organic Geochemistry 107, 21–32.
White, A., Sparrow, B., Leitch, E., Foulkes, J., Flitton, R., Lowe, A., Caddy-Retalic, S., 2012. AusPlots Rangelands Survey Protocols Manual, Terrestrial Ecosystem Research Network. University of Adelaide Press, University of Adelaide, p. 84.
Wright, I.J., Cannon, K., 2001. Relationships between leaf lifespan and structural defences in a low-nutrient, sclerophyll flora. Functional Ecology 15, 351–359.
Wright, I.J., Reich, P.B., Westoby, M., Ackerly, D.D., Baruch, Z., Bongers, F., Cavender-Bares, J., Chapin, T., Cornelissen, J.H.C., Diemer, M., Flexas, J., Garnier, E., Groom, P.K., Gulias, J., Hikosaka, K., Lamont, B.B., Lee, T., Lee, W., Lusk, C., Midgley, J.J., Navas, M.-L., Niinemets, U., Oleksyn, J., Osada, N., Poorter, H., Poot, P., Prior, L., Pyankov, V.I., Roumet, C., Thomas, S.C., Tjoelker, M.G., Veneklaas, E.J., Villar, R., 2004. The worldwide leaf economics spectrum. Nature 428, 821–827.
Xu, T., Hutchinson, M.F., 2013. New developments and applications in the ANUCLIM spatial climatic and bioclimatic modelling package. Environmental Modelling & Software 40, 267–279.
Yamamoto, S., Hasegawa, T., Tada, R., Goto, K., Rojas-Consuegra, R., Díaz-Otero, C., García-Delgado, D.E., Yamamoto, S., Sakuma, H., Matsui, T., 2010. Environmental and vegetational changes recorded in sedimentary leaf wax n-alkanes across the Cretaceous-Paleogene boundary at Loma Capiro, Central Cuba. Palaeogeography, Palaeoclimatology, Palaeoecology 295, 31–41.
Yamamoto, S., Kawamura, K., 2010. Compound-specific stable carbon and hydrogen isotopic compositions of *n*-alkanes in urban atmospheric aerosols from Tokyo. Geochemical Journal 44, 419–430.
Zaleha, M.J., 1997. Siwalik Paleosols (Miocene, northern Pakistan); genesis and controls on their formation. Journal of Sedimentary Research 67, 821–839.
Zech, M., Pedentchouk, N., Buggle, B., Leiber, K., Kalbitz, K., Marković, S.B., Glaser, B., 2011. Effect of leaf litter degradation and seasonality on D/H isotope ratios of *n*-alkane biomarkers. Geochimica et Cosmochimica Acta 75, 4917–4928.

Appendix 2. List of conference abstracts authored during candidature

Polissar, Pratigya J., Uno, Kevin T., Phelps, Samuel R., Karp, Allison, **Andrae, Jake**, Freeman, Katherine, McInerney, Francesca A. and deMenocal, Peter B. Environmental drivers of the Late Neogene expansion of C4 ecosystems. *AGU Fall Meeting (San Francisco, California, USA 2019).*

Karp, Allison T., **Andrae, Jake W.,** McInerney, Francesca A., Polissar, Pratigya J. and Freeman, Katherine H. Molecular insights on fire ecology and carbon cycling during the Neogene C4 expansion in Australia. *Geological Society of America Annual Meeting (Phoenix, Arizona, USA 2019).*

McInerney, F.A., **Andrae, J.W.,** Polissar, P.J., Sniderman, J.M.K., Howard, S., Hall, P.A., and Phelps, S.R. Late to the party: Australia's tardy expansion of C4 vegetation linked to Australian summer monsoon? *Mio-Meet 2019 (Stockholm, Sweden 2019).*

Andrae J., McInerney F., Polissar P., Sniderman J.M.K., Howard S., Hall P.A. & Phelps S. Plant Wax *n*-Alkanes Record Late Pliocene C_4 Vegetation Expansion in Australia. *AGU Fall Meeting (Washington D.C., USA 2018).*

Andrae J., McInerney F., Polissar P., Sniderman J.M.K., Howard S., Hall P.A. & Phelps S. The timing and drivers of the expansion of C_4 vegetation in Australia. *Australian Geoscience Council Convention (Adelaide, Australia 2018).*

McInerney F., **Andrae J.,** Polissar P., Sniderman J.M.K., Howard S., Hall P.A. & Phelps S. Late to the Party: Australia's Tardy Expansion of C4 Vegetation Linked to Australian Summer Monsoon. *Goldschmidt Conference (Boston, Massachusetts, USA 2018).*

Andrae, Jake W., McInerney, Francesca A., Polissar, Pratigya J., Hall, Tony and Tyler, Jonathan J. The Neogene expansion of C4 dominated ecosystems: An Australian perspective. *Geological Society of America Annual Meeting (Seattle, Washington, USA 2017).*

McInerney, Francesca A., Bush, Rosemary T., Baczynski, Allison A., **Andrae, Jake W.,** Bunney, Ellyse, Howard, Siân. Why do leaf wax *n*-alkane distributions change during the Paleocene-Eocene Thermal Maximum? *Geological Society of America Annual Meeting (Seattle, Washington, USA 2017).*

Jackson, Kevin E., Strömberg, Caroline A.E., **Andrae, Jake W.,** McInerney, Francesca A. The evolution of C4 grasslands in Australia: Phytolith assemblage data from Neogene marine cores. *Geological Society of America Annual Meeting (Seattle, Washington, USA 2017).*

Andrae, Jake W., McInerney, Francesca A., Tyler, Jonathan J. and Hall, Tony. The Neogene expansion of C4 dominated ecosystems: An Australian perspective. *19th Australian Organic Geochemistry Conference (Fremantle, Australia 2016).*

Andrae, Jake W., McInerney, Francesca A., Tyler, Jonathan J. and Hall, Tony. Ecosystem change through the Neogene in Australia: documenting the rise of C4 vegetation. *Palaeo Down Under 2 (Adelaide, Australia 2016).*

Andrae, Jake; McInerney, Francesca; Tibby, John; Barr, Cameron; Marshall, Jonathan; McGregor, Glenn and Westra, Seth. Variation in leaf wax *n*-alkane properties across a precipitation and temperature gradient. *Australian Earth Sciences Convention (Adelaide, Australia 2016).*